BIOPROCESS IMPROVEMENT FOR MANUFACTURING OF RECOMBINANT ADENO-ASSOCIATED VIRUS-BASED GENE DELIVERY VECTORS

Pranavkumar Joshi
Biological and Biomedical Engineering
McGill University, Montreal
Canada

December 2020

A thesis submitted to McGill University in partial fulfilment of the requirements of the degree of Doctor of Philosophy

Acknowledgement

Words may not do the justice to express my gratitude to those who have helped me throughout the journey of my Ph.D.; still, here is my honest attempt.

First and foremost, I want to thank Amine for providing me an exceptional opportunity to pursue my doctoral thesis under his mentorship. It seems like it was just yesterday that Amine and I sat down in UQAM's cafeteria and discussed what I'd be working on over the next what would be five years. While his futuristic vision was inspiring, his undivided attention and exemplary support throughout the years will always remain invaluable to me. The research facilities Amine has established in the lab are world-class, and the freedom of research offered to explore pertinent ideas was exceptional and unparalleled. Under his mentorship, I hone my critical thinking abilities, scientific writing, and presentation skills. Amine's significant contributions to this thesis have not only been limited to helping me navigate complex problems of my thesis, but also, he has worked tirelessly towards a critical evaluation of my research data and manuscripts. Amine, I will forever be indebted for this fantastic opportunity and for introducing me to the field of gene therapy.

I am also profoundly grateful to Parminder, my co-supervisor, for his invaluable support and guidance in every aspect of my doctoral research work. My hands-on training of complex AAV bioprocessing steps was conducted under his direct or indirect supervision at NRC. Through collaboration with him, I was able to access the advanced research facilities of NRC, without which many aspects of this doctoral thesis would have been incomplete. I am also thankful to him for always being a tough yet fair critic of my research work and my way of thinking, which ultimately shaped my understanding and attitude towards conducting the highest-quality scientific research over these years.

I would like to thank my committee members–Prof. Corinne Hoesli, Prof. Allen Ehrlicher, and Prof. David Juncker– for their time, support, and critical evaluation of my research progress.

I also want to extend my special gratitude to Alice Bernier-my colleague and a great mentor. My rigorous hands-on training on downstream processing and analytical technologies was conducted under her direct supervision, and she deserves much of the credit for a spectrum of biomanufacturing technical skills I possess today. I will also miss our lunch-time conversations and a series of short (you know how short they were!!) technical discussions.

I want to thank Dr. Joseph Schrag for training me on AAV analytical technologies and critically evaluating my research work. I will also miss our detailed scientific discussion on organic/inorganic chemistry, chromatography, and analytical technologies in general.

I want to extend my deepest gratitude to Julia from NRC to train me on AAV analytics, including HPLC. I would miss our technical brain-storming sessions and a long discussion on things that are not related to science.

I also want to thank other colleagues from NRC- Nasha, Marie-Helene, Renald, Johnny, Stephane, Mehul Bhai, and the team of HHT for their support and guidance.

I also want to thank all the past and current senior colleagues- Laura, Ernest, Ibrahim, Cuitla, Omar, Adeline, Cecile, Jean-Francois, Shini, Mounia, and Kumar for their guidance and support. Laura was the first friend and a mentor in the lab when I first arrived, who also trained me on insect cell culture and viral vector bioprocessing. Ernest provided invaluable guidance on overall virology and bioprocessing. Ibrahim trained me on qPCR technology and provided extended support during our time together in the lab. I also want to thank Kumar and Omar for their extensive support and guidance.

I want to convey special thanks to Alina, one of my closest friends and a fantastic colleague. I will miss our endless conversations on scientific and non-scientific topics. Thanks for being my go-to friend for every situation.

I also want to thank all the visiting and permanent lab members of the Viral Vectors and Vaccine Bioprocessing group- Ryan, Hanan, Javier, Irene, Xavier, Sascha, David, Aline, Michelle, Pablo, Marie-Angelique, Sean, Xingge, and others for being fantastic colleagues. I am also excited to see what the new members of the group accomplish in the upcoming years.

I want to thank my friends- Harsh, Tanushree, and Chetan for being the closest to the family away from home. Abdullah, I will miss the special friendship we share, our daily lunch sessions, casual conversations on life, Bollywood, and desi food.

I also want to thank Xavier, UQAM support staff, Bioengineering administrative staff, Pina, and BBME staff for their continued support. This journey would not have been easy and smooth without their support.

Finally, I want to thank my parents for their endless support throughout this journey. Mom and Dad, you have always been the source of endless inspiration and motivation for me, which fuelled my passion, driving me to achieve this milestone. I want to extend my deepest gratitude to my mom and my sister, two wonderful women in my life who laid the foundation of what I am today. I also want to thank my fiancée, Chitra, for being a supportive and understanding companion during this journey.

Dedicated to

Fall Armyworm *(Spodoptera frugiperda)*

The future of rAAV-based gene therapy medicines

“Failure is temporary, whereas success is autocatalytic.”

-Prof. G. D. Yadav

Table of Contents

Abstract

More than 5000 orphan diseases are caused by a hereditary or acquired genetic defect. Contrary to the common perception, orphan diseases are not that rare as approximately 10% of the world population suffer from orphan diseases; the total number is more than the patients of cancer and AIDS combined. Gene therapy in general and viral vector-based gene therapy medicines, in particular, have emerged as a promising approach for a long-lasting treatment of these genetic disorders. Of various viral vectors tested, the adeno-associated virus (AAV) has demonstrated notable safety profile and therapeutic efficacy in the clinical studies leading to the regulatory approval of three AAV-based gene therapy medicines by the European and U.S. regulatory authorities in the last decade. Because of proven clinical success and increased confidence in AAV-gene therapy candidates, there exists a massive demand for clinical-grade AAV material, which is difficult to meet with the current AAV production capacity and productivity levels. As a consequence, AAV gene therapy candidate pipelines are facing several years' delay before they reach the preclinical or clinical phase of the testing. The subject of this doctoral thesis aimed at improving the overall yield of the AAV manufacturing process to generate high-quality AAV vectors. This aim was achieved by finding answers to the challenges associated with three main phases of AAV manufacturing: AAV production (upstream), AAV purification (downstream), and AAV analyses and characterization.

To address the challenge related to the lower productivity of traditional transient transfection of adherent or suspension-mammalian cell culture-based AAV production systems, we employed an alternate well-established suspension cell culture-based scalable platform for AAV manufacturing, the insect cell-baculovirus expression vector system (IC-BEVS). A recent and more simplified version of IC-BEVS based on one baculovirus vector (One-Bac) was used for the production of

clinically relevant and evolutionary most divergent serotype, AAV5, as a model vector for our studies. Extensive studies were conducted to understand the effect of various upstream process parameters such as cell-density at infection, the multiplicity of infection of baculovirus, nutrient supplementation strategies, and its effect on AAV protein expression and eventual yield. Implementing process-intensification strategies, the optimized production process resulted in an overall 47-fold increase in volumetric production of AAV5 in high cell density fed-batch suspension culture of Sf9 insect cells. This scalable AAV production process demonstrated excellent reproducibility at small scale and was further validated in controlled bioreactor runs.

Comparable with other insect cell and mammalian cell culture production systems, the AAV5 produced by the One-Bac consisted of empty capsids (EC) of AAV5 in excess over the functional genome-containing capsids (GC). These empty capsids, devoid of any direct therapeutic effect, exhibit an immunogenic burden, and are considered AAV-related impurity in the clinical lots. Aligned with the final goal of producing high-purity AAV vectors, efforts were directed to develop a streamlined and scalable ion-exchange chromatographic approach (IEX) for the removal of empty capsids and consequent enrichment of samples by genome containing functional AAV5 vectors. Moreover, this chromatography process was designed to be modular such that it can be adapted to process other clinically relevant AAV serotypes as well to generate high-quality AAV vectors rapidly without necessitating significant changes. Detailed studies were conducted to understand the effect of various ionic species, chromatographic buffer composition, and processing mode on overall charge characteristics of AAV EC and GC capsids. Divalent ionic species were found to promote highly enriched preparations consisting of 80% of AAV5 GC under the selected optimal step-gradient mode of operation with an overall enrichment factor as high as 8-fold. These findings were further validated with serotypes AAV8, and AAV6 achieving highly enriched GC

vector preparations consisting of up to 95% of GC population and demonstrating the generic characteristics of the proposed chromatographic process.

Finally, a readily accessible high-performance liquid chromatography (HPLC) assay was developed for the detection and quantification of AAV5 EC and GC in the affinity-purified preparations before the enrichment step. The native amino acid-fluorescence based detection offered excellent linearity with a correlation coefficient of 0.9983 over two-log dilution of the sample. The LOD and LOQ values associated with the total AAV5 capsid assay are $3.14x10^9$ and $9.52x10^9$, respectively. A demonstrated orthogonality and comparability with other well-established methods makes this HPLC assay a suitable choice to support AAV characterization studies in academic labs and small-scale research organizations that do not have access to capital-intensive equipment such the analytical ultracentrifuge.

Overall, as an integrated approach, this doctoral thesis provides practical and actionable solutions to the challenges associated with the current AAV-manufacturing process.

Résumé

Plus de 5000 maladies rares sont causées par un défaut génétique héréditaire ou acquis. Contrairement à la perception générale, les maladies rares ne sont pas si exceptionnelles qu'on le croit, car environ 10 % de la population mondiale souffre de maladies rares; le nombre total de patients est supérieur à celui du nombre de patients atteints de cancer et de sida réunis. La thérapie génique en général et les thérapie génique exploitant les vecteurs viraux, en particulier, sont apparues comme des approches prometteuses pour un traitement durable de ces maladies génétiques. Parmi les différents vecteurs viraux testés, le virus adéno-associé (AAV) a démontré un profil de sécurité et une efficacité thérapeutique remarquables dans les études cliniques qui ont conduit à l'approbation réglementaire de trois médicaments de thérapie génique à base d'AAV par les autorités réglementaires européennes et américaines au cours de la dernière décennie. En raison des succès cliniques avérés et de la confiance accrue dans les thérapie génique utilisant les AAVs, il existe une demande massive de matériel AAV de qualité clinique, à laquelle il est difficile de répondre avec la faible productivité des AAVs et les capacités actuelles de production. En conséquence, les pipelines de production de candidats de thérapie génique AAV sont confrontés à un retard de plusieurs années avant d'atteindre la phase préclinique ou clinique des essais. Le sujet de cette thèse de doctorat visait à améliorer le rendement global du processus de fabrication des AAV afin de générer des vecteurs AAV de haute qualité. Cet objectif a été atteint en trouvant des réponses aux défis associés aux trois principales phases de la fabrication des AAV : La production de AAV (en amont), la purification de AAV (en aval), et les analyses et la caractérisation de AAV. Pour relever le défi lié à la faible productivité des systèmes de production d'AAV traditionnels par transfection transitoire des cultures de cellules mammifères adhérentes ou en suspension, nous avons utilisé une autre plate-forme évolutive bien établie basée sur la culture de cellules en

suspension pour la fabrication d'AAV : le système d'expression utilisant les cellules d'insectes et le baculovirus (IC-BEVS). Une version récente et plus simplifiée de IC-BEVS basée sur un vecteur baculovirus (One-Bac) a été utilisée pour la production du sérotype AAV5 comme vecteur modèle pour nos études. AAV5 est le serotype le plus pertinent d'un point de vue clinique mais le plus divergent du point de vue évolutif. Des études approfondies ont été menées pour comprendre l'effet de divers paramètres du processus en amont, tels que la densité cellulaire à l'infection, la multiplicité des infections par le baculovirus, les stratégies de supplémentation en nutriments, et leur effet sur l'expression des protéines AAV et le rendement final. En mettant en œuvre des stratégies d'intensification de procédés , le procédés de production optimisé a permis de multiplier par 47 la production volumétrique d'AAV5 dans une culture en suspension à haute densité cellulaire de cellules d'insectes Sf9. Ce procédé de production d'AAV évolutif a démontré une excellente reproductibilité à petite échelle et a été validé dans des lots produits en bioréacteur contrôlés.

Comparable à d'autres systèmes de production de cellules d'insectes et de cultures de cellules de mammifères, l'AAV5 produit par le One-Bac était constitué de capsides vides (EC) d'AAV5 en excès par rapport aux capsides contenant le génome fonctionnel (GC). Ces capsides vides, dépourvues de tout effet thérapeutique direct, présentent une charge immunogène, et sont considérées comme des impuretés liées aux AAV dans les lots cliniques. Conformément à l'objectif final de produire des vecteurs AAV de haute pureté, des efforts ont été mis en œuvre pour développer une approche chromatographique d'échange d'ions (IEX) facilement modulable pour l'élimination des capsides vides et l'enrichissement des preparations en AAV5 fonctionnels contenant le génome viral. En outre, ce procédé de chromatographie a été conçu pour être modulaire, de sorte qu'il puisse être appliqué à d'autres sérotypes d'AAV cliniquement pertinents

et générer rapidement des vecteurs AAV de haute qualité sans nécessiter de modifications importantes. Des études détaillées ont été menées pour comprendre l'effet de diverses espèces ioniques, de la composition des tampons chromatographiques et du mode de traitement sur les caractéristiques de charge globale des AAV EC et GC capsidiques. Il a été constaté que les espèces ioniques divalentes offraient des préparations hautement enrichies constituées de 80 % de GC AAV5 hautement enrichies dans le mode de fonctionnement optimal à gradient progressif selectionné, avec un facteur d'enrichissement global pouvant atteindre 8 fois. Ces résultats ont aussi été validés pour les sérotypes AAV8 et AAV6, en obtenant une préparation de vecteur GC hautement enrichie comprenant jusqu'à 95 % de la population démontrant ainsi, les caractéristiques génériques du procédé chromatographique proposé.

Enfin, un essai de chromatographie liquide haute performance (HPLC) facilement accessible a été mis au point pour la détection et la quantification de l'AAV5 EC et GC dans les préparations purifiées par affinité avant l'étape d'enrichissement. La détection basée sur la fluorescence des acides aminés natifs offre une excellente linéarité avec un coefficient de corrélation de 0,9983 sur une dilution de deux log de l'échantillon. Les valeurs LOD et LOQ associées au test de capside AAV5 total sont respectivement de $3.14x10^9$ et $9.52x10^9$.La comparabilité a été démontrées avec d'autres méthodes orthogonales bien établies qui fait de ce test HPLC un choix approprié pour soutenir les études de caractérisation des AAV dans les laboratoires universitaires et les organisations de recherche à petite échelle qui ne disposent pas d’équipements de caracterisation nécessitant des investissements capitaux inportants tel que l’ultra-centrifuge analytique.

De manière générale, en tant qu'approche intégrée, les résultats de cette thèse de doctorat apportent des solutions pratiques et réalisables aux défis liés au procédés courants de fabrication des AAV.

Contribution to original knowledge

The research work presented in this thesis expands all three aspects of the AAV manufacturing process, addressing three-key problems, each pertinent to one individual phase. Following are the findings, which are original in nature and scholarly contribution to the research field under study.

Chapter 3 (review paper manuscript) presents a comprehensive and critical review of the AAV production in insect-cell baculovirus platform from the bioprocess developer's standpoint. Summary of the key findings provides readers a holistic and rational view behind the systemic evolution of this platform. Our views on the future perspectives of this system are believed to offer the scientific community a fresh approach to drive future developments.

Chapter 4 studied the suitability and applicability of the One-Bac system for AAV vector production from the bioprocessing standpoint. A novel high-cell density infection, higher-MOI (MOI 3) fedbatch production process, validated at small shaker flask and bioreactor scale, resulted in an overall 47-fold higher yield than the control process and placed the One-Bac platform in the league of one of the highest AAV producer systems. The findings reporting exponentially higher yields of functional AAV particles at higher cell densities than the standard-low cell density process, indicated the importance of nutrient availability in the post-infection phase to enable cells to properly process the packaged capsids as they undergo the "capsid maturation" phase. This will provide a foundation for further research on developing media and nutrient feed formulation to offer AAV-specific enhancement properties to achieve an even higher yield of functional AAV vectors when produced in insect cell systems.

Chapter 5 studied the effect of different types of salts of differing valency on the separation efficiency of AAV empty and genome-containing capsids (GC). In contrast to conventional monovalent salt-based chromatography systems, the selection of sulfate-based divalent salt, based

on the systemic salt-screening study, provided better enrichment of GC capsids for a sample containing EC impurity in several-fold in excess. Moreover, the study of different cationic counterparts of the sulfate-salt (Na^+ and Mg^{2+}) provided evidence on their variable interaction with different AAV serotypes capsids and its consequent effect on separation efficiency. The overall two-step process involving affinity- capture step and anion-exchange polishing step provides a generic purification scheme for preparation GC-enriched vector preparation of multiple AAV serotypes without requiring significant changes in the proposed process. Notably, this was a critical finding and a step closer towards developing a more generic enrichment process.

Finally, the research work reported in chapter 6 focused on the development and validation of an HPLC method for analysis and quantification of EC and GC capsids of AAV5 samples. Importantly, exploring the high-resolution attributes of analytical chromatography systems, the use of a trivalent phosphate buffer system offered baseline resolution between EC and GC capsid populations. Differently from previously reported continuous gradient approaches, the proposed step-gradient analytical HPLC approach provided an accurate and precise means of AAV5 capsids quantification with better sensitivity of detection.

Contribution of authors

As a lead researcher and the first author of all the research publications included in this thesis, I was responsible for conceptualizing, designing, and executing all the experiments pertinent to AAV production, purification, characterization and HPLC analysis, data analyses, writing, and editing of all the manuscripts and this thesis.

Dr. Parminder Chahal (co-supervisor) and Prof. Amine Kamen (Supervisor) provided resources, critical evaluation, and guidance pertinent to the research work presented in all the manuscripts. As co-authors, both supervisors proof-read and edited the manuscripts. Prof. Amine Kamen was the corresponding author in all the manuscripts.

Notably, each co-author's contribution is provided as a part authors' contribution section of all the manuscripts (except chapter 3). Below is a detailed description of the contribution by each co-author.

Chapter 3

Dr. Alina Venereo-Sanchez provided critical inputs in the molecular biology sections of the review paper manuscript. She also contributed to the overall paper by critically reading the manuscript and providing valuable comments on the overall subject matter.

Chapter 4

Dr. Laura Cervera helped with my initial hands-on training with insect-cell culture techniques and AAV production in early-stage preliminary studies. Dr. Ibrahim Ahmed helped establish the qPCR analytical method, including the preparation and characterization of the plasmid standard. Dr. Joseph Schrag performed the *sv*-AUC analyses of all the AAV samples. Alice Bernier performed

initial chromatographic AAV purification runs on the AKTA FPLC system. She was also responsible for my training on the AKTA system and contributed significantly towards eventual independent AKTA purification runs performed by me.

Dr. Oleksandr Kondratov and Prof. Sergei Zolotukhin were the research collaborator from the University of Florida, Gainesville, U.S.A. They developed the One-Bac 3.0 system employed for AAV5 production and performed some of the molecular biology analyses of AAV samples.

Chapter 5

Alice Bernier and Dr. Joseph Schrag provided critical inputs on the design of experiments and evaluated and edited the manuscript. Dr. Joseph Schrag also trained me on the operation and data analyses of the *sv*-AUC runs for AAV characterization. Pablo Moço assisted with AAV serotypes production via transient transfection process in mammalian cells and analyses of AAV samples.

Chapter 6

Alice Bernier trained me on the operation and data analytics part of the HPLC instrument. She also operationalized the HPLC instrument for initial sample runs and provided critical guidance on the design of experiments of HPLC method development.

List of Tables

List of Figures

Abbreviations

AAV: adeno-associated virus

AcMNPV: *Autographa californica* multinuclear polyhedrosis virus

AEX: anion-exchange chromatography

AEX-HPLC: anion-exchange high-performance liquid chromatography

Ad5: adenovirus serotype 5

AUC: analytical ultracentrifugation

AUP: area under the peak

BHK: baby hamster kidney

BIIC: baculovirus infected insect cells

BR: bioreactor

BTP: bis-tris propane

BV: baculovirus

Cap: capsid proteins

CD-MS: charge-detection mass spectrometry

CG: capsids encapsidating genetic material

CMV: Cytomegalovirus

CQA: critical quality attributes

Cp: capsids

CV: column volumes

ddPCR: digital-droplet polymerase chain reaction

DOE: design of experiment

EC: empty capsids

EDTA: ethylenediamine tetraacetate

egt: ecdysteroid UDP-glucosyltransferase

ELISA: enzyme-linked immunosorbent assay

EMA: European medicines agency

ER: endoplasmic reticulum

ETU: enhanced transducing units

EU: emission unit

FL: fluorescence

FPLC: fast protein liquid chromatography

GC: genome-containing capsids

GFP: green fluorescence protein

GMP: good manufacturing practice

GOI: gene of interest

GTA: gene transfer assay

HEK293 cells: human embryonic kidney 293 cells

hGFP: humanised green fluorescence protein

Hi-5: High Five™ (*Trichoplusia ni*)

hpi: hours post infection

hr2: homologous region 2

HPLC: high-performance liquid chromatography

HSV: herpes simplex virus

IC-BEVS: insect cell baculovirus expression vector system

ICH: international council for harmonization

IE-1: immediate early 1

IEX: ion-exchange chromatography

IL-2: interleukin 2

INF-β: interferon beta

IS: ionic strength

ITR: inverted terminal repeat

IVP : infectious virus particle

LOD : limit of detection

LOQ: limit of quantification

LPL : lipoprotein lipase

MOI : multiplicity of infection

mRNA : messanger-RNA

µL: micro-litre

µV: micro-volt

NIIC: non-infected insect cells

O.D. : optical-density

ORF: open reading frame

PDA: photodiode array detector

pfu: plaque forming unit

qPCR: quantitative polymerase chain reaction

PTMs: post-translational modifications

rAAV: recombinant adeno-associated virus

r**BV:** recombinant baculovirus

RBE: Rep-binding element

Rep: replicase

RSD: relative standard deviation

SD: standard deviation

SDS-PAGE: sodium dedecylsulfate polyacrylamide gel electrophoresis

Sf9: *Spodoptera frugiperda*

SF: shake flask

STB: stirred-tank bioreactor

***sv*-AUC**: sedimentation velocity analytical ultracentrifugation

TEM: transmission electron microscopy

TT: transient transfection

TU: transducing units

UC: ultracentrifugation

USFDA: U.S. Food and Drug administration

VC: vector capsids

VG: viral genome

VP: viral proteins

wtAAV: wild-type adeno-associated virus

wtITR: wild-type inverted terminal repeat

Chapter 1 Introduction

In the 21st century, gene therapy has risen to fame as an emerging and promising approach for hereditary or acquired genetic disorders with the potential to offer a life-long cure upon a one-time administration of the gene therapy medicine[1]. Among various gene delivery systems, viral vectors are emerging as a vehicle of choice for highly efficient *in vivo* gene transfer, enabling sustained therapeutic gene expressions in the target tissue[2]. More specifically, because of exceptionally high safety-profile and sustained transgene expression in both dividing and non-dividing cells, adeno-associated virus (AAV)-based recombinant vectors are one of the preferred gene delivery systems in clinical trials for monogenic diseases indications[3]. In the last decade, three AAV-based gene therapy medicines have been granted regulatory approval via the European medicines agency (EMA) and U.S. food and drug administration (USFDA) for the treatment of hereditary genetic diseases[4].

Despite progressive evolution, low production yield, and limited availabilities of clinical-grade AAV material produced via traditional manufacturing platforms are among the major impediments in the development of AAV gene therapies. Moreover, newer neurological and hematological disease indications involving systemic administration require up to 10^{15} viral genomic particles (VG) per patient or up to 10^{17} VGs in total to conduct a phase-II/III clinical studies[5]. With the current low-cell density manufacturing process, at an approximately 50% overall recovery, the yield of up to 2-5x10^{13} VG/L of purified AAV is achieved, indicating that it would require approximately 100-250 L bioreactor scale production for one patient. Due to apparent higher production cost and a lack of a sufficient number of AAV gene therapy manufacturing facilities equipped with a large-scale production capacity, the resulting limited availability of AAV material delays the transition of AAV-based gene therapy candidates from the lab to the clinics.

At the upstream production stage, an excess of genome-less empty capsids, which is a major AAV related impurity, are co-produced regardless of the production platform[6]. Due to their immunogenic attributes and a lack of direct therapeutically beneficial effects *in vivo*, removing empty capsids at the downstream purification stage and quality-control analysis in the final product is crucial to ensure the potency and safety of the clinical-grade AAV material[7–9]. Current ultracentrifugation (UC)-based protocols are effective in separating these empty capsids (EC) from the functional genome-containing capsids (GC) of AAV[10–12]. Despite this, UC technology is not widely adopted for large-scale AAV production due to the lack of availability of large-scale UC equipment, operational complexity, and reservations against its integration in the current GMP facilities. On the other hand, in recent times, chromatographic approaches have shown notable success in generating empty-capsid free AAV preparations[13]. Chromatography remains a platform of choice due to linear scalability, robustness, and a history of successful commercial-scale operations in therapeutic biologics. Advancement in these chromatographic approaches with improved enrichment efficiency and operational simplicity to generate highly enriched preparations of GC of multiple AAV serotypes is highly desirable.

Evaluation of AAV manufacturing process or qualification of final AAV preparations requires detection and quantification of EC and GC via orthogonal analytical techniques such as transmission electron microscopy (TEM)[14], cryo-TEM[15], analytical ultracentrifugation (AUC)[16] and charge-detection mass spectrometry (CD-MS)[17]. However, due to a complete lack or limited availability of these advanced techniques, AAV-related research activities at academic or research labs are often restricted. The availability of an easily accessible and comparable assay method based on high-performance liquid chromatography (HPLC) offers a viable solution for such analyses to support AAV related research.

Three individual aims of the thesis specifically address each of these three research questions pertinent to the AAV production process using serotype 5 as a model vector produced using an advanced insect-cell baculovirus production system. Combinedly, these aims cover an entire spectrum of the AAV production process providing practical and actionable solutions to the current manufacturing challenges.

1.1 Main objective of the thesis

To improve overall AAV bioprocessing to generate high-yield, high-purity AAV gene delivery vectors.

1.2 Specific aims

1. To achieve a higher volumetric yield of AAV5 gene delivery vectors via process intensification.
2. To develop a scalable, robust, and generic chromatographic process to generate AAV vector preparations enriched in functional genome-containing capsids.
3. To develop a high-performance liquid chromatography (HPLC) assay for precise and accurate determination of empty and genome-containing capsid content in purified preparations of AAV serotype-5.

1.3 Thesis organization

Following the latest thesis preparation guidelines provided by McGill GPS, this thesis is organized in a manuscript-based format. Each of the four manuscripts constitutes the main body of the thesis. One manuscript (Chapter 4) has been already published, two manuscripts (Chapter 3 and Chapter

5) are under review and one manuscript (Chapter 6) is submitted for peer-review. The formatting of each chapter is in agreement with the guidelines of the original journal where the corresponding manuscript is either published or submitted. The existing inconsistencies in citation style or other aspects are cautious decision to abide by the guidelines pertinent to the manuscript-based thesis. For commonality purposes, the font characteristics (type and size) are harmonized in all chapters presented in this thesis.

The introduction chapter (**Chapter 1**) focuses on the rationale behind this doctoral thesis, main objective, specific aims, and thesis organization.

Following this is a separate chapter (**Chapter 2**) consisting of a comprehensive literature survey of gene therapy and AAV viral vectors.

Chapter 3 which exclusively focuses on the development of insect-cell baculovirus expression vector (IC-BEVS) platform for AAV production is a review paper manuscript. This manuscript was relevant to the current AAV production scenario and pertinent to the main theme of the thesis as the One-Bac system that has been primarily used for AAV production belongs to IC-BEVS platform.

Chapter 4, 5, and 6 are the research paper manuscripts focusing on AAV production (upstream), AAV purification and GC-enrichment (downstream), and AAV analytics aspect (HPLC analysis), respectively. The supplemental information sections corresponding to chapters 4, 5 and 6 are presented in the appendices (**Chapter 9**) in the same order of organization.

A comprehensive discussion (**Chapter 7**) covering critical aspects of all the findings is provided which is followed by the conclusive summary and future perspective (**Chapter 8**).

Finally, a reference list covering all the references cited in chapters 1, 2, 7, and 8 is provided in Chapter 10.

Chapter 2 Literature review

2.1 Why gene therapy

The genes are an encrypted storage form of genetic information in all life forms. The human genome consisting of approximately 25,000 genes, is responsible for the structural and functional architecture of the human body[18]. These genes encode a wide variety of proteins, the building blocks of various cellular organelles and tissues, which are also necessary for cellular homeostatic and regulated functioning of the biological process[19]. Over time, these genes undergo inevitable changes such as mutations, disruptions, or deletions rendering them partially or completely dysfunctional and can also be carried to the next generation[20]. These dysfunctional genes produce proteins with altered structures and functions, which in turn are often responsible for various types of diseases or disorders[21]. According to Global Genes and Orphanet, non-profit advocacy organizations for rare and genetic diseases, dysfunctional genes account for 80% of the 7,000 rare and genetic diseases reported to date, 95% of which do not have a treatment available. Nearly 400 million people, more than the population of the United States, are suffering from the genetic and rare diseases globally; unfortunately, half of them are children.

Substantial progress has been made in developing modern medicines representing the transition from small-molecular drugs to complex therapeutic biologics, including protein-based drugs such as a monoclonal antibody, transcription factors, and signaling proteins, gene editing enzymes, growth factors, hormones, blood factors, and antigens[22]. Although effective to a varying extent for many complex diseases such as various forms of cancers, neurodegenerative, and autoimmune diseases, the treatment is often symptomatic, temporary, and require lifelong interventions.

Moreover, in general, these drugs are designed to modulate pre- or post-transcription pathways and cellular functions, leaving a potential known genetic root-cause of a disease untouched.

Differently from these conventional forms of treatments, gene therapy aims at the genetic root-cause of the disease. It features the introduction of a therapeutic gene into the target cells/tissue, via viral or non-viral delivery means, to treat or prevent the disease by correcting (deletion or mutation of incorrect gene sequences) or completing (supplementation of missing or dysfunctional therapeutic gene) the underlying genetic cause[2]. Since this approach targets the natural genetic and protein processing pathways associated with the etiology of a hereditary disease, it has been envisaged as a potential one-time cure for many diseases and is currently being evaluated in clinics on a large scale with many gene therapy medicines being approved in last five years[23] (**Table 1**).

2.2 History of gene therapy

In 1928, Frederick Griffith, a British bacteriologist, first reported the bacterial transformation in which the R form of type I pneumococcus transformed into the virulent form upon incubation with the heat-inactivated S form of type II pneumococcus bacteria[24]. This work was also confirmed by other researchers[25,26] followed by the critical findings by Avery et al. in 1944, reporting that the deoxyribonucleic acid (DNA) in the cell-free extract was responsible for bacterial transformation[27]. This was the first report of DNA mediated genetic changes in a prokaryotic cell. In 1958, Joshua Landenberg received a Nobel prize for his ground-breaking work on bacterial genetics and bacteriophage. He first coined the term transduction to describe the inter-bacterial gene transfer through a virus-the bacteriophage, which resulted in a transformation of *Salmonella* Typhimurium into a drug-resistant variant[28]. This ground-breaking discovery laid the foundation

for the subsequent research on procaryotic and eventually eucaryotic viral gene delivery vectors, which are currently dominating the gene therapy clinical trial landscape.

In 1962, Waclaw Szybalski reported the transformation of human D98S cells via cellular uptake of the DNA[29]. Around the same time, in 1961, Howard Temin discovered that the genetic mutations resulting from a viral infection could be inherited in the chicken cells infected with the Rous sarcoma virus, an RNA virus, stably integrating the viral-specific gene mutations[30]. This was also the first demonstration of viral genome integration into the mammalian cells as well as the bi-directional flow of genetic information, RNA↔DNA, which was previously believed to be exclusively unidirectional from DNA→RNA. It became apparent that viruses possessed properties that could be explored for gene delivery into the target cells. The work on the virus-mediated gene transfer by Rogers and Pfuderer utilized the tobacco mosaic virus as a vector to introduce a polyadenylate stretch of viral RNA[31].

Building on the further advancement on the modes and vectors for viral gene transfer, in 1989, Rosenberg conducted the first officially approved gene therapy clinical trials in humans aimed at tracking the movements of tumor-infiltrating lymphocytes (TILs) blood cells via gene marking[32]. The encouraging results from this initial study led to the clinical trials in 1993, which were based on administering *ex vivo* modified TILs carrying tumor necrosis factor at the tumor sites resulting in localized tumor suppression at injection site[33]. The first clinical trial based on therapeutic gene delivery in a human was approved in 1990 for the treatment of adenosine-deaminase deficiency (ADA-SCID)[34]. Two children suffering from this monogenic disease condition were administered with *ex vivo* modified white blood cells, carrying the copy of the normal gene for producing adenosine deaminase, collected from the same patient. From the late '80s until the late '90s, the gene therapy field witnessed exponential growth. Several clinical trials were approved for a broad

spectrum of hereditary disease indications utilizing diverse viral and non-viral gene delivery platforms. However, in 1999, the tragic death of a patient as a result of an aggressive immune

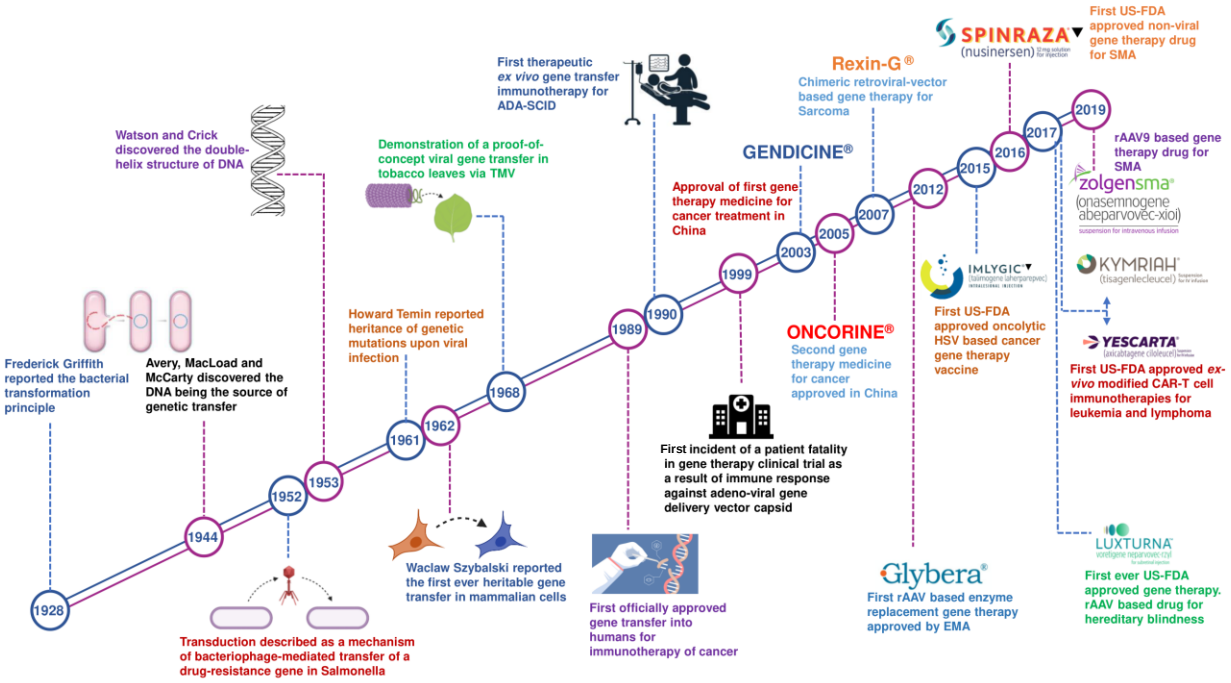

Figure 2.1 Timeline and critical milestones in gene therapy drug development

response against capsids protein of adenoviral vector during a clinical trial was a major setback for gene therapy. Since then, a large number of studies have been dedicated to enriching the understanding of the viral biology, transduction mechanism, and immune response against viral components in *in vitro* cell culture and animal models[35]. In the last decade, gene therapy has seen many clinical success stories, especially in virus-mediated gene delivery, resulting in the approval of many gene therapy drugs for various types of cancers, metabolic disorders, and neurological disease conditions (**Figure 2.1**).

2.3 Current status of gene therapy

Gene therapy has emerged as a new curative approach for several hereditary and acquired diseases. To date, more than 4500 gene therapy clinical trials have been registered in the US government's

clinical trials database. These clinical studies aimed at a wide variety of diseases, including cancer, neurological, metabolic, immunological, hematological, infectious diseases, muscular, cardiac, ocular, and genetic diseases, of which, cancer has been the most sought-after target for gene therapies in the clinics. Numerous gene delivery vehicles have been developed to deliver the therapeutic gene or the gene of interest to the target tissues. These vehicles are broadly categorized into two main classes: viral[36] and non-viral[37]. Non-viral delivery systems include but are not limited to electroporation, liposomes, cationic polymers, dendrimers, cell-penetrating peptides, and naked DNA, whereas the viral delivery systems are primarily based on adenovirus, adeno-associated virus (AAV), herpes simplex virus, retrovirus, and lentivirus (**Figure 2.2A**).

Although non-viral delivery vehicles are effective *in vitro* and in a localized gene delivery *in vivo*, their effectiveness and specificity are limited *in vivo* upon systemic administration. Conversely, the viral gene delivery systems provide efficient and better tissue-specific transduction resulting in persistent therapeutic gene expression[2]. Various improvements incorporated in next-generation viral vectors were aimed at improving immunological safety profile and transduction efficiency.

Among other viral vectors, which exhibit equal or even higher transduction efficiency, AAV stands apart from these viral vectors due to its ability of gene transfer in both dividing and non-dividing cells with a low degree of genome integration. The latter is responsible for its excellent safety profile[38]. AAV has emerged as a vector of choice in clinical studies with a consistently increasing number of clinical studies over the last decade (**Figure 2.2C**). AAV has demonstrated an excellent safety profile in clinics, and three drugs have been approved for marketing authorization post-phase-III human clinical studies. The recombinant AAV (rAAV) vector exhibits unique characteristics such as broad tissue tropism, non-pathogenicity, sustained transgene expression, and ease of production[4].

2.4 Evolution of AAV-based gene delivery vectors

2.4.1 AAV biology

Adeno-associated virus (AAV) was serendipitously discovered by Atchison and colleagues as a contaminant of simian adenovirus samples collected from the rhesus monkey cells and hence the name adeno-associated virus[39]. In the electro-micrograph, AAV appeared as a nano-dimensional (20-26 nm diameter), icosahedron capsids. When isolated from the larger adenovirus (~80 nm diameter) via ultrafiltration, AAV failed to autonomously replicate in *in vitro* cell culture. Later, AAV was also found in human and monkey primary kidney cells in a latent state and reportedly rescued from its latency upon adenovirus superinfection[40]. AAV belongs to the *Parvoviridae* family, and due to its replication-defective nature, it is classified in a *Dependovirus* genus. The viral genome is a single-stranded DNA of around 4.7 kb with three overlapping open reading frames encoding gene sequences for structural and regulatory viral protein expression flanked by an inverted T-shaped hairpin-like structure at both ends[41]. The four regulatory Rep proteins (Rep78, Rep68, Rep52, and Rep40) responsible for viral genome replication, integration, and rescue[42,43] are transcribed from two left ORF, whereas three viral capsid proteins (VP1, 2, and 3) and a viral capsid assembly activating protein are transcribed from a right ORF by alternative mRNA splicing mechanism. To date, at least 12 natural serotypes and over 100 engineered variants have been reported[44]. Naturally occurring serotypes were isolated from either human or monkey tissues. These serotypes exhibit different capsid protein amino-acid composition and display broad tissue tropism with a moderately high serotype dependent tissue specificity as a result of the presence of complementing cell surface receptor binding domain on the capsid surface.

AAV transduction pathway begins with a binding of the viral capsid with a primary cell-surface receptor and secondary co-receptor followed by viral integration inside the cells via endocytosis,

and clathrin-coated vesicles or other unknown mechanism[45,46]. Once inside the cells, the virus traverses through the endosomal pathway followed by a viral phospholipase-mediated escape from the late endosome, releasing the virus in perinuclear space[47]. The viral capsid enters into the nucleus via nucleopores[48,49], uncoats, and releases the viral ssDNA, which undergo second-strand synthesis[50,51], transcription and translational pathways resulting in viral protein synthesis and capsids assembly (**Figure 2.3**). In the presence of viral Rep proteins, which are responsible for viral genome integration, the viral genome undergoes partial genome integration at a specific site in human chromosome 19 (AAVS1), acquiring latency, however with a very low frequency (3-5 genome copies per diploid cellular genome)[52]. AAV serotype 2 (AAV2) has been widely used as a model in studies unveiling fundamental information on AAV biology, infection characteristics, and immune response.

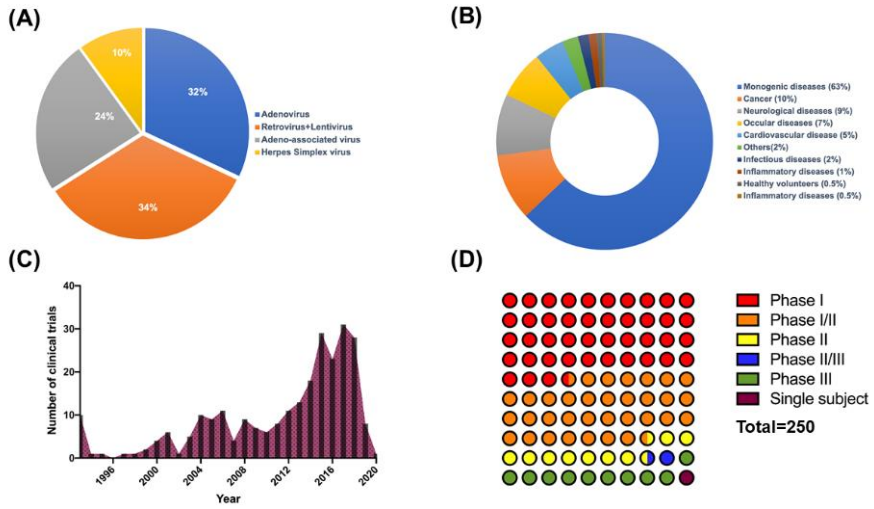

Figure 2.2 AAV clinical trials data

(**A**) Prominence of different viral vectors in clinical trials. (**B**) Disease indications for which AAV has been tested in clinical trials. (**C**) Growth of AAV vector-based gene therapy clinical trials. (**D**) Translation of AAV clinical trials through different phases of clinical trials. (data were collected from http://www.abedia.com/wiley/vectors.php)

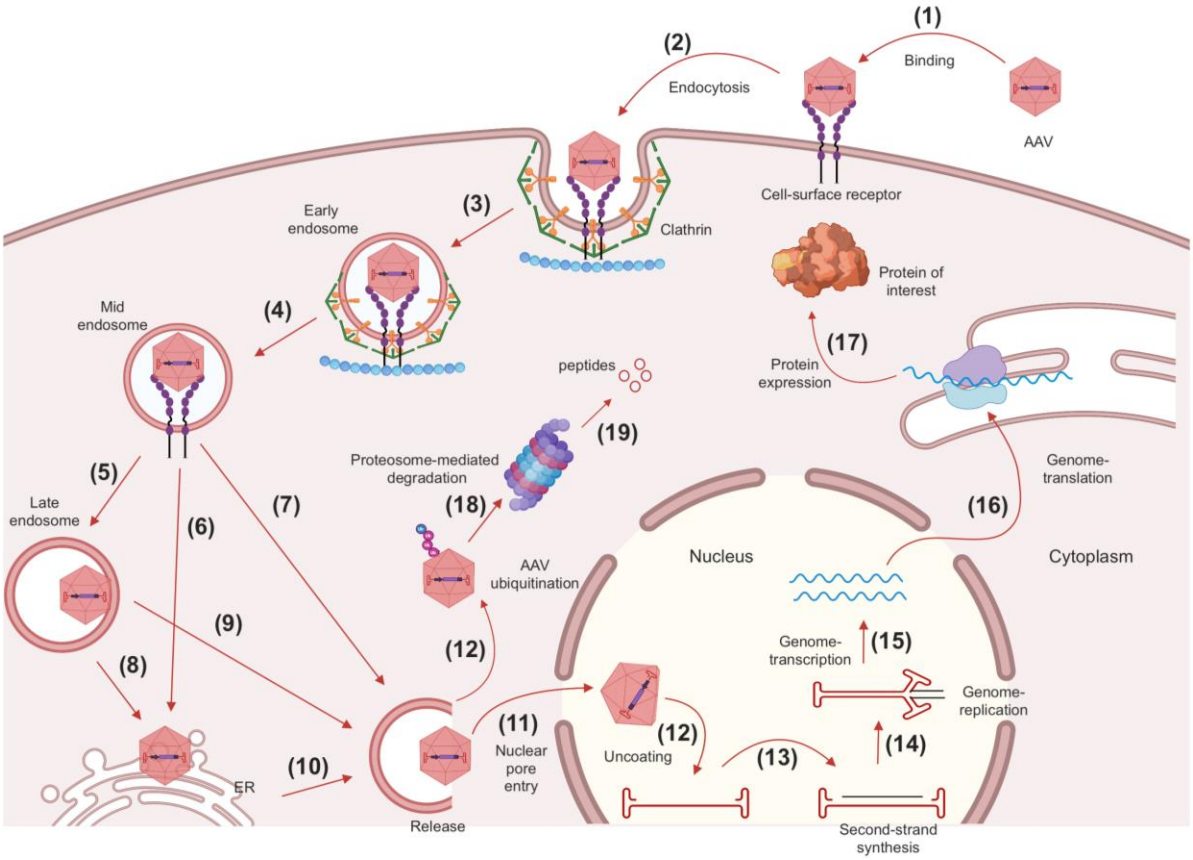

Figure 2.3 AAV-transduction pathway (adapted from Dan Wang et al.[3] and Chengwen Li et al.[4], and reproduced using biorender.com)

2.4.2 Recombinant-AAV vectors in clinical studies

In the recombinant vectors for gene delivery, the entire genome of the wild-type AAV, except the portion of the ITRs, is replaced with the gene of interest or a therapeutic gene in the recombinant vector, which follows the same viral transduction pathway as the wild-type virus. ITRs are retained as they are necessary for viral DNA replication, transcription, and viral genome packaging in the preassembled capsid. However, in the absence of Rep proteins, the viral genome remains episomal and provides persistent transgene expression[53].

AAV1 to AAV9 serotypes-derived vectors have been studied in clinical trials for various diseases (**Figure 2.2B**), where the suitable serotype is selected based on the tissue specificity[3]. For example, AAV1 displays very strong transduction in muscle tissues and was used as a gene delivery vector

in Glybera® developed to treat lipoprotein lipase (LPL) deficiency[54]. The rAAV1 vector carried the gene sequence for the LPL enzyme responsible for the metabolism of fatty acids in the patient suffering from hereditary LPL deficiency. Similarly, AAV2 showed higher transduction in the retina and was used in the development of Luxturna™, a gene therapy medicine for the treatment of hereditary retinal dystrophy[55]. Since AAV9 can cross the blood-brain barrier and facilitate gene delivery in neurons, it was used in the development of Zolgensma® for the treatment of spinal muscular atrophy, a devastating condition characterized by diminished motor neuron functionality[56].

As mentioned earlier, AAV has seen extensive growth in clinical studies over the last decades and has been a vector of choice in more than 240 clinical trials. These studies include cancer, neurological, cardiac, ocular, and inflammatory diseases (**Figure 2.2B**). Of particular note is the use of AAV as a vectored vaccine for infectious diseases such as HIV and Hepatitis C virus infection. By far, monogenic disease indications are the most studied disease type under clinical studies utilizing AAV as a gene delivery vector. It is interesting to note that even though AAV is not the dominant viral gene delivery vector in clinical studies, it has been by far the most successful with 24 drugs reaching the phase-III clinical studies (**Figure 2.2D**) and three gene therapy medicines approved for commercialization by regulatory authorities, including EMA and USFDA indicating a great promise offered by rAAV vectors.

2.5 AAV vector manufacturing

2.5.1 AAV production (upstream processing)

Currently, recombinant adeno-associated viral vectors are produced in mammalian and insect cell-based production platforms. Whereas the mammalian platform utilized various types of host cells such as HEK293[57,58], HeLa[59,60], and BHK[61,62], the insect cell platform features *Spodoptera*

frugiperda (Sf9) cells as a host for AAV production[63–65]. The traditional AAV production protocol was based on the transient transfection of adherent HEK293(T) cells with the three plasmids delivering the DNA sequences of packaging genes *(*pAAV-*rep/cap*), ITR-flanked transgene (pAAV-transgene), and the helper genes derived from adenovirus (p-Ad helper)[66]. This original platform evolved overtime to attain simplicity, scalability, and improvement in AAV production yield resulting in three main systems based on transient transfection of suspension-adapted HEK293 cells[57], HeLa-derived stable cell lines[59,60] and suspension-adapted BHK cells involving herpes simplex type-1 virus superinfection[61,67]. In the insect cell platform, the necessary gene sequences for AAV production (*rep*, *cap*, and ITR-*transgene*) are delivered via the AcMNPV baculovirus vector under the transcriptional control of insect promoters. Here, the helper function required for rescue and production of replication-deficient AAV is provided by the same baculovirus vectors[63].

While the most popular suspension-adapted HEK293 cell-based system is effective and scalable for AAV production, it is limited by the inefficiency of transient transfection (TT) mode of gene delivery at higher cell density, restricting the AAV production at up to 2 million cells/mL cell concentration and limiting the overall volumetric yield[57]. In contrast, the insect cell has been demonstrated to enable AAV production at a high-cell density of around 10-12 million cells/mL in the fed-batch cultures[68,69]. In general, the AAV production yield in the suspension-adapted HEK293/TT process is in the range of 2-8x10^{13} viral genomes (VG)/L[58,70], whereas in the high cell density insect cell cultures, the AAV yield can reach as high as 3x10^{14} VG/L[69]. Since its first report for AAV vector production in 2002, the insect cell platform has undergone significant improvements to streamline the production process by reducing the baculovirus vectors and producing AAV vectors of different serotypes with bioactivity similar to those produced in

mammalian cells, the natural host of AAV[64,65,71]. A detailed discussion on this topic is provided in Chapter 2, which is a review paper (accepted for publication) on the advancement of the insect-cell baculovirus platform for AAV production.

Notably, during the recombinant AAV production, the host cells do not efficiently encapsidate the vector genome in the pre-formed AAV capsids resulting in the co-existence of empty capsids in excess. The fractional content of these empty capsids is typically in the range of 50-90% in both mammalian[58,72] and insect cells[69,73]. These empty capsids exhibit no direct therapeutic effect and increase the immunogenic burden on the patient, and hence is considered an impurity in a clinical-lot of AAV vector.

2.5.2 AAV purification (downstream processing)

In general, the AAV vectors produced in the host mammalian and insect cells are intracellularly localized, and the primary recovery step requires the extraction of AAV via chemical or physical means of cell-lysis in the harvested cell cultures[12,74]. The insoluble cell-debris and high cell-density cellular components are removed via clarification step(s) involving high-speed centrifugation or depth-filtration or a combination of both[75]. Due to apparent co-extraction of other cellular components, including organelles, host cell-genome, and host cell proteins, AAV purification requires a multi-step process incorporating density-gradient ultracentrifugation or chromatography unit operations alone or in combination followed via ultrafiltration/diafiltration[13].

More amenable to small-scale, the ultracentrifugation protocol developed for AAV purification is based on either cesium chloride or iodixanol density gradient method[10–12]. A typical ultracentrifugation purification process involves two rounds of ultracentrifugation run. In the first round, AAVs are separated from other cellular impurities, and the fraction collected consists of a

mixture of empty capsids (EC) and genome-containing capsids (GC). This mixture is then subjected to a second-cycle of ultracentrifugation where EC (density: ~1.33 g/mL) and GC (~1.38-1.40 g/mL) are separated based on their minute differences in the buoyant densities[11,12]. The resultant EC-free material is highly enriched in genome-encapsidating vector particles with purity levels suitable for pre-clinical and clinical testing.

Easily scalable and widely used chromatography protocols were also developed in parallel for AAV purification. The primary capture step was based on either an AAV-specific affinity chromatography or a non-specific ion-exchange chromatography. Affinity chromatography techniques were based on (1) host cell-receptor binding domain of AAV (heparin affinity[76–79], cellufine sulfate[80] affinity and mucin affinity chromatography[81]), (2) immuno-affinity ligands raised against AAV capsids (AVB Sepharose[64,69], AAV8[72], AAV9[72], and AAVX chromatography) and (3) engineered AAV capsids (immobilized metal-affinity[82] and avidin-biotin affinity chromatography[83]). Exploring the ionic charge characteristics of AAV capsids, both anion[76]-and cation-exchange[74,84] chromatography processes have been used for the AAV capture step. Due to the non-specificity of ion-exchange chromatography, unlike affinity chromatography, the primary capture step is often combined with a secondary purification step involving another complementing ion-exchange step or hydrophobic chromatography step to attain purity levels comparable to affinity-chromatography step[13,74]. The purified AAV material generated after the primary capture step(s) is also a mixture of EC and GC, free-from cellular impurities. Anion-exchange chromatography has been reportedly used to separate genome-less empty capsids from genome-containing capsids based on minute differences in net negative charge at a pH above AAV's isoelectric point (≥ 8)[72,84,85]. This step is often combined as intermediate purification or polishing step with one or more capture steps to generate AAV material enriched in genome-

containing capsids. Finally, this material is subjected to ultrafiltration/diafiltration or size-exclusion chromatography to remove remaining high or small molecular weight impurities and buffer exchange in the formulation buffer.

Chapter 3 Advancements in Molecular Design and Bioprocessing of Recombinant Adeno-associated Virus Gene Delivery Vectors using the Insect-Cell Baculovirus Expression Platform

Pranav R.H. Joshi[1]

Alina Venereo-Sanchez[1]

Parminder S. Chahal[2]

Amine A. Kamen[1]

[1]Department of Bioengineering, McGill University, Montréal, QC, Canada

[2]Human Health Therapeutics Portfolio, National Research Council of Canada, Montréal, QC, Canada

Correspondence: Prof. Amine A. Kamen, Department of Bioengineering, McGill University, McConnell Engineering Building, Room 363, H3A 2K6, Montréal, QC, Canada.

E-mail: amine.kamen@mcgill.ca

Keywords: AAV-bioprocessing and gene therapy, Insect cell-baculovirus expression vector system, One-Bac, Three-Bac, Two-Bac

Published in "**Biotechnology Journal**".

Abbreviations: AAV, adeno-associated virus; **AcMNPV**, *Autographa californica* multinuclear polyhedrosis virus; **BIIC**, baculovirus infected insect cells; **BV**, baculovirus; **Cap**, capsid proteins; **Cp,** capsids; **DOE,** design of experiment; **egt,** ecdysteroid UDP-glucosyltransferase; **ELISA,** enzyme-linked immunosorbent assay; **GFP**, green fluorescence protein; **GMP**, good manufacturing practice; **GOI**, gene of interest; **HEK293**, human embryonic kidney 293; **hGFP**, humanised green fluorescence protein; **Hi-5**, High Five™ (*Trichoplusia ni*); **hpi**, hours post infection; **hr2**, homologous region 2; **HSV**, herpes simplex virus; **IC-BEVS**, insect cell baculovirus expression vector system; **IE-1**, immediate early 1; **IL-2**, interleukin 2; **INF-β**, interferon beta; **ITR**, inverted terminal repeat; **IVP**, infectious virus particle; **MOI**, multiplicity of infection; **mRNA**, messanger-RNA; **NIIC**, non-infected insect cells; **ORF**, open reading frame; **pfu**, plaque forming unit; **PLA_2**, phospholipase A_2; **PTMs**, post-translational modifications; **rAAV**, recombinant adeno-associated virus; r**BV,** recombinant baculovirus ; **RBE**, Rep-binding element; **Rep**, replicase; **Sf9**, *Spodoptera frugiperda*; **STB**, stirred-tank bioreactor; **TU**, transducing units; **USFDA**, U.S. Food and Drug administration; **VG**, viral genome; **VP**, viral proteins; **wtAAV**, wild-type adeno-associated virus; **wtITR**, wild-type inverted terminal repeat

Abstract

Despite rapid progress in the field, scalable high-yield production of AAV is still one of the critical bottlenecks the manufacturing sector is facing. The insect cell-baculovirus expression vector system (IC-BEVS) has emerged as a mainstream platform for the scalable production of recombinant proteins with clinically approved products for human use. In this review, we provide a detailed overview of the advancements in IC-BEVS for rAAV production. Since the first report of baculovirus-induced production of rAAV vector in insect cells in 2002, this platform has undergone significant improvements, including enhanced stability of Bac-vector expression and a reduced number of baculovirus-coinfections. The latter streamlining strategy led to the eventual development of the Two-Bac, One-Bac, and Mono-Bac systems. The one baculovirus system consisting of an inducible packaging insect cell line was further improved to enhance the AAV vector quality and potency. In parallel, the implementation of advanced manufacturing approaches and control of critical processing parameters have demonstrated promising results with process validation in large-scale bioreactor runs. Moreover, optimization of the molecular design of vectors to enable higher cell-specific yields of functional AAV particles combined with bioprocess intensification strategies may also contribute to addressing current and future manufacturing challenges.

3.1 Introduction

Since the establishment of the first successful continuous insect cell line from *Bombyx mori* in 1959 [1], sustained efforts have led to the establishment of insect cells as a workhorse for the expression of recombinant proteins for research and clinical applications. The discovery and isolation of *Autographa californica* multinuclear polyhedrosis virus (AcMNPV) in 1971 was instrumental in positioning the insect cell-baculovirus expression vector system (IC-BEVS) for heterologous protein expression [2]. Over the following years, extensive studies related to the biology of the baculovirus, infection kinetics, genome sequences, and structural variants were undertaken [3,4]. The first breakthrough was the discovery of the polyhedrin strong late promoter (*polh*) by Smith et al. in 1983 [5], which drives strong expression of the polyhdrin protein in the late infection phase in wild-type baculovirus (BV); however, it is not an essential element for a recombinant baculovirus vector. Smith et al. replaced the polyhedrin gene with that of human interferon-beta (INF-β) and interleukin-2 (IL-2), and demonstrated a *polh*-driven robust expression of these proteins using IC-BEVS [5,6]. A year later, another strong late promoter, *p10*, was discovered and its functionality in protein expression studies was demonstrated [7].

The cell line derived from the fall armyworm, *Spodoptera frugiperda* (Sf21 and derived clone Sf9) and the cabbage looper *Trichoplusia ni* (High Five™; Hi5) were established as continuous cell lines and extensively used due to their susceptibility to baculovirus infection and favorable growth characteristics in adherent, and thereafter, suspension cell cultures [8–12]. Despite their routine use, both cell lines showed notable differences. The Hi5 cells showed a comparatively higher yield of secretory proteins [13–15] and the addition of alpha1,3-fucose, a potentially immunogenic glycan structure, to the expressed proteins, which were absent in the proteins produced in Sf9 cells [16]. The Sf9 cells showed higher baculovirus susceptibility [17] and hence are often favored by researchers as host cells for both baculovirus and recombinant protein production. Despite these differences,

both cell lines have been routinely used to produce therapeutic biologics with a history of regulatory approval for human use [18,19].

In the early ’90s, cell culture engineers took the lead in studying the insect cell growth kinetics and metabolism in serum-supplemented and serum-free culture medium. Serum-free cell media with shear protective properties were developed, enabling insect cell growth in suspension cell cultures in shake flasks and bioreactors [20–23], demonstrating the scalability and robustness of the IC-BEVS process for protein production.

Initially employed for the production of baculoviruses as biopesticides, IC-BEVS quickly gained popularity for the expression of a broad spectrum of recombinant proteins, including enzymes, glycoproteins, recombinant viruses, and vaccines [13,24]. The IC-BEVS platform has been used for the production of veterinary vaccines such as Porcilis pesti, Circumvent PCV, CircoFLEX [25], and human vaccines such as Cervarix® [18,26], and Flublok® [11]. Regulatory approval of Cervarix®, a virus-like particle-based vaccine against cervical cancer, was a critical milestone as it was the first biologic produced in insect cells and approved for human use.

The adeno-associated virus (AAV) is currently gaining widespread popularity in gene therapy applications for the correction of monogenic disease conditions. In the last decades, there has been a steady growth in AAV-based gene therapy clinical studies, which have been supported by the accelerated development of IC-BEVS scalable production systems for AAV manufacturing. In addition to the approval of Glybera® by the European Medicines Agency in 2012 [27], from a regulatory perspective, a more recent and significant milestone was the breakthrough designation by the USFDA of BioMarin’s Hemophilia A gene therapy candidate, a recombinant adeno-associated virus 5 (rAAV5) gene delivery vector produced in insect cells using BEVS [28]. This

event further contributed to aligning the IC-BEVS manufacturing process of AAV with the current standard of Good Manufacturing Practice (GMP).

In this review, focusing exclusively on the advancements of the IC-BEVS as a platform for AAV production, we provide insights into the evolution of molecular designs of baculovirus vectors and their key features. AAV manufacturing technologies using IC-BEVS are discussed from a process developer's standpoint. It is foreseeable that further vector optimizations combined with innovative process intensifications may significantly contribute to addressing current and future manufacturing challenges, enabling higher cell-specific and total yields of functional AAV gene delivery vectors of different serotypes.

3.2 AAV taxonomy and genome organization

AAV is a single-stranded DNA virus that belongs to the family *Parvoviridae* and the genus *Dependovirus* because of its replication-deficient nature. Members of this family have evolved over the years, expanding their spectrum of hosts, which includes mammals and insects [29]. Although mammalian cells are the natural host of AAV, based on the common ancestral relationship (**Figure 3.1A**) and given that insect cells are the natural hosts of viruses belonging to the *Densovirinae* subfamily, they should facilitate the rescue and replication of AAV genes and support AAV protein expression. Ruffing et al. in 1992 reported baculovirus-mediated AAV gene delivery, AAV VP proteins expression and AAV capsids assembly in insect cells [30]. However, the first report of AAV Rep expression, Rep-mediated rescue of ITR-flanked *transgene* and production of functional AAV vector in insect-cell was published a decade later by Urabe et al. [31]. Both reports confirmed functionality of insect cells as a suitable host for AAV production. The

wild-type AAV (wtAAV) genome is a linear, single-stranded DNA with a size of approximately

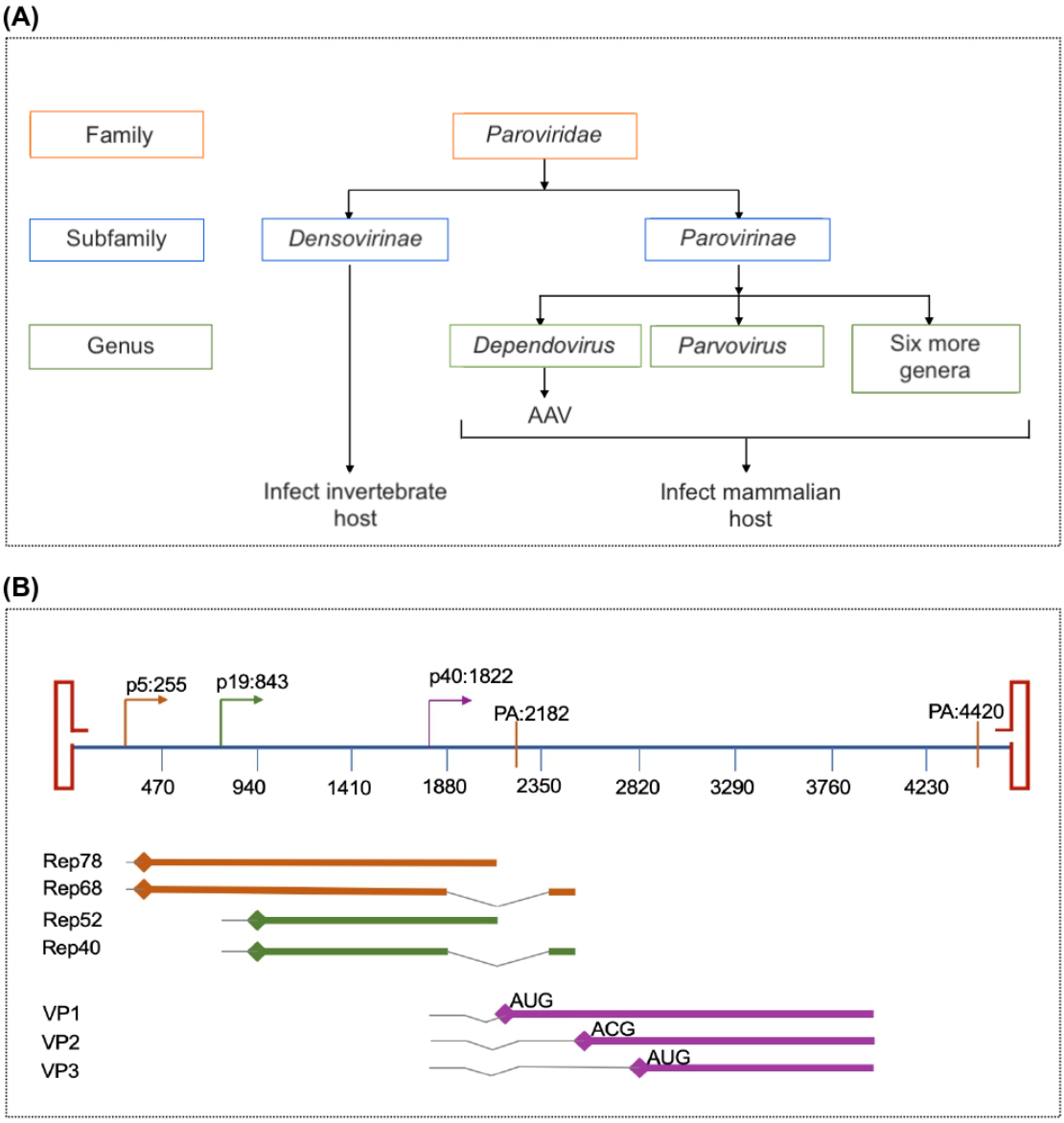

Figure 3.1 AAV family tree and wtAAV2 genome map and expression profile

(A) AAV family tree. The *Dependovirus* AAV mainly infects mammalian hosts and replicates in the presence of a helper virus. Though evolutionary distant yet related to the *Densovirinae* subfamily, it shares common structural and functional features with viruses from this subfamily, which mainly infect invertebrates hosts such as insects. **(B)** wtAAV2 genome map and protein expression profile. The AAV genome schematic illustrated is based on a previous publication [39]. The numbers represent the nucleotide position. The viral genome is flanked by two ITRs, one at each end. Two promoters in the Left ORF drive the expression of four regulatory Rep proteins, whereas a single promoter in the right ORF drives the expression of three capsid protein subunits (VP1, VP2, and VP3) from a single mRNA transcript. Intron splicing generates four Rep proteins of different sizes from two mRNA transcripts, whereas the leaky scanning of weak translational codons results in the production

of three VP proteins in a stochastic ratio of 1:1:10. The diamond shape represents the N-terminal of the peptide. Two polyadenylation (PA) signal sequences are shown via the orange line.

4.7 Kb [32]. Major coding regions consist of the genes responsible for the expression of non-structural regulatory Rep proteins and structural capsid proteins (Cap or VP). This coding region is flanked at both ends by an inverted terminal repeat (ITR) sequence, which acquires a T-shaped hairpin-like structure formed via complementary base pairing of palindromic sequences.

The wild-type AAV (wtAAV) genome is a linear, single-stranded DNA with a size of approximately 4.7 Kb [32]. Major coding regions consist of the genes responsible for the expression of non-structural regulatory Rep proteins and structural capsid proteins (Cap or VP). This coding region is flanked at both ends by an inverted terminal repeat (ITR) sequence, which acquires a T-shaped hairpin-like structure formed via complementary base pairing of palindromic sequences. Figure 3.1B represents the genomic map of wtAAV2 and its transcriptional and translational profile [32]. The recombinant AAV (rAAV) vector retains only the ITR from the wild-type virus, the element essential for vector genome encapsidation, whereas the *rep/cap* genes are replaced by an expression cassette consisting of a gene of interest flanked by ITR. The *rep/cap* genes essential for rAAV production are supplied in *trans* via a suitable vector, such as baculovirus vector in case of insect cells-based production system.

3.3 Molecular design of baculovirus expression vectors and cell lines for production of rAAV

Since insect cells are the heterologous host of AAV, substantial efforts have been made in the last two decades in applying molecular engineering approaches to achieve efficient AAV production employing the IC-BEVS platform. Building upon the intrinsic advantages of the IC-BEVS

platform, efforts have been directed towards achieving higher expression stability, improved AAV yield, and streamlining manufacturing processes. Below, we summarize the progressive development of various strategies and highlight features that might be of consideration when using IC-BEVS for AAV production. The bioprocessing features are discussed separately in Section 4.

3.3.1 First generation IC-BEVS: Three-Bac

The production of functional rAAV2 vectors in insect cells was first reported in 2002 by Urabe et al. [31]. This system required co-infection of *Spodoptera frugiperda* (Sf9) cells with three baculovirus expression vectors (BEVs), each delivering one of the three essential genes (*rep:* Bac-Rep, *cap*: Bac-Cap, and ITR-flanked gene of interest*:* Bac-ITR-GOI) for AAV generation, hence the name Three-Bac (**Figure 3.2A**). The successful AAV vector production demonstrated that AAV genes, when delivered as an integral part of the baculovirus genome under the transcriptional control of insect promoters, can successfully undergo DNA and protein processing pathways in insect cells. They adequately provided the components and cellular machinery required for rescue and replication of AAV genes, AAV protein expression, capsid assembly, and viral genome encapsidation. Moreover, unlike mammalian cells, no additional helper virus (adenovirus or herpes simplex virus) superinfection or supplementation of helper genes was necessary for AAV production, indicating that the baculoviral vector provided all or any essential helper function(s).

3.3.2 Second generation IC-BEVS: Two-Bac, Mono-Bac, and One-Bac1.0

Although initially successful for AAV2 production, the Three-Bac did not achieve widespread application because of the genetic instability of BEVs and consequent loss of AAV yield, and the inability to produce functional AAV vectors of other serotypes [33,34]. These limitations were

partially resolved in the follow-on systems based on two and one BEV, namely, Two-Bac and One-Bac/Mono-Bac. In the Two-Bac system reported by Smith et al. [35] and Chen [36], *rep* and *cap* expression cassettes were introduced into a single BEV (Bac-Rep-Cap or Bac-*In*-Rep-Cap) (**Figure 3.2A**), therefore now requiring co-infection of only two baculoviruses. AAV production with Mono-Bac required Sf9 cells to undergo infection with a single BEV harboring all three essential genes [37]. In contrast to the Mono-Bac, the One-Bac1.0 reported by Aslanidi et al. consisted of baculovirus (BV) inducible stable Sf9 packaging cells harboring the *rep2* (AAV2 *rep*) and *capX* (X = serotype of interest) genes [38]. Infection of these cells with a single baculoviral vector carrying an ITR-flanked *transgene* cassette resulted in an inducible and amplified expression of AAV proteins offering up to 10-fold higher cell-specific yield of AAV2 vector particles compared to the Three-Bac. Comprehensive reviews providing detailed insights into the molecular design of each of these systems have been published previously [39,40].

3.3.3 Advancements in IC-BEVS

The development of the first- and second-generation BEV systems and their subsequent improvements were driven by the combined aims of achieving sustained expression of AAV proteins (Rep and Cap) in stoichiometric proportions, improved AAV production yield and functionality, and overall vector quality. The following sections summarize the various strategies undertaken to achieve each of these goals.

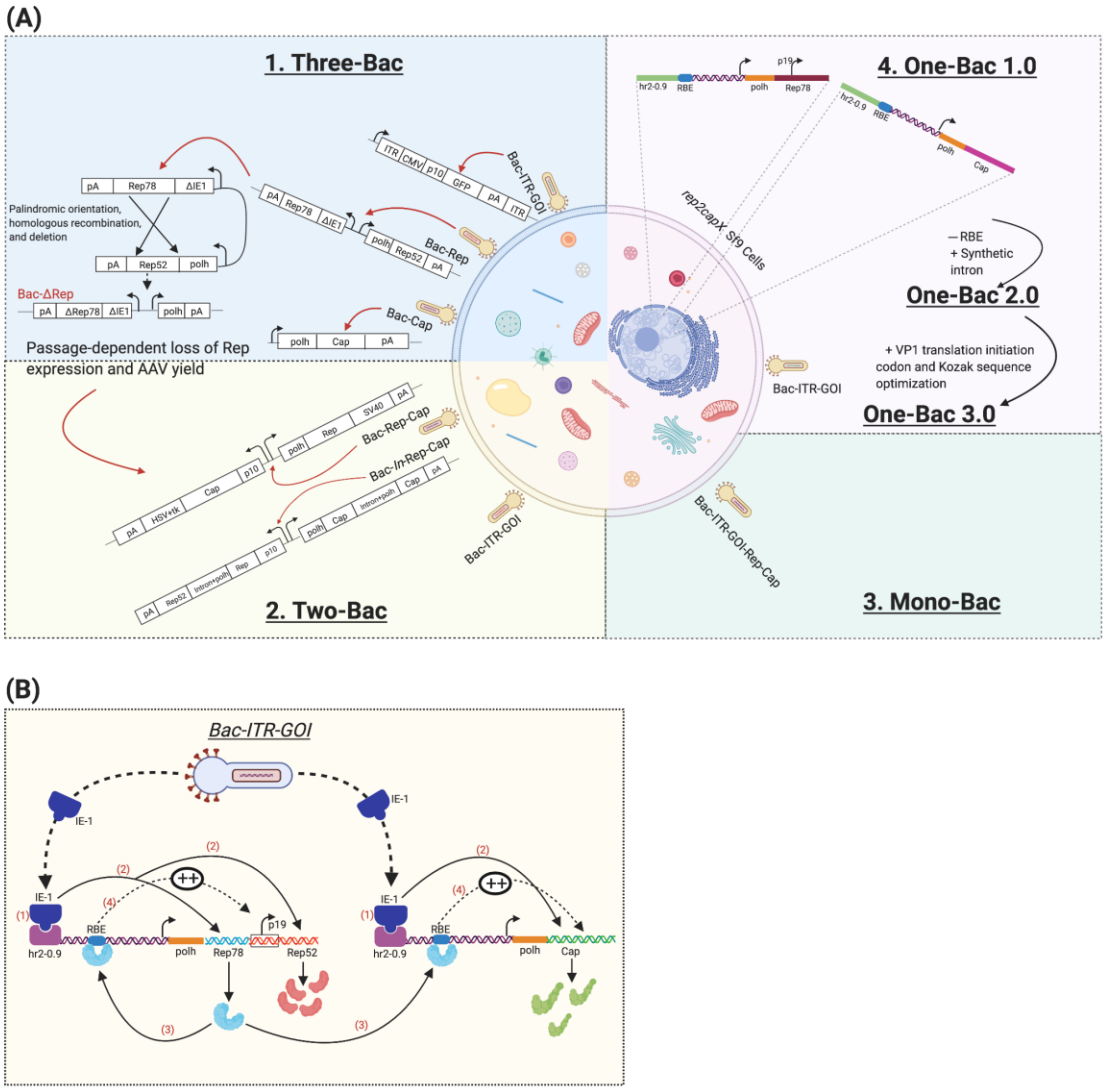

Figure 3.2 AAV insect cell baculovirus expression systems for AAV production and mechanism of inducible expression in One-Bac

(A) Four major systems for rAAV production using the IC-BEVS. The Three-Bac system consisted of three rBEVs vectors, each carrying a specific gene sequence [31]. Further study with this system identified critical shortcomings, related to the expression stability of rBEVs and the underlying mechanism [33]. The follow-on systems exhibited better expression stability of rBEVs over extended passage numbers and required only two rBEVs' co-infections for AAV production. The systems such as One-Bac or Mono-Bac further simplified the manufacturing process requiring only a single rBEV co-infection. One-Bac consists of *a rep2capX* packaging cell line and a Bac-GOI vector [38], whereas in Mono-Bac, a single BEV carries all the necessary gene (Bac-ITR-GOI-Rep2-CapX) sequences [37]. **(B)** The postulated mechanism of induction and amplification of *rep/cap* genes in One-Bac1.0. Bac-ITR infection provides IE-1, which activates hr2-0.9 (1) and induces Rep78/52 or Cap expression (2). The expressed Rep78 further forms a complex with RBE (3) and induces the second round of amplification of Cap or Rep52 expression (4), resulting in a higher Rep52:Rep78 ratio which is reported to favor

higher vector yield [38]. The schematics of Bac-vector expression cassettes depicted in this figure were adapted from the original publications and recreated using Biorender.com.

3.3.3.1 Enhancement in AAV Rep expression

The head-to-head orientation of Rep78 and Rep52 expression cassettes of the Three-Bac's Bac-Rep vector was found to be genetically unstable due to palindromic orientation (**Figure 3.2A**), causing passage dependent loss of Rep78/Rep52 expression and substantially low functional AAV titer [33]. Kohlbrenner et al. restored expression stability by isolating the Rep78 and Rep52 sequences onto different baculovirus vectors, although quadruple infection was now required, complicating the Three-Bac-based AAV production process even more [33].

Chen et al. reported stable Bac-Rep expression by introducing a synthetic intron in the Rep coding region [36]. The *polh* promoter of this synthetic intron drove the Rep52 expression independent of Rep78, resulting in stable expression of both proteins from two different mRNAs for extended passage numbers. In contrast, in the Two-Bac system, Smith et al. modified the nucleotide sequences of the Rep78 translational initiation codon providing weak Kozak consensus and the codons downstream of Rep78 [35]. The resulting leaky ribosomal scanning of Rep78 and concomitant expression of both Rep78/Rep52 proteins from a single mRNA transcript showed Bac-Rep stability up to seven passages.

A more recent modification utilized the weak initiation codon for Rep78, which enabled partial exon skipping and subsequent expression of downstream Rep52 from a single expression cassette and reportedly enhanced Bac-Rep stability for at least five passages [41].

In the Mono-Bac [37], the *rep-cap* expression cassette reported in Two-Bac [35] was integrated into the *egt* (ecdysteroid UDP-glucosyltransferase) locus of the baculovirus genome. The very late phase expression of Rep proteins, specifically after baculovirus DNA replication, minimized Rep-

induced excision of the *rep-cap* expression cassette from the baculovirus genome, resulting in sustained expression stability. Furthermore, this late phase expression of Rep proteins was also critical to avoid Rep-induced excision of AAV expression cassette [42] and its integration stability in baculovirus genome as this can ultimately affect the stability of Mono-Bac BEV and overall production titer of AAV vectors.

In contrast to some of the above systems where a separate strong polh promoter was used for Rep52 expression, Aslanidi et al. retained the partially active native p19 promoter of Rep52 to drive its expression in One-Bac 1.0 insect cells [38]. The introduction of the Rep-binding element (RBE) resulted in Rep52 expression higher than Rep78 via a feed-forward loop achieving a desirably higher Rep52:Rep78 ratio (**Figure 2B**). The modified version of the One-Bac Sf9 cell line harboring a stably integrated rep-cap cassette demonstrated higher expression stability than previously described Bac-Rep vectors, up to at least 35 cell-culture passages [43].

3.3.3.2 Restoration of VP1 expression proportion for improved AAV functionality

In mammalian cells, the natural host of AAV, the combination of alternate mRNA splicing and leaky ribosomal scanning of a weak VP2 translational initiation codon enables the expression of three VP proteins in their prototypic ratio (VP1:VP2:VP3 = 1:1:10) from a single mRNA transcript [32]. Sufficient expression and subsequent incorporation of VP1 subunit, harboring phospholipase A_2 (PLA_2) like enzymatic domain, in the AAV capsid are critical as the PLA_2 is reportedly responsible for late endosomal escape and consequent perinuclear localization which are essential steps for the transduction efficiency of AAV vectors [44,45]. Initial failures at attaining the expression of three VP proteins in given prototypic proportions using Three-Bac necessitated the use of a

weak VP1 translational initiation codon, which, leveraging leaky ribosomal scanning, produced three VP proteins in the desired ratio [31]. Although successful for AAV2, the Three-Bac was later reported to produce sub-optimal expression levels of VP1 of other clinically relevant serotypes such as AAV5 and AAV8, generating defective/non-tranducive vector particles [33,34].

Based on the original findings by Kozak [46,47], Urabe et al. hypothesized that, compared to AAV2 VP1, a single nucleotide difference at a critical position in the Kozak sequence surrounding the AAV5 VP1 translational initiation codon may be responsible for sub-optimal ribosomal scanning efficiency and reduced VP1 expression levels. Building on this hypothesis, complete or partial VP1 domain swapping strategies have been shown to generate AAV chimeric vectors (AAV2/5 or AAV2/8) with restored VP1 expression levels and improved transduction efficiency [33,34].

Chen achieved sufficient VP protein expression by placing VP1 under the transcriptional control of a strong polh promoter, whereas the VP2/3 expression was governed by a synthetic intron [36]. As a result, higher and stable expression of all VP proteins was achieved from two separate mRNA transcripts.

Similar to the original Three-Bac, the Two-Bac [48] and the One-Bac systems, harboring the weak VP1 translational initiation codon, also showed suboptimal expression levels of VP1 proteins in certain serotypes other than AAV2 [49]. Bosma et al. reported that the selection of a modified optimal VP1 translation initiation codon and the associated downstream nucleotide sequence resulted in optimal stoichiometric expression of all three VP proteins generating an AAV5 vector with improved functionality in the Two-Bac system [48]. In One-Bac2.0, the second-generation One-Bac, the original strong VP1 codon and a synthetic intron were introduced to restore the expression level of AAV5 VP1 [50]. In a more recent modification, the third-generation One-Bac3.0, a combination of the modified translational initiation codon and Kozak sequences offered

suboptimal translation efficiency yet sufficiently high VP1 expression levels in more than one serotype, reportedly in both AAV5 and AAV9, resulting in highly transducive vectors [51].

Differently from previous reports, Galibert et al. found that baculovirus protease-driven degradation of VP1 led to the production of defective/VP1 deficient AAV vectors of serotype 1, 6, and 8 in insect cells [52]. Deletion of cathepsin expressing *v-cath* locus from the baculovirus genome or the use of the E64 protease inhibitor improved the post-expression stability of VP1 and restored the potency of the vector.

A novel strategy involving the use of the 5'-untranslated region (5'-UTR) to regulate AAV VP protein expression levels was reported [53]. The engineered 5'-UTR sequence, forming a hairpin-like secondary structure, was introduced upstream of the VP1 codon to generate AAV2 and AAV9 vectors with the desired VP1 level.

3.3.3.3 Improved efficiency and specificity of vector genome packaging

Concerns regarding the co-packaging of non-vector nucleotide sequences, including antibiotic selection marker genes from the bacmid backbone, were first raised during the regulatory evaluation of Glybera® [54]. The baculovirus DNA sequences proximal to the AAV ITR in the Bac-ITR vector are also prone to reverse packaging due to ITR's role as a packaging signal [55]. Even though collaterally packaged baculoviral gene sequences, in general, are not expressed in mammalian cells, the delivery of such non-transgene elements may evoke a potential immunogenic response in vivo and hence is considered a safety risk. Therefore, dedicated efforts have been invested in improving packaging efficiency and specificity.

The inverted terminal repeat sequence of the AAV genome is the only element from the wild-type AAV virus that is maintained in a recombinant vector and is present in cis in a transgene expression

cassette. A recent report by Savy et al. showed that the unmodified AAV2 wild-type ITR (wtITR) sequence promotes enhanced and specific encapsidation of the rAAV8 vector sequence in contrast to truncated ITRs, which is found in traditional packaging plasmids such as pSUB201 and its variants [56]. The latter was found to be responsible for non-specific packaging. Specifically, with the use of intact wtITR, two-dimensional improvements were reported. First, the relative proportion of packaged capsids increased to 40% from 10%, and second, the packaging of non-specific sequences was reduced by 10-fold [56].

The incorporation of RBE in the original One-Bac1.0 was responsible for high-frequency co-packaging of rep/cap sequences in AAV capsids, confirming its role as a packaging signal [50]. Excision of the RBE component in the One-Bac2.0/AAV5 cell line resulted in more than 3- and 4-log reductions in the frequency of rep and cap sequence co-packaging, respectively, with final rep/cap packaging levels reaching as low as 0.001% and 0.02%, respectively [50]. The AAV vector produced using RBE-negative One-Bac3.0 also demonstrated a lower frequency of the co-packaging of all non-vector-specific sequences (rep/cap, baculoviral, and Sf9 genome) in the range of 0.003–0.4% [51].

Recently, BEVs generated via homologous recombination, in contrast to the traditional Tn-7 transposition protocol, showed improved expression stability and lack of co-packaging of bacterial or transposase-derived sequences, providing a high-quality AAV vector preparation [57].

3.4 Bioprocessing of rAAV using the IC-BEVS manufacturing platform

In addition to the molecular design of expression systems, the bioprocessing aspect of IC-BEVS is equally essential for the successful manufacturing of AAV. AAV production in insect cells is inducible upon BV infection, a process based on the complex dynamics of insect cell baculovirus

interaction and kinetics of baculoviral and AAV gene expression, which in turn affects the extent and kinetics of AAV protein production and overall AAV quality and yield. This process has been primarily and extensively documented in peer-reviewed research publications with the Three-Bac system, which has been the workhorse of AAV production and bioprocessing research for more than a decade. In the following sub-sections, a detailed discussion on AAV bioprocessing from the Three-Bac standpoint is provided, highlighting important process intensification strategies. The key features of recent improvements in the AAV production process related to the Two-Bac and the One-Bac systems and critical areas of future improvements are discussed in later sections. **Table 3.1** summarizes the AAV yield at various scales employing different IC-BEVS production systems. A schematic overview of the AAV production process employing the IC-BEVS platform is shown in **Figure 3.3**.

3.4.1 Multiplicity of infection of Baculovirus: cell population and kinetics of Baculovirus Infection

Multiplicity of infection (MOI), defined as the number of active viral particles (BV in this context) infecting one cell, has been shown to influence the kinetics and extent of infection and protein expression, which ultimately affect the overall yield and composition of the product of interest [58–61]. In the Three-Bac system, the productive infection and consequent AAV generation necessitate the insect cells to receive all the essential genes (rep, cap, and transgene) delivered by three BEVs [31].

Statistically, at an MOI of 1 for each of the three BEVs, while 95% of cells are infected with at least one BEV, only 22% of cells receive three BEV productive infections, leaving 78% of the cells unproductive in the primary BV infection [62]. This productive cell population is even lower at a higher MOI. Meghrous et al. reported that at an optimal MOI of 5, less than 12% of cells are

AAV-productive in the primary infection cycle [63]. In two baculovirus systems (Two-Bac), the productive cell-population proportion ranges between 60–70% [40], with a one baculovirus system, it can reach as high as 95% (based on the MOI used) in the first wave of infection [62]. The single baculovirus infection follows the Poisson distribution, and the relationship between the MOI and protein expression as a function of the productive cell population is a hyperbolic up to an MOI of 5 [62,64,65]. It is believed that this increase in the productive cell population in Two-Bac may be responsible for the higher AAV yield [40]. However, this can be challenged given that the average cell-specific yield of AAV2 viral genomes (VG) achieved with Three-Bac (45,000 VG/cell) [31] is not significantly different from that of Two-Bac (78,000 VG/cell) [35]. A somewhat higher titer with Two-Bac might be correlated to higher AAV Rep protein expression stability, which is necessary for vector genome rescue, replication, and encapsidation [35,66,67]. The lower productive cell population at the primary BEV infection can be circumvented via subsequent waves of infections where BEV progenies produced after the primary infection round infect the remaining cell population, providing near 100% productive infection. This phenomenon is characteristic of asynchronous baculovirus infection caused by low MOI used in the primary infection round [68]. This process has been used for the production of enveloped virus-based vaccine candidates in insect cells and mammalian cells [69,70].

When applied to AAV production using Three-Bac, Mena et al. and Negrete et al. reported that at both low and high MOIs, the overall volumetric yields of AAV are comparable [68,71]; however, in the case of a low MOI process, the culture harvest time is delayed by an additional 24–48 h post-infection (~96 hpi) due to an apparent delay in the transition to the productive infection phase as compared to the standard high MOI process [68]. A full factorial DOE study conducted by Aucoin et al. provided detailed insight into single-factor and multifactorial interaction effects of MOI of

the three baculoviruses on AAV yields and the timing of expression for each AAV protein [72]. This study suggested a self-controlling nature of the insect cell-baculovirus infection process, where differing MOIs or delaying the infection of one of the three baculoviruses did not lead to significant changes or improvements in overall AAV yield when reported in combination with the relative proportions of total, genome containing, and infective virus particles (Cp: VG: IVP).

Besides, obviously low BEV stock requirements, another advantage of the low MOI process, relate to the lower production of non-functional defective interfering particles (DIP) of BV progenies after the primary infection [73]. Therefore, a low MOI is also recommended for BV/BEV production. It has been reported that during BV production, the co-synthesized DIP can lack up to 43% of the original BV genome [73], the missing elements may be complemented by a high MOI infection facilitating DIP co-production. In contrast, a low MOI primary infection reduces this genetic complementation and probability of DIP progeny formation, hence minimizing DIP-mediated non-AAV-productive infections during the AAV production process.

3.4.2 Cell density effect and mode of cell culture operation

The cell density effect, which refers to the loss of cell-specific yield of the product of interest above specific cell density (breakpoint) in the cell culture, has been widely reported in the literature, including with respect to AAV production [43,63,68,74,75]. This effect has been associated with metabolic limitation of the culture, especially in the productive infection phase, and has been successfully alleviated via supplementation of fresh growth medium (medium replacement strategy) or bolus supplementation of the nutrient cocktail under the fed-batch mode of operation [63,75]. While commercially available serum-free growth media for insect cell culture such as SF-900™-II or-III can support a peak cell density of up to 13 million cells during a standard growth

curve (our unpublished data), they fail to sustain protein expression in baculovirus-infected high cell density cultures. When analyzed for AAV production using Three-Bac, the optimal cell density at the time of infection was reported to be approximately 1 million cells/mL in the EX-CELL® 420 medium [63] or 3.5 million cells/mL in SFX serum-free medium [76]. Similarly, during AAV5 production in One-Bac3.0 Sf9 cells using Sf900™-II or Sf900™-III medium, the cell density breakpoint was approximately 2.0 million cells/mL [43]. Any combination of cell density at the time of infection and an MOI that resulted in a peak cell density above the breakpoint resulted in a drop in the cell-specific yield, limiting the AAV volumetric titer in a low-cell density culture. Such a low-cell density culture process operating under a batch mode of cultivation generally results in a lower volumetric yield of AAV, necessitating large-scale bioreactor production to meet the exceptionally high demand of AAV vector material (up to 10^{17} VGs) for late-phase clinical studies [39].

A straightforward way to boost the overall volumetric titer is to infect and induce AAV production at higher cell densities while maintaining the cell-specific yield. The medium replacement strategy was used to attain increased AAV production at cell density as high as 7.5 million cells/mL in shake-flasks, and the process was further validated at the 3L and 20L bioreactor scale at up to 2.5 million cells/mL cell density [63]. Similarly, in Sf21 cells, the fresh growth medium supplementation successfully alleviated nutrient limitation at 1 million cells/mL density offering increased cell-specific yield compared to controlled production runs [77]. The fed-batch mode of operation combined with low MOI infection of Three-Bac BEVs resulted in an almost 1-log increase in volumetric yield of functional AAV2 particles when the nutrient cocktail was provided at the time of infection and 24 h before and after infection (**Table 3.1**) [68]. In this case, Sf9 cells were infected at ~5 million cells/mL at a low MOI of 0.1 (for each BV), which resulted in non-infected cells

growing up to 48 hpi, attaining a peak cell density as high as ~10 million cells/mL followed by a sustained AAV production phase.

3.4.3 Effect of temperature

The temperature modulation strategy is reported to affect protein expression yield and glycosylation in insect cells [78–81], which grow best at temperatures between 27 °C and 30 °C. Aucoin et al. reported higher functional AAV2 vector production in Sf9 cells at a higher temperature [82]. Of different temperatures tested (21, 24, 27, 30, and 33 °C), the highest yield of AAV functional particles was achieved at 30 °C, which was 2.5 times and 5 times more than at 27 °C and temperatures below that, respectively. In addition, temperature modulation affected the onset of expression and kinetics of AAV protein production. The use of temperature-responsive promoters or other regulatory elements to achieve inducible production of AAV proteins at a controlled rate or expression levels remains open to further investigation.

3.4.4 AAV production in small and large-scale stirred-tank bioreactors and Wave™ bioreactors

The attractive features of insect cell baculovirus platforms include the ability of insect cells to grow in suspension culture at a high cell density, proven linear scalability, and a history of regulatory acceptance of the platform for the production of various biologics [11,26]. A commercial-scale fed-batch manufacturing process for Flublok® in Sf9 cells was successfully scaled-up and demonstrated at 2,500 L stirred-tank bioreactor (STB) [11] with targeted production at a > 20,000 L scale. Multiple reports of AAV production in either conventional STBs (glass, stainless steel, or disposable vessel) [63,76,83]or Wave™ bioreactors [83] suggest comparable yields and quality of rAAV vector material (**Table 3.1**). In a controlled bioreactor environment maintained at optimal cell-

culture conditions, the AAV production yield improved compared to a shake flask run, as demonstrated in a 20 L scale bioreactor production, which generated around 5×10^{12} AAV2 functional particles [63](**Table 3.1**). Subsequent reports of AAV production using an improved Three-Bac system indicated AAV volumetric yield in the range of 5×10^{12}–3×10^{13} VG/L with a comparable consistency at various scales of Wave™ (up to 20 L) and STB (up to 40 L), respectively [83]. Even though the reported yield was somewhat lower, the bioreactor scale process performance, when expressed as the ratio of genomic: transducing units (VG: TU), was consistent in all production runs.

Although simple and straightforward at a smaller-scale, AAV production using Three-Bac at a large scale was challenging due to a multitude of reasons. First, a large amount of three different BEV stock, required to infect large-scale production cultures, necessitates the parallel production of these BEVs. During this BEV production step, BEVs may undergo high passage numbers, resulting in lower and variable expression stability and presenting a direct source of plausible process variability. Second, the parallel production, quantification, and characterization of three different baculoviral vectors remain cumbersome and resource-extensive steps. Moreover, if a high MOI process is selected (> 3 MOI for each BEV), the total volume of three-BEV stock (1×10^8 pfu/mL) required may be as high as 20% v/v, leading to a substantial dilution of production culture volume at the time of infection. To address these challenges, an alternate approach to the proven low-MOI process [68] was reported by Cecchini et al., where the low MOI infection characteristics were mimicked and reproduced in situ by expansion of a mixture of cryo-preserved baculovirus-infected insect cells (BIIC) and non-infected insect cells (NIIC) [76]. BIIC and NIIC, originally mixed in a 1:10,000 ratio, eliminated the need for exogenous baculovirus infection during production, and offered consistent baculovirus infection kinetics and AAV expression yield. When

assessed at different scales (shake flask to 200 L bioreactor) for different serotypes (AAV-6 and -9), a comparable yield of AAV serotypes was reported[76](**Table 3.1**).

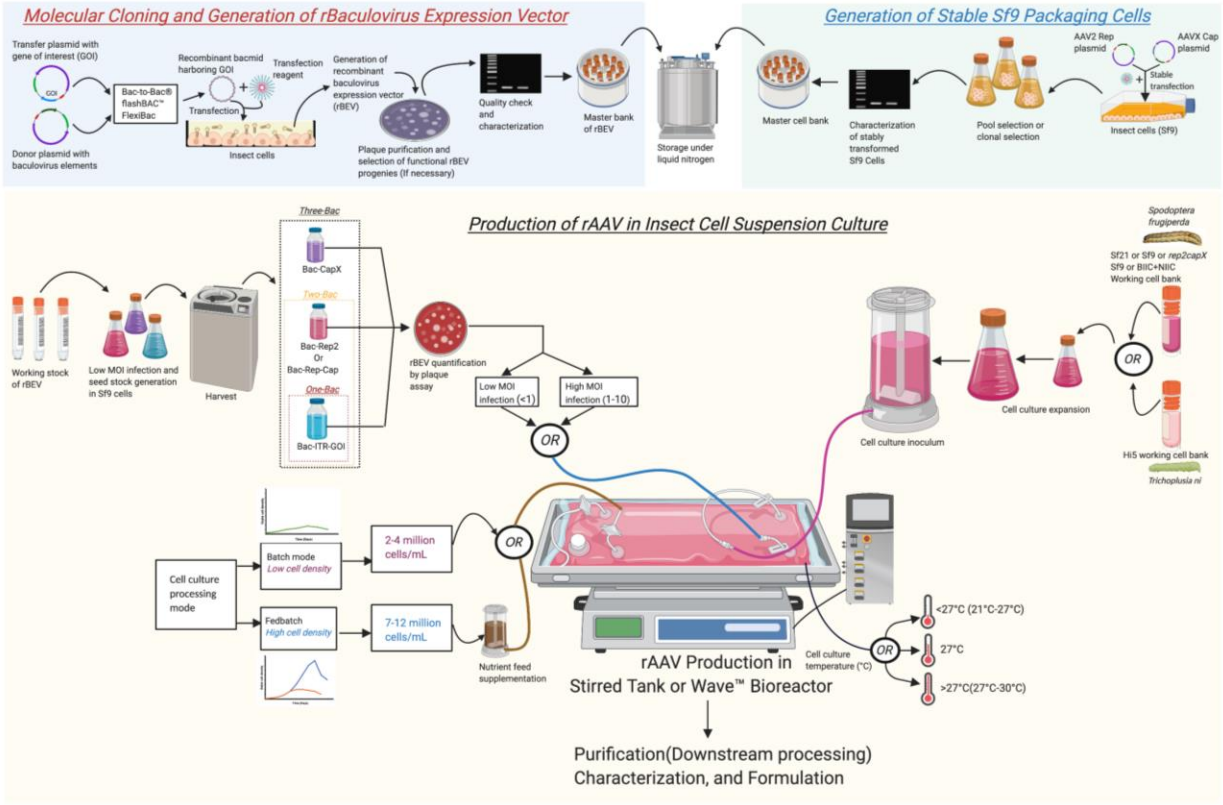

Figure 3.3 Overview of process flow for rAAV production employing the IC-BEVS platform

AAV production using the IC-BEVS platform consists of two stages: 1. Generation of recombinant baculovirus expression vectors (rBEVs) and additionally *rep2capX* Sf9 packaging cells in the case of the One-Bac system (Top section), and 2. AAV production at the bioreactor scale in suspension culture of insect cells followed by purification and formulation (bottom part). The first part requires molecular cloning, transient expression, plaque purification, and characterization of rBEVs. Similarly, *the rep2capX* cells are generated via stable transfection of respective shuttle plasmid vectors and selection followed by characterization and master cell bank preparation. During the production stage, the rBVES and insect cells (Sf9 or Hi5) are sequentially expanded, as required for stirred tank or Wave™ production scale bioreactors. At the production stage, the insect cells are infected with rBEVs at an appropriate multiplicity of infection (low, < 1 or high, 1-10) and at optimal cell density. Generally, under the batch mode of cultivation, the cells are infected at a low cell density of approximately 1–3 million cells/mL, whereas in the fed-batch or medium-exchange mode, the cells reach a higher peak cell density before infection, at 7–12 million cells/mL. The cultivation temperature for insect cells is generally set at 27 °C, although one study reported AAV production at higher and lower temperatures, and their effect on yield and production kinetics. Post-infection, at 72–96 h, the culture is harvested, and cells are lysed to recover AAV. Next, the lysate is subjected to a multistep purification process followed by formulation in an appropriate buffer as a final step. The artwork in the figure was created using Biorender.com.

3.4.5 AAV production process monitoring in bioreactors

In addition to the pH, temperature, and dissolved oxygen concentration sensors, various in-line process monitoring tools have been reported for AAV production. These tools include dielectric spectroscopy [84] and capacitance sensors for monitoring cell growth, productive infection, infection kinetics, and relative permittivity of insect cells [43,68]. Infrared sensors for measuring the carbon dioxide evolution rate of cell culture [68] and recently reported on-line digital holographic microscopy for AAV production yield and cell concentration measurement have also been documented [85]. These tools provide a practical approach for process optimization and process control, including making the decision on culture harvest time.

3.5 Recent advancements in the AAV production process

As discussed in the previous section, the extensive documentation of AAV production employing Three-Bac (**Table 3.1**) provided the key learnings that laid the foundation of the current manufacturing systems and process using improved and follow-on IC-BEVS. Recently, there has been a shift towards a simpler and more straightforward Two-Bac system for AAV production, as it combines the flexibility of Three-Bac and the process simplicity of the less flexible One-Bac/Mono-Bac system to some extent. The two-baculovirus system has been reportedly used for large-scale AAV production by AAV vector manufacturers [86,87].

Although Mono-Bac provides a higher volumetric titer[37], it has not been extensively documented. Generating a stable baculoviral vector harboring all three gene sequences is technically challenging. Moreover, it is the least modular system compared to the Three-Bac or the Two-Bac systems, making it difficult to produce a library of AAV capsids in the early screening phase.

Current standard protocols for AAV production involve Rep proteins and ITR packaging functions from AAV2, whereas the serotype and vector expression cassettes are selected based on in vivo/in vitro transduction studies conducted at the screening phase. In accordance with this rationale, a modified version of the original Two-Bac, Duo-Bac was reported, which consists of Bac-Rep and Bac-CapX-GOI (gene of interest) baculoviruses [48,87]. Similarly, a modified version of One-Bac consisting of only the rep-expressing Sf9 cell line and Bac-CapX-GOI for AAVX (X = serotype) production has also been recently reported [88].

A study by Joshi et al. reported AAV5 production in high-cell density fed-batch cultures using One-Bac3.0, with a final volumetric yields exceeding 2×10^{14} VG/L of cell culture [43]. In contrast to the previously reported fed-batch process [68], the culture at a 10 million cells/mL cell density was infected at a higher optimal MOI of 3, which resulted in the transition of the cell culture to the AAV-production phase from the growth phase within 24 hpi. The nutrient cocktail was supplied to maintain the cell culture in the mid-exponential phase before infection and support AAV production in the post-infection stage to alleviate nutrient limitation, resulting in a 6-fold increase in VGs and an 18-fold increase in bioactive AAV5 particles as compared to the standard low-cell density batch process [43].

In compliance with regulatory and GMP requirements, newer yeastolate-free and chemically defined serum-free media such as ExpiSF™ [89–91] or TheraPEAK™-SfAAV™ [92] have been developed as alternatives to traditional yeastolate-based serum-free media such as Sf900™-II.

Table 3.1 Summary of AAV Production in IC-BEVS Platform

Author, year and production system	Sero type	Bac-MOIs (Absolute values) Rep: Cap: ITR	Transgene	Culture volume	Cell density[a] (cells/mL)	VG/cell	VG/mL	IVP or TU/cell	IVP or TU/mL	Cp: VG: IVP(TU)	Specific notes
Urabe et al.[31] (2002) Three-Bac	2	5:5:5	GFP	200mL	$2x10^{6}$ [b]	$4.5x10^{4}$± ($0.32x10^{4}$ [c])	NA	NA	NA	NA: 1344:1[d] ±283	First report of rAAV production in Sf9 cells
Meghrous et al.[62] (2005) Three-Bac	2	1.6:1.6:1.6	GFP	60mL	$3x10^{6}$ [b]			168	$4.75x10^{8}$ [f]	NA	AAV production in Sf9 cells at high MOI
	2	1.6:1.6:1.6	GFP	60mL	$1x10^{6}$ [e]			185	$4.38x10^{8}$ [f]	NA	AAV production in Hi5 cells at high MOI
	2	5:5:5	GFP	60mL	$2.5x10^{6}$ [b]			75	$3.73x10^{8}$ [f]	NA	Low cell density, batch mode production
	2	5:5:5	GFP	60mL	$2.5\ x10^{6}$ [b]			122	$5.90x10^{8}$ [f]	NA	Low cell density with medium exchange
	2	5:5:5	GFP	60mL	$5.0\ x10^{6}$ [b]			105	$8.78x10^{8}$ [f]	NA	High cell density with medium exchange
	2	5:5:5	GFP	60mL	$7.5\ x10^{6}$ [b]	NA	NA	116	$11.60x10^{8}$ [f]	NA	High cell density with medium exchange
	2	5:5:5	GFP	3L	$2.6X10^{6}$ [b]			250	$6.52x10^{8}$ [f]		Infection in a fresh Ex-Cell 420 medium
	2	5:5:5	GFP	3L	$3.08x10^{6}$ [b]			132	$4.09x10^{8}$ [f]	1640[g]: NA: 1	AAV production process scalability demonstration
	2	5:5:5	GFP	20L	$1.7x10^{6}$ [b]			253	$4.46x10^{8}$ [f]	830[g]: NA: 1	
Urabe et al.[34] (2006) Three-Bac	5	1:1:1	hGFP	NA	$2x10^{6}$	$5.6x10^{4}$± ($0.32x10^{4}$ [h])	NA	NA	NA	NA	Bac-Cap modification, VP1 domain swapping to produce functional AAV5 vector particle
					$2x10^{6}$	$7.67x10^{4}$ ± ($2.12x10^{4}$ [i])					
Aucoin et al.[71] (2006) Three-Bac	2	9:1:1	GFP	20mL	NA	NA	$2x10^{10}$ [j]	NA	$5x10^{7}$ [f]	3400[g]:400:1	MOI optimization study.
	2	9:9:9	GFP	20mL			$2x10^{9}$ [j]		$1.7x10^{8}$ [f]	3000[g]:12:1	
Negrete et al.[70] (2007) Three-Bac	2	0.3:0.3:0.3	GFP	20mL	$2x10^{6}$	NA	$2x10^{12}$ [c]	NA	$2x10^{11}$ [k]	NA: 10: 1	Screening of low Bac-MOIs and cell density to economize AAV production
	2	3:3:3	GFP	20mL	$2x10^{6}$		$3.6x10^{12}$ [c]		$3.2x10^{12}$ [k]	NA: 1.12: 1	
	2	0.03:0.03:0.03	GFP	10L	$1x10^{6}$		$2x10^{11}$		NA	NA	
Negrete and Kotin [82] (2007) Three-Bac	2	3:3:3	GFP	200mL	$2x10^{6}$ [b]	NA	~$3x10^{10}$ [j]	NA	~$1x10^{9}$ [k]	NA: 30:1	Three-Bac system with a modified Bac-Cap sequence.
	2	3:3:3	GFP	5L-Wave™	$2x10^{6}$ [b]		~ $9x10^{9}$ [j]		~$5x10^{8}$ [k]	NA: 18:1	
	2	3:3:3	GFP	20L-Wave™	$2x10^{6}$ [b]		~$5x10^{9}$ [j]		~$3x10^{8}$ [k]	NA: 16:1	Demonstration of AAV process scalability at large scale
	2	3:3:3	GFP	10L-STB	$2x10^{6}$ [b]		~$2x10^{10}$ [j]		~$5x10^{8}$ [k]	NA: 40:1	
	2	3:3:3	GFP	40L-STB			~$4.33x10^{10}$ [j] (±$4.1x10^{10}$)		~$7.5x10^{8}$ [k] (±$2.5x10^{8}$)	NA: 20:1	

Aucoin et al.[81] (2007) Three-Bac	2	10:10:3	GFP	25mL	~2x10[6]	~12000	NA	200[f]	4x10[8]	4600:79:1	Temperature modulation study and its effect on AAV yield
Mena et al.[67] (2010) Three-Bac	2	0.1:0.1:0.1	GFP	20mL	1x10[6]	NA	4.8x10[10 j] (±0.19x10[10])	NA	4.7x10[8 j f] (±0.19x10[8])	NA: 102:1	Low MOI, Batch production
	2	3:3:3	GFP	20mL	1x10[6]		1.3x10[10 j] (±0.17x10[10])		1.8x10[8 j f] (±0.17x10[8])	NA: 72: 1	High MOI, Batch production
	2	0.1:0.1:0.1	GFP	20mL	5x10[6]		2.9x10[10 j] (±0.19x10[10])		6.8x10[8 j f] (±0.25x10[8])	NA: 43: 1	High cell density, medium exchange before the infection
	2	3:3:3:	GFP	20mL	5x10[6]		3.34x10[10 j] (±0.17x10[10])		7.2x10[8 j f] (±0.61x10[8])	NA: 46: 1	High cell density, medium exchange before the infection
	2	0.1:0.1:0.1	GFP	20mL	9.43x10[6 l]		1.17x10[11 j] (±0.12x10[11])		2.9x10[9 j f] (±0.32x10[9])	NA: 40:1	Low MOI, Fed-batch production
	2	0.1:0.1:0.1	GFP	3L	9.5x10[6 l]		2.2x10[11 j]		2.35x10[9 j f]	NA: 94:1	Low MOI, Fed-batch production
Liu et al.[76] (2010)	2	45:45:5	GFP	50mL	1x10[6]	NA	NA	122	1.22x10[8]	NA	Batch production
Three-Bac	2	45:45:5	GFP	50mL	1x10[6]			240	2.4x10[8]	NA	Fed-batch production
Cecchini et al.[75] (2011) Three-Bac	9		GFP	10L	3.55x10[6 l]	2.24x10[4]	7.9x10[10 j]				AAV production employing BIIC strategy.
	9		U7smOPT		3.23x10[6 l]	2.41x10[4]	7.8x10[10 j]				
	8		GFP	20L	3.88x10[6 l]	1.48x10[4]	4.44x10[10 j]				
	6	BIIC: NIIC (1:10000)	U7smOPT	100L	4.29x10[6 l] (±1x10[6])	2x10[4] (±0.3x10[4])	8.75x10[10 j] (±4.04x10[10])	NA	NA	NA	Demonstration of AAV production process robustness at bioreactor scale regardless of the type of transgene
	6		PLS	200L	4.41x10[6 l]	1.82x10[4]	7.45x10[10 j]				
	6		PLS	20L	3.44x10[6 l]	2.07x10[4]	5x10[11 j]				
Chen[36] (2008)	2	1:1:1	GFP		5x10[6 b]		1.37x10[11 j] (±0.34x10[11])				Bac-Intron constructs of baculovirus vector
Three-Bac					5x10[6 b]						Baculovirus with enhanced passage dependent stability
	6	1:1:1	GFP		5x10[6 b]		3.53x10[10 j]				
	8	1:1:1	GFP	NA	5x10[6 b]	NA	9.65x10[10 j]	NA	NA	NA	
	1	1:1:1	GFP				4.41x10[10 j]				Bac-*In*-Rep-Cap and Bac-*In*-ITR
Two-Bac Bac-*In*-Rep-Cap					5x10[6 b]						
	2	1:1	GFP				1.19x10[11 j]				
Smith et al.[35] (2009) Two-Bac	1	1:1	GFP	200mL	2.4x10[6 b]	NA	1.07x10[13 m] (±0.46x10[13])	NA	5.08x10[10 m n] (±5.9x10[10])	NA: 200:1	Bac-Rep-Cap and Bac-ITR based two

Bac-Rep-Cap	2	1:1	GFP	200mL	$1.2x10^{6}$ [b]		$6.5x10^{12}$ [m]		$1.9x10^{10}$ [m n]	NA: 350:1	baculovirus vectors with improved stability
Aslanidi et al. [38] (2009) *rep2capX*One-Bac 1.0	2 1	3 3	GFP GFP	NA	NA	$1.4x10^{5}$ $7.3x10^{4}$	NA	NA	NA	NA	Inducible packaging Sf9 cell line for AAV production
Mietzsch et al. [48] (2014) One-Bac 1.0	1-11 12	3 3	GFP GFP	NA	NA	$\sim10^{4}$-10^{5} [o] $\sim10^{3}$ [o]	NA	NA	NA	NA	Production of all AAV serotypes employing One-Bac system
Mietzsch et al. [49] (2015) One-Bac 2.0	5	5	GFP	NA	NA	$1x10^{5}$ [o]	NA	NA	NA	NA	One-Bac system with VP ratio restoration to improve AAV5 vector functionality
Joshi et al. [42] (2019) One-Bac 3.0	5	3	GFP	25ml	$1.6x10^{6}$ [l]	$2.4x10^{4}$ ($\pm0.45x10^{4}$)	$2.7x10^{11}$ [j] ($\pm0.37x10^{11}$)	6±1.4	$1.7x10^{7}$ [j p] (0.25 ± 10^{7})	NA: 15600:1	Robust, High MOI, Fedbatch AAV5 production process. Process validation at bioreactor scale.
	5	3	GFP	25mL	$12x10^{6}$ [l]	$3x10^{4}\pm$ ($0.4x10^{4}$)	$3.8x10^{11}$ [j]	20±5	$1.9x10^{8}$ [j p] ($\pm0.43x10^{8}$)	NA: 1400:1	
	5	3	GFP	1L	$12x10^{6}$ [l]	$3.16x10^{4}$	$2.6x10^{11}$ [j]	22±5	$2.1x10^{8}$ [j p]	9600[q]: 2400[r]:1	The improved volumetric yield of genomic and functional AAV5 vector
	5	3	GFP	3L	$12x10^{6}$ [l]	$2.7x10^{4}$		15±5	$1.4x10^{8}$ [j p]	9400[q]: 2500[r]:1	
Yang et al. [87] (2019) One-Bac 3.0+	2	3	GFP	NA	$2x10^{6}$	$1.35x10^{5}$ $\pm0.46x10^{5}$	NA	NA	NA	NA	One-Bac based Rep2 expressing transformed Sf9 cell line.
	8	3	GFP		$2x10^{6}$	2.16x105 $\pm0.53x10^{5}$					Offer more flexibility for the production of multiple AAV serotypes production
	9	3	GFP		$2x10^{6}$	$1.80x10^{5}$ $\pm0.39x10^{5}$					

[a] Sf9 cells have been dominantly used for AAV production regardless of the production systems except a single report by Meghrous et al. (2005) where Hi5 cells were used.

[b] Cell density at the time of infection.

[c] value reported for fraction collected from the CsCl purification run.

[d] Determined by infecting HEK293 cells and subsequent analysis under a fluorescence microscope for GFP positive cells. Originally reported as transducing units (TU).

[e] AAV2 production in Hi5 cells.
[f] Determined via infecting HEK293 EBNA cells with AAV vector in the presence of a helper virus and subsequent analysis via flow cytometry for GFP positive cells.
[g] Total virus capsids (Cp) analyzed via ELISA.
[h] Value of rAAV5-hGFP produced using Rep52 of Serotype 1.
[i] Value of rAAV5-hGFP generated via AAV2 VP1 domain swapping (VP1 2/5) and Rep52 of serotype 1.
[j] Value reported for per milliliter of cell culture.
[k] Analyzed via infecting adherent HEK293 cells and subsequent analysis via flow cytometry.
[l] The peak cell density during the production run.
[m] Value reported per milliliter of AVB-Sepharose affinity-purified eluate fraction.
[n] Determined via infecting HEK293A cells via AAV in the absence of helper virus and subsequent analysis using a fluorescence microscope.
[o] Titer value reported from the analysis of a one-step AVB-Sepharose Affinity purified sample.
[p] Analyzed via infecting suspension adapted HEK293 cells with AAV in the presence of helper virus and subsequent analysis by flow cytometry.
[q] Determined via analytical ultracentrifugation analysis of one-step AVB-Sepharose Affinity purified sample and originally reported as enhanced transduction units (ETU).
[r] The value of the relative ratio is derived from ETU units determined for AVB affinity-purified samples.
NA: Not available in the published report
GFP: Green Fluorescence Protein
hGFP: Humanized Green Fluorescence Protein
STB: Stirred-tank bioreactor

3.6 Future perspectives

3.6.1 Insect cell and baculovirus engineering

Although insect cells have been in use for AAV production for more than 15 years, the first major question yet unanswered relates to the uncertainty of whether the maximum cellular protein production/processing capacity has been reached. One-Bac1.0 reported almost 1-log higher cell-specific AAV yield (~500,000 VG/cell) [38] compared to the original Three-Bac (~45,000 VG/cell) [31], which indicates that current AAV production protocols demonstrating routine cell-specific yield of up to ~100,000 VG/cell (**Table 3.1**) may be under-utilizing the insect-cell's AAV production capacity.

The second question is related to the efficiency of vector genome packaging in insect cells. In general, insect cells have been reported to produce more AAV empty capsids [43,56,93] compared to mammalian cell platforms [94–96], which counteracts any success achieved with increased cell-specific AAV yield and necessitates active efforts towards engineering insect cells or BEVs to improve packaging efficiency and produce more functional particles. A head-to-head comparison of mammalian cell versus insect cells for wild type AAV production may help identify any insect-cell specific limitations for producing packaged AAV particles because mammalian cells, the natural host of AAV, have been reported to produce nearly 100% genomic and functional particles of wtAAV in the presence of helper virus functions [97]. Moreover, in contrast to well-defined and well-characterized helper genes of adenovirus or HSV [98,99], the baculovirus helper elements have not yet been fully identified, even though their helper function has been known for almost two decades [31]. Aslanidi et al. reported the absolute requirement of baculovirus genomic elements such

as homologous region (hr2-0.9) in *cis* as a part of the rep expression cassette for its rescue and replication in insect cells upon BV infection [38]. Identifying similar helper elements to modulate AAV gene expression and subsequent genome-encapsidation efficiency of insect cells presents an opportunity for further research.

Another critical factor requiring significant consideration is the functionality of ITR, which is not yet fully understood [100], especially in the context of insect cells. In contrast to traditional AAV2 Rep/ITR, the selection of optimal combinations of serotype-specific Rep/ITR also remains an open area of investigation to further support the findings of a single report by Urabe et al. studying the effect of such a combination on genome packaging efficiency and overall yield of AAV5 [34].

The exclusive use of Sf9 cells over Hi5 for AAV production has not been supported with sufficient documentation despite proven commercial viability and regulatory acceptance of Hi5 cells for the production of therapeutic biologic for use in humans [11,26]. Meghrous et al. reported a somewhat higher cell-specific yield of AAV2 in Hi5 cells compared to Sf9 [63]. However because of the known ease of baculovirus production in Sf9 cells over Hi5 cells [17], the former was selected for both AAV and BEV production, streamlining the overall process. With the demonstrated success of AAV production in the One-Bac Sf9 packaging cell line, the generation of a similar Hi5 cell line remains open to further evaluation. Additionally, in the context of a recent report regarding the effect of post-translational modifications (PTMs) of AAV capsids on vector transduction efficiency [93], a side-by-side comparison of AAV produced in Sf9 and Hi5 cell lines might provide new insights into the vector quality attributes (PTMs, in vivo potency) imparted by different cell lines.

It should be noted that in recent years, commercially available Sf9 and expres*SF+*, and Hi5 cell lines have been found to produce rhabdovirus [101,102] and nodavirus[103], respectively, wherein the latter was found to acquire latency in Hi5 cells in the absence of baculovirus superinfection. As

such, rhabdovirus can not replicate in human or monkey cell lines [101,104]; therefore, it is deemed harmless, whereas the host range of nodavirus is not yet clear. Importantly, the team from Glyobac recently established and characterized rhabdovirus-negative Sf9 cell line [102] and nodavirus-negative Hi5 cell line [105], which showed the absence of corresponding adventitious viruses over extended cell passages making these cell lines preferentially more suitable for biologics manufacturing than the current Sf9 and Hi5 cell lines in use because of improved product safety. Notably, none of these new cell lines have been reportedly used for AAV production and remain open to further investigation.

AAV production using IC-BEVS is a transient phenomenon. Because of the lytic nature of baculovirus infection, AAVs are recovered by harvesting the cell culture within 96 hpi, preferably at viability > 70% [43], to minimize potential degradation of AAV capsids by cellular-proteases released as a result of cell apoptosis. At this time, AAV VG titer often reaches a plateau; however, this may not be the optimal harvest time since packaged virions are believed to undergo a so-called "capsid maturation" phase reflected as delayed onset in infective virus particles[43,106]. Extending the time of harvest while maintaining insect cells at higher viability offers a plausible solution to increase the overall yield of the functional AAV vectors. Expression of anti-apoptotic proteins such as vankyrins has been shown to maintain > 90% viability at 96 hpi in both Sf9 and Hi5 cells [107]. Similarly, the anti-apoptotic p35 gene expression also showed a 4-fold increase in GFP titer while maintaining the culture at > 50% viability at approximately 120 hpi [108]. Incorporation of these advancements in the AAV production process and their effect on AAV yield could be of potential interest in the future.

The protease-driven degradation of secreted recombinant proteins produced via IC-BEVS has been known for a while, which prompted the use of a chitinase and cathepsin gene-deleted BEV [109].

Similarly, recent observations reported on the degradation of VP proteins of specific serotypes suggest further exploration in this area to identify other protein-degrading elements of the baculovirus genome [52]. Further identification and deletion of such detrimental or non-essential genes may facilitate the insertion of multiple copies of AAV gene expression cassettes in the baculoviral vector. In this way, more copies of AAV genes, compared to standard baculoviral vectors, can be delivered to insect cells without increasing the MOI, enabling a lower overall requirement of baculoviral vector stock and an economized approach to AAV bioprocessing.

3.6.2 AAV bioprocessing

In addition to molecular and cellular engineering, improvements in high cell density production processes can also contribute to addressing the challenges of high-yield production by incorporating advancements in the field of biologics manufacturing. The strategies involved are not limited to the development of cellular proteomics- and metabolomics-based optimized insect cell medium formulation, nutrient cocktail or AAV titer enhancer formulations. Moreover, a detailed understanding of the critical process parameters guided by the critical quality attributes of AAV serotype therapeutic products is crucial for a robust manufacturing process.

The high-cell density upstream process should be designed with consideration of downstream processing. AAV is an inherently intracellular product and the primary recovery step involves cell lysis and release of intracellular AAVs in lysis buffer [110]. In high cell density cultures, the removal of co-extracted cellular components (host cell genome, proteins, and other components) released upon cell lysis exerts a significant burden on downstream processing. It would be appealing to study if the AAV capsids can be modified, without altering the functionality, to direct AAV

secretion in cell-culture supernatant to continuously recover them with minimum contamination of intracellular impurities.

Another futuristic approach is the development of a producer insect cell line that constitutively integrates and inducibly expresses all the genes necessary, including baculovirus helper functions, AAV proteins, and AAV vector production, using an alternative inducible system(s) not requiring baculovirus superinfection [111–113]. The Sf9 genome was published recently [114] and CRISPR-mediated knockout of genes expressing viral restriction factors in insect cells or targeted integration of AAV genes in the transcriptionally active regions of the insect cell genome are attractive strategies for producer cell-line generation. These strategies, combined with high-viability insect-cell cultures as discussed above, can be used to design a semi-continuous perfusion process that facilitates ultra-high cell density. Such a process may offer a significantly higher volumetric yield of AAV enabling a large amount of vector generation, even at a small-scale cGMP facility with reduced frequency of production runs.

3.7 Summary and Conclusion

Supported by sustained efforts in baculovirus and insect-cell engineering, the IC-BEVS platform has undergone significant improvements to produce AAV vectors with better yield, quality and process simplicity. Although the key understanding of AAV production in insect cells was based on the original Three-Bac system, more advanced and simplified versions, including Two-Bac and One-Bac, are being adopted for large-scale AAV production, accommodating and continuously improving the existing Three-Bac manufacturing process. Moreover, the emergence of novel process monitoring technologies and continuous improvements in process intensification strategies with demonstrated success in other eukaryotic expression platforms (e.g., CHO cell line)

also presents a futuristic direction for AAV manufacturing. In conclusion, due to increased regulatory acceptance, ease of scale-up, and recent advancements in production technologies, insect cell baculovirus systems are being more broadly adopted for the production of multiple AAV serotypes (**Table 3.1**). As a result, more insect cell-produced AAV vectors can be expected in clinical trials in the future.

3.8 Acknowledgments

P.R.H.J. is financially supported through a grant from the Natural Sciences and Engineering Research Council (NSERC RGPIN-2015-05132) of the government of Canada. A.A.K. is a recipient of a Canada Research Chair (CRC/240394).

3.9 Conflict of interest

The authors declare no financial or commercial conflicts of interest.

3.10 References

[1] Gaw, Z. Y., Liu, N. T., Zia, T. U. (1959). Tissue culture methods for cultivation of virus grasserie. Acta. Virol., 3, 55-60.

[2] Vail, P. V., Sutter, G., Jay, D. L., Gough, D. (1971). Reciprocal infectivity of nuclear polyhedrosis viruses of the cabbage looper and alfalfa looper. J. Invertebr. Pathol., 17(3), 383-388.

[3] Kool, M., Vlak, J. M. (1993). The structural and functional organization of the Autographa californica nuclear polyhedrosis virus genome. Arch. Virol., 130(1-2), 1-16.

[4] Summers, M. D. (2006). Milestones leading to the genetic engineering of baculoviruses as expression vector systems and viral pesticides. Adv. Virus. Res., 68, 3-73.

[5] Smith, G. E., Summers, M. D., Fraser, M. J. (1983). Production of human beta interferon in insect cells infected with a baculovirus expression vector. Mol. Cell. Biol., 3(12), 2156-2165.

[6] Smith, G. E., Ju, G., Ericson, B. L., Moschera, J., Lahm, H. W., Chizzonite, R., Summers, M. D. (1985). Modification and secretion of human interleukin 2 produced in insect cells by a baculovirus expression vector. Proc. Natl. Acad. Sci. U.S.A., 82(24), 8404-8408.

[7] Kuzio, J., Rohel, D. Z., Curry, C. J., Krebs, A., Carstens, E. B., Faulkner, P. (1984). Nucleotide sequence of the p10 polypeptide gene of Autographa californica nuclear polyhedrosis virus. Virology, 139(2), 414-418.

[8] Kirnbauer, R., Booy, F., Cheng, N., Lowy, D. R., Schiller, J. T. (1992). Papillomavirus L1 major capsid protein self-assembles into virus-like particles that are highly immunogenic. Proc. Natl. Acad. Sci. U.S.A., 89(24), 12180-12184.

[9] Wickham, T. J., Davis, T., Granados, R. R., Shuler, M. L., Wood, H. A. (1992). Screening of insect cell lines for the production of recombinant proteins and infectious virus in the baculovirus expression system. Biotechnol. Prog., 8(5), 391-396.

[10] Felberbaum, R. S. (2015). The baculovirus expression vector system: A commercial manufacturing platform for viral vaccines and gene therapy vectors. Biotechnol. J., 10(5), 702-714.

[11] Buckland, B., Boulanger, R., Fino, M., Srivastava, I., Holtz, K., Khramtsov, N., ... and Cox, M. M. (2014). Technology transfer and scale-up of the Flublok® recombinant hemagglutinin (HA) influenza vaccine manufacturing process. Vaccine, 32(42), 5496-5502.

[12] van Oers, M. M., Pijlman, G. P., Vlak, J. M. (2015). Thirty years of baculovirus–insect cell protein expression: from dark horse to mainstream technology. J. Gen. Virol., 96(1), 6-23.

[13] Bruinzeel, W., Yon, J., Giovannelli, S., Masure, S. (2002). Recombinant insect cell expression and purification of human β-secretase (BACE-1) for X-ray crystallography. Protein. Expr. Purif., 26(1), 139-148.

[14] Granados, R. R., Li, G., Blissard, G. W. (2007). Insect cell culture and biotechnology. Virol. Sin., 22(2), 83-93.

[15] Krammer, F., Nakowitsch, S., Messner, P., Palmberger, D., Ferko, B., Grabherr, R. (2010). Swine-origin pandemic H1N1 influenza virus-like particles produced in insect cells induce hemagglutination inhibiting antibodies in BALB/c mice. Biotechnol. J., 5(1), 17-23.

[16] Rendić, D., Wilson, I. B., Paschinger, K. (2008). The glycosylation capacity of insect cells. Croat. Chem. Acta., 81(1), 7-21.

[17] Wilde, M., Klausberger, M., Palmberger, D., Ernst, W., Grabherr, R. (2014). Tnao38, high five and Sf9-evaluation of host–virus interactions in three different insect cell lines:

baculovirus production and recombinant protein expression. Biotechnol. Lett., 36(4), 743-749.
[18] Cervarix. Human papillomavirus vaccine Type 16 and 18 (Recombinant, AS04 adjuvanted), Suspension for injection, Active immunizing agent, ATC code: J07BMO2. GlaxoSmithKline Inc. 2019.
[19] Assessment Report. Glybera. European Medicines Agency. EMA/882900/2011. Committee for medicinal products for human use. 2012.
[20] Kamen, A. A., Bédard, C., Tom, R., Perret, S., Jardin, B. (1996). On-line monitoring of respiration in recombinant-baculovirus infected and uninfected insect cell bioreactor cultures. Biotechnol. Bioeng., 50(1), 36-48.
[21] Kamen, A. A., Tom, R. L., Caron, A. W., Chavarie, C., Massie, B., Archambault, J. (1991). Culture of insect cells in helical ribbon impeller bioreactor. Biotechnol. Bioeng., 38(6), 619-628.
[22] Kamen, A. A., Chavarie, C., Andre, G., Archambault, J. (1992). Design parameters and performance of a surface baffled helical ribbon impeller bioreactor for the culture of shear sensitive cells. Chem. Eng. Sci., 47(9-11), 2375-2380.
[23] Maranga, L., Cunha, A., Clemente, J., Cruz, P., Carrondo, M. J. (2004). Scale-up of virus-like particles production: effects of sparging, agitation and bioreactor scale on cell growth, infection kinetics and productivity. J. Biotechnol., 107(1), 55-64.
[24] Mena, J. A., Kamen, A. A. (2011). Insect cell technology is a versatile and robust vaccine manufacturing platform. Expert. Rev. Vaccines, 10(7), 1063-1081.
[25] Desrosiers, R., Clark, E., Tremblay, D., Tremblay, R., Polson, D. (2009). Use of a one-dose subunit vaccine to prevent losses associated with porcine circovirus type 2. J. Swine. Health. Prod., 17(3), 148-154.
[26] Harper, D. M. (2008). Impact of vaccination with Cervarix™ on subsequent HPV-16/18 infection and cervical disease in women 15–25 years of age. Gynecol. Oncol., 110(3), S11-S17.
[27] Ylä-Herttuala, S. (2012). Endgame: glybera finally recommended for approval as the first gene therapy drug in the European union. Mol. Ther., 20(10), 1831-1832.
[28] AAV5-hFVIII-SQ (BMN 270). Annex III A. BioMarin Pharmaceutical Inc. 2017.
[29] Kailasan, S., Agbandje-McKenna, M., Parrish, C. R. (2015). Parvovirus family conundrum: what makes a killer? Annu. Rev. Virol., 2, 425-450.
[30] Ruffing, M., Zentgraf, H., Kleinschmidt, J. A. (1992). Assembly of viruslike particles by recombinant structural proteins of adeno-associated virus type 2 in insect cells. J. Virol., 66(12), 6922-6930.
[31] Urabe, M., Ding, C., Kotin, R. M. (2002). Insect cells as a factory to produce adeno-associated virus type 2 vectors. Hum. Gene. Ther., 13(16), 1935-1943.
[32] Srivastava, A., Lusby, E. W., Berns, K. I. (1983). Nucleotide sequence and organization of the adeno-associated virus 2 genome. J. Virol., 45(2), 555-564.
[33] Kohlbrenner, E., Aslanidi, G., Nash, K., Shklyaev, S., Campbell-Thompson, M., Byrne, B. J., ... and Zolotukhin, S. (2005). Successful production of pseudotyped rAAV vectors using a modified baculovirus expression system. Mol. Ther., 12(6), 1217-1225.
[34] Urabe, M., Nakakura, T., Xin, K. Q., Obara, Y., Mizukami, H., Kume, A., ... and Ozawa, K. (2006). Scalable generation of high-titer recombinant adeno-associated virus type 5 in insect cells. J. Virol., 80(4), 1874-1885.
[35] Smith, R. H., Levy, J. R., Kotin, R. M. (2009). A simplified baculovirus-AAV expression

vector system coupled with one-step affinity purification yields high-titer rAAV stocks from insect cells. Mol. Ther., 17(11), 1888-1896.
[36] Chen, H. (2008). Intron splicing–mediated expression of AAV Rep and Cap genes and production of AAV vectors in insect cells. Mol. Ther., 16(5), 924-930.
[37] L. Galibert, O-W. Merten, A. Jacob (Genethon), US 2018/0305717 A1, 2018.
[38] Aslanidi, G., Lamb, K., Zolotukhin, S. (2009). An inducible system for highly efficient production of recombinant adeno-associated virus (rAAV) vectors in insect Sf9 cells. Proc. Natl. Acad. Sci. U.S.A., 106(13), 5059-5064.
[39] Galibert, L., Merten, O. W. (2011). Latest developments in the large-scale production of adeno-associated virus vectors in insect cells toward the treatment of neuromuscular diseases. J. Inverterb. Pathol., 107, S80-S93.
[40] Merten, O. W. (2016). AAV vector production: state of the art developments and remaining challenges. Cell. Gene. Ther. Insights, 2(5), 521-551.
[41] W. T. Johannes, M. C. Hermens, S. J. K. Haast, D. J. Biesmans, A. C. Bakker (uiQure IP B.V.) US 2017/0152525 A1, 2017.
[42] Savy, A., Kaikkonen, M. U., Léger, A., Dickx, Y., Galibert, L., Merten, O. W. (2018). Genetics instability of wtAAV2 genome and AAV promoter activities in the Baculovirus/Sf9 cells system. PloS One, 13(7), e0199866.
[43] Joshi, P. R., Cervera, L., Ahmed, I., Kondratov, O., Zolotukhin, S., Schrag, J., ... and Kamen, A. A. (2019). Achieving high-yield production of functional AAV5 gene delivery vectors via fedbatch in an insect cell-one baculovirus system. Mol. Ther. Methods. Clin. Dev., 13, 279-289.
[44] Girod, A., Wobus, C. E., Zádori, Z., Ried, M., Leike, K., Tijssen, P., ... and Hallek, M. (2002). The VP1 capsid protein of adeno-associated virus type 2 is carrying a phospholipase A2 domain required for virus infectivity. J. Gen. Virol., 83(5), 973-978.
[45] Grieger, J. C., Snowdy, S., Samulski, R. J. (2006). Separate basic region motifs within the adeno-associated virus capsid proteins are essential for infectivity and assembly. J. Virol., 80(11), 5199-5210.
[46] Kozak, M. (1986). Point mutations define a sequence flanking the AUG initiator codon that modulates translation by eukaryotic ribosomes. Cell, 44(2), 283-292.
[47] Kozak, M. (1999). Initiation of translation in prokaryotes and eukaryotes. Gene, 234(2), 187-208.
[48] Bosma, B., du Plessis, F., Ehlert, E., Nijmeijer, B., de Haan, M., Petry, H., Lubelski, J. (2018). Optimization of viral protein ratios for production of rAAV serotype 5 in the baculovirus system. Gene. Ther., 25(6), 415-424.
[49] Mietzsch, M., Grasse, S., Zurawski, C., Weger, S., Bennett, A., Agbandje-McKenna, M., ... and Heilbronn, R. (2014). OneBac: platform for scalable and high-titer production of adeno-associated virus serotype 1–12 vectors for gene therapy. Hum. Gene Ther., 25(3), 212–222.
[50] Mietzsch, M., Casteleyn, V., Weger, S., Zolotukhin, S., Heilbronn, R. (2015). OneBac 2.0: Sf9 cell lines for production of AAV5 vectors with enhanced infectivity and minimal encapsidation of foreign DNA. Hum. Gene. Ther., 26(10), 1-24.
[51] Kondratov, O., Marsic, D., Crosson, S. M., Mendez-Gomez, H. R., Moskalenko, O., Mietzsch, M., ...and Zolotukhin, S. (2017). Direct head-to-head evaluation of recombinant adeno-associated viral vectors manufactured in human versus insect cells. Mol. Ther., 25(12), 2661-2675.
[52] Galibert, L., Savy, A., Dickx, Y., Bonnin, D., Bertin, B., Mushimiyimana, I., ... and Merten,

O. W. (2018). Origins of truncated supplementary capsid proteins in rAAV8 vectors produced with the baculovirus system. PloS One, 13(11), e0207414.
[53] Cecchini, S., Slack, J., Maranga, L. (2020). Engineering of 5 ' UTR to control the expression and incorporation level of VP1 during rAAV vector production using a baculovirus system. ASGCT 23rd Annual Meeting.
[54] Bryant, L. M., Christopher, D. M., Giles, A. R., Hinderer, C., Rodriguez, J. L., Smith, J. B., ... and Wilson, J. M. (2013). Lessons learned from the clinical development and market authorization of Glybera. Hum. Gene Ther. Clin. Dev., 24(2), 55-64.
[55] Wright, J. F. (2008). Manufacturing and characterizing AAV-based vectors for use in clinical studies. Gene. Ther., 15(11), 840-848.
[56] Savy, A., Dickx, Y., Nauwynck, L., Bonnin, D., Merten, O. W., Galibert, L. (2017). Impact of inverted terminal repeat integrity on rAAV8 production using the baculovirus/Sf9 cells system. Hum. Gene. Ther. Methods, 28(5), 277-289.
[57] Jacob, A., Brun, L., Gil, P. J., Ménard, L., Bouzelha, M., Broucque, F., ... and François, A. (2020). Homologous recombination offers advantages over transposition-based systems to generate recombinant baculovirus for adeno-associated viral vector production. Biotechnol. J. DOI: 10.1002/biot.202000014.
[58] Hu, Y. C., Bentley, W. E. (2001). Effect of MOI ratio on the composition and yield of chimeric infectious bursal disease virus-like particles by baculovirus co-infection: Deterministic predictions and experimental results. Biotechnol. Bioeng., 75(1), 104-119.
[59] Jiang, B., Barniak, V., Smith, R. P., Sharma, R., Corsaro, B., Hu, B., Madore, H. P. (1998). Synthesis of rotavirus-like particles in insect cells: Comparative and quantitative analysis. Biotechnol. Bioeng., 60(3), 369-374.
[60] Palomares, L. A., López, S., Ramírez, O. T. (2002). Strategies for manipulating the relative concentration of recombinant rotavirus structural proteins during simultaneous production by insect cells. Biotechnol. Bioeng., 78(6), 635-644.
[61] Mena, J. A., Ramírez, O. T., Palomares, L. A. (2006). Intracellular distribution of rotavirus structural proteins and virus-like particles expressed in the insect cell-baculovirus system. J. Biotechnol., 122(4), 443-452.
[62] Rosinski, M., Reid, S., Nielsen, L. K. (2002). Kinetics of baculovirus replication and release using real-time quantitative polymerase chain reaction. Biotechnol. Bioeng., 77(4), 476-480.
[63] Meghrous, J., Aucoin, M. G., Jacob, D., Chahal, P. S., Arcand, N., Kamen, A. A. (2005). Production of recombinant adeno-associated viral vectors using a baculovirus/insect cell suspension culture system: From shake flasks to a 20-L bioreactor. Biotechnol. Prog., 21, 154-160.
[64] Mena, J. A., Ramírez, O. T., Palomares, L. A. (2007). Population kinetics during simultaneous infection of insect cells with two different recombinant baculoviruses for the production of rotavirus-like particles. BMC. Biotechnol., 7(1), 1-11.
[65] Kotin, R. M., Snyder, R. O. (2017). Manufacturing clinical grade recombinant adeno-associated virus using invertebrate cell lines. Hum. Gene. Ther., 28(4), 350-360.
[66] King, J. A., Dubielzig, R., Grimm, D., Kleinschmidt, J. A. (2001). DNA helicase-mediated packaging of adeno-associated virus type 2 genomes into preformed capsids. EMBO. J., 20(12), 3282–3291.
[67] Collaco, R. F., Kalman-Maltese, V., Smith, A. D., Dignam, J. D., Trempe, J. P. (2003). A biochemical characterization of the adeno-associated virus Rep40 helicase. J. Biol.,

278(36), 34011-34017.
[68] Mena, J. A., Aucoin, M. G., Montes, J., Chahal, P. S., Kamen, A. A. (2010). Improving adeno-associated vector yield in high density insect cell cultures. J. Gene. Med., 12(2), 157-167.
[69] Thompson, C. M., Petiot, E., Mullick, A., Aucoin, M. G., Henry, O., Kamen, A. A. (2015). Critical assessment of influenza VLP production in Sf9 and HEK293 expression systems. BMC Biotechnol., 15(1), 31.
[70] Kiesslich, S., Losa, J. P. V. C., Gélinas, J. F., Kamen, A. A. (2020). Serum-free production of rVSV-ZEBOV in Vero cells: Microcarrier bioreactor versus scale-X™ hydro fixed-bed. J. Biotechnol., 310, 32-39.
[71] Negrete, A., Yang, L. C., Mendez, A. F., Levy, J. R., Kotin, R. M. (2007). Economized large-scale production of high yield of rAAV for gene therapy applications exploiting baculovirus expression system. J. Gene. Med., 9(11), 938-948.
[72] Aucoin, M. G., Perrier, M., Kamen, A. A. (2006). Production of adeno-associated viral vectors in insect cells using triple infection: Optimization of baculovirus concentration ratios. Biotechnol. Bioeng., 95(6), 1081-1092.
[73] Kool, M., Voncken, J. W., Van Lier, F. L. J., Tramper, J., Vlak, J. M. (1991). Detection and analysis of Autographa californica nuclear polyhedrosis virus mutants with defective interfering properties. Virology, 183(2), 739-746.
[74] Bernal, V., Carinhas, N., Yokomizo, A. Y., Carrondo, M. J., Alves, P. M. (2009). Cell density effect in the baculovirus-insect cells system: A quantitative analysis of energetic metabolism. Biotechnol. Bioeng., 104(1), 162-180.
[75] Elias, C. B., Zeiser, A., Bédard, C., Kamen, A. A. (2000). Enhanced growth of sf-9 cells to a maximum density of 5.2×10^7 cells per mL and production of β-galactosidase at high cell density by fed batch culture. Biotechnol. Bioeng., 68(4), 381-388.
[76] Cecchini, S., Virag, T., Kotin, R. M. (2011). Reproducible high yields of recombinant adeno-associated virus produced using invertebrate cells in 0.02-to 200-liter cultures. Hum. Gene. Ther., 22(8), 1021-1030.
[77] Liu, Y. K., Yang, C. J., Liu, C. L., Shen, C. R., Shiau, L. D. (2010). Using a fed-batch culture strategy to enhance rAAV production in the baculovirus/insect cell system. J. Biosci. Bioeng., 110(2), 187-193.
[78] Cain, K. D., Byrne, K. M., Brassfield, A. L., LaPatra, S. E., Ristow, S. S. (1999). Temperature dependent characteristics of a recombinant infectious hematopoietic necrosis virus glycoprotein produced in insect cells. Dis. Aquat. Organ., 36(1), 1-10.
[79] Donaldson, M., Wood, H. A., Kulakosky, P. C., Shuler, M. L. (1999). Glycosylation of a recombinant protein in the Tn5B1-4 insect cell line: Influence of ammonia, time of harvest, temperature, and dissolved oxygen. Biotechnol. Bioeng., 63(3), 255-262.
[80] Hara, T., Nonaka, K., Kawaguchi, H., Ogata, S., Etou, N. (1993). Effects of temperature on Escherichia coli β-galactosidase expression in baculovirus-insect cell system. Biosci. Biotechnol. Biochem., 57(6), 996-997.
[81] Reuveny, S., Kim, Y. J., Kemp, C. W., Shiloach, J. (1993). Effect of temperature and oxygen on cell growth and recombinant protein production in insect cell cultures. Appl. Microbiol. Biotechnol., 38(5), 619-623.
[82] Aucoin, M. G., Perrier, M., Kamen, A. A. (2007). Improving AAV vector yield in insect cells by modulating the temperature after infection. Biotechnol. Bioeng., 97(6), 1501-1509.
[83] Negrete, A., Kotin, R. M. (2007). Production of recombinant adeno-associated vectors using

two bioreactor configurations at different scales. J. Virol. Methods, 145(2), 155-161.
[84] Negrete, A., Esteban, G., Kotin, R. M. (2007). Dielectric Spectroscopy monitoring for optimum harvest time determination during large-scale production of recombinant adeno-associated vectors. Appl. Microbiol. Biotechnol., 76(6), 761-772.
[85] Pais, D. A., Galrão, P. R., Kryzhanska, A., Barbau, J., Isidro, I. A., Alves, P. M. (2020). Holographic Imaging of Insect Cell Cultures: Online Non-Invasive Monitoring of Adeno-Associated Virus Production and Cell Concentration. Processes, 8(4), 487.
[86] Bosma, B., du Plessis, F., Sanders, B., S. van Dveventer, A., J. Lubelski. (2020). Generation of a DuoBac expression system for improved AAV production. ASGCT 23rd Annual Meeting.
[87] Horowitz, E. D. (2020). Biophysical and in-vitro comparability analysis of an AAV vector produced by the baculovirus/Sf9 system and HEK triple transfection system. ASGCT 23rd Annual Meeting.
[88] Wu, Y., Mei, T., Jiang, L., Han, Z., Dong, R., Yang, T., Xu, F. (2019). Development of Versatile and Flexible Sf9 Packaging Cell Line-Dependent OneBac System for Large-Scale Recombinant Adeno-Associated Virus Production. Hum. Gene. Ther. Methods., 30(5), 172-183.
[89] Pesic, M., Ahamed, T., Golinska, M., Lubelski. J. (2020). Production of recombinant AAV vectors in chemically defined media. ASGCT 23rd Annual Meeting.
[90] Thompson, K., Bundy, M., Irvin, K., Yocheva, M., Barnes, M., van den Berg, A., ... and Zmuda, J. (2020). Recombinant adeno-associated virus (AAV) production in the ExpiSf™ expression system. ASGCT 23rd Annual Meeting.
[91] J. Kurasawa, A. Park, C. Sowers, R. Halpin, A. Tovchigrechko, C. Dobson, A. Schmelzer, C. Gao, S. Wilson, Y. Ikeda. (2020). Chemically-defined, high-density insect cell-based expression system for scalable AAV vector production. ASGCT 23rd Annual Meeting.
[92] Jacques, J., Jones, A., Xing, D., Low, K., Bossie, A. (2020). Evaluation of AAV production in insect cells using chemically defined media. ASGCT 23rd Annual Meeting.
[93] Rumachik, N. G., Malaker, S. A., Poweleit, N., Maynard, L. H., Adams, C. M., Leib, R. D., ... and Sinn, P. (2020). Methods Matter--Standard Production Platforms for Recombinant AAV Produce Chemically and Functionally Distinct Vectors. Mol. Ther. Methods. Clin. Dev., 18, 98-118.
[94] Grieger, J. C., Soltys, S. M., Samulski, R. J. (2016). Production of recombinant adeno-associated virus vectors using suspension HEK293 cells and continuous harvest of vector from the culture media for GMP FIX and FLT1 clinical vector. Mol. Ther., 24(2), 287-297.
[95] Martin, J., Frederick, A., Luo, Y., Jackson, R., Joubert, M., Sol, B., ... and Vincent, K. (2013). Generation and characterization of adeno-associated virus producer cell lines for research and preclinical vector production. Hum. Gene. Ther. Methods, 24(4), 253-269.
[96] Thorne, B. A., Takeya, R. K., Peluso, R. W. (2009). Manufacturing recombinant adeno-associated viral vectors from producer cell clones. Hum.Gene. Ther., 20(7), 707-714.
[97] Zeltner, N., Kohlbrenner, E., Clément, N., Weber, T., Linden, R. M. (2010). Near-perfect infectivity of wild-type AAV as benchmark for infectivity of recombinant AAV vectors. Gene. Ther., 17(7), 872-879.
[98] Geoffroy, M. C., Salvetti, A. (2005). Helper functions required for wild type and recombinant adeno-associated virus growth. Curr. Gene Ther., 5(3), 265-271.
[99] Meier, A. F., Fraefel, C., Seyffert, M. (2020). The Interplay between Adeno-Associated Virus and Its Helper Viruses. Viruses, 12(6), 662.

[100] Tai, P. W. (2020). ITRs: The terminal frontier. Hum. Gene Ther., 31(3-4), 143-144.
[101] Ma, H., Galvin, T. A., Glasner, D. R., Shaheduzzaman, S., Khan, A. S. (2014). Identification of a novel rhabdovirus in Spodoptera frugiperda cell lines. J. virol., 88(12), 6576-6585.
[102] Maghodia, A. B., Geisler, C., Jarvis, D. L. (2016). Characterization of an Sf-rhabdovirus-negative Spodoptera frugiperda cell line as an alternative host for recombinant protein production in the baculovirus-insect cell system. Protein Expr. Purif., 122, 45-55.
[103] Li, T. C., Scotti, P. D., Miyamura, T., Takeda, N. (2007). Latent infection of a new alphanodavirus in an insect cell line. J. Virol., 81(20), 10890-10896.
[104] Maghodia, A. B., & Jarvis, D. L. (2017). Infectivity of Sf-rhabdovirus variants in insect and mammalian cell lines. Virology, 512, 234-245.
[105] Maghodia, A. B., Geisler, C., Jarvis, D. L. (2020). A new nodavirus-negative Trichoplusia ni cell line for baculovirus-mediated protein production. Biotechnol. Bioeng., 117(11), 3248-3264.
[106] Cecchini, S., Negrete, A., Kotin, R. M. (2008). Toward exascale production of recombinant adeno-associated virus for gene transfer applications. Gene. Ther., 15(11), 823-830.
[107] Steele, K. H., Stone, B. J., Franklin, K. M., Fath-Goodin, A., Zhang, X., Jiang, H., ... and Geisler, C. (2017). Improving the baculovirus expression vector system with vankyrin-enhanced technology. Biotechnol. Prog., 33(6), 1496-1507.
[108] Gómez-Sebastián, S., López-Vidal, J., Escribano, J. M. (2014). Significant productivity improvement of the baculovirus expression vector system by engineering a novel expression cassette. PLoS One, 9(5), e96562.
[109] Kaba, S. A., Salcedo, A. M., Wafula, P. O., Vlak, J. M., van Oers, M. M. (2004). Development of a chitinase and v-cathepsin negative bacmid for improved integrity of secreted recombinant proteins. J. Virol. Methods, 122(1), 113-118.
[110] Chahal, P. S., Aucoin, M. G., Kamen, A. (2007). Primary recovery and chromatographic purification of adeno-associated virus type 2 produced by baculovirus/insect cell system. J. Virol. Methods, 139 (1), 61-70.
[111] Hegedus, D. D., Pfeifer, T. A., Hendry, J., Theilmann, D. A., Grigliatti, T. A. (1998). A series of broad host range shuttle vectors for constitutive and inducible expression of heterologous proteins in insect cell lines. Gene, 207(2), 241-249.
[112] Pfeifer, T. A. (1998). Expression of heterologous proteins in stable insect cell culture. Curr. Opin. Biotechnol., 9(5), 518-521.
[113] Kempf, J., Snook, L. A., Vonesch, J. L., Dahms, T. E., Pattus, F., Massotte, D. (2002). Expression of the human μ opioid receptor in a stable Sf9 cell line. J. Biotechnol., 95(2), 181-187.
[114] Nandakumar, S., Ma, H., Khan, A. S. (2017). Whole-genome sequence of the Spodoptera frugiperda Sf9 insect cell line. Genome. Announc., 5(34), e00829-17.

Achieving High-yield Production of Functional AAV5 Gene Delivery Vectors via Fedbatch in Insect cell/One Baculovirus System

Preamble

Cell culture process development is the first step after the design and molecular engineering of the suitable insect-cell baculovirus system for AAV production. This chapter focuses on the cell culture process development achieving high-yield volumetric production of AAV5 vectors in IC-BEVS. Various strategies for high-yield AAV5 production including optimization of multiplicity of baculovirus infection, cell -density at the time of infection, and high-cell density fedbatch production culture were tested to achieve the volumetric yield exceeding $2x10^{14}$ VG/L of cell culture. Under optimal cell culture process conditions, sustained cell-specific yield and product quality characteristics were reported which were consistent with the current state of the art in the field. Moreover, this study establishes the recent modification of One-Bac platform, as a suitable system for large-scale AAV vector production. The supplemental data associated with this chapter are provided in the **appendix, 9.1** (**Page number 204-216**).

Chapter 4 Achieving High-Yield Production of Functional AAV5 Gene Delivery Vectors via Fedbatch in Insect cell/One Baculovirus System

Pranav R.H. Joshi[1], Laura Cervera[1], Ibrahim Ahmed[1], Oleksandr Kondratov[2], Sergei Zolotukhin[2], Joseph Schrag[3], Parminder Singh Chahal[3], Amine Kamen[1]*

[1] Viral Vectors and Vaccine bioprocessing group, Department of Bioengineering, McGill University, Montreal, Quebec, H2X 1Y4, Canada.

[2] Department of Pediatrics, University of Florida College of Medicine, Gainesville, FL 32610, USA.

[3] Human Health Therapeutics portfolio, National Research Council of Canada, Montreal, Quebec, H4P 2R2, Canada.

* Correspondence should be addressed to Amine Kamen (amine.kamen@mcgill.ca)
Department of Bioengineering, McGill University.

Short title: High cell density AAV5 production using One Bac 2.0+

Published in "**Molecular therapy: methods and clinical development**"

Abstract

Despite numerous advancements in production protocols, manufacturing AAV to meet exceptionally high demand (10^{16}-10^{17} VGs) in late clinical stages and eventually systemic delivery poses significant challenges. Here, we report an efficient, simple, scalable and robust AAV5 production process utilizing the most recent modification of the One-Bac platform. An increase in volumetric yield of genomic particles by ~ 6-fold and functional particles by ~ 20-fold was achieved operating a high cell density process in shake flasks and bioreactors that involves Sf9-based *rep/cap* stable cell line grown at a density of about 10 million cells/mL infected with a single baculovirus. The overall volumetric yields of genomic (VG) and bioactive particles (ETU) in representative fedbatch bioreactor runs ranged from 2.5 to 3.5x10^{14} VG/L and 1 to 2x10^{11} ETU/L respectively. Analytical ultracentrifugation analyses of affinity-purified AAV vector samples from a side by side batch and fedbatch production runs show vector preparations with a full/empty particle distribution of 20-30% genomic and 70-80% empty particles. Moreover, the stoichiometric analysis of capsid proteins from fedbatch production in shake flask and bioreactor run samples demonstrates the incorporation of higher VP1 subunits resulting in better functionality.

4.1 Introduction

Recombinant adeno-associated virus (rAAV) has emerged as one of the versatile vectors for therapeutic gene delivery in both dividing and non-dividing cells for the treatment of monogenic disease conditions.[1,2] The regulatory approval of Glybera® by the European Medicines Agency (EMA) in 2012 for lipoprotein lipase deficiency[3] and recent approval of Luxturna™ by the USFDA and EMA for the treatment of hereditary retinal dystrophy are two key milestones in the AAV-based gene therapy field.

Extensive research and sustained efforts have been dedicated to the development of various production platforms to deliver large quantities of functional AAV vectors. Traditional methods of AAV production involve 2-D cell culture processes where adherent mammalian cell lines are transiently transfected with plasmids carrying all the necessary genes along with co-infection of a helper virus.[4–9] The latter was eventually replaced with a plasmid carrying helper functions. Restricted scalability of this system led to the development of a production method based on a suspension-adapted mammalian cell line in combination with transient transfection[10] or recombinant herpes simplex virus-based infection for delivery of necessary genes. Although very promising, these systems faced challenges associated with a lower volumetric yield.[10,11] Further work involving alternative modes of cell cultivation and advancement in the processing led to the improvement of these expression systems.[12–15]

The first report of rAAV production in *Spodoptera frugiperda* insect cells (Sf9) using triple *Autographa californica* multiple nuclear polyhedrosis baculovirus infections (Three-Bac) brought about a new excitement in the field of scalable AAV production.[16] This system offered comparable per cell yield of AAV and the possibility of enhanced volumetric yields due to the ability of Sf9 cells to grow at a high cell density in a suspension culture. This original system was further improved addressing its key shortcomings and followed after were 2Bac and One Bac, more

simpler systems.[17–21] The recently reported One Bac has only two components: an inducible and stable Sf9-based packaging cell line incorporating integrated copies of *rep* and *cap* genes, and a baculovirus carrying a Bac-rAAV cassette (One-Bac). This system was further improved to achieve optimal VP composition and functionality in AAV5 and AAV9 vectors comparable to vector produced in the mammalian platform. This recent improvement also demonstrated minimized encapsidation of foreign DNA in the vector particle.[22,23]

Although serotype-dependent compared to 2Bac and 3Bac, the One Bac system studied in this manuscript essentially provides an efficient packaging cell line and presents advantages for large-scale manufacturing of an AAV delivery system with serotype 5 because of the relative simplicity of operation from a process standpoint. Generating a stable cell line and establishing a master cell bank for manufacturing clinical grade material require a significant undertaking. More generally, in the context of manufacturing of biologics, primary work has relied on transient expression, followed thereafter by stable expression systems. In the case of viral vectors, the transient expression systems, packaging cell lines and producing cell lines are scenarios that might be considered depending on the viral product characteristics and end use. We believe that the stable cell line approach has the potential to be a preferable platform for a well-established and clinically proven vector candidates such as AAV5, and AAV9.

Aligned with our continuing efforts to improving AAV manufacturing platforms, in this report, we have further explored the One Bac system from a process standpoint for AAV5 fedbatch production mode focusing solely on the upstream process phase. The consistency of the production process was assessed in shake flask and was further validated in a 1L, and 3L controlled bioreactor runs. The purified AAV was characterized for its quality attributes including *in vitro* functionality,

capsid protein composition and relative proportion of empty and genomic particles in affinity-purified AAV preparations.

4.2 Results

4.2.1 Genetic stability of the packaging cell line and *Rep/Cap* copy number analysis

During a traditional commercial scale production, the cells undergo numerous doubling cycles, and any loss of expression of integrated *rep/cap* genes can result in lower yields and hence it is important to assess their expression stability over the extended passage numbers. The working cell bank of given packaging cells was at passage number 3 (P3). The cells were infected at various passage numbers: P4 (vial thaw+1), P8 (vial thaw+5), and P35 (vial thaw+32) at a multiplicity of infection (MOI) of 1 pfu/cell. The clarified cell lysate containing Cap and Rep proteins was analyzed by Western blot, the results of which are shown in **supplemental data, Figure S1**. The data show no significant loss of expression with either of the proteins. Furthermore, the same clarified lysate samples were analyzed for total viral genome copies (VG) via quantitative polymerase chain reaction (qPCR). The cell-specific yield in all three samples is around 15000 VG/cell. This VG shows no passage dependent loss of cell-specific yield in *rep2cap5* packaging cell line suggesting stable expression of the AAV helper genes up to 35 passages. It should be noted that this preliminary set of experiments was conducted in an early phase of the project under non-optimal conditions of MOI and the cell density at the time of infection. The Sf9 cell line (B8 clone) was found to have 9.97 copies of *cap5* and 1.25 copies of *rep2* integrated per cell (**Table 4.3**).

4.2.2 AAV production culture characteristics

In the present study, we investigate AAV production using regular and high cell density culture. For ease of understanding throughout the paper, the regular cell density and high cell density production processes are referred to as batch and fedbatch processes (modes) respectively. Also respectively, in the batch and fedbatch processes, cells were infected at low cell density and high cell densities. In the latter case, the cultures in pre- and post-infection phases are supplemented with an additional nutrient feed which has been reported on several occasions by research groups.[24–26] The cell density and viability profiles during AAV production in batch (triplicate shake flasks runs) and fedbatch (triplicate shake flasks and bioreactor runs) modes are shown in Figure 4.1A. In both modes, the cells were infected in their mid-exponential growth phase which is followed by a characteristic baculovirus induced cell growth arrest and protein expression phase. Preliminary experiments were conducted to screen the suitable cell density at the time of infection and the multiplicity of infection in the low cell density process. The findings suggested that 1.2-1.4 million cells/mL is a suitable cell density for infection and the MOI of 3 pfu/cell gives higher cell-specific yield (data not shown). Any combination of cell density and MOI that results in an overall cell density above 2-2.5 million cells/mL during AAV production results in reduced cell-specific and volumetric yield. This can be due to culture medium limitation and its inability to support protein expression in the post-infection phase. Similar work was conducted for AAV production in fedbatch mode for preliminary screening (supplemental data, Figure S2). In batch mode, when cells were infected at a cell density around 1.2-1.4 million cells/mL, cells density increased to 1.5-1.7 million cells/mL within 24 hpi followed by progressive decline in cell density and cell viability. Similarly, in the high cell density process (fedbatch mode), the cells were infected at 9.5-10 million cells/mL, and the cell density increased to 10.5-11 million cells/mL

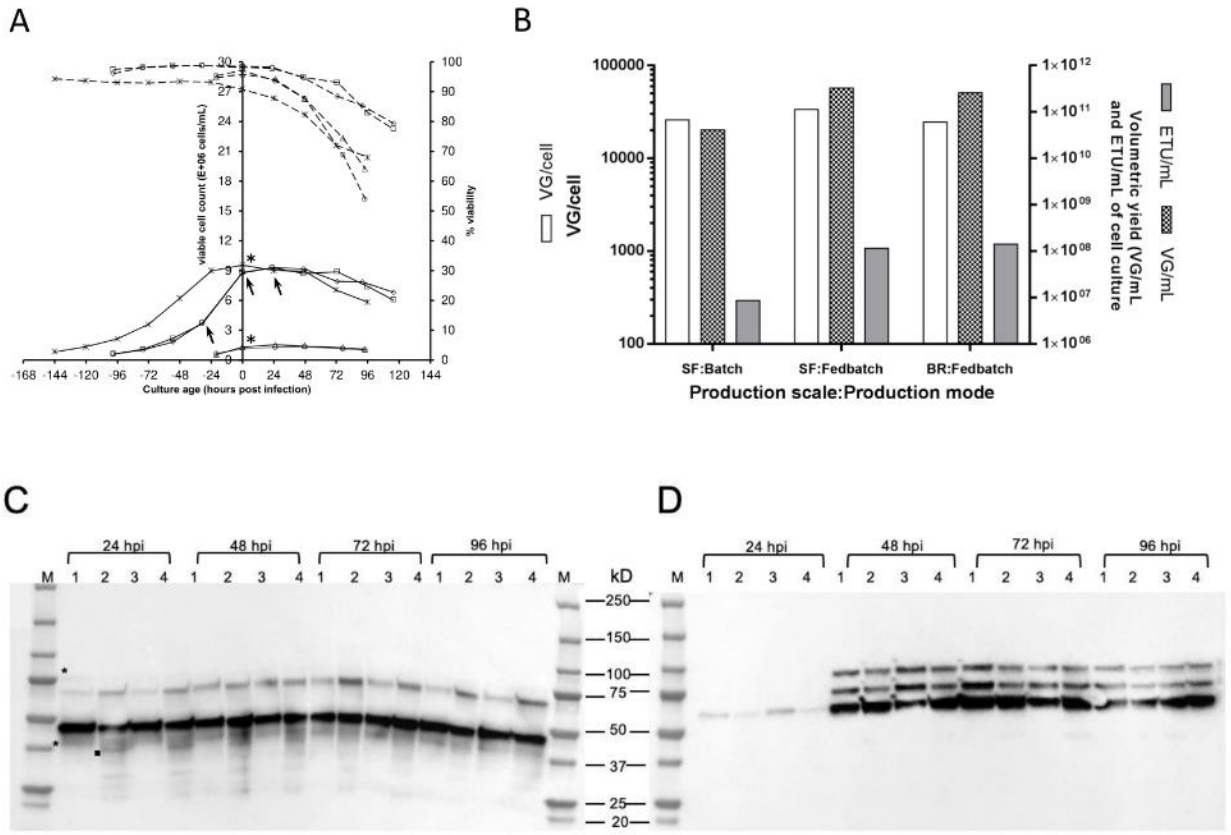

Figure 4.1 AAV production characteristics

(A) Insect cell culture characteristics during AAV5 production runs. The data shown are for AAV batch production (shake flask 1&2) and fedbatch production (shake flask 1&2 and bioreactor). Asterisk marks represent the time point of infection in batch and fedbatch process. The three arrow marks represent the time points of nutrient feed supplementation. The cell density data are shown via solid line (__) whereas the data of % cell viability is shown via dotted lines (----). **[legends-o: SF Batch F1, □: SF Fedbatch F1, Δ SF Batch F2, ◊: SF Fedbatch F2, ✳: Bioreactor]**. **(B)** Bar graph representation of overall cell-specific and volumetric yield of AAV5 production in batch and fedbatch mode in shake flask (SF) and bioreactor (BR). Note the logarithmic scale on left y-axis. **(C)** Kinetic of AAV Rep expression in post-infection phase. 1: SF Batch flask 1, 2: SF Fedbatch flask 1, 3: SF Batch flask 2, 4: SF Fedbatch flask 2. Rep 78 and Rep 40 are shown by asterisk and small molecular weight fragment of Rep 52 is shown via a dot. **(D)** Kinetics of AAV5 Cap expression in post-infection phase. 1: SF Batch flask1, 2: SF Fedbatch flask 1, 3: SF Batch flask 2, 4: SF Fedbatch flask 2. BR: bioreactor, ETU: enhanced transducing units, hpi: hours post infection, M: molecular weight marker, SF: shake flask, VG: viral genomes.

within 24 hpi followed by a sequential decline in both viable cell density and viability. In fedbatch mode, the addition of nutrient feed and baculovirus stock results in partial dilution of the culture,

the effect of which is reflected on the final cell density. The viability of the cells at the time of harvest (96 hpi-120 hpi) was found to be between 70%-80% in fedbatch and 50%-60% in batch mode. After infection at MOI 3, the majority of the cells are infected within 24 hours (**supplemental data, Figure S3**). The peak expression of Rep and Cap proteins were obtained at 48h (**Figure 4.1C and 1D**). A graphical representation of AAV yield at different scales (shake flask and bioreactor run) and in different production modes (batch and fedbatch) is shown in **Figure 4.1B**. The cell-specific (VG/cell) and volumetric yields (VG/mL) of genomic particles were found to be 25,000-27,000 VG/cell and 4-5x10^{10} VG/mL of culture in batch mode. In shake flask and bioreactor runs under fedbatch mode, around 25,000-35,000 VG/cell and 2-3x10^{11} VG/mL titers were obtained. The volumetric yield of enhanced transducing units (ETU) otherwise reported as infective virus particles[27] were around 1x10^{7} and 1-2x10^{8} ETU/mL in batch and fedbatch processes, respectively. The inline profile of various bioreactor sensors and process parameters during AAV production in a fedbatch bioreactor run is also shown in **Figure 4.2.**

4.2.3 AAV5 characterization

4.2.3.1 Analysis of AAV5 vector heterogeneity via Analytical Ultracentrifugation (AUC)

AUC is increasingly becoming a valuable tool for routine analysis of structural variants in AAV vector preparations where the real-time sedimentation analysis data provides a qualitative and quantitative measurement of vector heterogeneity, i.e., empty particle, full particle and the continuum of the population in between.[28] To obtain the samples with a purity necessary for AUC analysis, the AAV5 produced in multiple runs in shake flasks and bioreactors were prepared by affinity chromatography. The clarified cell lysate was subjected to single-step affinity chromatography, and the eluted AAV was collected, neutralized and buffer exchanged against

suitable buffer. The characteristic chromatogram is shown in **supplemental data, Figure S4** with a magnified image of the eluate peak containing the virus.

The AUC analysis of affinity eluate samples from multiple AAV production runs show two major peaks at around 62-67s and 93-98s. The sharp peak at 62-67s corresponds to empty particles, whereas, the intermediate population and the peak around 93-98s correspond to capsids with a genomic content and a prevalence of capsid incorporating complete rAAV genome (93-98s).

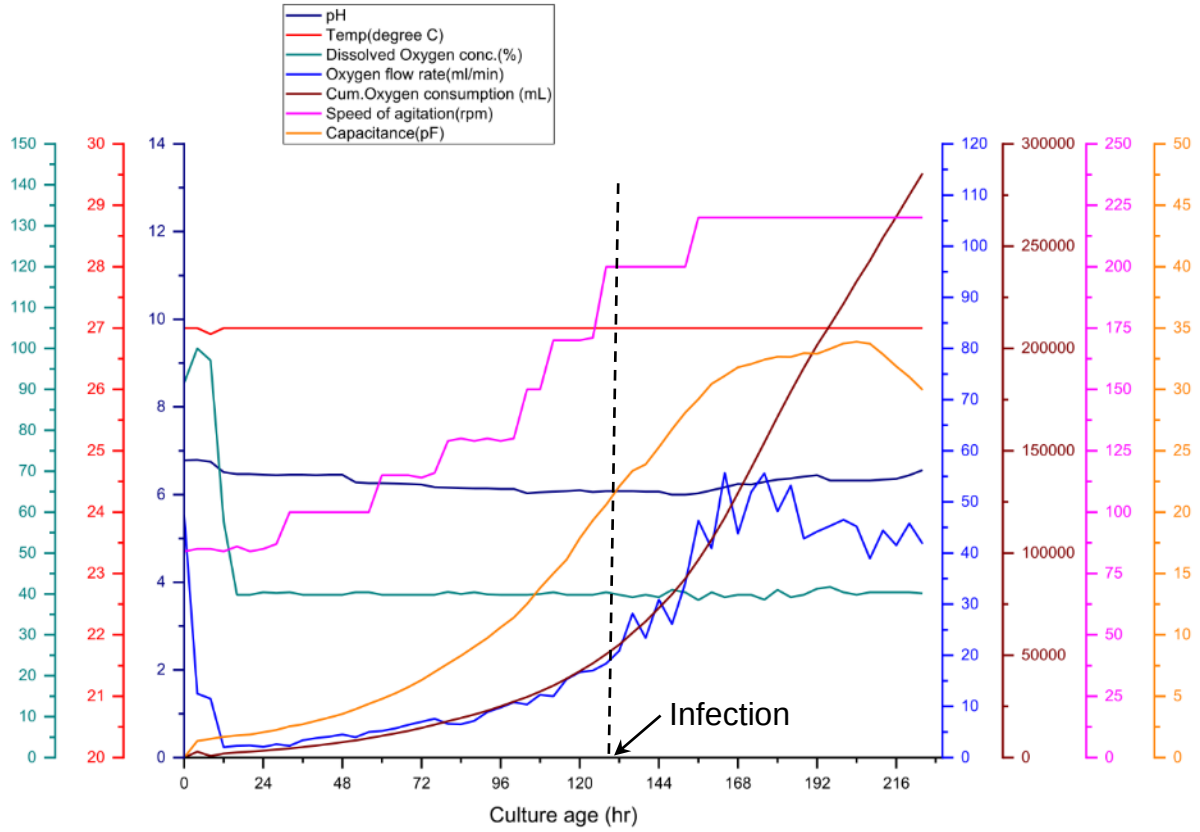

Figure 4.2 In-line sensors profile during AAV production in a bioreactor

Profile of various bioreactor sensors and process parameters during AAV production in a bioreactor. The speed of agitation was increased gradually as the cells grew. The pH, dissolved oxygen concentration and temperature were maintained to their respective set-points throughout the run. Note the change in capacitance and oxygen consumption post infection, an indication of cells undergoing productive infection phase. pF: picofarads.

The AUC profile at the 260nm scan of each representative sample from batch and fedbatch runs at various scale is shown in **Figure 4.3C**. The relative proportion of empty and genomic capsids was found to be ~70-80% and ~20-30% respectively. The AUC histogram for each of the AAV production runs (n=3) in batch and fedbatch mode in shake flasks is provided in **supplemental data, Figure S5** along with detailed data in **Table S1.** A detailed description of the calculation method is provided in the **supplemental methods**.

4.2.3.2 Transmission electron microscopy (TEM) of AAV

The sample used for AUC was recovered from the sample chamber after analysis and used for TEM analysis. The uranyl acetate negatively-stained AAV sample was analyzed at 180,000 x magnification. A representative image is shown in **Figure 4.3A**. The TEM image shows a mixed population of empty and genomic particles, and the diameter of the particles is in the range of 20-23 nm which is consistent with the reported values.

4.2.3.3 AAV5 VP composition analysis via SDS-PAGE and densitometry

The best possible linearity between VP band intensity and VG was found to be in the concentration range $5.5x10^8$-$7.3x10^8$ VG loaded (**supplemental data, Figure S6**). The stoichiometric composition of VP subunits is somewhat different compared to the previous report.[23] The incorporation of more VP1 is reported to be associated with the enhanced functionality of the vector preparation.[23,29–31] The results of VP composition from analysis of AAV samples of multiple production runs are shown in (**Figure 4.3B**). Please see the **supplemental data, Table S2** for details of VP composition data for each sample.

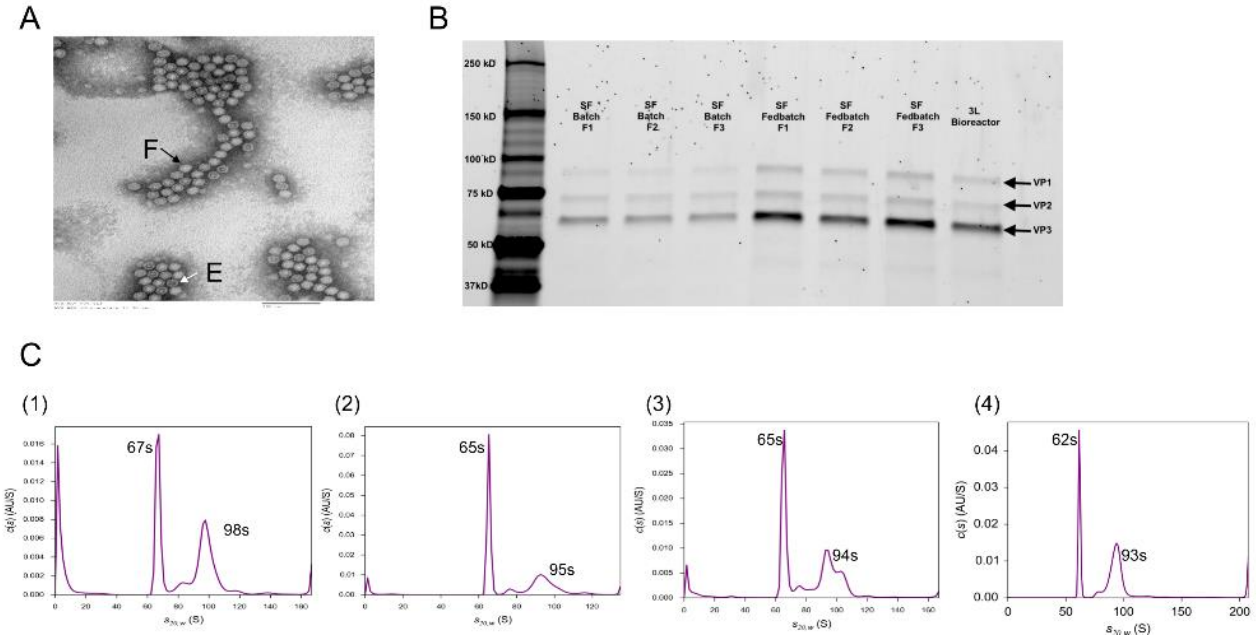

Figure 4.3 AAV purification and characterization

(A) TEM image of affinity-purified AAV5 which shows a mixed population of full particles [F] and empty capsids [E] with a characteristic particle diameter of 20-23 nm **(B)** VP stoichiometry analysis via Flamingo™ stained SDS-PAGE gel of affinity purified sample of n=3 production runs of AAV in batch mode (Shake flask: SF) and Fedbatch mode (Shake flask: SF and 3L bioreactor). The total VG loading per well was in the range of $5x10^8$-$7x10^{8.}$ The VP band intensities in all samples are similar and comparable to that of the 1L bioreactor sample. **(C)** AUC histogram representing 260mn absorbance profile of representative samples of an affinity-purified AAV5 from production in (1) batch mode in shake flask (2) fedbatch mode in shake flask (3) fedbatch mode in 3L bioreactor and (4) fedbatch mode in 1L bioreactor. Different components in an affinity-purified AAV5 sample as a function of sedimentation coefficient are shown. A very sharp peak around 62-67s represents the presence of an empty capsid and a major peak around 93-98s and intermediate population between these two major peaks represent genomic capsids. The peaks corresponding to the intermediate population may represent the form of a particle with encapsidation of partial AAV genome or collaterally packaged contaminating DNA. (See also Figure S4-S6, and Table S1-S2). SF: shake flask.

4.2.4 Assessment of *in vitro* functionality via gene transfer assay (GTA)

The titer values obtained from GTA for different samples analyzed have been summarized in **Table 4.1** (clarified lysate) and **Table 4.2** (AVB-affinity eluate samples). For batch and fedbatch production processes, the functional titers were found to be of $1x10^7$ ETU/mL and $1x10^8$ ETU/mL, respectively, wherein the latter reflected a 1 log increase in titer in the fedbatch process corresponding to high cell density.

4.2.5 The relative ratio of genomic and functional virus particle (VG: ETU ratio)

To quantify the respective ratio, the data were compiled from AAV analyses via qPCR and GTA for the clarified cell lysate and the affinity purified sample. The genomic to functional particle ratio (VG: ETU) for the cell lysate sample of the batch production was around 3600:1 and that of the fedbatch production was 1400:1 (shake flask) and about 1700:1(bioreactors). In the case of the purified sample, this ratio is somewhat higher eventually resulting from possible loss of the functional particles/functionality during the low pH elution necessary in affinity chromatography. Additionally, the variability of the assay may also contribute to the variability of this ratio.

Table 4.1 Summary of AAV production yield in a clarified lysate

Sample	Culture Volume (mL)	ETU[c]/mL	VG[d]/mL	ETU/cell	VG: ETU
[a]Shake flask/Batch	25	$1.1x10^{7}$ $\pm 2.53x10^{6}$	$4.0x10^{10}$ $\pm 0.56x10^{10}$	6±1.4	~3600:1
[b]Shake flask/Fedbatch	25	$1.9x10^{8}$ $\pm 0.43x10^{8}$	$2.7x10^{11}$ $\pm 0.37x10^{11}$	20±4.6	~1400:1
Bioreactor 1/Fedbatch	740	$2.1x10^{8}$ $\pm 0.48x10^{8}$	$3.8x10^{11}$ $\pm 0.53x10^{11}$	22±5	~1700:1
Bioreactor 2/Fedbatch	2250	$1.4x10^{8}$ $\pm 0.32x10^{8}$	$2.6x10^{11}$ $\pm 0.27x10^{11}$	15±3.5	~1700:1

ETU: enhanced transducing units
VG: viral genome copies or genomic particle
[a]values shown for multiple runs (n=6), relative standard deviation, 19%
[b] values shown for multiple runs (n=6), relative standard deviation, 18%
[c]GTA variability: relative standard deviation, 23%
[d]qPCR assay variability: relative standard deviation, 14%

The cell-specific yield of the functional particles was found to be around 6 ETU/cell (shake flask: batch), 20 ETU/cell (shake flask: fedbatch) and around 15-20 ETU/cell (bioreactors: fedbatch). It is important to note that the values of ETU obtained from the GTA are highly dependent on the detection method and the cell line used in the bioassay. In particular, the transduction susceptibility of the cell line used in the GTA is AAV serotype dependent. Our group has previously reported that HEK293 and HeLa cells based GTA display significant differences in the AAV serotype titer values.

Table 4.2 Summary of AAV5 characterization in AVB affinity-purified samples

Sample	Eluate Volume (mL)	ETU[c]/mL	VG[d]/mL	VG: ETU	% empty capsid	% genomic capsids
[a]Shake flask/Batch	3.5	$8.2x10^7$ $\pm1.9x10^7$	$3.2x10^{11}$ $\pm0.41x10^{11}$	~3800:1	[e]74.1% ±0.6%	[e]25.9% ±0.6%
[b]Shake flask/Fedbatch	3.5	$5.3x10^8$ $\pm1.23x10^8$	$1.3x10^{12}$ $\pm0.29x10^{12}$	~2500:1	[f]80.6% ±1.0%	[f]19.3% ±1.1%
Bioreactor 1/Fedbatch	3.5	$4.0x10^8$ $\pm0.92x10^8$	$1.0x10^{12}$ $\pm0.14x10^{12}$	~2500:1	68%	32%
Bioreactor 2/Fedbatch	3.5	$3.57x10^8$ $\pm0.82x10^8$	$8.48x10^{11}$ $\pm1.35x10^{11}$	~2400:1	78.8%	21.2%

ETU: enhanced transducing units
VG: viral genome copies or genomic particle
[a]values shown for triplicate runs (n=3)
[b]values shown for triplicate runs (n=3)
[c]GTA variability: relative standard deviation, 23%
[d]qPCR assay variability: relative standard deviation, 14%
[e]average value for n=3 runs
[f] average value for n=3 runs

Specifically, when AAV2 and AAV5 serotypes were produced side by side via a triple transfection process in suspension-adapted HEK293 cells, the genomic titer (VG/mL) of both serotypes was identical whereas the functional titer via GTA assay resulted in approximately 2 log lower quantification values for AAV5 (~$1x10^7$ ETU/mL) in the HEK293-based GTA and 1 log lower quantification value (~$1x10^8$ ETU/mL) in the HeLa-based GTA as compared to AAV2 (~$1x10^9$ ETU/mL). Because of these reasons, caution needs to be exercised when comparing the functional titers of different serotypes with that of AAV2.[10]

4.2.6 Characterization of the fedbatch production process

It is expected that AAV5 production at high cell density in fedbatch mode might add a dimension to the complexity and possible process variability, therefore, it is important to assess the robustness and consistency of the AAV production process under this mode of operation. Three AAV5 fedbatch productions in shake flasks were run in parallel and analyzed for consistency of the production, as well as the final titer of genomic and functional virus particles. Moreover, side-by-side AAV productions in the fedbatch mode in shake flask and bioreactor runs were conducted to validate the process. The kinetics data of AAV VG productions in shake flasks is provided in **Figure 4.4B**. The variability in cell-specific and volumetric yield of three replicates at different time points post-infection is shown, wherein the error bar represents the relative standard deviation. As the data suggest, there is significant consistency in AAV5 VG kinetics at different time points and in the final titer of the three replicates. There is a consistent increase of approximately 7,000-10,000 VG/(cell*day) between 48 hpi and 96 hpi. The overall cell-specific and volumetric yield at the time of harvest is in the range of 27,000-30,000 VG/cell and 2-$3x10^{11}$ VG/mL, respectively. In the case of the side by side comparison of AAV production kinetics in a

shake flask and bioreactor (**Figure 4.4A**), a similar trend in AAV production kinetics is observed for both scales. The genomic particles increased up to 96 hpi followed by a plateau between 96 hpi to 120 hpi. The ETU/mL data follows a similar trend but with a late onset where the functional particles were only detected at 48 hpi.

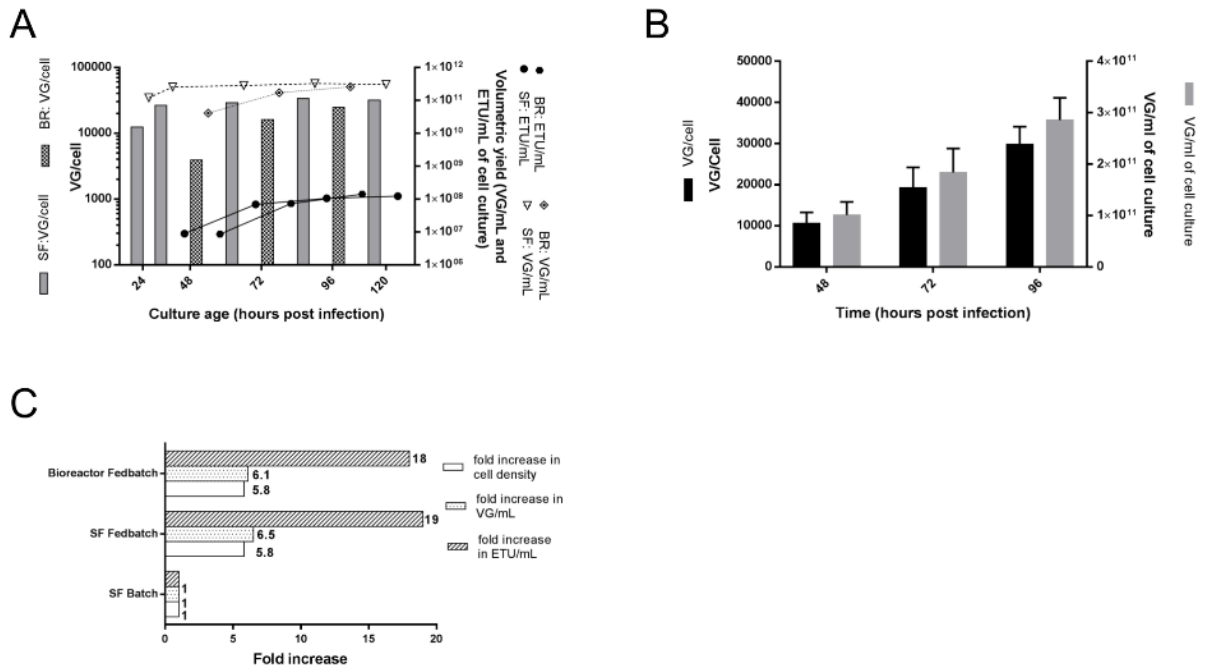

Figure 4.4 Fedbatch process characterization

(A) AAV production kinetics data of parallel runs of AAV productions in a shake flask and bioreactor in fedbatch mode. At different time points post-infection, the VG/cell, VG/mL and the ETU/mL values are shown via a bar graph, dotted trend line, and a solid trend line respectively. The maximum cell-specific and volumetric yields are achieved by 96 hpi with no further noticeable increase afterward and hence the harvest time was decided to be 96 hpi. **(B)** Consistency analysis of production kinetics and overall yield of AAV in fedbatch mode in shake flasks in triplicate parallel runs. The error bar in the bar graph represents the relative standard deviation of titers. **(C)** Comparative analysis of batch and fedbatch processes at shake flask and bioreactor scale. In the fedbatch process, the overall cell density is increased by a factor of ~6 compared to the batch process. This resulted in ~6fold increase in volumetric yield of genomic particles and ~20fold increase in that of transducing particles during AAV productions in shake flask and bioreactor runs. This exponential increase in volumetric yield is believed to be due to confounding positive effect of nutrient supplementation in a fedbatch mode of production. (See also Table S3). BR: bioreactor, SF: shake flask, ETU: enhanced transducing units, VG: viral genome.

This trend represents a typical AAV production kinetics where capsid protein expression commences immediately after the baculovirus infection followed by transgene rescue, replication, and packaging into preformed capsids. It is postulated that the preformed capsid with encapsidated genome undergoes conformational changes/capsid maturation in later stage and hence the functional titer values appear typically after 24 hpi. The final volumetric yield of AAV5 genomic titer in shake flask, bioreactor1, and bioreactor2 runs are $2.7x10^{14}$ VG/L, $3.8x10^{14}$ VG/L and $2.6x10^{14}$ VG/L respectively and that of the functional titer is $1.9x10^{11}$ ETU/L, $2.1x10^{11}$ ETU/L and $1.4x10^{11}$ ETU/L respectively. The overall summary of these results expressed as a factorial increase in volumetric yield is given in **Figure 4.4C**. To further extend the process characterization, representative samples from AAV production in batch mode and fedbatch mode at 72 hpi were analyzed for *rep/cap* copy number to determine the degree of *rep/cap* amplification post baculovirus infection alongwith non-infected Sf9 B8 as a control.(**Table 4.3**). The data suggest around 47x and 28x amplification in fedbatch and batch mode of production respectively.

Table 4.3 Determination of the number of integrated/rescued cap and rep genes copies per cell of Sf9 B8 stable cell line during AAV production in different modes and scales

Production method	Cap5 copies per cell	Rep2 copies per cell	Cap/Rep ratio	Bursting effect, times
Batch_SF_72hpi	286.56	29.55	9.7	28.7
Fedbatch_SF_72hpi	472.80	47.38	9.98	47.4
Fedbatch_BR_72 hpi	467.64	48.98	9.55	46.9
Not infected B8	9.97	1.25	7.99	N/A

SF: shake flask
BR: bioreactor
hpi: hours post infection

4.3 Discussion

Progression of AAV-based gene delivery vector candidates into late clinical stages necessitates a higher amount of clinical grade vector material. This poses a critical challenge and confers further burden on vector production processes because of a low volumetric yield of current AAV production platforms. The therapeutic dosage of AAV for a systemic administration in humans ranges from 10^{12} -10^{14} VG/kg, depending on indication.[32,33] This translates into an overall requirement of 10^{16}-10^{18} VG in a typical phase three clinical trial study. Utilizing traditional plasmid transfection protocols with adherent HEK293 cells to generate that much virus makes it impractical for commercial-scale production.[16] Recently, various bioreactors based on alternative modes of adherent cell cultivation such as CellFactory™, CellSTACKs®, and iCELLis® have been used to generate AAV material for clinical studies.[14,34,35] The most straightforward approach is a three-dimensional suspension cell culture which offers linear scalability and eventually a higher volumetric yield. Production platforms based on suspension-adapted HEK293 cell, and insect cell cultures represent a more viable option where the typical volumetric yield of AAV at a regular cell density (~ 1 million cells/mL) production cultures is about $1x10^{10}$ VG/mL and requires 100 L-10,000 L scale bioreactor production for late-stage clinical studies.[10,36–38] Among the insect cell culture-based systems for AAV production, the One-Bac platform is the simplest from a process standpoint as it consists of only two components. It reportedly provides cell-specific yields comparable to that of other two systems.[22] It was further fine-tuned for the VP1:VP2: VP3 capsid composition and minimum encapsidation of foreign DNA.[23] Hereby, we have examined this system from a process stand point. The volumetric yield was enhanced by around six-fold (**Figure 4.4C**) using fedbatch mode of production in shake flask and bioreactor formats.

The One-Bac system generates functional AAV particles upon infection with a single baculovirus. The detailed description of this system has been reported previously.[20–22] The expression level of

Rep, and Cap proteins is reported to have a direct impact on AAV yield.[17] The passage stability of the expression of the Rep proteins helper suggests a potential shift to higher molecular weight proteins Rep78 and 52, however without any noticeable effect on per cell yield of VGs. It can be inferred that the necessary expression level of these two Rep proteins for maximum replication and encapsidation of vector DNA is maintained irrespective of passage numbers up to 35 (the maximum passage tested). At the high cell density AAV productions under fedbatch mode, the timely addition of a nutrient feed is crucial for two key attributes: 1) in the pre-infection phase, it supports and helps to maintain high cell density culture in an exponential growth phase prior to infection, and 2) in the post-infection phase, it supports elevated nutrient demand to sustain high protein and genomic material expression. The high MOI infection which results in a cell growth arrest within 24 hpi metabolically shifts the overall culture from the cell growth phase to the protein expression phase, unlike low MOI (e.g., MOI of 0.1) infection where this shift is often delayed by an additional cell growth cycle.[26,39] As shown here, the peak expression of Rep and Cap proteins is attained within 48 hpi and the nutrient supplementation addition at the time of infection and at 24 hpi sufficiently fulfills the metabolic need of the culture. Similar findings have been reported with a three baculovirus system where the high cell density was achieved via infection of the Sf9 cell culture at 5 million cells/mL with a low MOI of 0.1 pfu/cell.[26] Comparative analysis of the volumetric yields in batch and fedbatch modes shows that even at the high cell density, the cell-specific yield was maintained. There is a proportionate increase in volumetric yield of genomic and transducing virus particle titer with an increase in cell density. This further suggests that the feeding formulation and feeding regime applied at this high cell density successfully led to the process intensification. The data from the bioreactor production runs provide further validation of the process. Also, improved cell-specific yield of functional virus particles (ETU/cell) in fedbatch

compared to batch processes (**Table 4.1**) suggests that the requirement of essential nutrients to support cellular processing in the late infection phase was fulfilled with the fedbatch feeding regime. The overall cellular processing seems to be impacted with the cell culture and extracellular environmental parameters (cell viability, pH, osmolarity, accumulation of toxic metabolites and depletion of essential nutrient). The VP1 capsid protein subunit can be directly correlated with virus infectivity due to the presence of an integrated phospholipase A_2-like enzymatic domain and its postulated role in virion escape from a late endosomal stage. It has been reported on several occasions that insect cell-produced AAV vectors exert inferior infectivity compared to that produced in mammalian cells due to an altered capsid composition resulting in a low incorporation of VP1.[17,23] The analysis of capsid composition of the bioreactor-produced AAV5 shows a higher ratio of VP1 compared to the previous report,[23] and it is believed to be responsible for the improved infective virus particle titer.

Given that the same GTA protocol was used for the analysis of both samples, it provides an opportunity for direct comparison of two different platforms (One-Bac and HEK293). The functional virus particle titer of the fedbatch bioreactor-produced AAV5 is comparable to that of AAV5 produced in suspension-adapted HEK293-based triple plasmid transfection method as reported previously by our research group.[10] This data confirms that the One-Bac system used for AAV5 production here, in conjunction with the proposed production process generates AAV5 with identical functionality.

4.4 Materials and Methods

4.4.1 Cells and medium

Stably-transformed *rep2cap5* packaging Sf9 cell line B8 was designed essentially as described previously.[23] These cells were used for the production of AAV. rAAV-encoding BEV stocks used to infect B8 cells were grown in naïve Sf9 cells in serum-free insect cell medium: sf900-II or sf900-III (Thermo Fisher scientific: Waltham, Massachusetts). For high cell density AAV productions in fedbatch mode, B8 cells were supplemented with a single proprietary nutrient feed formulation. Both insect cell cultures were maintained in sterile PETG disposable flasks (Fisher Scientific: Hampton, New Hampshire) in serum-free medium in a 27°C incubator at 110 rpm agitation speed. The suspension-adapted HEK293 cells used for the gene transfer assay are described in our previous studies and are maintained in CD HEK293 medium (Irvine Scientific: Santa Ana, California) supplemented with L-glutamine at a final concentration of 4mM. The suspension cell culture was maintained in a shaker incubator set at 37°C, 5% CO_2, and 85% relative humidity. The cell density analyses from routine maintenance flasks and virus production runs were performed using the Vi-Cell XR cell counter (Beckman Coulter: Brea, California). This instrument works on the principle of Trypan blue dye exclusion and captures 50 images and provides an average value for viable cell density, percent viability, and cell diameter. The accuracy of the instrument is ±10% in the range of 0.2-10x10^6 cells/mL.

4.4.2 Baculovirus

The recombinant baculovirus carrying the AAV transgene expression cassette (Bac-GFP) consisted of AAV-ITR flanking eGFP under the control of chicken ß-actin-CMV hybrid promoter The baculovirus stock was plaque-purified, and five baculovirus isolates expressing a high level

of transgene cassette were collected. A highly potent Bac-GFP isolate was further selected based on AAV5 DNase-resistant particle titer analyzed from cell lysates of B8 cells infected with these individual isolates. The selected working isolate was volumetrically expanded using naive Sf9 cells where the clarified cell culture supernatant from 72-96 hours post infection (hpi) was stored in the dark at 4°C (for short-term use) or at -80°C (longer term use). This Bac-GFP working stock quantified via standard baculovirus plaque assay protocol was found to have a functional titer of 3-5x10^8 pfu/mL. This working baculovirus stock was at passage three (P3) with respect to the primary stock.

4.4.3 Analysis of the genetic stability of the packaging B8 cell line

The *rep2cap5* expressing insect cells at extended passage numbers (vial thaw+1: P4, vial thaw+5: P8 and vial thaw+32: P35) were infected with Bac-GFP at a multiplicity of infection (MOI) of 1pfu/cell, and cells were harvested 96 hpi and lysed via a triple freeze-thaw cycle. Clarified lysate was used for the analysis of Rep and Cap expression by Western blotting. A detailed protocol of culture harvest and cell lysis is given in a separate section that follows later.

4.4.4 Analysis of rep2/cap5 copy number

To characterize the AAV5-producing B8 Sf9 stable cell line for the number of rep and cap copies, the real time qPCR using Cap5-, and Rep2-specific primers, as well as Sf9 house-keeping gene Innexin2 (Inx2)[20] was used. Briefly, 0.3 µg of total DNA isolated by Zymo Research Quick DNA kit (Zymo research: Irvine, California) was digested by 20U of BamH HF enzyme (New England Biolabs: Ipswich, Massachusetts) for 1 h. Then, 30 ng of digested DNA was amplified using PowerUp SYBR Green Master Mix kit (Applied Biosystems: Foster city, California). Linearized

plasmid DNA spiked by Sf9 wild-type gDNA was used as a reference for calculation of Cap5 and Rep2 copies per cell. For calculation of input genomes per qPCR reaction, *Spodoptera frugiperda* Sf9 insect cell line genome size was assumed to be 451 Mbp.[40] The sequences of primers used in this study are provided in **supplemental data, Table S3.**

4.4.5 AAV5 production in low and high cell density cultures at shake flask scale

For all AAV production runs at shake flask scale, 125 mL sterile PETG flasks were used with 25 mL working volume, and the cells were maintained in a 27°C incubator at 110 rpm agitation speed. The insect cells at mid-exponential phase (2.5-3.5x10^6 cells/mL) were used to seed the subsequent culture and the seeding density at the beginning of the culture was always kept at around 0.65-0.75 million cells/mL. In the low cell density production, the B8 cells at a cell density of 1.2-1.4 million cells/mL were infected with Bac-GFP at MOI of 3 pfu/cell. At 96 hpi, the culture was harvested, cells were lysed, and the clarified lysate was collected for subsequent analysis. In the high cell density culture process, the insect cells were infected when the cell density was around 9.5-10 million cells/mL. Cell culture was harvested at 96 hpi and processed for AAV recovery and analysis. In the high cell density process, the pre- and post-infection phases were supported by fedbatch mode where cells were supplemented with a single nutrient cocktail at specific time points: 24 hours before infection (4% v/v), at the time of infection (0 hpi- 8% v/v) and 24 hpi (8% v/v). Cell culture samples were collected every 24 h for analysis throughout the run. The addition of nutrient cocktail in two aliquots at 24 h interval during the post-infection phase provides a nutrient-rich environment to support maximum protein expression for up to 48 hpi; time phase where the cell density reaches a plateau and AAV Rep/Cap expression is at its peak.

4.4.6 Fedbatch process characterization

In fedbatch process characterization, process consistency and AAV production kinetics analysis were studied. AAV production runs were performed in triplicate in 125 mL sterile shake flasks with 25 mL working volume. Samples were collected at every 24 h post infection for analysis.

4.4.7 AAV5 production at high cell density in bioreactors

High cell density in 1L (bioreactors 1) and 3L (bioreactor 2) bioreactors was achieved by growing cells in fedbatch mode applying the same nutrient feeding strategy as described previously for the shake flask. The bioreactor (Applikon Biotechnology: Delft, Netherlands) was equipped with a single marine impeller, a pH sensor, a temperature sensor, dissolved oxygen (DO) concentration sensor and a micro sparger with 100 µm pore size. The pH, temperature and DO parameters were set at 6.3±0.3, 27°C±1°C and 40% air saturation±2% at their corresponding units, respectively. In addition, the 3L bioreactor was equipped with a capacitance probe for in-line monitoring of the culture characteristics such as cell growth and progress of the infection. The bioreactor control unit equipped with a PID controller suit ensured controlled conditions of process parameters within the given operational range throughout the run. The B8 cells from shake flask at a mid-exponential growth phase were used to inoculate the bioreactor at 0.65-0.75 million cells/mL density. When cells were at 9.5-10 million cells/mL, they were infected with a Bac-GFP at MOI of 3 (pfu/cell) and harvested at 96 hpi for further processing.

4.4.8 Culture harvesting and AAV recovery.

The whole cell culture at 96 hpi was lysed *in-situ* in a shake flask and a bioreactor via addition of 10 % v/v of lysis buffer (20 mM $MgCl_2$, 500 mM Tris-HCl, pH 7.5, 1% Triton™ X-100) supplemented at final concentration of 50 U/mL of Benzonase® DNase (Millipore Sigma;

Burlington, Massachusetts). The cell culture was incubated with this lysis buffer for 1.5-2 h at 27°C with agitation followed by addition of $MgSO_4$ to achieve the final concentration of 37.5 mM. This step is followed by an additional incubation for 30 min at the same temperature. The later step results in an ionic strength of more than 200 mM where the presence of the high salt concentration assists in AAV release, prevent/minimize interparticle AAV aggregation (Mg^{2+} being more effective) and AAV-cell debris/AAV-DNA complexes.[36] In the case of samples for virus titration, the crude lysate underwent a further 3 freeze/thaw cycles to ensure efficient cell lysis of less fragile insect cells and complete AAV release in the high ionic strength lysate. Following this, the lysate was clarified via centrifugation at 3000 *g* for 30 min to eliminate cellular debris, and the supernatant containing released AAV5 particles was collected for further processing.

4.4.9 AAV Characterization

Clarified cell lysate and affinity purified material containing AAV5 was used for quantitative and qualitative analytical assays. The purified samples for various characterization assays were generated via a single step immune-affinity chromatography method. AAV5 purification was performed via a single step affinity chromatography using the AVB Sepharose resin and the ÄKTA Avant25 (GE Healthcare: Chicago, Illinois) chromatographic system. The AVB resin harboring a single domain monoclonal antibody fragment is reported to selectively bind a majority of AAV serotypes.[21] Based on SDS-PAGE and Western Blot analysis, this single step column purification yields a high purity vector free from major cellular and baculovirus components (data not shown). Specifically, a 1mL Hi-Trap prepacked AVB Sepharose column was equilibrated with 10 column volumes of loading buffer (20 mM Tris, 500 mM NaCl, pH 8) followed by the loading of 100 mL

of lysate filtered via 0.45µm modified polyethersulfone membrane filter. The column was washed with loading buffer until the 260/280 nm baseline returned to zero. The elution was done by the introduction of a low pH elution buffer (0.1 M Glycine, pH 2.5) which resulted in a sharp pH gradient and the low pH environment inside the column induced detachment of bound AAV. The acidic eluate containing AAV5 was immediately neutralized via dropwise addition of neutralizing buffer (1M Tris, pH 8.8) until the pH shifted to neutral/alkaline values. This neutralized AAV material was further buffer-exchanged in a suitable buffer using PD-10 desalting columns (GE Healthcare: Chicago, Illinois). The chromatographic process flowrate throughout the operation was kept at 75 cm/h. The process monitoring was done using built-in UV-VIS, conductivity and pH sensors. The affinity purified material was used for subsequent quantitative and qualitative characterization.

4.4.10 Quantitative analysis

4.4.10.1 Quantification of DNase-resistant genomic particles (viral genomes: VGs) by quantitative polymerase chain reaction (qPCR)

Clarified lysate or affinity purified material was incubated with 5 U/ml of Benzonase® for 30 min at 37°C before viral DNA extraction. Benzonase®-treated undiluted and 1:10 diluted samples were used for viral DNA extraction using High Pure Viral DNA Extraction kit (Roche Diagnostics: Risch-Rotkreuz, Switzerland). In the end, 200 µL of lysate sample resulted in 50 µL of purified and concentrated viral DNA. This viral DNA, serially diluted to 1:10, 1:100 and 1:1000 was used as a template for subsequent qPCR analysis via probe-based reaction. The forward primer (5`-ATAGGGACTTTCCATTGACGTC-3`), the reverse primer (5`- TGATACACTTGATGTACTGCCAAG-3`) and the probe (FAM 5`-TGGGTGGACTATTTACGGTAAACTGCC-3`BHQ) targeting CMV enhancer sequence used in the qPCR reaction were purchased from Integrated DNA Technologies (Coralville, Iowa). The 20

µL qPCR reaction mixture consisted of 10 µL of Ssoadvanced™ Universal Probes Supermix (Bio-Rad Laboratories: Hercules, California), 1.2 µL of 10µM forward primer, 1.2 µL of 10 µM reverse primer, 1 µL of 5 µM probe, 1.6 µL of qPCR grade water and 5 µL of DNA template. The temperature programming for qPCR reaction used was: preincubation at 95°C/3 min for denaturation and 40 cycles of 95°C/15 sec and 54.5°C /30 secs. Vector genome standard was prepared using AAV-GFP plasmid (Addgene: Cambridge, Massachusetts). Purified and linearized plasmid in the concentration range of $1.7x10^2$ copies/uL -$1.7x10^7$ copies/uL was used for qPCR standard curve. The qPCR reaction was performed using the CFX-96 Touch™ Real-time PCR system (Bio-Rad Laboratories: Hercules, California).

4.4.10.2 Gene transfer assay (GTA) for quantification of enhanced transducing units (ETU)/functional particles

Over time, various protocols have been developed for *in vitro* assessment of AAV vector functionality. The suspension adapted-HEK293 cells were infected with serial dilutions of AAV5 (clarified lysate or affinity-purified) and co-infected with an E1, E3 deleted adenovirus serotype 5-(ΔE_1E_3Ad5) at an MOI-5 infectious particles/cell. In the case of cell lysates, the samples were heated at 60°C for 15 min before infection to deactivate existing baculovirus and to prevent false positive results. At 22-24 hpi, the cells were harvested via centrifugation at 300 *g* for 5 min, and the cell pellet was resuspended and fixed in freshly prepared cold fixation buffer (final concentration 2% paraformaldehyde in PBS) at 4°C for minimum 30 min. Later, the cell suspension was analyzed for GFP-positive cells via flow cytometry. Here, only ΔE_1E_3Ad5 infected negative control samples were used to set the gate, and the total of 10000 events were recorded for data analysis. The linear range of quantification was established to be between 2-20% GFP positive cells.

4.4.11 Qualitative analysis

4.4.11.1 AAV2 Rep and AAV5 Cap Western blot

Clarified cell lysate samples were filtered using 0.45 µm filter and used for western blot analysis. Lysate samples equivalent of $6x10^4$ cells were mixed with preformulated 4x Laemlli sample buffer to which was added a reducing agent as per manufacturer`s instructions (Bio-Rad Laboratories, Hercules, California), heated to 95°C for 15 min and loaded onto TGX Stain-free gel, 4-15% acrylamide (Bio-Rad Laboratories, Hercules, California). The gel was run at 120 V for 90 min. Once the run was complete, the protein was transferred to a nitrocellulose membrane using the Transblot Turbo Transfer System (Bio-Rad Laboratories: Hercules, California) as per manufacturer`s instruction. Next, the nitrocellulose membrane was placed in a blocking buffer-PBS containing 0.1% v/v Tween™ - 20 (PBST) and 5% w/v skimmed milk and incubated for 1 h at room temperature. Afterwards, the membrane was incubated overnight at 2-8°C with mouse IgG anti-AAV5 VP primary antibody (American Research Products Inc: Waltham, Massachusetts) at a 1:2000 dilution prepared in PBST (PBS containing 0.1%v/v Tween™-20), and anti-AAV2 Rep primary antibody (American Research Products Inc: Waltham, Massachusetts) at a 1:100 dilution prepared in PBST. Following this, the membrane was washed three times with PBST and incubated at room temperature with an HRP-conjugated rabbit polyclonal against mouse IgG secondary antibody (Abcam: Cambridge, United Kingdom) at a 1:10000 dilution prepared in PBST. Finally, the membrane was washed three times with PBST, incubated with ECL chemiluminescence reagent (Bio-Rad Laboratories, Hercules, California) and visualized using Bio-Rad's ChemiDoc imager.

4.4.11.2 AAV5 VP proteins stoichiometry analysis

Stoichiometric analysis of AAV5 VP subunits was performed via SDS-PAGE of the affinity-purified sample. Purified vector was serially diluted within 1 log range of viral genomes (VGs) with the resulting amount loaded per well in the range of $2.2x10^8$-$2.2x10^9$ VGs. After the run, the gel was stained using Flamingo™ fluorescent stain as per manufacturer`s protocol (Bio-Rad Laboratories, Hercules, California). This stain was selected because it offers similar sensitivity and better linear range of quantification in comparison to silver stain. The stained gel was visualized via the ChemiDoc Imager, and the densitometric analysis of the resolved bands was performed using the Image Lab software suite. The linear range of quantification was established by plotting the VP band intensity as a function of VG amount. The best possible linearity between VP band intensity and VG was found to be in the concentration range $5.5x10^8$-$7.3x10^8$ VG loaded (**supplemental data, Figure S5**). Also within this range, the VP3 band intensity was normalized, arbitrarily set to 10, and the relative band intensities of the three VP subunits were determined.

4.4.11.3 Analytical ultracentrifugation (AUC) analysis of the affinity-purified AAV5

For analytical ultracentrifugation analysis, the affinity-purified AAV5 material ($2x10^{12}$ VG/mL) was buffer exchanged into PBS and concentrated using 30 kD molecular weight cut off centrifugal filter device such that the 260 nm absorbance value for the concentrate is between 0.4-0.8. The concentrated sample was then analyzed using the Beckman proteomelab XL-1 (Beckman Coulters: Brea, California). The sample chamber is charcoal filled-epon, two sector centerpieces with 1.2 cm pathlength. The reference chamber was filled with 420 µL PBS (blank) and the sample chamber with concentrated AAV5. After the sample chamber was placed in the rotor, it was allowed to equilibrate at 20°C with full vacuum applied for 1h. The sedimentation analysis run was performed at 20,000 rpm for 2 h at 20°C. The real-time data was captured using a 260 nm optics. The Sedfit

software was used for post-run data analysis. This free access software was developed by a research group from NIH.

4.4.11.4 AAV analysis via transmission electron microscopy (TEM)

10 µL of the virus dispersion, fixed with 2% paraformaldehyde, was dropped on a carbon-formvar-coated nickel grid for 10 min. Grids containing fixed viruses were washed with water prior to staining. 10 µL of 1% Uranyl Acetate was applied on the grid for 30 sec. The excess of the sample and negative stain solution was blotted with a Whatman filter paper, and the grid was air-dried prior to the observation in TEM. The examination was performed with a Philips CM100 transmission electron microscope. Electron micrographs were captured using an AMT XR80 digital camera.

4.5 Authors contributions:

Conceptualization, P.J., P.S.C. and A.K.; Methodology, P.J., L.C., I.A., J.S., O.K., S.Z., P.S.C. and A.K.; Execution P.J., Writing-original draft, P.J.; Review & Editing, P.S.C., S.Z., and A.K.; Funding acquisition, A.K.; Resources, P.S.C. and A.K.; Supervision, P.S.C and A.K.

4.6 Acknowledgement

P.J. is financially supported by a fellowship from the Faculty of Engineering, McGill University and a grant from Natural Sciences and Engineering Research Council (NSERC RGPIN-2015-05132) of government of Canada. The authors also thank Diane Gingras for AAV TEM analysis, Marie-Hélène Venne for initial setup of GTA and Alice Bernier for assistance in chromatographic processing and critical reading of the manuscript.

4.7 Conflict of interest

S.Z. is a co-founder of Lacerta Therapeutics, a licensee of the insect cell technology used in this research.

4.8 References

1. Huang, S., Kahimira, M. (2013). Development of hybrid viral vectors for gene therapy. Biotechnol. Adv. 31, 208-223.
2. Waehler, R., Russell, S J., Curiel, DT. (2007). Engineering targeted viral vectors for gene therapy. Nat. Rev. Genet. 8, 573-587
3. Ylä-Hertuala, S. (2012). Endgame: Glybera finally recommended for approval as the first gene therapy drug in the European Union. Mol. Ther. 20, 1831-1832
4. Clark, KR., Liu, X., McGrath, JP, Johnson, PR. (1999). Highly purified recombinant adeno associated virus vectors are biologically active and free of detectable helper and wild type-viruses. Hum. Gene. Ther. 10, 1031-1039.
5. Collaco, RF., Cao, X., Trempe, JP. (1999). A helper virus-free packaging system for recombinant adeno-associated virus vectors. Gene. 238, 397-405.
6. Collaco, RF., Trempe, JP. (2003). A method for helper virus-free production of adeno-associated virus vectors. Methods. Mol. Med. 76, 237-254.
7. Gao, G., Qu, G., Faust, LZ., Engdahl, RK., Xiao, W., Hughes, JV, et al. (1998). High-titer adeno-associated viral vectors from a Rep/Cap cell line and hybrid shuttle virus. Hum. Gene. Ther. 9, 2353-2362.
8. Harris, JD., Beattie, SG., Dickson, JG. (2003). Novel tools for production and purification

of recombinant adeno-associated viral vectors. Methods. Mol. Med. 86, 255-267.

9. Xiao, X., Li, J., Samulski, RJ. (1998). Production of high-titer recombinant adeno-associated virus vectors in the absence of helper adenovirus. J. Virol. 72, 2224-2232.
10. Chahal, PS., Schulze, E., Tran, R., Montes, J., Kamen, A. (2014). Production of adeno-associated virus (AAV) serotypes by transient transfection of HEK293 cell suspension cultures for gene delivery. J. Virol. Methods. 196, 163-173.
11. Clément, N., Knop, DR., Byrne, BJ. (2009). Large-scale adeno-assocaited viral vector production using a herpesvirus-based system enables manufacturing for clinical studies. Hum. Gene. Ther. 20, 796-806.
12. Adamson, SL., Potter, M., Bryne, BJ., Clément, N. (2017). Sodium Chloride Enhances Recombinant Adeno-Associated Virus Production in a Serum-Free Suspension Manufacturing Platform Using the Herpes Simplex Virus System. Hum. Gene Ther Methods. 28 (1); 1-14.
13. Clément, N., Grieger, JC. (2016). Manufacturing of recombinant adeno-associated viral vectors for clinical trials. Mol Ther Methods Clin Dev. 3:16002
14. Emmerling, VV., Pegel, A., Milian, EG., Venereo-Sanchez, A., Kunz, M., Wegele, J. et al. (2016). Rational plasmid design and bioprocess optimization to enhance recombinant adeno-associated virus (AAV) productivity in mammalian cells. Biotechnol J. 11(2):290-297
15. Durocher, Y., Pham, PL., St-Laurent, G., Jacob, D., Cass, B., Chahal, P. et al. (2007). Scalable serum-free production of recombinant adeno-associated virus type 2 by transfection of 293 suspension cells. J Virol Methods.144(1):32-40.
16. Urabe, M., Ding, C., Kotin, RM. (2002). Insect cells as a factory to produce adeno-

associated virus type 2 vectors. Hum. Gene. Ther. 13, 1935-1943.

17. Kohlbrenner, E., Aslanidi, G., Nash, K., Shklyaev, S., Thompson, MC., Bryne, BJ., et al. (2005). Successful production of pseudotyped rAAV vectors using a modified baculovirus expression system. Mol. Ther. 12, 1217-1225.
18. Chen, H. (2008). Intron splicing-mediated expression of AAV rep and cap genes and production of AAV vectors in insect cells. Mol. Ther. 16, 924-930.
19. Smith, RH., Levy, JR., Kotin, RM. (2009). A simplified baculovirus-AAV expression vector system coupled with one-step affinity purification yields high-titer rAAV stocks from insect cells. Mo. Ther. 17, 1888-1896.
20. Aslanidi, G., Lamb, K., Zolotukhin, S. (2009). An inducible system for highly efficient production of recombinant adeno-associated virus (rAAV) vectors in insect sf9 cells. Proc. Natl. Acad. Sci. USA. 106, 5059-5064.
21. Mietzsch, M., Grasse, S., Zurawski, C, Weger, S., Bennett, A., Agabandje-McKenna, M. et al. (2014). One Bac: platform for scalable and high-titer production of adeno-associated virus serotype 1-12 vectors for gene therapy. Hum. Gene. Ther. 25, 212-222.
22. Mietzsch, M., Casteleyn, V., Weger, S., Zolotukhin, S., Heilbronn, R. (2015). OneBac 2.0: sf9 cell lines for production of AAV5 vectors with enhanced infectivity and minimal encapsidation of foreign DNA. Hum. Gene. Ther. 26, 1-24.
23. Kondratov, O., Marsic, D., Crosson, SM., Mendez-Gomez, HR., Moskalenko, O., Mietzsch, M. et al. (2017). Direct head-to head evaluation of recombinant adeno-associated viral vectors manufactured in human versus insect cells. Mol. Ther. 25, 2661-2675.
24. Bédard, C., Kamen A., (1994). Maximization of recombinant protein yield in the insect cell / baculovirus system by one-time addition of nutrients to high-density batch cultures.

Cytotechnology. 15, 129-138.

25. Elias, CB., Zeiser, A., Bédard, C., Kamen, AA. (2000). Enhanced growth of Sf-9 cells to a maximum density of $5.2x10^7$ cells per mL and production of beta-galactosidase at high cell density by fed batch culture. Biotechnol Bioeng. 68(4), 381-388.
26. Mena, AJ., Aucoin, MG., Chahal, PS., Kamen, AA. (2010). Improving adeno-associated vector yield in high density insect cell cultures. J. Gene. Med. 12, 157-167.
27. Aucoin, MG., Perrier, M., Kamen, AA. (2008). Critical assessment of current adeno-associated viral vector production and quantification methods. Biotechnol. Adv. 26,73-88.
28. Burnham, B., Nass, K., Kong E., Mattingly, A., Woodcock, D., Song, A. et al. (2015). Analytical ultracentrifugation as an approach to characterize recombinant adeno-associated viral vectors. Hum. Gene. Ther. Methods. 26, 228-242.
29. Girod, A., Wobus, CE., Zádori, Z., Ried. M., Leike, K., Tijssen, P. (2002). The VP1 capsid protein of adeno-associated virus type 2 is carrying a phospholipase A_2 domain required for virus infectivity. J. Gen. Virol. 83, 973-8.
30. Dorsch, S., Liebisch, G., Kaufmann, B., Landenberg, PV., Hoffmann, JH., Drobnik, W. et al. (2002). The VP1 unique region of parvovirus B19 and its constituent phospholipase A2-like activity. J. Virol. 76, 2014-2018.
31. Vihinen-ranta, M., Wang, D., Weichert, WS., Parrish, CR. (2002). The VP1 N-terminal sequence of canine parvovirus affects nuclear transport of capsids and efficient cell infection. J. Virol. 76, 1884-1891.
32. Wells, DJ. (2017). Systemic AAV gene therapy close to clinical trials for several neuromuscular diseases. Mol. Ther. 25, 834-835.
33. Galibert, L., Merten, O-W. (2011). Latest developments in the large-scale production of

adeno-associated virus vectors in insect cells towards the treatment of neuromuscular diseases. J. Invertebr. Patho. 107, S80-S93.

34. Allay, JA., Sleep, S., Long, S., Tillman, DM., Clark, R., Carney, G. et al. (2011). Good manufacturing practice production of self-complementary serotype 8 adeno-associated viral vector for a Hemophilia B clinical trial. Hum. Gene. Ther. 22, 595-604.
35. Powers, AD., Piras, BA., Clark, RK., Lockey, TD., Meagher MM. (2016). Development and optimization of AAV hFIX particles by transient transfection in an iCELLis® fixed-bed bioreactor. Hum. Gene. Ther. Methods. 27, 112-121.
36. Chahal, PS., Aucoin, MG., Kamen, A. (2007). Primary recovery and chromatographic purification of adeno-associated virus type 2 produced by baculovirus/insect cell system. J. Virol. Methods. 139, 61-70.
37. Meghrous, J., Aucoin, MG., Jacob, D., Chahal, PS., Arcand, N., Kamen, AA. (2005). Production of recombinant adeno-associated viral vectors using baculovirus/insect cell suspension culture system: From shake flasks to a 20-L bioreactor. Biotechnol. Prog. 21, 154-160.
38. Nagrete, A., Kotin, RM. (2007). Production of recombinant adeno-associated vectors using two bioreactors configurations at different scales/ J. Virol Mehtods. 145, 155-161.
39. Mena, JA., Ramirez, OT., Palomares, LA. (2007). Population kinetics during simultaneous infection of insect cells with two different recombinant baculoviruses for the production of rotavirus-like particles. BMC Biotechnol. 7:39.
40. Nandankumar, S., Ma, Hailun., Khan, AS. (2017). Whole-genome sequence of the Spodoptera frugiperda Sf9 Insect cell line. Genome Announc. 5(34).

Development of a Scalable and Robust Anion-exchange Chromatographic Method for Enriched Recombinant Adeno-Associated Virus Preparations in Genome Containing Vector Capsids of Serotype- 5, 6, and 8.

Preamble

Following the upstream cell-culture process development, the next step for AAV process development is the downstream purification process. The next chapter, more specifically, focuses on the improvement of downstream process with regards to the removal of empty capsid population from the material generated at the upstream stage. An end-to-end chromatographic process was proposed that consisted of a two-step chromatography approach; immune-affinity capture chromatography for selective capture of AAV capsids and anion-exchange chromatography process for high-resolution separation and removal of empty capsids. Exploring the fundamental principles of anion-exchange chromatography process, the optimized process was further validated for additional serotypes, confirming its functionality a potentially genetic platform. Overall, this report provides a simple, scalable, and a robust approach for generating high-purity AAV preparations enriched in capsids containing genetic material. The supplemental data associated with this chapter are provided in the **appendix, 9.2** (**Page number 217-225**).

Chapter 5 Development of a Scalable and Robust Anion-Exchange Chromatographic Method for Enriched Recombinant Adeno-Associated Virus Preparations in Genome Containing Vector Capsids of Serotypes- 5, 6, and 8

Pranav R. H. Joshi[1], Alice Barnier[1], Pablo D. Moço[1], Joseph Schrag[2], Parminder S. Chahal[2], Amine Kamen[1]*

[1] Viral Vectors and Vaccine Bioprocessing Group, Department of Bioengineering, McGill University, Montreal, Quebec, Canada.

[2] Human Health Therapeutics, National Research Council of Canada, Montreal, Quebec, Canada.

* Correspondence should be addressed to Amine Kamen (amine.kamen@mcgill.ca)
Department of Bioengineering, McGill University.

Short title: Generic chromatographic process for AAV vector capsid purification

Submitted to "**Molecular therapy: methods and clinical development**"

Abstract

Removal of empty capsids from adeno-associated virus (AAV) manufacturing lots remains a critical step in the downstream processing of AAV clinical-grade batches. Because of similar physico-chemical characteristics, the AAV capsid populations totally lacking or containing partial viral DNA are difficult to separate from the desired vector capsid populations. Based on minute differences in density, ultracentrifugation remains the most effective separation method and has been extensively used at small-scale, but has limitations associated with availabilities and operational complexities in large-scale processing. In this paper, we report a scalable, robust, and versatile anion-exchange chromatography (AEX) method for removing empty capsids and subsequent enrichment of vectors of AAV serotypes 5, 6, and 8. On average, AEX resulted in about 9-fold enrichment of AAV5 in a single-step containing 80±5% genome containing vector capsids, as verified and quantified by analytical ultracentrifugation. The optimized process was further validated using AAV6 and AAV8, resulting in over 90% vector enrichment. The AEX process showed comparable results not only for vectors with different transgenes of different sizes but also for AEX runs under different geometries of chromatographic media. The herein reported sulfate salt-based AEX process can be adapted to different AAV serotypes by appropriately adjusting step-gradient elution conditions to achieve enriched vector preparations.

5.1 Introduction

Recombinant adeno-associated virus (rAAV) based vectors have emerged as a platform of choice for therapeutic gene delivery in both dividing and non-dividing cells[1,2]. The clinical success and resulting regulatory approval of three rAAV based drug products, namely Glybera®, Luxturna™, and Zolgensma® for single-dose curative gene therapy in hereditary monogenic disease indications have set new milestones[3–5].

The progressive understanding of clinical and pharmacological implications of the presence of inadvertently co-synthesized empty capsids (EC) in AAV lots during clinical studies opened new areas of investigation[6]. Devoid of a therapeutic transgene, these EC do not exert direct clinical benefits. Many reports have suggested ECs' role in reducing transduction efficiency (while being in excess) through competition for receptor binding[6], inducing dose-dependent capsid-neutralizing antibody response[7], and cytotoxic T-lymphocytes mediated destruction of transduced cells displaying capsid associated peptide-MHC complexes[8,9]. On the other hand, a potential beneficial effect of excess ECs through its role as a decoy against immune response, protecting functional vector particles has been suggested[10]. In this view, a resultant strategy proposed admixing sequence-modified, non-receptor binding empty capsids of the same serotype in a precisely tailored ratio to a clinical lot of functional vector material (EC-free)[11]. Importantly, in both scenarios, the removal of "co-existing" empty capsids remains a critical step. From a bioprocessing standpoint, the similarity in size and surface charge characteristics of these empty capsids with vector capsids (VC) make their removal challenging.

Ultracentrifugation (UC) approaches developed to remove EC were based on density gradient media such as cesium chloride or iodixanol, where EC and VC were separated based on their buoyant density[12–14]. Although large-scale ultracentrifugation has been industrially demonstrated in viral vaccine[15,16] and AAV vector purification[17], the capital investment associated with this

technology makes it difficult to implement in small and medium-size cGMP facilities. In parallel, various chromatographic protocols developed alone or in combination with UC to generate EC free high-purity clinical grade AAV material have been reviewed in detail and published[18].

To further address UC-associated challenges, especially relevant in high dose vector preparation for systemic administration (10^{12}-10^{14} VG/Kg)[19,20] and achieving an end-to-end linear scalability in the manufacturing process, multimodal chromatographic approaches emerged as a tool for overall downstream processing, including removal of EC. These chromatographic protocols incorporate primary capture steps and intermediate purification steps of a specific modality[21–37] followed by an anion-exchange chromatography (AEX) step for removal of empty capsids[31,38–41]. Moreover, anion-exchange protocols involving chromatography media with improved mass-transfer, such as monolithic stationary phases[41] or adsorptive membranes, have also been reported[40,42]. These reports were specific to a particular serotype, such as AAV1[40], AAV2[43], AAV6[44], and AAV8[40–42]. A recent report on vector capsids enrichment of natural and engineered rAAV vectors from the affinity-purified preparations employing an AEX protocol demonstrated a step closer towards a generic AAV purification method[31].

As part of our sustained efforts directed at improving AAV manufacturing technology, we report herein the development of a simple and scalable AEX protocol for removal of EC and consequent enrichment of AAV5 VC produced in insect-cell cultures. The generic nature of this AAV5-AEX protocol was further validated using AAV6 and AAV8 produced in mammalian cell cultures, demonstrating adaptability to different serotypes. Importantly, the discontinuous gradient elution process, carefully tailored for each serotype, showed the robustness amenable to cGMP operation.

5.2 Results

5.2.1 AAV Sample Preparation for Anion-exchange Chromatography (AEX)

In this study, immuno-affinity-purified AAV was used as a starting material. Besides providing high recovery in a single-step, the affinity purification step substantially increases the concentration of AAV and reduces the amount of non-AAV-related impurities. The immuno-affinity step recovery of genomic particles (VGs) for various AAV serotypes was found to be around 80-85% despite the starting lysate material originating from two different production platforms: (1) insect-cell and (2) mammalian-cell cultures, containing different host-cell impurities. **Table 5.1** shows a summary of overall recovery in flow-through, wash, and eluted AAV collections during affinity-purification runs of insect-cell produced AAV5-*gfp* and mammalian cell-produced AAV6-*gfp*, AAV6-*cas9*, and AAV8-*gfp*.

5.2.2 Screening of Different Salts and their Effect on AAV5 Elution Profile in AEX

The prime task was to optimize the anion-exchange conditions such that the minute difference in net negative charge between AAV5 EC and VC can be exploited at a preparative scale. The screening of various mono (NaCl) and divalent (Na_2HPO_4, and Na_2SO_4) salts was conducted to understand the effect of the valence of the anionic counter-ions (chloride, monohydrogen phosphate, or sulfate) on the resolution and separation efficiency of AAV5 EC over a continuous elution gradient. The affinity-purified AAV5 material was loaded onto an anion-exchange medium (CIMac™ AAV empty/full 0.1 mL, 1.3 μm pore diameter), and after wash, it was subjected to a 20-420 mM linear salt concentration gradient over 200 column volumes (CV) (**Figure 5.1**). Each salt produced a distinct elution pattern where AAV5 particles eluted at low ionic strength, indicated as the peaks 1 (EC) and 2 (VC) (**Figure 5.1)**. The divalent salts not only provided better resolution

Table 5.1 Summary of Affinity-Purification Process Characteristics

Sample	VG/mL	Volume (mL)	Total VGs	% VG Recovery
AAV5-*gfp*/AVB Sepharose [a, b]				
Feed	8.03×10^{10}	1000	8.03×10^{13}	-
Flowthrough	3.07×10^{09}	1000	3.07×10^{12}	3.82
Column Wash	7.13×10^{08}	50	3.57×10^{10}	<1%
Elution	6.72×10^{12}	10	6.72×10^{13}	83.69
AAV8-*gfp*/Capture Select AAVX [c, d]				
Feed	3.19×10^{10}	1000	3.19×10^{13}	-
Flowthrough	5.47×10^{08}	1000	5.47×10^{11}	1.71
Column Wash	9.81×10^{07}	50	4.91×10^{09}	<1%
Elution	2.61×10^{12}	10	2.61×10^{13}	81.82
AAV6-*gfp*/Capture Select AAVX [d]				
Feed	2.87×10^{10}	1000	2.87×10^{13}	-
Flowthrough	7.24×10^{08}	1000	7.24×10^{11}	2.52
Column Wash	1.13×10^{08}	50	5.65×10^{09}	<1%
Elution	2.33×10^{12}	10	2.33×10^{13}	81.18
AAV6-*cas9*/Capture Select AAVX [d]				
Feed	2.58×10^{10}	1000	2.58×10^{13}	
Flowthrough	5.44×10^{08}	1000	5.44×10^{11}	2.11
Column Wash	8.75×10^{07}	50	4.38×10^{09}	<1%
Elution	2.15×10^{12}	10	2.15×10^{13}	83.33

VG, viral genomes analyzed via ddPCR

[a, c] Average value for multiple runs (n=3), relative SD <±10%

[b] 5 mL prepacked column, [d] 5 mL prepacked column

of AAV associated two peaks but also displayed 260/280 nm absorbance ratios with values close to that representative of EC and VC (**Table S1**). Compared to NaCl, AAV5 elution at a lower salt concentration of divalent monohydrogen phosphate and sulfate indicate their higher displacement strength. Moreover, relative to NaCl, the peaks eluted with divalent salts were narrower and with less peak overlapping (**Figure 5.1**), suggesting improved enrichment and separation of vector capsids from empty capsids by divalent anions.

To account for the 3-fold difference in ionic strengths resulting from the different valences of the Cl^- and SO_4^{2-} ions, elution was studied by matching the ionic strength (IS) of the gradient and the slope. Based on the previous elution of AAV5 capsids in the range of 20-30 mM Na_2SO_4, the continuous gradient was run from 60-90 mM ionic strength at gradient slope adjusted to 2 mM IS/CV for both NaCl and Na_2SO_4. In Na_2SO_4 gradient, the AAV5 capsids eluted at 60-90 mM ionic strength. In contrast, no AAV5 elution occurred in this range of the gradient in NaCl, where instead, elution occurred at higher ionic strength (100-130 mM). The separation of EC and VC peaks in NaCl remained similar to that shown in **Figure 5.1A**.

The sulfate salt was selected over monohydrogen phosphate based on the relative ratio of signal intensity and absorbance peak area at 260 nm and 280 nm for EC and VC peaks. For monohydrogen phosphate, the higher peak area of peak 2 compared to peak 1 indicated EC being co-eluted with VC (**Table S1**). The $A_{260/280}$ ratios and peak areas in sulfate were more representative of empty and vector capsids, as confirmed by a comparative analysis of these peak areas against sedimentation velocity analytical ultracentrifugation (*sv*-AUC) profiles (**Table S1**).

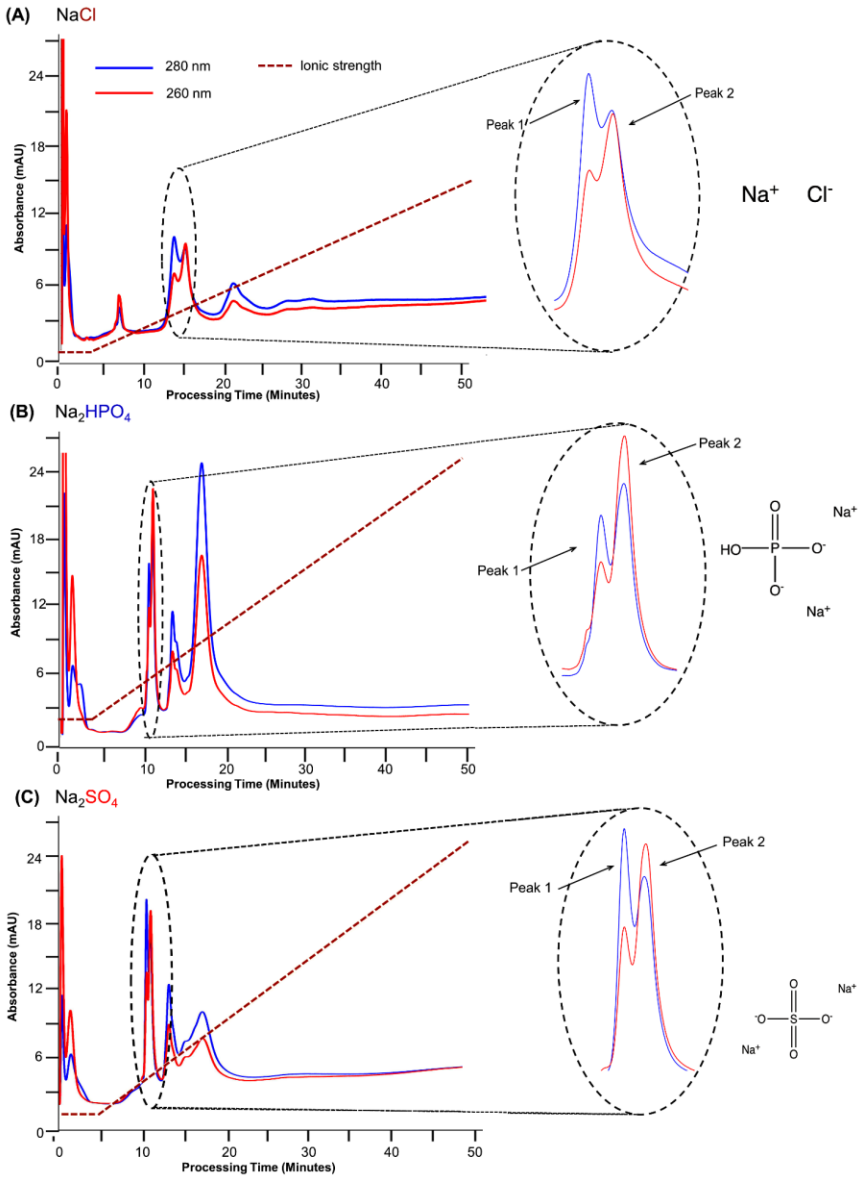

Figure 5.1 AAV5-gfp AEX Elution Profile Under Continuous Gradient of Different Salts

The AEX column used in this study was a CIMac Q 0.1 AAV, processing buffer is 25 mM BTP, pH 9.0, and salt concentration gradient ranges from 20-420 mM in 200 CV with the slope of 2 mM salt/CV. The process flowrate was 0.5 mL/min. The magnified image of the AAV5 capsids peaks (peak 1 and 2), and corresponding salts' chemical structures are shown on the right-hand side. **(A)** AAV5-*gfp* elution in a NaCl continuous gradient. AAV5 capsid elution range is 100-130 mM. **(B)** AAV5-*gfp* elution in a Na_2HPO_4 continuous gradient with AAV5 eluting in the range of 25-35 mM. The larger area under peak (AUP) of the VC peak does not correlate with the VC proportion relative to EC when compared with the *sv*-AUC profile of starting material. This indicates the co-elution of empty capsids in VC peak fraction. **(C)** AAV5-*gfp* elution in a Na_2SO_4 continuous gradient where EC and VC peaks elute at a concentration range of about 20-30 mM. The 260/280 nm signal ratio closely corresponds with the known values of the EC and VC standards and *sv*-AUC results. AEX, anion-exchange chromatography; *sv*-AUC, sedimentation velocity analytical ultracentrifugation; AUP, area under the peak; CV, column volume; EC, empty capsids; VC, vector capsids.

5.2.3 Chromatographic Buffer Composition and Mode of Operation

A pH screening study at pH 9.0, 9.5, and 10.0 was conducted to investigate its effect on the separation efficiency. No improvement in separation efficiency was observed above pH 9. Preparative scale process optimization was conducted on an FPLC system employing a 1 mL scale AEX monolith column (CIMmultus™ QA 1 mL, 0.95-1.15 µm pore diameter) using bis-Tris propane (BTP) buffer (pH 9.0 ± 0.02) with 50 mM Na_2SO_4 salt in the elution buffer. A shallow continuous gradient (0.66 mM IS/CV) process (**Figure 5.2A**), which efficiently separated empty and vector capsid populations (**Figure 5.2B**), was developed. The peak fractions containing AAV capsids were identified via anti-AAV VP Western blot (**Figure 5.2C**). The empty capsids eluted first in early elution fractions followed by vector capsids as analyzed via digital-droplet polymerase chain reaction (ddPCR) (**Figure 5.2D, Table S2**). From this continuous gradient elution, a step-gradient elution process that resolved two capsid populations with operational simplicity was derived (**Figure 5.2E)**. The *sv*-AUC analyses indicated 80% VC and 20% EC (**Figure 5.2I**) in the genomic peak fraction (**Figure 5.2F**), whereas the EC peak fraction showed over 95% EC (**Figure 5.2H**). As a result, the VC content was enriched by ~9-fold from the initial ~9%, and EC content was reduced 4.5-fold from an initial ~91% (**Figure 5.2G**). It is notable that the relative proportion of the 79S population with respect to 95S also got reduced from 37% to 18% in the VC peak fraction. The summary of *sv*-AUC analyses expressed as fold improvement in VC enrichment is provided in **Table 5.2**. Notably, the 95S VC population of the starting material (**Figure 5.2G**) appeared as an 89S population in the VC capsids (**Figure 5.2I**) collected in the AEX process. Interestingly, the packaged genome size was similar in both of these samples as analyzed via alkaline agarose gel electrophoresis (**Figure 5.3D,** AAV5-*gfp***, lane 1 and 3**).

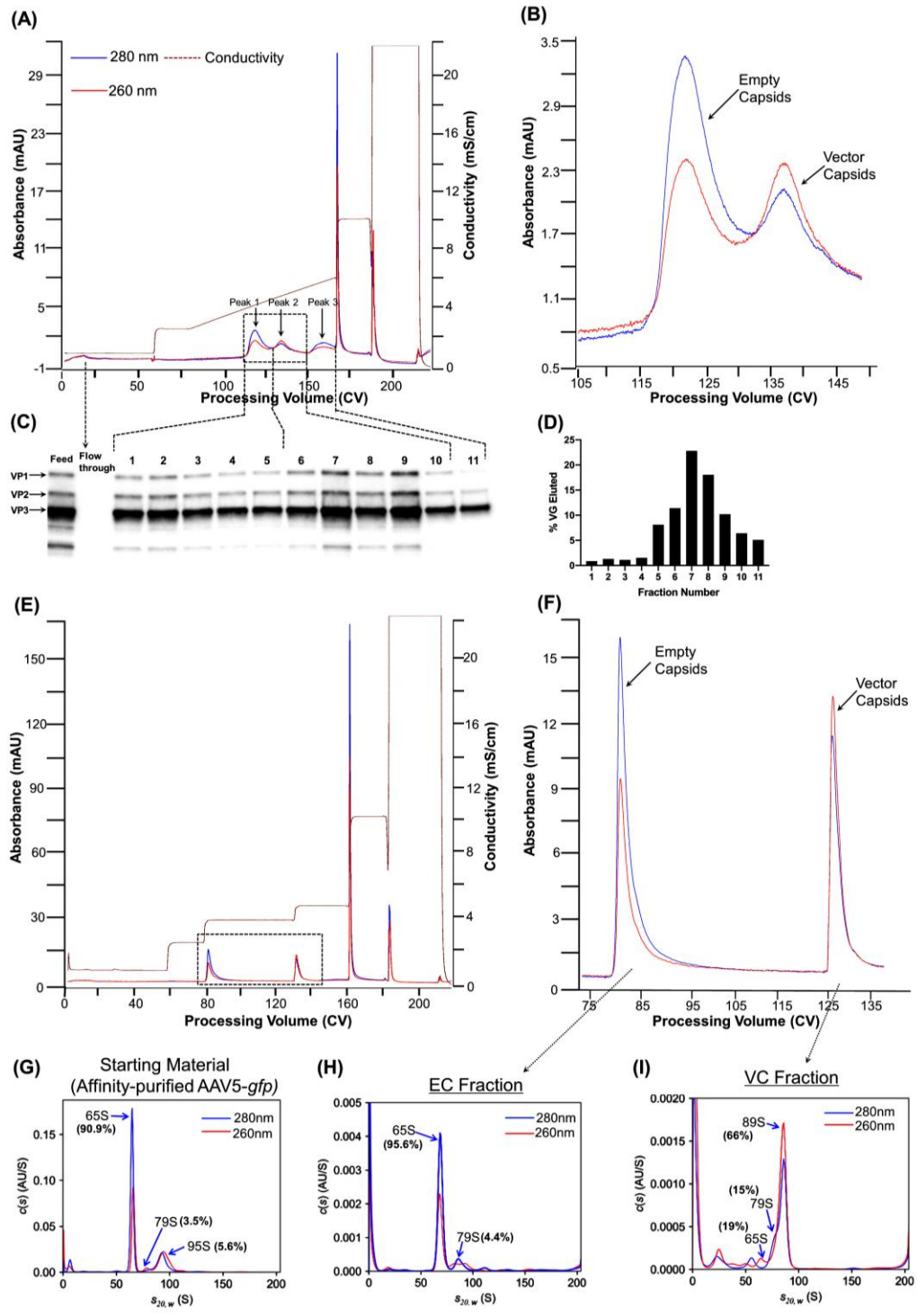

Figure 5.2 AAV5-gfp AEX Process Development

(A) AEX-process chromatogram of AAV5-*gfp* in a continuous gradient of elution buffer. Peaks eluting in this continuous gradient (peak 1, 2, and 3) and corresponding to AAV capsids are shown in a box. Multiple fractions were collected and analyzed by Western blot against AAV VP proteins and ddPCR to determine the presence of AAV capsids and packaged genome, respectively **(B)** Magnified image of AAV5 EC and VC capsid peaks eluted

in a continuous gradient. **(C)** Western blot analysis of multiple fractions collected from a continuous gradient run. Three bands corresponding to three VP subunits indicate the presence of the AAV capsid. Peak 3 shows the AAV VP bands, indicating residual AAV VC capsids eluted at high salt wash step (100%B). The high UV 280 nm signal in peak 3 may also indicate the co-elution of residual protein impurities present in the affinity-purified material. **(D)** VG analyses, via ddPCR, of multiple fractions collected from continuous gradient run. A total of 13% VGs were detected in peak 1 (Fraction 1-5), whereas around 70% of VG were detected in peak 2 (Fraction 6-10). The presence of ~5%VGs in fraction 11 represents the elution of residual AAV VC capsids in peak 3 at the high salt wash (100%B) step. **(E)** AAV5-AEX chromatographic profile employing optimized process conditions (10 mM BTP and Na_2SO_4 as an eluent salt) of a step-gradient run. AAV5 EC and VC peaks are shown in a box. **(F)** Magnified image of AAV EC and VC peak fractions (as confirmed by SDS-PAGE and ddPCR). The first peak with AUP value for $A_{260/280}$ ratio of 0.58 corresponds to empty capsids, whereas the second peak with AUP value for $A_{260/280}$ ratio of 1.21 indicates predominantly the genome containing vector capsids. **(G)** *sv*-AUC profile of the affinity-purified AAV5-*gfp*. Three distinct AAV capsid populations with unique sedimentation coefficients were detected: (1) light capsids-65S (EC), (2) Heavy capsids-95S (VC), and (3) Intermediate population-79S. The relative percentages of each of these AAV5 variants are 91% (65S), 3.5% (79S) and 5.5% (95S). **(H)** *sv*-AUC profile of AAV5 EC fraction. The dominant peak of EC at 65S and a second small peak of intermediate species at 79S translate to their relative proportion of 95.6% and 4.4%, respectively. The absence of a peak at 95S indicates no detectable co-elution of VC in this fraction. **(I)** *sv*-AUC profile of AAV5 VC fraction. The three distinct populations at 65S, 79S, and 89S have a relative proportion of ~19%, ~15%, and ~66%, respectively. ddPCR, digital-droplet polymerase chain reaction; VG, viral genome copies.

Although not clear, the higher S values (95S) could be due to the interaction of the VC population with other sample matrix components present in the affinity-purified material. The VC and EC contents of the same fractions were also analyzed by the optical-density measurement method[45], and these results are in agreement with the *sv*-AUC results, as shown in **Table 5.3**. It should be noted that within the scope of this paper, the term VC refers to the entire population of AAV capsids encapsidating genomic material unless otherwise specified.

5.2.4 AAV5 AEX-step Reproducibility

For the reproducibility study, the affinity-purified AAV5 material from three different production runs was subjected to the AEX step-gradient protocol. The *sv*-AUC profiles of VC peak fractions

Table 5.2 Summary of VC Enrichment via AEX

Sample	% Relative proportion			Fold VC Enrichment	Relative Ratio (EC: VC)	Relative Ratio (Heavier: Intermediate capsids)
	EC	VC				
	Lighter Capsids	Intermediate Population	Heavier Capsids			
AAV5-*gfp* [a,b]						
	66S	79S	95S	-	-	-
Affinity-purified AAV5	90.91	3.43	5.66	-	10:1	1.6:1
EC Peak Fraction	95.6	4.4	ND	-	-	-
VC Peak Fraction	19.81	14.69	65.50 (89S)	8.8x	1:4	4.4:1
AAV8-*gfp* [a,b,]						
	63S	74S	84S	-	-	-
Affinity-purified AAV8	62.56	2.03	35.41	-	1.7:1	17.4:1
EC Peak Fraction	96.6	ND	3.4	-	-	-
VC Peak Fraction	3.13[c]	4.22	92.65	2.6x	1:31	22:1
AAV6-*gfp* [d]						
Affinity-purified AAV6	63.17	36.83		-	1.71:1	-
EC Peak Fraction	93.28	6.72		-	-	-
VC Peak Fraction	5.36	94.64		2.6x	1:18	-
AAV6-*cas9* [d]						
Affinity-purified AAV6	60.59	39.41		-	1.54:1	-
EC Peak Fraction	95.72	4.38		-	-	-
VC Peak Fraction	4.54	95.46		2.4x	1:21	-

AEX, anion-exchange chromatography; EC, empty capsids; VC, vector capsids; ND, not detected

[a] Average value for multiple runs (n=3), relative SD <±5%

[b] Values reported from *sv*-AUC analyses for determination of the relative proportion of empty capsid and vector capsid

[c] No visible peak of AAV8 63S was observed in AUC profiles of VC fraction (**Figure 5.4E and 5.5A**). In the sample with a very low UV signal, a small peak at 63S was observed (e.g., **Figure 5.5A, Lot#2**). Although not

clear if it was the noise of the UV-detection as the absorbance was below 0.001, calculations were made based on the UV signal peak area at this 63S position not to exclude the possibility of the 63S population present in trace amount.

[d] Values reported from the optical-density method for determination of the relative proportion of empty capsid and vector capsid.

and graphical representation of reproducibility in VC enrichment from *sv*-AUC data are shown in

Figures 5.3A and 5.3B. A lot-to-lot enrichment of samples in VCs with a relative standard deviation <5% was achieved.

5.2.5 AAV5 AEX-step Reproducibility

For the reproducibility study, the affinity-purified AAV5 material from three different production runs was subjected to the AEX step-gradient protocol. The *sv*-AUC profiles of VC peak fractions and graphical representation of reproducibility in VC enrichment from *sv*-AUC data are shown in **Figures 5.3A and 5.3B**. A lot-to-lot enrichment of samples in VCs with a relative standard deviation <5% was achieved.

5.2.6 Characterization of AEX-processed AAV5 lot

In addition to *sv*-AUC analysis, the purified and enriched VC preparations of AAV5 were analyzed for identity, purity, VP proteins ratio, and vector genome packaging using SDS-PAGE and alkaline agarose gel electrophoresis (**Figure 5.3C, 5.3D**). The SDS-PAGE profile confirms (1) EC and VC fractions with reduced protein impurities and (2) three VP subunit proteins in a near prototypic ratio (1:1:10). The alkaline agarose gel electrophoresis profile also displayed two characteristics.

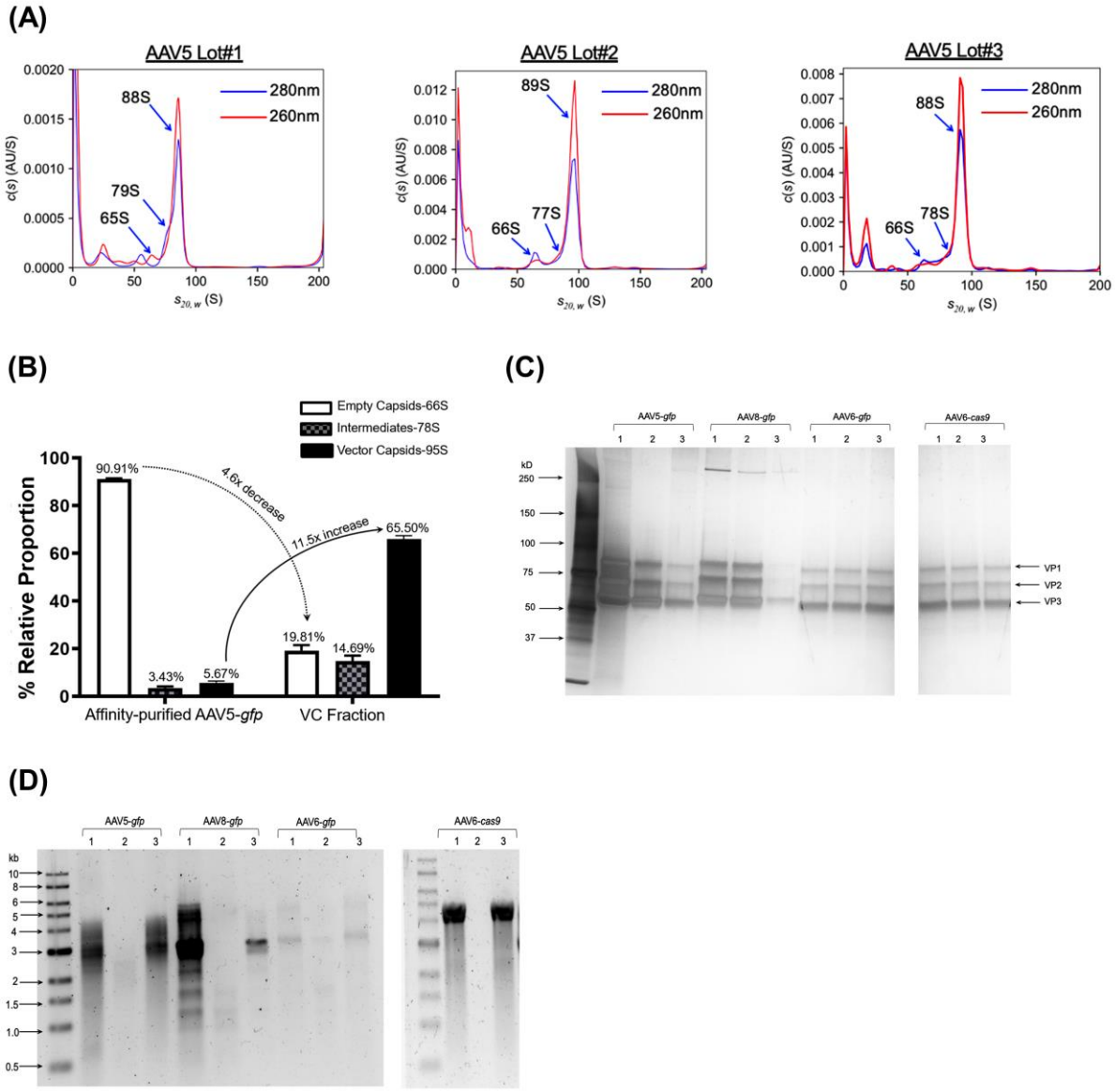

Figure 5.3 AAV5-AEX Process reproducibility and Characterization of AEX-processed AAV material

(A) *sv*-AUC profiles of OneBac/Insect cell produced AAV5 VC peak fractions collected from three different runs representative of three different production batches of AAV5. **(B)** Graphical representation of the AEX process reproducibility data for AA5-*gfp*. The individual column represents the percent relative proportion of empty capsids, vector capsids, and intermediate capsids determined from *sv*-AUC data of affinity-purified starting material and VC peak fractions. The VC peak fractions were collected from a representative optimized discontinuous gradient AEX process. The variability is represented by an error bar (RSD <5%). **(C) SDS-PAGE analysis of AEX processed AAV fractions.** Lane 1, 2, and 3 correspond to the affinity-purified starting material, empty capsid fraction, and vector capsids fractions, respectively. For all serotypes, three major bands correspond to three VP subunits of AAV capsids. The gel image shows an absence of major protein impurities except that

of >250 kDa in EC and VC (panel 2 and 3) fractions. **(D) Alkaline agarose gel electrophoresis profile for vector genome analysis of AEX processed AAV fractions**. Lane 1, 2, and 3 correspond to the affinity-purified starting material, empty capsid fraction, and vector capsids fractions, respectively. Notably, the size of the expression cassette (from ITR-to-ITR) for AAV5-*gfp*, AAV8/6-*gfp*, and AAV6-*cas9* is 3.79 kb, 2.9 kb, and 4.8 kb, respectively. **(1) AAV5-*gfp***. In the case of affinity-purified AAV5-*gfp* sample (lane 1), the maximum packaged size is around 4.7 kb followed by a continuous smear between 3-4.5 kb, two visible bands around 3 kb and 2.8 kb, and finally a smear below 2.8 kb. In EC fraction, a smear of size up to 2.4 kb is visible, indicating the presence of capsids packaging small molecular weight DNA. A similar trend is also visible as 79S intermediate capsid in the *sv*-AUC profile. In VC capsid fraction (lane 3), similar to affinity-purified sample, high molecular weight packaged DNA (3-4.5 kb), and low molecular weight DNA (<3 kb) are visible. **(2) AAV8-*gfp***. In the case of affinity-purified, the maximum packaged size for AAV8-*gfp* (lane 1) is around 5 kb, which is followed by a smear (3-5 kb) and multiple distinct bands <3 kb. In the EC fraction (lane 2), three bands <2 kb in size are visible, indicating the presence of capsids packaging small size DNA. In VC capsid fraction (lane 3), similar to affinity-purified sample, high molecular weight DNA bands, a faint band at ~5 kb, and two dominant bands of 2.8kb and 3kb size are visible. Low signal intensities in this sample indicate a low sample amount compared to lane 1, which may be due to possible loss of during concentration step using centrifugal filters or low sample recovery after the *sv*-AUC run. The band at ~3 kb indicates the presence of capsids primarily and preferentially packaging complete vector (ITR-to-ITR). A trend similar to AAV8-*gfp* is also visible in **(3) AAV6-*gfp*** fractions, where, in the VC fraction (lane 3), a dominant band at ~3 kb indicates capsids with primarily packaging complete vector sequence. **(4) AAV6-cas9**. In both affinity-purified (lane 1) and enriched VC fractions (lane 3), dominant high molecular weight DNA bands around 5 kb and 4 kb are visible, suggesting capsids preferentially packaging larger size (high molecular weight) vector sequence. The faint smear below 4kb size indicates a continuum of intermediate capsid population packaging non-specific fragments of DNA. No visible band of small molecular size DNA in AAV6-*cas9* EC fraction may attribute to either their presence at the level below the LOD or absence in the sample. ITR, inverted terminal repeats; LOD, limit of detection; RSD, relative standard deviation.

First, in EC capsid fraction, a genome of <3 kb in size was detected in the form of a smear **(Figure 5.3D,** AAV5-*gfp***, lane 2),** whereas the band(s) representing large-size genome (>3 kb) was too faint to detect. Second, both a small-size genome (<3 kb) and a high molecular weight genome (3-4.5 kb) were present in the vector capsid fraction (**Figure 5.3D,** AAV5-*gfp***, lane 3**). The small genome (<3 kb) may represent fragments smaller than the vector expression cassette (3.8 kb), and the larger genome (>3.8 kb) may potentially represent co-packaging of other fragments with vector cassette.

The alkaline agarose gel results were also supported by the AUC profile of (1) empty capsid fraction (**Figure 5.2H**) where the capsid population encapsidating small size genome appeared as 79S peak and (2) vector capsid fraction (**Figure 5.2I**), which showed the presence of residual 79S capsids and capsids encapsidating large size genome as 89S. Combined results of AUC and alkaline agarose gel suggest that AAV capsids encapsidating small-sized intermediate genomic material co-eluted in the first empty capsid fraction and the remainder of these also eluted in VC fraction.

Table 5.3 Comparability evaluation between *sv*-AUC and optical-density measurement for determination of relative % empty capsids and % vector capsids in purified AAV preparations

Sample	***sv*-AUC analyses**		**Optical-Density method**[45]	
	% Empty Capsids	**% Vector Capsids**	**% Empty Capsids**	**% Vector Capsids**
Affinity-purified AAV5-*gfp*	90.91	9.09	89.71	10.29
AAV5-*gfp*/EC Peak Fraction	95.6	4.4	89.32	10.68
AAV5-*gfp*/VC Peak Fraction	19.81	80.19	10.57	89.43
Affinity-purified AAV8-*gfp*	62.56	37.44	61.07	38.93
AAV8-*gfp*/EC Peak Fraction	96.60	4.4	90.56	9.44
AAV8-*gfp*/VC Peak Fraction	3.13	96.87	4.37	95.63

sv-AUC, sedimentation velocity analytical ultracentrifugation; EC, empty capsids; VC, vector capsids

5.2.7 AEX-step Generalization for AAV6 and AAV8 serotypes

The AEX process generalization was studied by assessing its efficiency in the enrichment of VC for other clinically relevant serotypes, AAV8, and AAV6. We decided to use 10 mM BTP, pH 9.0, and sulfate salt with the monolith column. The affinity-purified material of serotypes AAV8 and AAV6 was first subjected to the continuous gradient elution process (**Figure S1**) and, thereafter, a discontinuous gradient process. Specific to serotypes, gradient step, and buffer composition were adjusted to optimize the separation of EC and VC (**Figure 5.4**).

The sodium sulfate salt used for AAV5 was replaced with magnesium sulfate for AAV8. Magnesium sulfate offered slightly higher VC enrichment, as indicated by *sv*-AUC analysis of the VC peak fraction (**Figure S2-A and B**). The magnesium sulfate salt was also used in the AAV6-AEX process, but initially, AAV6 eluted as a single broad peak (**Figure S2-C**). The addition of 5 mM $MgSO_4$ to both the column equilibration buffer and the buffer-exchanged sample solved the problem of single peak elution, and AAV6 ECs and VCs eluted as separate peaks in a continuous gradient (**Figure S2-D**). The 5 mM salt supplementation strategy was ultimately applied to AAV5 (Na_2SO_4) and AAV8 ($MgSO_4$) as well. This additional salt supplementation helps retain components in flow-through, which may otherwise bind in the absence of additional salt and elute at 5 mM salt.

The chromatograms of representative step-gradient AEX processes for AAV8 and AAV6 vectors and *sv*-AUC profiles of AAV8 EC and VC peak fractions are shown in **Figure 5.4**. The proportion of VC capsid population (74S+84S) in the VC peak fraction of AAV8 was increased to near 100% from the 37% observed in starting material as analyzed by *sv*-AUC (**Figure 5.4A-4E**), whereas no visible peak at 63S corresponding to AAV8 EC was observed in this fraction. Comparable results were also obtained by the optical-density method (**Table 5.3**). Because of limited access to the AUC instrument and demonstrated comparability between *sv*-AUC and optical-density method

determination of relative percentage EC and VCs, the AAV6 samples were analyzed only by the latter method. Similar to AAV8, the final vector preparation of AAV6 also consisted of over 90% VCs (**Table 5.2**). The AEX process recovery and yield results for all serotypes are shown in **Table S3**.

Further characterization of AEX-processed lots via SDS-PAGE confirmed the purity of enriched vector capsid fractions of AEX purified AAV8-*gfp* and AAV6-*gfp*, which showed no major detectable protein impurities except a visible band of >250 kDa (**Figure 5.3C**). The alkaline agarose gel electrophoresis profiles of AAV8-*gfp* also showed the bands of <2 kb in size in the EC fraction (**Figure 5.3D,** AAV8-*gfp***, lane 2**), indicating the co-elution of AAV8 capsids carrying small-size intermediate genomic material. In the case of AAV6-*gfp*, the band of the size of the expression vector (2.9 kb), as well as smaller genome fragment (<2 kb), were detected in EC fraction (**Figure 5.3D,** AAV6-*gfp***, lane 2**).

The AEX-step reproducibility, as demonstrated earlier for insect cell produced AAV5-*gfp*, was also assessed for HEK293-produced AAV8-*gfp* vectors. Three production lots of immuno-affinity purified AAV8 vectors were subjected to the step-gradient AEX process (**Figure 5.4A**). The *sv*-AUC analysis of empty and vector capsid fractions collected from these runs also showed a lot-to-lot reproducibility (**Figure 5.5A, 5B**) in VC enrichment with a variability of < 5% RSD.

5.2.8 Further Generalization of AEX-step

The versatility, herein defined as the ability of the AEX process to exhibit transgene-independent separation efficiency of EC and VC, was assessed for serotype 6 derived recombinant vectors. AAV6 was selected due to its reported potential in cell therapy and gene delivery applications[46]**.** An additional AAV6-*cas9* (4.8 kb) vector was selected for this study. The affinity-purified AAV6-

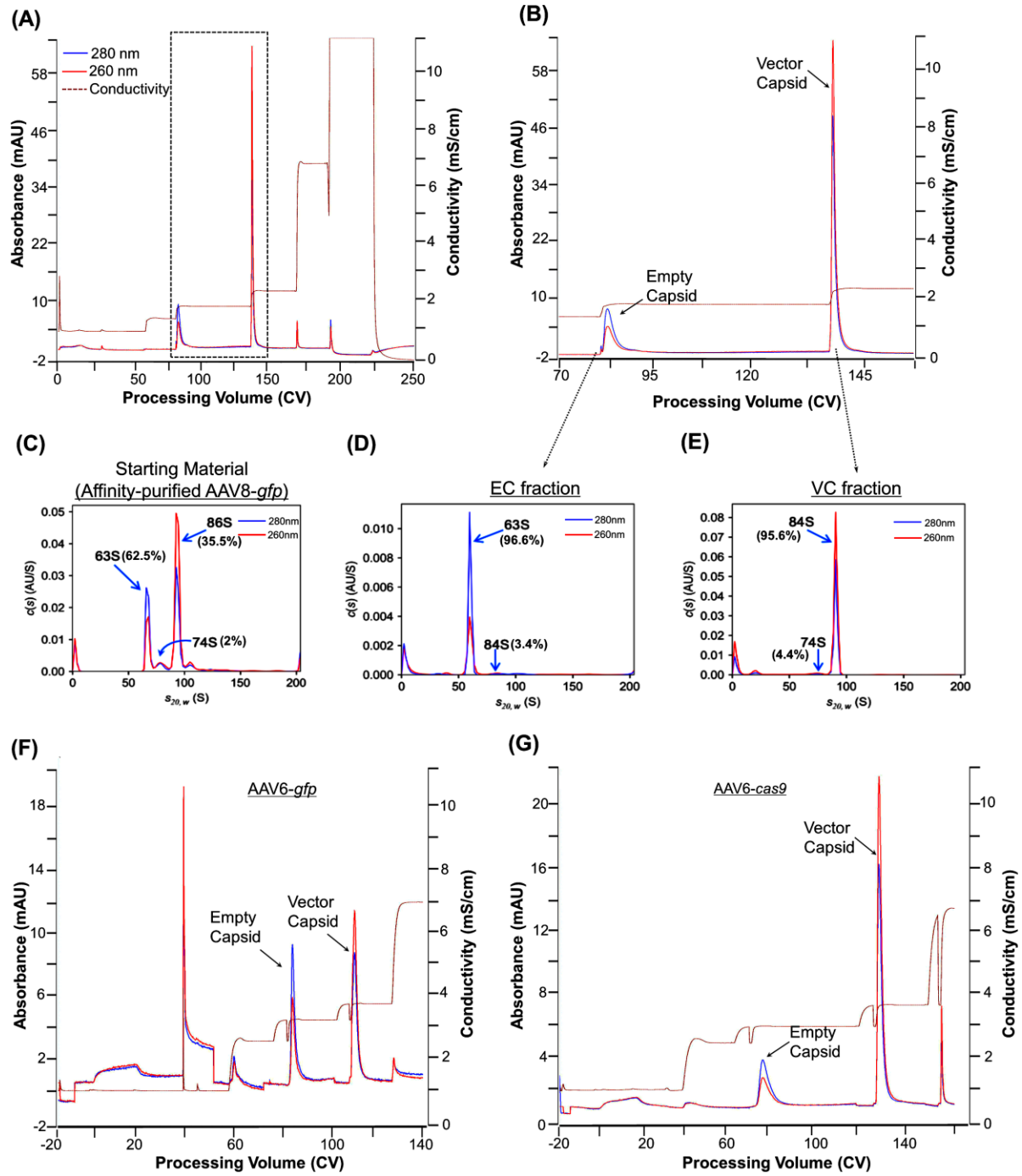

Figure 5.4 AAV-AEX Process Generalization demonstration for AAV6 and AAV8 serotype

(A) AAV8 AEX chromatographic profile employing optimized process conditions of step-gradient AEX run. **(B)** Magnified image of two peaks corresponding to AAV8 capsids, as confirmed by SDS-PAGE and ddPCR. The first peak with $A_{260/280}$ ratio of 0.53 correlates to empty capsids, whereas the second peak with for $A_{260/280}$ ratio of 1.33 correlates to the genome containing capsids. **(C)** *sv*-AUC profile of AAV8 starting material

(affinity-purified AAV8-*gfp*). Three distinct AAV capsid populations with unique sedimentation coefficient are (1) light capsids-63S (EC), (2) heavy capsids-86S (VC), and (3) intermediate population-74S. The relative percentages of each AAV8 capsid variants are 62.5 % (63S), 2 % (74S) and 35.5 % (84S). Note the differential 260/280 nm signal profile for EC and VC, the intensities of which directly correspond to molar absorption coefficients of AAV8 capsid protein, packaged DNA, and their proportion. **(D)** *sv*-AUC profile of AAV8 EC fraction collected from a representative AEX run. The dominant peak of EC at 63S and a small peak of VC at 84S correlate to their relative proportion of 96.6% and 3.4%, respectively. **(E)** *sv*-AUC profile of AAV8 VC fraction. The two populations detected are intermediate species (74S) and heavy capsids-VC (84S), with their relative proportion of 4.4% and 95.6%, respectively. Step-gradient run profile employing optimized process conditions AAV6-*gfp* **(F***)* and AAV6-*cas9* vectors **(G)**. The higher 260 nm signal intensity in the VC peak of AAV6-*cas9* **(G)** compared to AAV6-*gfp* **(F)** potentially corresponds to the difference in the molar absorption coefficients due to different size vector DNA (*gfp*-2.9 kb Vs. *cas9*-4.8 kb).

cas9 vector, when subjected to the AAV6-*gfp* AEX process (under both linear and step-gradient elution modes), eluted at the same salt ionic strength (%B steps) and showed EC and VC elution profiles identical to that of AAV6-*gfp* (**Figures 5.4F, 4G, and S1-C, S1-D**). Both quantitative (**Table 5.2**) and qualitative enrichment (**Figure 5.3C, 3D**) of AAV6-*cas9* vector capsid were comparable to that of AAV6-*gfp*.

The AEX process developed for AAV8 was further assessed in a chromatography medium with a different resin matrix geometry and chemistry. The affinity-purified AAV8-*gfp* vector material was subjected to the same continuous gradient AEX process using two different anion-exchange column configurations and matrices: monolith and packed-bed. Notably, in both cases, the range of the salt gradient and its slope (1 mM IS/CV) were kept the same, whereas the flow rate was reduced from 10 mL/min on a monolith to 3 mL/min for packed-bed to be within acceptable backpressure limits. Representative chromatograms of the AAV8-*gfp* purification are superimposed in **Figure 5.5C**. No substantial differences in the AAV8 EC and VC elution profiles and characteristics (**Table S4**) were observed.

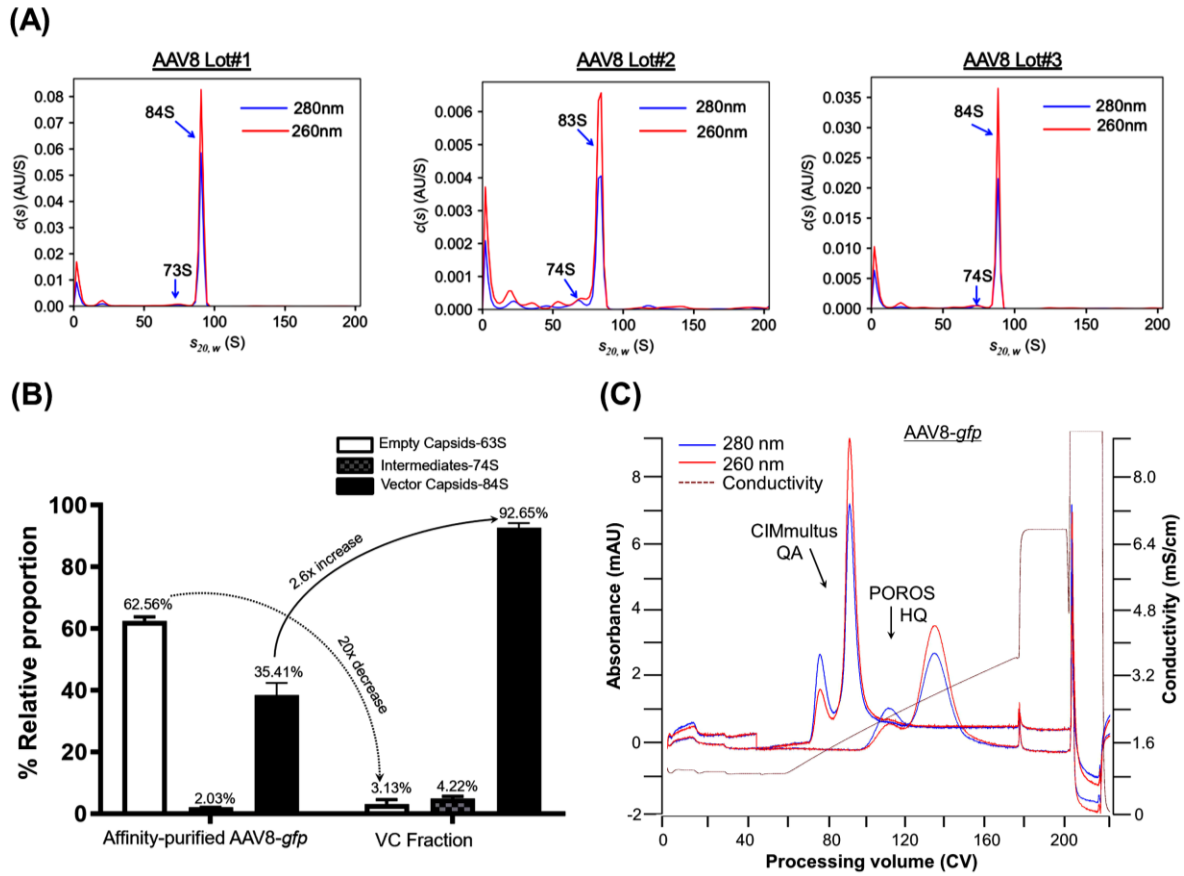

Figure 5.5 AEX-step reproducibility and adaptability demonstration for AAV8-gfp vectorsFigure **(A)** *sv*-AUC profiles of for HEK293SF cell produced AAV8-*gfp* VC peak fractions collected from three different production batches of AAV8 demonstrating reproducible enrichment. **(B)** Graphical representation of the AEX process reproducibility data AA8-*gfp*. Each plot represents the relative % proportion of empty capsids, vector capsids, and intermediate capsids determined from *sv*-AUC data for starting material and VC peak fractions. The VC peak fractions were collected from a representative optimized discontinuous gradient AEX process. The variability is represented by an error bar (RSD <5%). **(C)** Superimposed chromatographic elution profiles of AAV8-*gfp* AEX run using monolith (CIMmultus™ QA-1 mL) and packed-bed (POROS™ HQ-1 mL) under $MgSO_4$ salt gradient from 20-120 mM ionic strength over 100 CV. In the case of monolith column, AAV8 EC and VC eluted at 36.5 mM and 50.5 mM ionic strengths, whereas, in the case of packed bed column, EC and VC eluted at higher ionic strengths of 65.5 mM and 87.5 mM, respectively. RSD, relative standard deviation.

5.3 Discussion

The utilization of universal and highly effective ultracentrifugation-based protocols for large-scale AAV vector capsid enrichment is limited by the availability, reservations to adapt and install, and operational feasibility in current GMP facilities for AAV production. Various GMP amenable ion-

exchange column chromatography protocols have also been reported to separate empty and vector capsids based on minute differences in net capsid charges obtaining varying degrees of VC enrichment. Many of these reported protocols were serotype-specific with limited application to other serotypes, and in recent times, interest has grown in developing an AEX protocol that can be rapidly adapted to different serotypes to generate EC-free vector material. Aligned with this interest, in this paper, we have reported a scalable anion-exchange chromatographic process for AAV5 VC enrichment with its adaptability demonstrated for serotypes 6 and 8 with minor adjustments.

During the salt-screenings study, AAV5 elution in a continuous NaCl gradient displayed poor resolution and separation with substantial overlapping between EC and VC peaks (**Figure S1**). Compared to monovalent chloride salt, the high ionic-strength divalent anionic salts, sodium monohydrogen phosphate (HPO_4^{2-}), and sodium sulfate (SO_4^{2-}) eluted AAV5 EC and VC with high-resolution separation of EC and VC (**Figure 5.1**), resulting in better VC enrichment as shown by $A_{260/280}$ ratio (**Table S1**). This observation was different from the previous AAV5 related publications where the VC enrichment was achieved using either a weak anion exchanger (POROS PI) and a salt of monovalent chloride anions (KCl)[39] or a strong anion exchanger (POROS HQ) and salt of acetate (Tris-acetate)[31] or chloride (NaCl)[30,42]. Better resolution and separation of AAV1 empty and vector capsids on HPLC-scale column packaging analytical-grade nonporous 3 µm Mini Q™ beads was reported upon replacement of NaCl with kosmotropic salts of NH_4^+, $(CH_3)_4N^+$, PO_4^{3-}, and SO_4^{2-} [47].

The intrinsic net negative charge differences of AAV5 EC and VC were exploited, employing a shallow elution gradient (0.66 mM IS/CV) of sodium sulfate salt, which resulted in improved resolution and separation compared to previous results. Although improved from the previous

value of 0.49, the resolution coefficient of 0.77 was still less than ideal (>1.5) with reduced yet evident co-elution of EC and VC. A discontinuous (isocratic/step) gradient elution protocol was then developed, specifically tailored to ensure maximum EC removal, maximizing the VC enrichment and recovery. As a result of step optimization, a substantial elution of empty capsids was achieved in the fraction preceding the VC elution step. The partial co-elution of the intermediate population in both empty and vector capsid (encapsidating full-length genome: ~ 4.7 kb) fraction indicated that its net negative charge lies between the two populations at the extremities. The VC elution step was also optimized to ensure minimum co-elution of contaminants (eluting just after the VC peak, **Figure 5.2A**, peak 3) present in the affinity-purified starting material. A slightly lower salt concentration step was selected to achieve this, which resulted in high purity and VC recovery (73%) at the expense of only 6% of VGs co-eluting in the later fractions with other contaminants. The collective recovery of the VGs in all fractions was above 90% (**Table S3**).

The 80% AAV5 VC proportion in the step-gradient VC fraction as determined via *sv*-AUC analysis was comparable to the 82% (also analyzed via *sv*-AUC) recently reported from the team of Sanofi[31]. In both cases, despite different AAV5 production platforms and technology (One-Bac/Sf9 in our case and HEK293/triple plasmid transfection at Sanofi), the affinity-purified starting material consisted of approximately similar fractional content of empty capsids (91% in our case and 86% in the case of Sanofi) resulting in comparable fold reduction in empty capsids (~5x) after AEX step. In other reports, the AAV5 VC content in the purified preparation was reported 90%[39] or near 100%[30] as determined from negatively stained TEM analysis. The AEX-step recovery of 73% for AAV5 reported herein is higher than the previous reports of 6%[39] and 54%[31].

The sulfate-based step-gradient elution approach initially developed for AAV5 was also successfully applied to gfp expressing AAV6 and AAV8 vectors and cas9 expressing AAV6 vector. For both serotypes, the step-elution profiles, VC enrichment (>90%), and recovery (80-83%) were similar, demonstrating the versatility of the protocol independent of the serotype or the transgene. More than 95% VC proportion in AAV8-*gfp* preparation was comparable to previous AAV8 specific reports utilizing membrane anion-exchangers[40,42]. The AEX-step-gradient recovery of 81% is higher than the previous reports, where it was reported to be 43% [40] or 67%[42]. Similarly, for AAV6-*gfp* also, the >90% VC proportion in the final preparation is comparable with the previous report[31].

It was observed that the efficiency of chromatographic resolution of empty and vector capsid under continuous elution gradient and consequent VC enrichment in a step-gradient process was inversely related to the relative proportion of EC in the affinity-purified starting material. The EC and VC peak resolution of the AAV5 sample containing 90% empty capsid fractional content was lower (R_s:0.77) than the AAV8 or AAV6 (R_s:1.1-1.3) sample having 65% of fractional empty capsid content. Similar to peak resolution, the consequent enriched VC content (% VC) in a step-gradient process was also lower for AAV5 (81% VC) compared to AAV6 or AAV8 (>90% VC). These findings are also in agreement with the previous report, where AAV5 VC enrichment was reportedly as high as 100% when the starting material consisted of 55% of empty capsids as opposed to the AAV5 starting material with 86% EC, which resulted in 82% of VC post-single-step AEX[31]. Both these reports suggest that further VC enrichment may be achieved with an additional AEX cycle by removing residual ECs. Moreover, while comparing the efficiency of different chromatographic VC enrichment processes, the fractional content of EC and VC in both starting and enriched material should be considered for an accurate evaluation.

For AAV8, $MgSO_4$ provided slightly better VC enrichment than Na_2SO_4 (**Figure S2 A and B**). Given that the anion is the same, that indicates that the cation (Na^+/Mg^{2+}) plays some role in the separation. In the case of AAV6, 5 mM $MgSO_4$ salt supplementation was found to be a prerequisite for EC and VC separation in the form of two peaks (**Figure S2**), suggesting a potential interaction with the AAV6 capsid. Similarly, better separation and enrichment of AAV6[44] and AAV2[48] VCs was reported when 2 mM magnesium salt ($MgCl_2$) was supplemented into the elution buffer. In contrast, we found VC enrichment for AAV5 using $MgSO_4$ to be inferior compared to that achieved with Na_2SO_4 (data not shown).

The exact mechanism of AEX based separation of AAV EC and VC is not yet clear. Although competitive anionic displacement is a well-accepted elution model in AEX, the potential role of salt-induced charge neutralization and/or conformational change in the AAV capsids should not be overlooked. Further investigation on the interaction of salts with genome-less AAV empty capsids and genome-encapsidating vector capsids would be useful to better understand the separation mechanism.

Employing various AAV characterization techniques including *sv*-AUC/optical-density analyses, ddPCR, SDS-PAGE, and alkaline agarose gel analysis, we have demonstrated that the step elution protocol using sodium or magnesium sulfate salt can efficiently generate preparations highly enriched in AAV vector capsids and can be potentially applied to multiple AAV serotypes. Similar elution profiles of AAV8 capsids under the shallow continuous gradient run in both monolith and packed bed resin columns indicate that our AEX process can be readily adapted to two widely used chromatography media without requiring significant changes. We have also demonstrated the effectiveness of this protocol for serotypes produced in two widely used platforms for commercial manufacturing of AAV vectors.

5.4 Materials and Methods

5.4.1 Cell Culture and Baculovirus

Stably-transformed *rep2cap5* packaging Sf9 cells (B8) and suspension adapted mammalian cells (HEK293SF) used for rAAV viral vector production were provided by Dr. Zolotukhin (University of Florida: Gainesville) and Dr. Chahal (National Research Council of Canada, Montreal), respectively. The Sf9/B8 and HEK293SF-cells were maintained in serum-free suspension cultures at appropriate cell-culture conditions (27°C for Sf9 and 37°C, 5% CO_2, and 85% relative humidity for HEK293 cells) in a shaker incubator (Infors, Basel, Switzerland) at 120 rpm speed of agitation. The maintenance and production medium for insect cells and mammalian cells were Sf900-II (Thermo Fisher scientific: Waltham, Massachusetts) and Hycell™ TransFx-H (Cytiva Life Sciences: Chicago, Illinois) (additionally supplemented with 0.1% w/v of Kolliphor® P188 and 4 mM Glutamax™), respectively. The cell density analysis for routine maintenance flasks and virus production run was performed using the Vi-Cell XR cell counter (Beckman Coulter: Brea, California). The recombinant baculovirus carrying the AAV transgene expression cassette (Bac-*gfp*) consisted of an AAV2-ITR flanking *egfp* under the control of chicken ß-actin-CMV hybrid promoter. The recombinant baculovirus stock used for rAAV5 production was generated using naïve Sf9 cells following a standard protocol, as published in our previous report[49].

5.4.2 Recombinant AAV Vector Production

AAV5 production in insect cells and AAV6 and AAV8 production in HEK293SF cells was carried out applying baculovirus infection and triple-plasmid transient transfection protocols, respectively, as previously reported[49,50]. In brief, for AAV5 production, B8 Sf9 cells were infected with Bac-GFP baculovirus at a MOI of 3 in a high cell density (~10 million cells/mL) fed-batch suspension

cultures. The cell culture was provided with nutrient feed formulation in pre- and post-baculovirus infection phases at specific time points[49]. For AAV6 and AAV8 productions, the HEK293SF cells at 1-1.2 million cells/mL were transiently transfected using 5% v/v PEI: DNA complex at a ratio of 2:1. The final concentrations of plasmid DNA and PEI (Catalog number:23966-1, Polysciences, Warrington, Pennsylvania) were 1 µg/mL and 2 µg/mL of cell culture, respectively. The three plasmids used for AAV production were as follows: (1) Rep2Cap-6/-8 (Provided by Dr. Samulski, University of North Carolina, Chapel Hill), (2) pAdDeltaF6-helper (a gift from James M. Wilson, Catalog number:1128677, Addgene, Watertown, Massachusetts), and (3) pAAV-CAG-GFP (a gift from Edward Boyden, Catalog number:37825, Addgene, Watertown, Massachusetts) or pAAV-PGK-saCas9-U6-sgRNAsa (Catalog number: C306, Applied Biological Materials, Richmond, Canada). The AAV production scale was 1L and 3L cell culture for AAV5/Sf9 and AAV-6, -8/HEK293SF, respectively.

5.4.3 Culture Harvest, Primary Recovery and Affinity Purification

The insect cells and mammalian cells were harvested at 72 hours post-infection and 48 hours post-transfection, respectively. The insect cells were harvested through an *in-situ* whole broth cell lysis protocol, whereas the mammalian cells were harvested by cell pellet lysis. In both cases, the cell culture or the cell pellets were mixed with lysis buffer such that the final concentration of buffer components was 50 mM Tris-HCl, pH 7.5, 0.1% Triton™ X-100, 2 mM $MgCl_2$, and 50 U/mL of Benzonase® DNase (Millipore Sigma, Burlington, Massachusetts). The cell lysate was incubated with lysis buffer at 37°C for 2h, followed by the addition of $MgSO_4$ to increase the overall ionic strength of the lysate to 600 mM with an additional half an hour incubation before the clarification step. The lysate was clarified using an Optiscale® capsule filter consisting of a Milligard®

membrane-1.2/0.5 µm (Catalog number: SWSCA47HH3, Millipore Sigma, Burlington, Massachusetts). The clarified lysate was then subjected to a single-step affinity capture chromatography using commercially available 5 mL prepacked immuno-affinity resin columns, AVB Sepharose (Cytiva Life Sciences: Chicago, Illinois) for AAV5 or CaptureSelect AAVX (Thermofisher Scientific, Waltham, Massachusetts) for AAV6 and AAV8. The affinity purification process was conducted on the ÄKTA Avant25 FPLC system. The affinity-resin bound AAVs were eluted in 0.1 M Glycine (pH 2.5) and were immediately neutralized via addition of 10% v/v of 1 M Tris, pH 8.8. The neutralized AAV material was buffer exchanged into a suitable buffer using PD-10 desalting columns (Cytiva Life Sciences: Chicago, Illinois). The linear flow rate of the process was 75 cm/h, providing 2 min residence time. The pH, conductivity, and UV-Vis absorbance were monitored throughout the process.

5.4.4 Anion-Exchange Chromatography (AEX) for AAV Genome Containing Capsid Enrichment

The salt screening study was conducted using an analytical-scale anion-exchange monolith column (CIMac™ AAV empty/full 0.1 mL, 1.3 µm pore diameter) on the Waters Alliance HPLC system. The affinity-purified AAV5 material was buffer exchanged in 25 mM bis Tris propane, pH 9 buffer, and injected onto the column. The bound AAV5 capsids were eluted under a continuous salt gradient of elution buffers containing specific eluent salt (NaCl or Na_2HPO_4 or Na_2SO_4) at 0.5 mL (5CV)/min flowrate. For preparative scale AEX processing, the Affinity purified AAV material was buffer-exchanged into the AEX column equilibration buffer before loading. The anion-exchange chromatography medium used was either monolithic (CIMmultus™ QA 1mL) or packed-bed (POROS™ HQ-1mL). The buffers were, **A**: 10 mM BTP, pH 9.0; **B**: 10 mM BTP, pH 9.0 + either 50 mM Na_2SO_4 (AAV5) or 50 mM $MgSO_4$ (AAV6 and AAV8), and **C**:2 M NaCl. The

chromatographic steps in a continuous gradient elution process were as following: Equilibration: 90% A+10% B (20 CV), Sample loading: (10 CV), Column wash-1**:** 90% A+10% B (30 CV), Elution: 10% B→50% B (150 CV), Column Wash-2: 100% B (20 CV), and Column Wash-3: 100% C. The process flow rate for the monolith column run was 10 mL/min, whereas, for the packed-bed column, it was 3 mL/min. Derived from the continuous elution gradient was the discontinuous (step) gradient process. The column equilibration, column wash 1, 2, and 3 steps were as indicated above. The finalized discontinuous gradient steps for elution of EC and VC of various AAV serotypes were as follows: (1) AAV5 EC (37.5% B) and VC (46% B) (2) AAV8 EC (15.5% B) and VC (23% B), and (3) AAV6 EC (35% B) and VC (43% B). The elution step (% B) for EC was selected such that it will ensure a maximum EC elution without significant co-elution of VC (and hence without significant loss of VC) before the next step applied to elute VC. The UV signal returning to the baseline for each step was achieved by appropriately adjusting the step-gradient length, ensuring the near-complete elution of a given component. Additional column wash steps before and after the AAV capsids elution were added to remove impurities, as indicated above. The AEX-process runs, conducted on the ÄKTA Avant25 FPLC system, were monitored using inline pH, conductivity, and UV-VIS sensors.

5.4.5 Process Reproducibility Study

Three individual vials from a working cell bank of packaging insect cells (*rep2cap5* Sf9) B8 or HEK293SF were used. Three different lots of recombinant baculovirus or plasmids stock were used at the upstream processing stage to produce three batches of AAV5 or AAV8 vectors. The AAV5 or AAV8 material generated was then subjected to affinity-chromatography and AEX steps.

All chromatographic runs were carried out on different days involving different lots of freshly prepared chromatography processing buffers for each run.

5.4.6 Quantification of DNase Resistant Genomic Particles (viral genomes: VGs) by Digital-Droplet Polymerase Chain Reaction (ddPCR)

The clarified lysate or chromatography processed material was incubated with 5U/mL of Benzonase® for 30 min at 37°C before viral DNA extraction. Benzonase® treated samples both undiluted and 1:10 diluted were used for viral DNA extraction using a High Pure Viral DNA Extraction kit (Roche Diagnostics: Risch-Rotkreuz, Switzerland). The ddPCR assay was conducted using the QX200 Digital Droplet PCR system (Bio-Rad Laboratories: Hercules, California) as per the manufacturer's instructions. The reaction mixture for the AAV5-*gfp* sample consisted of a forward primer (5'-ATAGGGACTTTCCATTGACGTC-3'), a reverse primer (5'-TGATACACTTGATGTACTGCCAAG-3'), and a probe (FAM 5'-TGGGTGGACTATTTACGGTAAACTGCC-3'BHQ) targeting the CMV enhancer sequence. For AAV6/AAV8-*gfp*, the reaction mixture consisted of a forward primer (5'-CTGCTGCCCGACAACCAC-3') and a reverse primer (5'-TCACGAACTCCAGCAGGAC-3') designed to target the transgene (*egfp*) sequence. The primer set for AAV6-*cas9* vector is as follows: forward primer (5'-GGCCAGATTCAGGATGTGCT-3') and reverse primer (5'-CATCATCCACAGAAGCGTGT-3'). The primers and a probe were purchased from Integrated DNA Technologies (Coralville, Iowa). The thermocycling temperature programming for AAV5-*gfp* (preincubation at 95°C/15 min for denaturation and 40 cycles of 95°C/15 sec and 54.5°C /30 secs) and AAV6-/AAV8-*gfp* (preincubation at 95°C/15 min for denaturation and 40 cycles of 94°C/30 sec and 60°C /1 min) were optimized explicitly for specific primers set.

5.4.7 Immuno-Blotting Analysis

Multiple elution fractions collected from continuous gradients of AAV5-AEX run were subjected to SDS-PAGE using TGX-Stain-free gels. After the electrophoresis run, the protein bands were transferred to a nitrocellulose membrane using the Transblot Turbo Transfer System (Bio-Rad Laboratories, Hercules, California) as per the supplier's instructions. Following the blocking step, the nitrocellulose membrane was sequentially incubated with mouse IgG Anti-AAV VP primary antibody (PROGEN Biotechnik GmbH, Heidelberg, Germany) (1:5000 dilution) and HRP-conjugated rabbit anti-mouse IgG polyclonal antibody (Abcam, Cambridge, United Kingdom) (1:100000 dilution). Following the subsequent washing steps, the membrane was incubated with enhanced chemiluminescence reagent and visualized with the ChemiDoc Imager (Bio-Rad Laboratories, Hercules, California).

5.4.8 Sedimentation Velocity Analytical Ultracentrifugation (*sv*-AUC) Analyses

For analytical ultracentrifugation analyses, the samples from affinity-purification or AEX process fractions containing AAV capsids were buffer exchanged into PBS and concentrated using Amicon® Ultra (Millipore Sigma, Burlington, Massachusetts) centrifugal filter with a 30 kDa molecular weight cut off. The concentrated sample was then analyzed using a Beckman Proteomelab XL-1 ultracentrifuge (Beckman Coulter: Brea, California). The centerpieces were charcoal filled-epon, two-sector centerpieces with a 1.2 cm pathlength. The reference sector was filled with 420 µL PBS and the sample sector with a concentrated AAV sample. Samples were temperature equilibrated at 20°C with a full vacuum applied for 1h. The sedimentation analysis run was performed at 20,000 rpm for two hours at 20°C using absorbance detection at 260 and 280 nm. Data analysis was performed using Sedfit[51]. The data visualization plots were created using Gussi freeware[52].

5.4.9 SDS-PAGE Analysis

AEX process fractions were used for the analysis of purity and identity of components via SDS-PAGE. The concentrated elution fractions or concentrated samples recovered after *sv*-AUC analysis were subjected to denaturing protein electrophoresis run conditions. After the run, the gel was stained using Silver Stain Plus™ (Bio-Rad Laboratories, Hercules, California) as per supplier's instructions and visualized using the ChemiDoc Imager (Bio-Rad Laboratories, Hercules, California).

5.4.10 Alkaline Agarose Gel Electrophoresis

The concentrated elution fractions or concentrated samples recovered after *sv*-AUC analysis were subjected to alkaline agarose gel electrophoresis. The recovered sample was mixed with 6x alkaline loading buffer (180 mM NaOH, 6 mM EDTA, 18% Ficoll 400, 0.15% Bromophenol Blue, and 0.25% Xylene Cyanol) in 6:1 proportion to get the final concentration of alkaline loading buffer to 1x. The alkaline running buffer comprises of 30 mM NaOH, 2 mM EDTA in Milli-Q water. The 0.7% agarose gel was prepared by dissolving agarose powder in the alkaline running buffer. 30 µL of samples and 10 µL of Quick-Load® 1kb DNA ladder (New England Biolabs, Ipswich, Massachusetts) in 1x alkaline loading buffer were loaded on the gel and run at 3.5 V/cm for extended hours until the dye had migrated approximately 2/3 length of the gel. Post electrophoresis, the gel was washed with 0.5 M Tris-HCl, pH 8 buffer for 30 min, and was incubated with staining buffer (1x SYBR™ Safe stain in TE buffer, pH 8) for one hour, followed by gel imaging using the ChemiDoc Imager.

5.5 Authors' Contributions

Conceptualization, P.R.H.J., P.S.C., and A.K.; Design of Experiments, P.R.H.J., A.B., J.S., P.S.C., and A.K.; Chromatographic Process Development, P.R.H.J.; AAV Production and Characterization, P.R.H.J., J.S., and P.D.M.; Writing-original draft, P.R.H.J.; Review & Editing, P.S.C., A.B., J.S., and A.K.; Funding acquisition, A.K.; Resources, P.S.C., J.S., and A.K.; Supervision, P.S.C, and A.K.

5.6 Acknowledgment

P.R.H.J. is financially supported through a grant from the Natural Sciences and Engineering Research Council (NSERC RGPIN-2015-05132) of the government of Canada. A.K. is a recipient of a Canada Research Chair (CRC/240394). The authors would like to thank Aleš Štrancar (BIA separation) for providing gift sample of monolith anion-exchange columns, Mehul Patel (National Research Council of Canada, Montreal) for providing a gift sample of POROS™-HQ prepacked 1 mL column, and Orjana Terova and Alejandro Baccera (Thermofisher Scientific) for providing gift samples of CaptureSelect AAVX resin and prepacked columns for preliminary studies. The authors would also like to thank Marie-Hélène Venne (National Research Council of Canada, Montreal) for providing a protocol for vector genome analysis.

5.7 Conflict of interest

The authors declare no financial or commercial conflict of interest.

5.8 References

1. Huang, S., and Kamihira, M. (2013). Development of hybrid viral vectors for gene therapy. Biotechnol Adv. *31*, 208–223.
2. Waehler, R., Russell, S. J., and Curiel, D. T. (2007). Engineering targeted viral vectors for gene therapy. Nat Rev Genet. *8*, 573–587.
3. Ylä-Herttuala, S. (2012). Endgame: Glybera finally recommended for approval as the first gene therapy drug in the European Union. Mol Ther. *20*, 1831–1832.
4. FDA advisory committee briefing document. Spark Therapeutics, Inc. Luxturna™ (voretigene neparvovec). Meeting of the cellular tissue, and gene therapies advisory committee. 1–149 (2017).
5. Byrnes, A. ZOLGENSMA. Summary basis for regulatory action. Office of the tissue and advanced therapies signatory authority. 1-16 (2019).
6. Wright, J. F. (2014). AAV empty capsids: for better or for worse? Mol Ther. *22*, 1-2.
7. Mingozzi, F., and High, K. A. (2011). Immune responses to AAV in clinical trials. Curr Gene Ther. *7*, 316–324.
8. Li, H., Lasaro, M. O., Jia, B., Lin, S. W., Haut, L. H., High, K. A., and Ertl, H. CJ. (2011). Capsid-specific T-cell responses to natural infections with adeno-associated viruses in humans differ from those of nonhuman primates. Mol Ther. *19*, 2021–2030.
9. Mingozzi. F., Maus, M. V., Hui, D. J., Sabatino, D. E., Murphy, S. L., Rasko, J. E. J., Ragni, M. V., Manno, C. S., Sommer, J., Jiang. H. et al. (2007). CD8(+) T-cell response to adeno-associated virus capsid in humans. Nat Med. *13*, 419-422.
10. Hoffman, B. E., and Herzog, R. W. (2013). Covert warfare against the immune System : decoy capsids, stealth genomes, and suppressors. Mol Ther. *21*, 1648–1650.
11. Martino, A. T., Basner-Tschakarjan, E., Marjusic, D. M., Finn, J. D., Hinderer, C., Zhou,

S., Ostrov, D. A., Srivastava, A., Ertl, H. C. J., Terhorst, C. et al. (2013). Engineered AAV vector minimizes in vivo targeting of transduced hepatocytes by capsid-specific $CD8^+$ T cells. Blood. *121*, 2224–2233.

12. Ayuso, E., Mingozzi, F., Montane, J., Leon, X., Anguela, X. M., Haurigot, V., Edmonson, S. A., Africa, L., Zhou, S., High, K.A. et al. (2009). High AAV vector purity results in serotype- and tissue-independent enhancement of transduction efficiency. Gene Ther. *13*, 419–422.
13. Mueller, C., Ratner, D., Zhong, L., Esteves-sena, M., and Gao, G. (2012). Production and discovery of novel recombinant adeno-associated viral vectors. Curr Protoc Microbiol. 14D.1–21.
14. Zolotukhin, S., Byrne, B. J., Mason, E., Zolotukhin, I., Potter, M., Chesnut, K., Summerford, C., Samulski, J., and Muzyczka. (1999). Recombinant adeno-associated virus purification using novel methods improves infectious titer and yield. Gene Ther. *6*, 973–985.
15. Morita, M., Aizawa, M., Toi, H., Fukuhara, E., and Hashimoto K. (2011). Continous flow ultracentrifuge system for production of infection prevention vaccines. Hitachi Review. *60*, 257-261.
16. Reimer, C. B., Baker, R. S., van Frank, R. .M., Newlin, T. E., Cline, G. B., and Anderson, N. G. (1967). Purification of large quantities of influenza virus by density gradient centrifugation. J Virol. *1*, 1207-1216.
17. Meriño, S. F., and Haifeng, C. WO 2016/114991 A2.
18. Qu, W., Wang, M., Wu, Y., and Xu, R. (2015). Scalable downstream strategies for purification of recombinant adeno-associated virus vectors in light of the properties. Curr

Pharm Biotechnol. *16*, 684–95.

19. Wells, D. J. (2017). Systemic AAV gene therapy close to clinical trials for several neuromuscular diseases. Mol. Ther. *25*, 834–835.

20. Galibert, L., and Merten, O. W. (2011). Latest developments in the large-scale production of adeno-associated virus vectors in insect cells toward the treatment of neuromuscular diseases. J Invertebr Pathol. *107*, S80–S93.

21. Auricchio, A., O'Connor, E., Hildinger, M., and Wilson, J.M. (2001). A single-step affinity column for purification of serotype-5 based adeno-associated viral vectors. Mol Ther. *4*, 372-374.

22. Auricchio, A., Hildinger, M., O'connor, E., Gao, G. P., and Wilson, J. M. (2001). Isolation of highly infectious and pure adeno-associated virus type 2 Vectors with a single-step gravity-flow column. Hum Gene Ther. *12*, 71–76.

23. Zolotukhin, S., Potter, M., Zolotukhin, I., Sakai, Y., Loiler, S., Fraites, Jr, T. J., Chiodo, V. A., Phillipsberg, T., Muzyczka, N. et al. (2002). Production and purification of serotype 1, 2, and 5 recombinant adeno-associated viral vectors. Methods. *28*, 158–167.

24. Smith, R. H., Levy, J. R., and Kotin, R. M. (2009). A simplified baculovirus-AAV expression vector system coupled with one-step affinity purification yields high-titer rAAV stocks from insect cells. Mol Ther. *17*, 1888–1896.

25. Anderson, R., Macdonald, I., Corbett, T., Whiteway, A., and Prentice, H. G. (2000). A method for the preparation of highly purified adeno-associated virus using affinity column chromatography, protease digestion and solvent extraction. J Virol Methods. *85*, 23-34.

26. Harris, J. D., Beattie, S. G., and Dickson, J. G. (2003) Novel tools for production and purification of recombinant adeno-associated viral vectors. Methods Mol Med. *76*, 255–267

27. Auricchio, A., O'Connor, E., Hildinger, M., and Wilson, J. M. (2001) A single-step affinity column for purification of serotype-5 based adeno-associated viral vectors, Mol Ther. *4,* 372–374.

28. Koerber, J. T., Jang, J. H., Yu, J. H., Kane, R. S., and Schaffer, D. V. (2007) Engineering adeno-associated virus for one-step purification via immobilized metal affinity chromatography. Hum Gene Ther. *18,* 367–378.

29. Potter, M., Chesnut, K., Muzyczka, N., Flotte, T., and Zolotukhin, S. (2002) Streamlined large-scale production of recombinant adeno-associated virus (rAAV) vectors, Methods Enzymol. *346,* 413–430.

30. Brument, N., Morenweiser, R., Blouin, V., Toublanc, E., Raimbaud, I., Chérel, Y., Folliot, S., Gaden, F., Boulager, P., Kroner-Lux, G. et al. (2002). A versatile and scalable two-step ion-exchange chromatography process for the purification of recombinant adeno-associated virus serotypes-2 and -5. Mol Ther. *6,* 678–686.

31. Nass, S. A., Mattingly, M. A., Woodcock, D. A., Burnham, B. L., Ardinger, J. A., Osmond, S. E., Frederick, A. .M, Scaria, A., Cheng, S. H., and O'Riordan, C. R. (2018). Universal method for the purification of recombinant AAV vectors of differing serotypes. Mol Ther Methods Clin Dev. *9,* 33–46.

32. Gao, G., Qu, G., Burnham, M. S., Huang, J., Chirmule, N., Joshi, B., Yu, Q-C., Marsh, J. A., Conceicao, C. M., and Wilon, J. M. (2000). Purification of recombinant adeno-associated virus vectors by column chromatography and its performance in vivo. Hum Gene Ther. *11,* 20179-2091.

33. Chahal, P. S., Aucoin, M. G., and Kamen, A. (2007). Primary recovery and chromatographic purification of adeno-associated virus type 2 produced by baculovirus/insect cell system. J

Virol Methods. *139*, 61–70.

34. Zhou, A. & Llp, F. WO 2010/148143 Al (74). **98075**, (2010).

35. Zhou, J., Yang. X., Wright, J. F., High, K. A., Couto, L., and Qu, G. (2011). PEG-modulated column chromatography for purification of recombinant adeno-associated virus serotype 9. J Virol Methods. *173*, 99–107.

36. O'Riordan, C. R. O., Lachapelle, A. L., Vincent, K. A., and Wadsworth, S. C. (2000). Scaleable chromatographic purification process for recombinant adeno-associated virus (rAAV). J Gene Med. *2*, 444–454.

37 Clark, K. R., Liu, X., Mcgrath, J. P., and Johnson, P. R. (1999). Highly purified recombinant adeno-associated virus vectors are biologically active and free of detectable helper and wild-type viruses. Hum Gene Ther. *10*, (1999).

38. Qu, G., Bahr-Davidson, J., Prado, J., Tai, A., Cataniag, F., McDonnell, J., Zhou, J., Hauck, B., Luna, J., Sommer, J. M. et al. (2007). Separation of adeno-associated virus type 2 empty particles from genome containing vectors by anion-exchange column chromatography. J Virol Methods. *140*, 183–192.

39. Kaludov, N., Haandelman, B., and Chiorini, J. A. (2002). Scalable purification of Adeno-associated virus type 2, 4 and 5 using ion-exchange chromatography. Hum Gene Ther. *13*, 1235-1243.

40. Okada, T., Nonaka-Sarukawa, M., Uchibori, R., Kinoshita, K., Hayashita-Kinoh, H., Nitahara-Kasahara, Y., Takeda, S., and Ozawa, K. (2009). Scalable purification of adeno-associated virus serotype 1(AAV1) and AAV8 vectors, using dual ion-exchange adsorptive membranes. Hum Gene Ther. *20*, 1013-1021.

41. Lock, M., Alvira, M. R., and Wilson, J. M. (2012). Analysis of particle content of

recombinant adeno-associated virus serotype 8 vectors by ion-exchange chromatography. Hum Gene Ther Methods. *23*, 56–64.

42. Davidoff, A. M., Ng, C. Y. C., Sleep, S., Gray, J., Azam, S., McIntosh, J. H., Karimipoor, M., et al. (2004), Purification of recombinant adeno-associated virus type 8 vectors by ion exchange chromatography generates clinical grade vector stock. J Virol Methods. *121*, 209-215.

43. Fu, X., Chen, W. C., Argento, C., Clarner, P., Bhatt, V., Dickerson, R., Bou-Assaf, G. et al. (2019). Analytical strategies for quantification of adeno-associated virus empty capsids to support process development. Hum Gene Ther Methods. *30*, 144-152.

44. Wang, C., Mulagapati, S. H. R., Chen, Z., Du, J., Zhao, X., Xi, G., Chen, L., et al. (2019). Developing an anion exchange chromatography for determining empty and full capsid contents in AAV6.2. Mol Ther Methods Clin Dev. *26*, 257-263.

45 Sommer, J. M., Smith, P. H., Parthasarathy, S., Isaacs, J., Vijay, S., Kieren, J., Powell, S. K., McClelland, A., and Wright, J. F. (2003). Quantification of adeno-associated virus particles and empty capsids by optical density measurement. Mol Ther. *7*, 122–128

46. Moço, P. D., Aharony, N., and Kamen, A. (2020). Adeno-associated viral vectors for homology-directed generation of CAR-T Cells. Biotechnol J. *15*, 1900286, 1–6.

47. Urabe, M., Xin, K. Q., Obara, Y., Nakaura, T., Mizukami, H., Kume, A., Okuda, K., and Ozawa, K. (2006). Removal of empty capsids from type 1 adeno-associated virus vector stocks by anion-exchange chromatography potentiates transgene expression. Mol Ther. *13*, 823-828.

48. Dickerson, R., Argento, C., Peracci, J., and Bakhshayeshim M. (2020). Separating empty and full rAAV particles using isocratic anion exchange chromatography. Biotechnol

Journal. doi: 10.1002/bab.202000015.

49. Joshi, P. R. H., Cervera, L., Ahmed, I., Kondrotov, O., Zolotukhin, S., Schrag, J., Chahal, P. S., and Kamen, A. A.(2019). Achieving high-yield production of functional AAV5 gene delivery vectors via fedbatch in an insect cell-one baculovirus system. Mol Ther Methods Clin Dev. *13*, 279-289.

50. Chahal, P. S., Schulze, E., Tran, R., Montes, J., and Kamen, A. A. (2014). Production of adeno-associated virus (AAV) serotypes by transient transfection of HEK293 cell suspension cultures for gene delivery. J Virol. Methods. *196*, 163–173.

51. Schuck, P. (2000). Size-distribution analysis of macromolecules by sedimentation velocity ultracentrifugation and Lamm equation modeling. Biophys. J. *78*, 1606–1619.

52. Brautigam, C. A. (2015). Calculations and publication-quality illustrations for analytical ultracentrifugation data. Methods Enzymol. *562*, 109-133.

Development and Validation of an Anion-Exchange High-Performance Liquid Chromatography Method for Analysis of Empty Capsids and Capsids Encapsidating Genetic Material in a Purified Preparation of Recombinant Adeno-associated Virus Serotype 5.

Preamble

After developing the upstream and downstream processes, as reported in Chapter 4 and 5, Chapter 6, focuses on the development of an analytical assay for quantification of AAV capsids population in primarily purified (affinity-purified) and highly purified final AAV samples completing the triad of AAV manufacturing process. Herein, we report a simple and readily accessible high-performance liquid chromatography method for absolute and relative quantification of AAV capsid population in a purified preparation. Exploring a high-resolution separation under anion-exchange chromatographic process, a native fluorescence-based detection method offers high-sensitivity of detection, requiring only a small amount/volume of the total AAV capsids in a sample, in contrast to the current methods of analysis that often requires a large amount of AAV sample. The supplemental data associated with this chapter are provided in the **appendix, 9.3** (**Page number 226-236**).

Chapter 6 Development and Validation of an Anion-Exchange High-Performance Liquid Chromatography Method for Analysis of Empty Capsids and Capsids encapsidating genetic material in a Purified Preparation of Recombinant Adeno-Associated Virus Serotype 5

Pranav R. H. Joshi[1], Alice Bernier[1], Parminder S. Chahal[2], Amine Kamen[1]*

[1] Viral Vectors and Vaccine Bioprocessing Group, Department of Bioengineering, McGill University, Montreal, Quebec, Canada.

[2] Human Health Therapeutics, National Research Council of Canada, Montreal, Quebec, Canada.

* Correspondence should be addressed to Amine Kamen (amine.kamen@mcgill.ca)
Department of Bioengineering, McGill University.

Short title: HPLC method for AAV5 empty/filled capsid quantification

Submitted to "**Human gene therapy methods**"

Abstract

The development of various manufacturing platforms and analytical technologies has substantially contributed to successfully translating the recombinant adeno-associated viral vector from the lab to the clinic. The active deployment of these analytical technologies for process and product characterization has helped define critical quality attributes (CQA) and improve the quality of the clinical grade material. In this manuscript, we report an anion-exchange high-performance liquid chromatography (AEX-HPLC) method for relative and as well as absolute quantification of empty capsids (EC) and capsids encapsidating genetic material (CG) in purified preparations of AAV using serotype 5 as a model. The selection of optimal chromatographic buffer composition and step-gradient elution protocol offered baseline separation of EC and CG in the form of two peaks, as validated with the respective reference standards. The native amino acid-fluorescence based detection offered excellent linearity with a correlation coefficient of 0.9983 over two-log dilutions of the sample. The LOD and LOQ values associated with the total AAV5 capsid assay are 3.1E+09 and 9.5E+09, respectively. AEX-HPLC showed method comparability with the analytical ultracentrifugation (AUC) method for determination of the relative proportions of empty and capsids containing genetic material, supporting the reported HPLC method as an easy-to-access alternative to AUC with operational simplicity. Moreover, rapid and easy adaptation of this method to AAV8 material also demonstrated the robustness of the proposed approach.

6.1 Introduction

With three clinically approved products and many more drug candidates under evaluation in clinical trials, the recombinant adeno-associated virus (rAAV) emerged as one of the preferred gene delivery vehicles in the curative gene therapy approach of many hereditary diseases[1–4]. In contrast to the wild-type AAV sample, which has near 100% of the genome-containing functional particles[5], the rAAV vector preparations contain genome-less empty capsids (EC) in excess. Having no direct therapeutic effect, these empty capsids are generally considered a product-related impurity in clinical lots[6]. A better understanding of these empty capsids' role in *in vivo* AAV transduction efficiency and potential impact on the final clinical outcome[7,8] has led the development of various analytical technologies for detection, identification, and quantification of empty capsids and capsids containing genetic material (CG).

These methods include sedimentation velocity analytical ultracentrifugation (*sv*-AUC)[9], transmission electron microscopy (TEM)[10,11], a combination of ELISA and quantitative polymerase chain reaction (qPCR) for total capsids and CG analysis, respectively[12], charge-detection mass spectrometry (CD-MS)[13], and optical-density measurement[14]. Although effective to a varying extent, these methods also have specific drawbacks. For example, TEM or Cryo-TEM based analyses are subjected to manual intervention for both the differentiation between EC and CG and their quantification, potentially affecting the accuracy and precision of the final results. In the ELISA-based analysis of total AAV capsids, both TEM and qPCR are used as validation methods for establishing the concentration of empty capsids in the standard provided with the kit. Because of this, the ELISA, besides its own inherent error, may also confound the errors associated with the methods for quantification of the standard. The accuracy of optical-density measurements for both relative and absolute quantification of EC and CG depends on the purity level of the sample. In the absence of *in situ* sample fractionation, in contrast to HPLC run, an impurity of any

nature, DNA, or protein, even when present in trace amounts, will absorb at 260 and 280 nm and can substantially impact the overall results. A recently reported charge-detection mass spectrometry method differentiates the EC and CG based on the difference in mass-to-charge ratio and associated migration velocity under applied electric field[13]. Notably, a more robust and accurate method is *sv*-AUC, where the sedimentation coefficient (S), a practical expression of the buoyant density, is determined for EC, CG, and the intermediate population during a centrifugation run. The S values reported for the CG capsid population linearly correlates to the size of the genome encapsidated in an empty capsid[9].

Ion-exchange chromatography has been reported for high-resolution separation of charge variants of complex biological molecules such as monoclonal antibodies[15–17]. Similarly, various anion-exchange HPLC (AEX-HPLC) methods demonstrating separation of EC and CG, based on the differences in the net negative charge, have also been reported to determine empty and genome-containing capsids of AAV serotypes such as AAV1[18], AAV2[19,20], AAV8[21], and AAV6[22].

Building on the intrinsic resolution power of anion-exchange chromatography and the operational advantage of HPLC, in this manuscript, we report a simple AEX-HPLC protocol for the simultaneous quantification of relative and absolute values of EC and CG population in an affinity-purified AAV5 sample. Combining a step-gradient elution approach, which enabled a baseline separation of EC and CG populations, with the native fluorescence-based detection, improved the accuracy and sensitivity of the detection and quantification. Demonstrated comparability with other existing methods, including *sv*-AUC, for EC and CG determination provides an opportunity to establish this protocol as an additional tool for orthogonal analyses with better accessibility and operational simplicity.

6.2 Materials and Methods

6.2.1 Recombinant AAV5 vector production, harvest, and immuno-affinity purification

The rAAV5-*gfp* vector material was produced using the One-Bac 3.0 platform and the fed-batch mode of high-cell density production cultures, as reported in our previous publication[23]. For AAV5 production, B8 Sf9 cells[24] were infected with Bac-GFP baculovirus (harboring the AAV expression cassette of 3.79kb in size, consisting of ITR flanked GFP transgene sequence) at an MOI of 3. The B8 Sf9 cell line is a third-generation One-Bac inducible packaging insect cell line harboring the *rep2cap5,* which upon infection with a single baculovirus carrying the transgene sequence, produces the AAV5[24]. The cell culture was provided with nutrient feed formulation in pre- and post-baculovirus infection phases at specific time points. At 72 hours post-infection, the insect cell culture was harvested through *in-situ* whole broth cell lysis via the addition of 10% v/v of the lysis buffer. AAV8-*gfp* used for the demonstration of the method robustness was produced via triple-plasmid transfection protocol as reported previously[25]. The suspension-adapted HEK293 cells at 1-1.2 million cells/mL were transiently transfected using 5% v/v PEI: DNA complex at a ratio of 2:1. The final concentrations of plasmid DNA and PEI (Catalog number:23966-1, Polysciences, Warrington, Pennsylvania) were 1 µg/mL and 2 µg/mL of cell culture, respectively. The three plasmids used for AAV8 production were as follows: (1) Rep2Cap8 (Provided by Dr. Samulski, University of North Carolina, Chapel Hill), (2) pAdDeltaF6-helper (a gift from James M. Wilson, Catalog number:1128677, Addgene, Watertown, Massachusetts), and (3) pAAV-CAG-GFP (a gift from Edward Boyden, Catalog number:37825, Addgene, Watertown, Massachusetts, 2.9 kb in size). The HEK293 cells were harvested 48 hours post-transfection and lysed via addition of 10% v/v of lysis buffer. Post addition of a lysis buffer, the final concentration of buffer components in the lysate is 50 mM Tris-HCl, pH 7.5, 0.1% Triton X-100, 2 mM $MgCl_2$,

and 50 U/mL of Benzonase® DNase (Millipore Sigma, Burlington, Massachusetts). Following the incubation at 37°C for 2 h, magnesium sulfate was added to increase the overall ionic strength of the lysate to 600 mM coupled with an additional half an hour incubation before the clarification step. The high-ionic strength lysate was clarified using the Optiscale® capsule filter consisting of a Milligard® membrane-1.2/0.5 µm (Cat# SWSCA47HH3, Millipore Sigma, Burlington, Massachusetts). The clarified lysate was then subjected to a single-step affinity capture chromatography step using commercially available 5 mL prepacked immune-affinity resin columns, AVB Sepharose (Cytiva Life Sciences: Chicago, Illinois) for AAV5 and AAVX (Thermofisher Scientific: Waltham, Massachusetts) for AAV8. The affinity purification process was conducted on the ÄKTA Avant 25 chromatography system. The AAV5 and AAV8 capsids, which were bound to the affinity resin, were eluted with a low pH buffer (0.1 M Glycine, pH 2.5). The eluate was immediately neutralized by adding 10% v/v of neutralization buffer (1M Tris, pH 8.8). The neutralized AAV5 and AAV8 material was buffer exchanged against a suitable buffer using a PD-10 desalting column (Cytiva Life Sciences: Chicago, Illinois) for further analysis.

6.2.2 Anion-Exchange High-Performance Liquid Chromatography Method of AAV5 and AAV8

Affinity-purified AAV5 material or the AAV5 empty and vector capsid reference standards were buffer-exchanged against the AEX-HPLC equilibration buffer that enables the binding of AAV capsid to the anion-exchange medium. The separation of AAV5 empty and genome-containing capsids was achieved using a 0.106 mL anion-exchange monolithic disc column (CIMac™ Q 0.1 AAV full/empty) connected to a Waters Alliance HPLC system. This HPLC system was equipped with a separation module, a column chamber, a UV-VIS photodiode array detector, and a fluorescence detector. The separation module consisted of a four-channel mixing chamber

allowing buffer composition prepared from four different stock solutions. The low extra column volume (~1 mL) associated with the Alliance system ensures minimum band broadening of the sample injection and provides sharper peaks. The chromatography buffers used in the AEX method were as follows: **A**: 10 mM BTP-phosphate, pH 9.0; **B**: 10 mM BTP-phosphate, pH 9.0 + 20 mM sodium phosphate tribasic (Na_3PO_4), **C**: Milli-Q water, and **D**: 2 M NaCl. The continuous gradient elution protocol consisted of the following steps: Equilibration: 95% A + 5% B (25 CV), Elution 1: 5% B → 50% B (100 CV), Elution 2: 100% B (20 CV, 0.45% B/CV), Column Wash: 10% A+15%C+75%D, and re-equilibration: 95%A+5%B. The optimized step-gradient protocol comprises of the following steps: Equilibration:95% A+5% B (25 CV, conductivity: 0.348 mS/cm), Elution Step 1 (EC elution): 88% A+12% B (50 CV, conductivity: 0.9 mS/cm), Elution Step 2 (CG elution,): 82% A+18% B (50 CV, conductivity: 1.13 mS/cm), Elution step 3: 50% A+50% B (50 CV, conductivity: 2.4 mS/cm), Elution step 4: 100% B (30 CV conductivity: 4.2 mS/cm), Column Wash: 10% A+15% C+75% D (30 CV) , and re-equilibration: 10% A+ 90% C (30 CV) and 95% A+5% B (35 CV). The HPLC method robustness was demonstrated for an additional serotype, AAV8-*gfp* vector. The affinity-purified AAV8 material was subjected to the following continuous gradient elution protocol: Equilibration: 60% A + 40% B (20 CV), Elution 1: 40% B → 80% B (200 CV), Elution 2: 100% B (30 CV), Column Wash: 10% A+15%C+75%D (30 CV), and re-equilibration: 10% A+ 90% C (35 CV) and 95% A+5% B (35 CV). For both continuous gradient and step-gradient elution protocols, the process flow rate and column chamber temperature were 0.5 mL/min (5 CV/min) and room temperature (around 23 °C), respectively. The column pressure at given flow rate was between 160-180 psi. Since the Waters Alliance HPLC system used for this study is not equipped with an in-line conductivity sensor, the conductivity of eluted fractions was measured via an off-line conductivity sensor.

The sample injection volume for all the samples, including reference standards, was fixed to 40 µL. To account for the sample loop volume and associated injection volume, which may vary depending on the HPLC system hardware, all the method validation parameters such as LOD, LOQ, and linear quantification range are reported as a function of the total AAV capsid amount instead of the capsid concentration (capsids/mL). The conversion of these values in the AAV concentration unit (capsids/mL) can simply be attained by dividing the total amount with the injection volume.

The real-time chromatographic run monitoring via UV absorbance was conducted at 260 nm and 280 nm wavelengths using a photodiode array detector (PDA), whereas the native amino-acid fluorescence was monitored at 280 nm excitation and 336 nm emission wavelengths. The automated post-run data analysis was performed using the Empower® 3 software. The peak area calculation was conducted using a preset apex-track algorithm that integrates peak area from the valley-to-valley arrangement. For calculations of the relative percentage of empty and genomic capsids from the 260/280 nm absorbance signal, their molar absorption coefficient, as previously reported[14], and the peak area corresponding to each wavelength were used. The DNA does not significantly emit at 336 nm upon excitation at 280 nm[26,27] and the single-stranded AAV genome's contribution to the fluorescence signal is negligible. Therefore, the relative values of peak area were directly correlated to the percent proportion of EC and CG capsids.

6.2.3 AAV5 empty and vector capsid reference standards characterization via orthogonal analyses

AAV5 empty and vector capsid reference standards were prepared by a two-step anion-exchange chromatographic process. An affinity-purified preparation containing the mixture of empty and vector capsids was subjected to the first cycle of anion-exchange chromatography where a highly-

enriched empty capsid fraction was collected. The moderately enriched vector capsid fraction (still containing the residual empty capsids), collected from the this first cycle was then subjected to a second cycle of anion-exchange chromatography under a continuous gradient elution to further reduce the residual empty capsid content, and increase the extent of enrichment in vector capsid preparation. This way, a two-step process enabled generation of enriched empty and vector capsids preparation with minimized co-presence of another component. To certify these preparations as reference standards, they were comprehensively characterized for purity (SDS-PAGE), identity (*sv*-AUC, alkaline agarose gel electrophoresis analysis), and quantification (ddPCR, optical density measurement, and total protein assay-Avagadro equation-based total capsid quantification).The individual component was concentrated and buffer-exchanged against a suitable buffer using a 30 kDa molecular weight cut off centrifugal filter, the Amicon® Ultra (Millipore Sigma, Burlington, Massachusetts). The concentrated standards were then used for sedimentation velocity analytical ultracentrifugation (*sv*-AUC) analysis. After the *sv*-AUC run and standards were recovered and along with the starting affinity-purified material were subjected to orthogonal characterization, which includes optical-density measurement for empty/full capsids analysis, SDS-PAGE, and alkaline agarose gel electrophoresis. The optical-density measurement assay was carried out as per the method reported previously[14]. The quantitative characterization assays include the RC DC™ assay (Bio-Rad Laboratories, Hercules, California) for total capsid (protein) analysis and digital droplet quantitative polymerase chain reaction (ddPCR) analysis for quantification of DNA encapsidating genomic capsids. The total protein amount determined from the RC DC assay was used to total capsids based on the known molecular weight of the AAV5 capsid (~4000 kDa) and the Avogadro equation.

6.2.3.1 Sedimentation-velocity analytical ultracentrifugation (sv-AUC) analyses

Due to the lower sensitivity of absorbance measurement in general, the sample concentration step was necessary to achieve the O.D. value of 0.2-0.8 AU for *sv*-AUC analyses. The affinity-purified AAV5 samples and EC and VC reference standards, buffer exchanged in PBS, were analyzed using the Beckman proteomelab XL-1 (Beckman Coulters: Brea, California). The centerpieces were charcoal filled-epon, two-sector centerpieces with a 1.2 cm pathlength. The reference sector was filled with 420 µL PBS (blank) and the sample sector with either the concentrated AAV reference standards or affinity-purified sample. After placement in the rotor, the sample cell was allowed to equilibrate at 20°C with a full vacuum applied for 1h. The sedimentation analysis run was performed at 20,000 rpm for two hours at 20°C. During the velocity-sedimentation run, the real-time sedimentation data were collected using absorbance detected at 260 and 280 nm optics simultaneously in a single run. Data analysis was performed using Sedfit as per previously published AAV related parameters[9]. The data visualization plots were created using GUSSI freeware[28].

6.2.3.2 Genomic capsid quantification via digital-droplet polymerase chain reaction (ddPCR)

The affinity-purified sample and reference standards were incubated with 5 U/ml of Benzonase® for 30 min at 37°C before viral DNA extraction. Benzonase® treated undiluted, and 1:10 diluted samples were used for viral DNA extraction using the High Pure Viral DNA Extraction kit (Roche Diagnostics: Risch-Rotkreuz, Switzerland). The ddPCR reaction was conducted using the QX200 digital droplet PCR system (Bio-Rad Laboratories: Hercules, California) as per the manufacturer`s instructions. In the case of the AAV5-*gfp* sample, the reaction mixture consisted of a forward primer (5'-ATAGGGACTTTCCATTGACGTC-3'), a reverse primer (5'-TGATACACTTGATGTACTGCCAAG-3'), and a probe (FAM 5'-

TGGGTGGACTATTTACGGTAAACTGCC-3'BHQ) targeting the CMV enhancer sequence. The primers and a probe were purchased from Integrated DNA Technologies (Coralville, Iowa). The thermocycling temperature programming was as following: preincubation at 95°C/15 min for denaturation and 40 cycles of 95°C/15 sec and 54.5°C /30 secs.

6.2.3.3 Purity analysis via SDS-PAGE

The AEX-HPLC process fractions and concentrated samples and standards recovered after the *sv*-AUC were subjected to denaturing protein electrophoresis run. After the run, the gel was stained using the Silver Stain Plus™ kit (Bio-Rad Laboratories, Hercules, California) as per supplier`s instructions and visualized using the ChemiDoc Imager (Bio-Rad Laboratories, Hercules, California).

6.2.3.4 Alkaline Agarose Gel Electrophoresis

The affinity-purified starting material and empty and vector capsid reference standards, recovered after sv-AUC analyses, were subjected to alkaline agarose gel electrophoresis. The 6x gel loading dye (New England Biolabs: Ipswich, Massachusetts), the running buffer, and the gel casting buffer were adjusted to alkaline pH by adding sodium hydroxide stock solution to the final concentration of up to 150 mM. 30 µL of 1x samples in gel loading dye and 10 µL of Quick-Load® 1kb DNA ladder (New England Biolabs: Ipswich, Massachusetts) in 1x alkaline gel loading buffer were loaded on the 0.7% alkaline agarose gel. The gel was run at 3.5 V/cm for extended hours until the dye had migrated approximately 2/3 length of the gel. Post electrophoresis run, the gel was washed with 0.5 M Tris-HCl, pH 8 buffer for 30 min. Later, the gel was incubated with staining buffer (1x

SYBR™ Safe stain in TE buffer, pH 8) for one hour, followed by imaging using the ChemiDoc Imager.

6.3 Results

6.3.1 Anion-exchange (AEX) high-performance liquid chromatography (HPLC) method development

6.3.1.1 Sample characteristics

The affinity-purified AAV5 material used for AEX-HPLC method development consisted of about 90% of EC, an undesirable AAV-related component, and 10% of capsids encapsidating genetic material (CG) as analyzed via *sv*-AUC (**Figure S1 A**)[23]. Here, CG refers to an entire AAV population consisting of intermediate capsids (encapsidating small-size fragments of genetic material: host cell DNA, RNA, and fragments of viral expression cassette) and vector capsids (encapsidating full-length vector expression cassette with or without other fragments) (**Figure S1 E-1**).

6.3.1.2 AEX-HPLC method development

Building on our preliminary data related to the selection of the pH, buffering agent, and eluent salt, the bis-Tris propane (BTP) buffer at pH 9 and sodium phosphate tribasic (Na_3PO_4) salt were selected as chromatographic buffer constituents for AEX method development. The BTP, having one of its pKa values at 9.1, was a suitable choice for buffers at pH 9. The trivalent sodium phosphate (PO_4^{3-}) was selected over monovalent and divalent salts such as sodium chloride or sodium sulfate because of its higher resolution power, potentially due to a higher ionic and

displacement strength. The higher pKa of phosphate groups of sodium phosphate results in a higher pH (>12.5) for the non-pH adjusted buffer; therefore, both the equilibration buffer (Buffer A) and the elution buffer (Buffer B) were pH adjusted to 9 using the phosphoric acid. Such a high pH, which is above the global isoelectric point of AAV capsids, induces strong net negative surface charges and dominantly promotes anionic exchange interactions with the quaternary ammonium ligands of the AEX-column matrix. The elution buffer, consisting of 20 mM sodium phosphate (equivalent to a 120 mM ionic strength), was used for gradient generation. Notably, the theoretical ionic strength of 1 M sodium phosphate salt concentration is 6 M. This relationship was used to calculate the ionic strength associated with a given salt concentration, as presented in the sections ahead. The other two solutions consisted of Milli-Q grade water and 2 M NaCl used for column wash and regeneration steps.

A continuous gradient method was developed after the initial fine-tuning of buffer B composition and salt gradient range. The AAV5 capsids bound to the anion-exchange column were eluted with 5-50% B shallow gradient (6-60 mM ionic strength) over 100 column volume (CV) at a gradient slope of 0.54 mM/CV. First, the AAV5 EC eluted, followed by CG, both in the 16.5-27.5% B range (**Figure 1A and 1B**). The notable feature of the EC and CG elution profile was the absence of a baseline separation and very close elution points, indicating a partial overlapping (and co-elution) of EC and CG at the intersection point. The relative proportion of EC and CG determined from the continuous gradient run data collected for all three sensors (260 nm, 280 nm, and fluorescence: FL) and analyzed via both modes (peak height and integrated peak area) indicated a lack of comparability with the *sv*-AUC values (**Figure S2 A and B**). These data suggested that the continuous gradient run was not suitable for accurate determination of % EC and % CG populations in a given sample. Under the given AEX conditions, the extent of EC and CG co-

elution is a combined function of (1) minute differences in the net negative charge and consequent equilibrium coefficients between these populations, (2) a continuum of the population between empty capsids and complete vector capsids encapsidating a full-length vector genome, and (3) a very high anionic displacement strength of the eluent (phosphate).

Following this, we decided to develop a step-gradient elution process where each elution step would represent a single population (EC or CG) with a minimum co-elution of other components. Further fine-tuning of the method resulted in the EC (retention time: 8.9 min) and CG capsids (retention time: 19 min) eluting in two separate peaks (12% and 18% B, respectively) (**Figure 1C and 1D**). It should be noted here that the length of the step elution gradient was adjusted to ensure that the signal reaches the baseline, which represents a near-complete elution of the first component (EC) before beginning the elution of the following species (CG). The identity and purity of EC and CG peak fractions were assessed via SDS-PAGE, where both fractions displayed three bands corresponding to AAV VP proteins with no additional detectable bands upon silver staining (**Figure 1E**). The peak fractions following the CG peak (Fraction# 4, 5, and 6) showed the presence of residual of AAV capsids that eluted at higher salt concentration and other small molecular weight impurities present in the affinity-purified AAV5 sample. Furthermore, the viral genome copies (VG) analyses via ddPCR also confirmed the presence of the majority of genomic particles in the second peak (CG peak), which consisted of approximately 87% of the total VGs loaded on the column upon sample injection (**Figure 1F**).

The native fluorescence in the protein is predominantly exhibited by tryptophan with excitation, and emission maxima reported to be approximately 280 nm and 350 nm, respectively [29,30]. Due to apparently higher sensitivity than absorbance, we decided to use the native fluorescence as an additional detection signal besides UV-VIS (260 and 280 nm). The excitation and emission

wavelengths for affinity-purified AAV5 material in AEX-chromatographic buffer (10 mM BTP-phosphate, pH 9.0) were found to be approximately 280 and 336 nm, respective, confirming no effect of AEX-buffer formulation on the tryptophan fluorescence. The analysis of step-gradient run suggested that the peak area-based determination of the relative proportions of % EC and % CG offered better accuracy than the peak height when compared with *sv*-AUC results (**Figure S2 C and D**), where the values from all three signals (260 nm, 280 nm, and FL) were comparable to the *sv*-AUC (**Figure S2 D**). Therefore, while the 260/280 nm relative ratio was employed for visual identification of EC and CG peaks in a chromatogram, the more sensitive fluorescence signal was used for the quantitative analyses and HPLC method validation reported in the following sections.

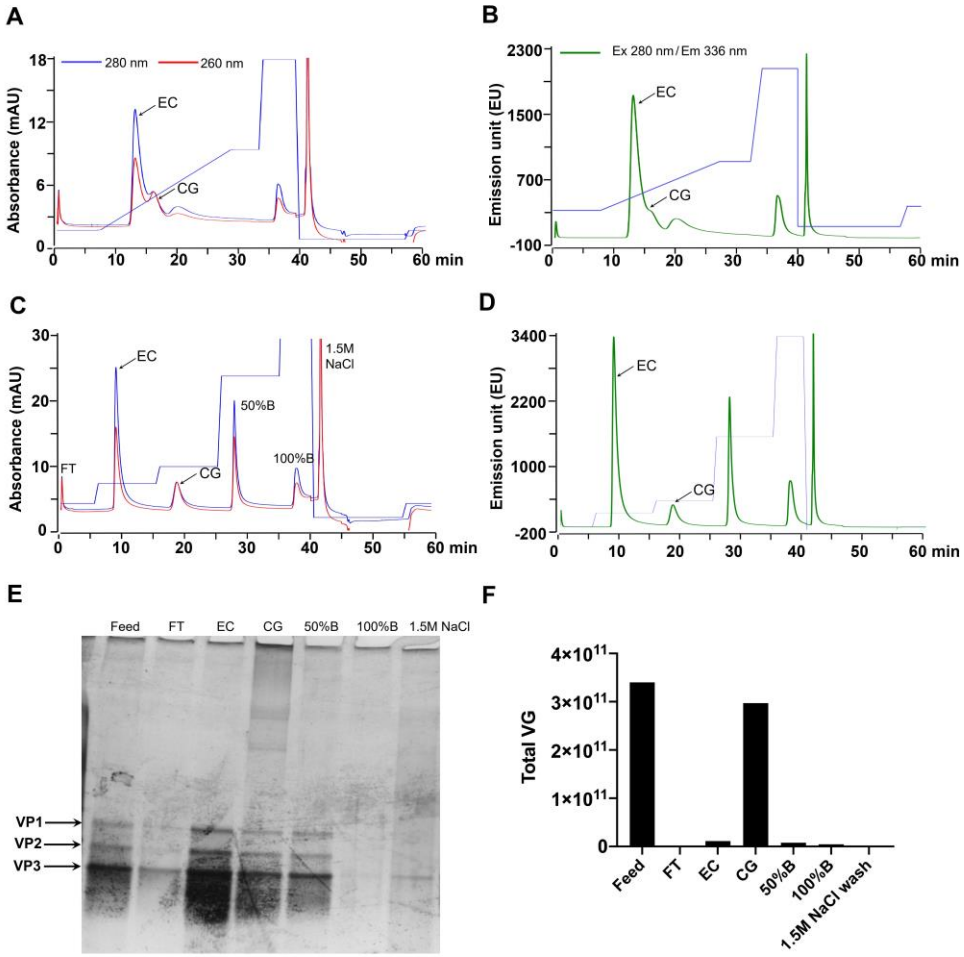

Figure 6.1 AAV5 AEX-HPLC method development

AAV5 AEX-chromatogram with UV signal **(A)** and FL signal **(B)** under 6-60 mM ionic strength sodium phosphate continuous-gradient run. AAV5 EC and CG are indicated by an arrow. AEX-chromatogram with UV signal **(C)** and FL signal **(D)** for an optimized step-gradient elution protocol for AAV5 EC (peak 2) and CG (peak 3) with baseline separation. Notice the differential 260/280 nm profile for empty and vector capsid peaks, a characteristic associated with these variants. Peak (fraction) 1: flowthrough, peak 2: 12 %B, Peak 3: 18 %B, peak 4: 50% B, peak 5: 100% B, and peak 6: 1.5 M NaCl wash. **(E)** SDS-PAGE/Silver staining image of AAV5 step-gradient elution fractions collected during the run and concentrated using Amicon ultra centrifugal filters (30 kDa MWCO). 25 µL of each sample (Feed 1:10 diluted, FT:1x concentrated sample, EC and CG: 1:20 dilution of concentrated sample, 50%B, 100%B, and 1.5M NaCl wash:1x concentrated sample) was loaded on the gel. Feed refers to an affinity-purified AAV5 sample subjected to the AEX-HPLC run. Lane EC and CG primarily shows three AAV5 VP bands, potentially suggesting a highly purified fraction as a result of *in situ* sample fractionation during the AEX separation run. **(F)** ddPCR analysis of each of the AEX-HPLC step gradient fractions. Approximately 87% of viral genome copies detected in vector capsid fraction (Fraction#3, CG peak 3) confirms the presence of the majority of genome-containing capsids of AAV5. AEX: anion-exchange chromatography, CG: capsids containing genetic material, EC: empty capsids, FL: fluorescence, FT: flowthrough, MWCO: molecular weight cut-off.

6.3.2 Specificity and comparability of AEX-HPLC

The finalized AEX-HPLC step gradient method (**Figure 1C and 1D**) was analyzed for two key attributes: specificity and comparability. The method specificity, which in this context is a measure of the degree of selectivity in the separation of EC and CG populations, was confirmed via AEX-HPLC run of in-house reference standards of AAV5 empty and vector capsids (VC), where the later was enriched in capsids containing full-length genomes (**Figure S1 C**). These standards generated via a two-step ion-exchange chromatographic process were orthogonally characterized. The relative percent proportion and purity in these standards were confirmed via *sv*-AUC and SDS-PAGE analyses, respectively (**Figure S1 B-D**). The alkaline agarose gel and ddPCR were used to analyze packaged genome size (**Figure S1 E)** and total VG quantification (**Table S1**), respectively. The AEX-chromatograms of EC and VC reference standards, the affinity-purified sample, and buffer blank are shown in **Figure 2**. While the peak at 19 min in EC reference standard (**Figure 2A and 2B**) correspond to the residual presence of the intermediate populations of AAV5 packaged capsids (~4.0%) as confirmed already via *sv*-AUC (**Figure S1 B**) and alkaline agarose

gel electrophoresis (**Figure S1 E-2**), the peak at 9 min (**Figure 2C and 2D**) represents residual empty capsids (~19%) in the VC standard as confirmed via *sv*-AUC (**Figure S1 C**). Similar to affinity-purified AAV5 material, the determination of % relative proportion of EC and CG in each reference standard from AEX-HPLC run, the peak area-based analyses of FL signal showed better compatibility with *sv*-AUC values over UV signals and peak height-based determination (**Figure S2 A-D**).

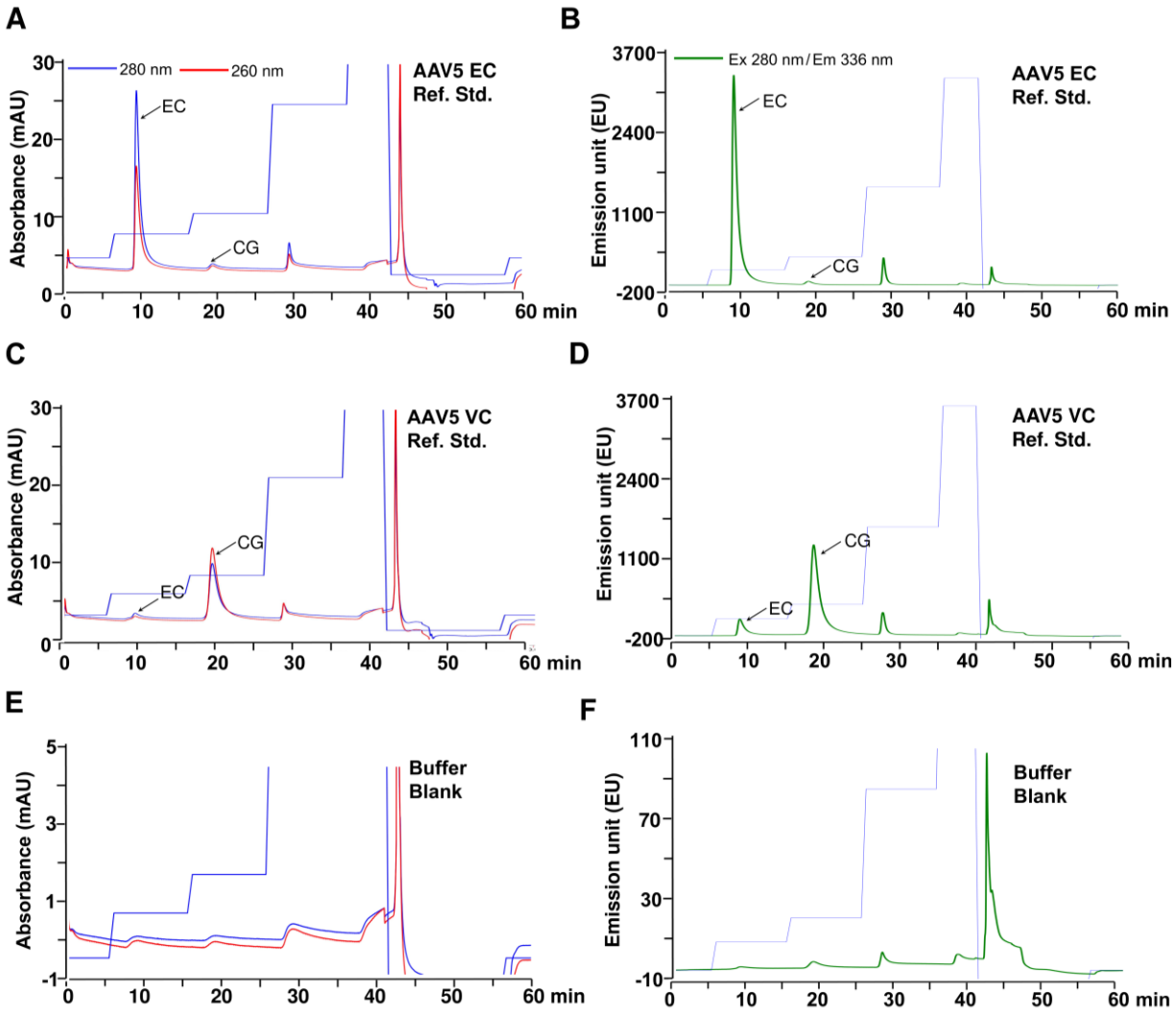

Figure 6.2 Confirmation of specificity of the AAV5 AEX-HPLC step-gradient protocol for EC and GC peaks

UV absorbance (**A)** and FL **(B)** profiles of AAV5 EC reference standard. AEX-chromatograms of AAV5 VC reference standard with UV **(C)** and FL **(D)** profiles and those for buffer blank are represented in **(E)** and **(F)**, respectively. Note the matching elution points of EC and CG in their respective reference standards and that with

the EC and CG peaks in the affinity-purified starting material (**Figure 1C and 1D**). Negligible signal contribution from buffer blank indicates that all peaks (peak 1 to 5, as shown in **Figure 1C**) appearing in the chromatogram are associated with AAV5 sample components.

The AEX-HPLC method comparability was evaluated against two other established methods: *sv*-AUC analysis[9] and optical-density measurement[14]. **Table 1** provides a summary of the percent relative proportion of EC and CG in the affinity-purified sample and respective reference standards when analyzed side-by-side via AEX-HPLC, *sv*-AUC, and optical-density measurement methods (refer to the supplementary calculation section for more details).

Table 6.1 Orthogonal quantitative analysis and Inter-method comparability of an affinity-purified AAV5 sample and a reference standard

% Relative proportions of empty capsids (EC) and capsids encapsidating genetic material (CG)						
Analytical Method	Affinity-purified AAV5 (mixture of EC and CG)		Empty capsid reference standard		Vector capsid reference standard	
	EC	CG	EC	CG	EC	CG
Analytical Ultracentrifugation	90.09[a]	9.91[a]	96.84[a]	3.16[a]	18.81[a]	81.19[a]
	91.08[b]	8.92[b]	95.6[b]	4.4[b]	19.13[b]	80.87[b]
Optical density measurement	89.71	10.29	90.32	9.68	10.57	89.43
HPLC	95.04[a]	4.96[a]	98.06[a]	1.94[a]	18.54[a]	81.46[a]
	94.68[b]	5.32[b]	99.34[b]	0.66[b]	20.82[b]	79.18[b]
	91.47[c]	8.53[c]	98.03[c]	1.97[c]	16.98[c]	83.02[c]

[a] Calculation based on 280 nm absorbance signal data; [b] Calculation based on 260 nm absorbance signal data.
[c] Calculation based on fluorescence signal (emission unit) data.
The calculations are based on the integrated peak area where applicable.

Despite small differences in the reported values with the other two methods, which is a function of the inherent inter-method variability, the overall data from **Table 1** confirm the comparability of the herein reported AEX-HPLC method. It further supports the AEX-HPLC method as an effective alternative to current methods and an additional tool for orthogonal characterization of affinity-purified AAV5 samples.

6.3.3 AAV5 AEX-HPLC method validation

Following the confirmation of method specificity and comparability, the AEX-HPLC method was validated as per standard analytical method validation guidelines from ICH[31] and USFDA[32]. The method validation parameters tested include linearity, sensitivity, precision, accuracy and recovery, and carryover analysis.

6.3.3.1 Linearity of calibration

The linearity of the fluorescence signal as a function of AAV5 capsids was established using the AAV5 VC reference standard. In addition to the orthogonal analyses, as reported in the previous section, this reference standard was further quantified for packaged vector genome copies using ddPCR and total protein assays. It should be noted that SDS-PAGE analysis of the VC reference standard did not show many bands associated with other major impurities except a faint band at 250 kDa, therefore, the contribution of any trace protein impurities in the total protein value was ignored while calculating the total AAV capsids from the protein amount determined via appropriate assay. From the total capsid amount (protein assay) and known molecular weight of AAV5 capsid (~4000 kDa), total capsids were quantified (Cp/mL) applying the Avogadro equation. The VG/mL value was then derived from the known ratio of total capsids and VGs from

the *sv*-AUC analysis. Notably, this VG/mL quantification values showed comparable results with that analyzed via ddPCR. A summary of these orthogonal analyses is provided in **Table S1**.

For the linearity study, VC reference standard ($5.5x10^{12}$ VG/mL or $6.8x10^{12}$ total capsids/mL) was serially diluted with a dilution factor 2 (1:2, 1:4, 1:8, ..., 1:128) and injected in triplicate in the range of $1.0x10^{9}$-$1.9x10^{11}$ capsids. This capsid amount reported here is the value that corresponds to the VGs in the 40 µL injection. In the linearity curve, when the peak height and peak area values were plotted as a function of VG capsids over the given range, the correlation coefficient values were similar (**Figure S4 A and B**). However, because of the better suitability of the peak area over peak height for both relative and absolute quantification, as indicated previously, it was selected as a quantification method. The integrated vector capsid peak area plotted as a function of the total vector capsids was used to construct a standard curve and establish other parameters (**Figure S4 B**). The details of the linear curve parameters are shown in **Table 2**.

Since baseline resolution was achieved between EC and CG in the affinity-purified sample ($8.5x10^{12}$ VG/mL or $7.7x10^{13}$ Capsids/mL, **Table S1**) as well, it was also serially diluted over a two-log range and subjected to AEX-HPLC (**Figure S2**) run. The peak height and peak area were used to determine the relative proportion of % EC and CG in the sample, where again, peak area was found to be relatively more accurate across the entire dilution range tested (**Figure S4 C and D**). The inter-dilution RSD values for % EC and % CG in the given range was less than 12%. However, for the linear curve, both peak height and peak area indicated comparable correlation coefficients (**Figure S5 A-D**). When combined, linearity over a three-log range dilution with a correlation coefficient of > 0.998 was achieved when the total capsid loading was in the range of $2.3x10^{9}$-$2.8x10^{12}$ capsids.

6.3.3.2 Sensitivity: limit of detection and limit of quantification

The limit of detection (LOD) and the limit of quantification (LOQ) were derived from the linearity curve data generated from the vector capsid standard and determined from the formulas as per ICH guidelines. These equations are LOD = 3.3*σ/S, and LOQ = 10*σ/S; where σ corresponds to the standard deviation of the regression line or the y-intercept, and S represents the slope of the curve. The values of LOD and LOQ determined from these formulas and expressed as a signal response (peak area) are shown in **Table 2** and **Figure S4 B**. The LOD values corresponding to the standard

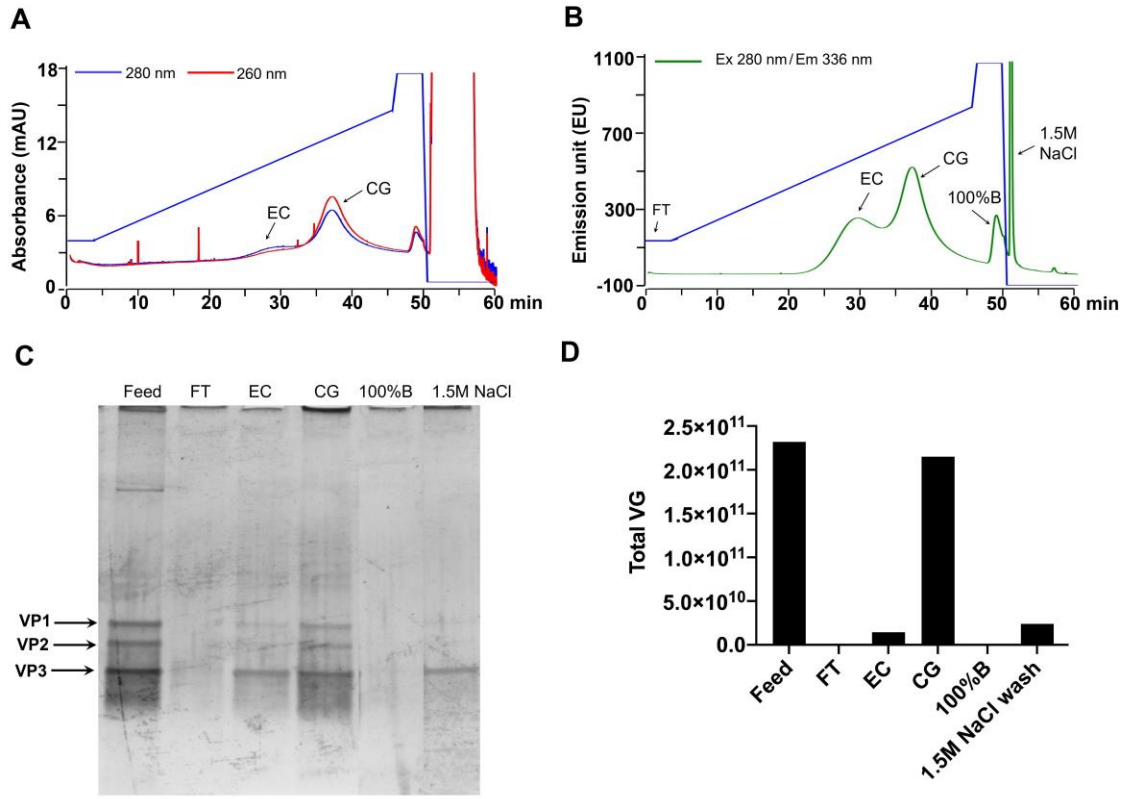

Figure 6.3 Demonstration of HPLC method robustness for AAV8

AAV8 AEX-chromatogram with UV signal **(A)** and FL signal **(B)** under 40-80% B continuous elution gradient run. AAV8 EC and CG are indicated by an arrow. The % EC and CG determined from FL signal was 54% and 465, respectively. Notice the differential 260/280 nm profile for empty and vector capsid peaks, a characteristic associated with these variants. Various peak fractions are shown with an arrow. **(C)** SDS-PAGE/Silver staining image of AAV8 continuous-gradient elution fractions collected during the run and concentrated using Amicon ultra centrifugal filters (30 kDa MWCO). **(D)** ddPCR analysis of each of the AEX-HPLC step gradient fractions.

Feed refers to the AAVX affinity-purified AAV8 sample. Around 90% of viral genome copies detected in CG fraction confirms the presence of the majority of genome-containing capsids of AAV8. AEX: anion-exchange chromatography, CG: capsids containing genetic material, EC: empty capsids, FL: fluorescence, FT: flowthrough, MWCO: molecular weight cut-off.

Table 6.2 Linearity curve characteristics of the vector capsid reference standard

Detection Signal/mode: Fluorescence/ Peak area	
Parameter	Value
Linearity curve equation	$Y=0.0012X-1.13x10^{6}$
R^2	0.9967
Linearity range tested	$1.5x10^{9}$-$1.9x10^{11}$ capsids
Based on the residual standard deviation of the regression line	
LOD (Peak area)	$1.3x10^{7}$
LOQ (Peak area)	$4.3x10^{7}$
The actual combined range for reliable quantification based on LOQ when expressed as total capsids	$3.7x10^{10}$-$1.9x10^{11}$ capsids
Based on the standard deviation of y-intercept of the regression line	
LOD (Peak area)	$2.6x10^{6}$
LOQ (Peak area)	$1x10^{7}$
The actual combined range for reliable quantification based on LOQ and when expressed as total capsids	$9.5x10^{9}$-$1.9x10^{11}$ capsids

deviation of the regression line and the y-intercept were found to be $1.3x10^7$ and $2.6x10^6$ (peak area unit: µV*sec), respectively equivalent of $1.2x10^{10}$ and $3.1x10^9$ AAV5 capsids. Similarly, The LOQ values (peak area unit) based on the standard deviation of the regression line and the y-intercept were $4.3x10^7$ and $1.0x10^7$, respectively, which correspond to $1.2x10^{10}$ and $3.1x10^9$ AAV5 capsids. A comprehensive summary of each of the standard curve parameters for both the vector capsid standard and the affinity-purified sample is provided in **Table 2** and **Table S2**, respectively. Based on the combination of the linearity range and LOQ values reported above, the effective range of quantification corresponding to AAV5 capsids is above $9.5x10^9$ capsids and up to $2.8x10^{12}$ capsids (**Table 2** and **Table S2**).

6.3.3.3 Precision

The two parameters for precision analysis employed in this study were repeatability (intra-day) and intermediate precision (inter-day). For this study, 40 µL injections of the affinity-purified AAV5 sample with a nominal concentration (the concentration that falls in the middle of the linear curve-$1.1x10^{12}$ VG/mL or $9.6x10^{12}$ Capsids/mL) was injected six times per day for three consecutive days. For each intra-day and inter-day points, the relative standard deviation of the peak area and retention time were determined for EC and CG. For the EC peaks, the % RSD value of the peak area and retention time, for both repeatability and inter-day precision parameters, was less than 3.5%. For the CG peaks, it was less than 5%. Similarly, the % RSD value of the relative proportion of empty and full capsids for both precision parameters was below 7%. **Table 3** provides the details of this study and the associated parameters.

6.3.3.4 Accuracy and recovery

For the accuracy and recovery study, a total of $4.8x10^{10}$ VG capsids of the AAV5 vector capsid reference standard were spiked in three samples corresponding to three concentrations (high:1x, medium-1:10, and low-1:20, **Table S3**) of the affinity-purified AAV5 sample. These spiked samples were subjected to the AEX-HPLC run, and the % recovery of spiked VGs was determined from the peak area corresponding to the CG peak (RT: 19 min) for each sample. The reported recovery of AAV5 VGs across all three samples was in the range of 93-99% (**Table S3**).

6.3.3.5 Method robustness

The robustness of the HPLC method reported herein was further studied for another serotype, AAV8. The affinity-purified material of AAV8 vector was subjected to the continuous gradient run HPLC method and two separate population of EC and CG was observed (**Figure 3A and 3B**), each representing characteristic $A_{260/280}$ profile (**Figure 3A**). When analyzed via SDS-PAGE, the EC and CG peak fraction were found to contain AAV capsids. ddPCR analysis of eluted fractions confirmed that the identity of the CG peak as it contained approximately 90% of total VGs with reference to total VGs injected in a sample. The % EC and CG, determined from FL signal applying valley to valley peak integration algorithm, was found to be 54% and 46%, respectively. These values were comparable to the optical-density measurement based analysis[14] of the same affinity-purified AAV8 material which was found to be 61% and 39% for EC and CG populations, respectively.

6.3.3.6 Carryover analysis

Carryover analysis is an integral part of an HPLC method validation as it provides information on any possible carryover of sample components during subsequent injections without additional column washing or re-generation steps. Moreover, since we have already incorporated a high salt wash and column re-equilibration steps in the herein reported HPLC method, carryover analysis provides us an opportunity to evaluate if these conditions are sufficient or any additional column-regeneration steps are required between successive sample injections. For carryover analysis, immediately after the AEX-HPLC run of the highest concentration sample ($2.9x10^{11}$ VGs in 40 µL injection volume), a buffer blank was injected. The peak area values, each corresponding to EC and CG, were used to calculate the carryover. The % carryover reported for EC peak, and CG peak was below 20% of LOQ (**Table S4**), meeting the USFDA guideline acceptance criteria[32]. It should be noted that the percent carryover reported here is a function of the total capsid amount injected, the amount of each component (EC and CG), the column matrix, and the ligand. It may be minimized by injecting sample in the lower dilution range of the standard curve and/or by adjusting the frequency and duration of the column's cleaning/re-equilibration conditions between the subsequent injections.

6.4 Discussion

With an increased understanding of the rAAV manufacturing process and pharmacological characteristics of AAV in the clinics, various analytical approaches have been developed, defining critical quality attributes (CQA) of an rAAV based clinical-grade material[6]. The removal of empty capsids, one of the major product-related components and an important CQA, during the

Table 6.3 Summary of the precision parameters for an AEX-HPLC run of an affinity-purified AAV5 sample

Precision parameter		EC peak fraction		CG peak fraction	
		Peak area (µV*sec)	Retention time (min)	Peak area (µV*sec)	Retention time (min)
Repeatability (Intra-day)	Mean	$2.4x10^8$	8.90	$4.4x10^7$	19.048
	SD	$7.6x10^6$	0.091	$1.7x10^6$	0.065
	% RSD	3.152	1.017	3.892	0.342
Intermediate precision (Inter-day)	Mean	$2.4x10^8$	8.940	$4.6x10^7$	19.020
	SD	$4.1x10^6$	0.052	$2.1x10^6$	0.022
	% RSD	1.712	0.587	4.52	0.119
% Relative proportion					
		% EC		% CG	
Repeatability (Intra-day)	Mean	91.47		8.53	
	SD	0.58		0.58	
	% RSD	0.64		6.82	
Intermediate precision (Inter-day)	Mean	91.25		8.75	
	SD	0.28		0.28	
	% RSD	0.31		3.23	

manufacturing process and analysis in the final clinical grade material, is of prime importance due to its impact on *in-vivo* transduction efficiency [7,33]. AAV serotype 5 is currently one of the vectors of choice in clinical studies for curative gene therapies in indications such as rheumatoid arthritis (NCT03445715, NCT02727764), acute intermittent porphyria (NCT02076763), and hemophilia A and B (NCT03520712, NCT03569891). In this paper, we are reporting a simple HPLC method to analyze EC and CG in a purified preparation of AAV5.

In contrast to the previously reported AEX-HPLC methods based on mono or divalent salts reported with continuous gradient elution protocols[18,20–22], we selected a trivalent sodium phosphate salt due to its higher efficiency for the separation between EC and CG capsids in the initial screening study. The phosphate salt was more effective than other mono- or divalent salts for our AAV5 sample where the percent proportion of the AAV-related undesirable component: empty capsids was much higher (~10x) than the genome-containing capsids, the product of interest.

The continuous gradient elution is regularly used in an analytical HPLC method due to its higher sensitivity for detection of multiple components in a sample; however, its effectiveness for an accurate quantification is limited when there is a lack of baseline resolution or the degree of co-elution between the impurity(ies) and the product of interest is higher, as observed in our AAV5 sample (**Figure 1A and 1B**). In previous reports of the AEX-HPLC method for determination of % EC and CG in other AAV serotypes, where the continuous gradient protocol was found to be effective, the % of CG was as high as 50%[20,22], which in turn compensates for the lack of baseline resolution, resulting in relatively lower co-elution between EC and CG. In contrast, in our AAV5 sample, due to 90% of EC content, the separation efficiency was not high enough to offer baseline resolution. As a result, a relatively higher degree of co-elution between EC and CG suggested that the quantification of % of EC and CG determined from this continuous gradient run was not accurate and differed significantly from the values reported with *sv*-AUC (**Figure S2 A and B**), the current standard method for such analysis.

To address this problem, a step-gradient elution protocol was developed. The EC and CG, two main populations of AAV capsids in an affinity-purified AAV sample, were separated as baseline-resolved discrete peaks. Because of the apparent higher purity of the sample, the amount of non-

AAV-related impurities and their interference in overall analysis and quantification is expected to be minimum in the step-gradient elution protocol, making it suitable for analytical HPLC purpose. Moreover, the specificity demonstrated with appropriate reference standards also demonstrated the effectiveness of the step-gradient AEX protocol.

The optimized step-gradient protocol offers various advantages over the classical continuous-gradient elution. First, under optimally defined step-elution conditions, peak overlapping, and resulting co-elution are minimized compared to a continuous gradient, as we have demonstrated in **Figure 1A, 1B**. Second, under clearly defined separation conditions, each tailored for EC and VC, the method is now independent of their relative proportion in the sample. Interestingly, the method can handle the relative proportions of EC and VC on both extremes. For example, the AEX method reported herein efficiently separated (1) the empty capsid standard where the individual proportion of EC and VC is >95% and <5%, respectively, and (2) the vector capsid standard where the full vector proportion is ~ 80%. Third, because EC and CG are eluted separately in different steps, the effect of chromatographic flow rate, which otherwise may have a substantial impact on the overall resolution under a continuous-gradient mode of elution, is negligible. Fourth, the step-gradient protocol also offered higher sensitivity and better accuracy in the analysis (**Figure S2 D**). Moreover, because of no peak-overlapping, the baseline and the peak area integration parameter (e.g., valley-to-valley, used for quantitation herein) were easier to define.

Notably, both peak height and peak area-based analyses were suitable for constructing the standard curve for absolute quantification of AAV capsids (**Figure S4 A and B, Figure S5**). However, peak area-based analysis offered better accuracy for the determination of % EC and CG (**Figure S4 C and D**) and hence selected for both absolute and relative quantification purposes.

While the 260/280 nm absorbance was used as an in-line detection and a direct method of differentiation between EC and CG, the native fluorescence was also used for both detection and quantitative analyses. Due to the higher sensitivity and specificity of the 280 nm Ex/ 336 nm Em signal for protein over DNA, it was adopted for the quantitative analysis and establishing method validation parameters, among others, such as sensitivity and linear range of quantification. The protein-specific response of the fluorescence detection allows quantifying EC and CGs not requiring capsid and vector DNA molar absorption coefficient values. In contrast, in UV absorbance-based analysis, these values have to be known or practically determined for accurate quantification. Moreover, a well-defined baseline under fluorescence mode (**Figure 1D**), compared to UV detection, had a lower noise and hence increased sensitivity of the detection as reflected in LOD values reported in **Table 2**.

Differently from widely used *sv*-AUC or TEM, the proposed AEX-HPLC method is more sensitive, thus not necessitating a highly concentrated sample (or a very high amount of the analyte). Moreover, unlike TEM, AEX-HPLC allows simultaneous quantification of both relative (% proportion) and the absolute amount of EC (Cp/mL) and CG (VG/mL) in an affinity-purified sample. The AEX-HPLC method can also be used as a readily accessible and additional tool for AAV drug product characterization in research or QC labs. A high degree of automation offered by HPLC also provides higher reproducibility and simplicity in the overall operation and handling of the sample.

In conclusion, primarily based on the net negative charge of a biomolecule, a universal property of AAV capsids, the herein proposed AEX-HPLC method demonstrated for AAV5 and AAV8 can also be adapted for other serotypes quantification by introducing serotype-specific adjustments in HPLC method conditions.

6.5 Acknowledgment

P.R.H.J. is financially supported through a grant from the Natural Sciences and Engineering Research Council (NSERC RGPIN-2015-05132) of the government of Canada. A.K. is a recipient of a Canada Research Chair (CRC/240394). The authors would like to thank Aleš Štrancar (BIA separation) for providing a gift sample of the monolith anion-exchange column. The authors would also like to thank Julia Transfiguracion (National research council of Canada, Montreal) for providing valuable guidance in HPLC operation and method development.

6.6 Authors' Contributions

Conceptualization, P.R.H.J., P.S.C., and A.K.; Design of Experiments, P.R.H.J., A.B., P.S.C., and A.K.; AEX-HPLC Method Development and Validation, P.R.H.J.; AAV5 Production, Purification, and Characterization, P.R.H.J.; Writing-original draft, P.R.H.J.; Review & Editing, P.S.C., A.B., and A.K.; Funding acquisition, A.K.; Resources, P.S.C., and A.K.; Supervision, P.S.C, and A.K.

6.7 Conflict of interest

The authors declare no financial or commercial conflict of interest.

6.8 References

1. Ylä-Herttuala S. Endgame: Glybera finally recommended for approval as the first gene therapy drug in the European union. Mol. Ther 2012;20:1831–1832.
2. FDA advisory committee briefing document, Meeting of the cellular tissue, and gene

therapies advisory committee. 1–149 (2017).

3. Byrnes A. ZOLGENSMA. Summary basis for regulatory action, Office of the tissue and advanced therapies signatory authority. 2019; 1-16.
4. Wang D, Tai PWL, Gao G. Adeno-associated virus vector as a platform for gene therapy delivery. Nat. Rev 2019;18:358-378.
5. Zeltner N, Kohlbrenner E, Clément N, et al. Near-perfect infectivity of wild-type AAV as benchmark for infectivity of recombinant AAV vectors. Gene Ther 2011;17:872-879.
6. Wright, JF. Product-related impurities in clinical-grade Recombinant AAV Vectors: Characterization and Risk Assessment. Biomedicines 2014;2:80–97.
7. Wright, JF. AAV Empty Capsids: For better or for worse? Mol. Ther 2014;22:1-2.
8. Mingozzi F, High KA. Immune responses to AAV in clinical trials. Curr Gene Ther. 2011;7:316–324.
9. Burnham B, Nass S, Kong E, et al. Analytical ultracentrifugation as an approach to characterize recombinant adeno-associated viral vectors. Hum Gene Ther Methods. 2015;26:228–242.
10. Kronenberg S, Kleinschmidt JA, Böttcher B. Electron cryo-microscopy and image reconstruction of adeno-associated virus type 2 empty capsids. EMBO Rep 2001;2:997–1002.
11. Subramanian S, Maurer AC, Bator CM, et al. Filling adeno-associated virus capsids : estimating success by cryo-electron microscopy. Hum Gene Ther 2019; 30: 1449-1460.
12. Grimm D, Kern A, Pawlita M, et al. Titration of AAV-2 particles via a novel capsid ELISA: packaging of genomes can limit production of recombinant AAV-2. Gene Ther 2019;6:1322–1330.

13. Pierson EE, Keifer DZ, Asokan A, et al. Resolving adeno-associated viral particle diversity with charge detection mass spectrometry. Anal Chem 2016;88:6718-6725.

14. Sommer JM, Smith PH, Parthasarthy S, et al. (2003). Quantification of adeno-associated virus particles and empty capsids by optical density measurement. Mol Ther 2003; 7:122–128.

15. Joshi V, Kumar V, Rathore AS. Rapid analysis of charge variants of monoclonal antibodies using non-linear salt gradient in cation-exchange high performance liquid chromatography. J Chromatogr A 2015;1406:175–185.

16. Ponniah G, Nowak C, Neill A, et al. Characterization of charge variants of a monoclonal antibody using weak anion exchange chromatography at subunit levels. Anal Biochem 2017;520:49–57.

17. Leblanc Y, Ramon C, Bihoreau N, et al. Charge variants characterization of a monoclonal antibody by ion exchange chromatography coupled on-line to native mass spectrometry : Case study after a long-term storage at + 5^0 C. J. Chromatogr B Analyt Technol Biomed Life Sci 2017;1048:130–139.

18. Urabe M, Xin KQ, Obara Y, et al. Removal of empty capsids from Type 1 adeno-associated virus vector stocks by anion-exchange chromatography potentiates transgene expression. Mol Ther 2006;13:823-828.

19. Qu, G, Bahr-Davidson J, Prado J, et al. Separation of adeno-associated virus type 2 empty particles from genome containing vectors by anion-exchange column chromatography. J Virol Methods 2007;140:183–192.

20. Fu X, Chen WC, Argento C, et al. Analytical strategies for quantification of adeno-associated virus empty capsids to support process development. Hum. Gene. Ther. Methods

2019;30:144–152.

21. Lock M, Alvira MR, Wilson JM. Analysis of particle content of recombinant adeno-associated virus serotype 8 vectors by ion-exchange chromatography. Hum Gene Ther Methods 2012; 23:56–64.

22. Wang C, Mulagapati SRH, Chen Z, et al. Developing an anion exchange chromatography assay for determining empty and full capsid contents in AAV6 . 2. Mol. Ther. Methods Clin. Dev. 2019; 15:257–263.

23. Joshi PRH, Cervera L, Ahmed I, et al. Achieving high-yield production of functional AAV5 gene delivery vectors via fedbatch in an insect cell-one baculovirus system. Mol. Ther. - Methods Clin. Dev. 2019;13:279-289.

24. Kondratov O, Marsaic D, Crosson SM, et al. Direct head-to-head evaluation of recombinant recombinant adeno-associated viral vectors manufactured in human versus insect cells. Mol. Ther. 2017;25:2661-2675

25. Chahal PS, Schulze E, Tran R. et al. Production of adeno-associated virus (AAV) serotypes by transient transfection of HEK293 cell suspension cultures for gene delivery. J. Virol. Methods. 2014; 196, 163–173.

26. Vayá I, Gustavsson T, Miannay FA, et al. Fluorescence of natural DNA: from the femtosecond to the nanosecond time scales. J Am Chem Soc 2010; 132:11834–11835.

27. Onidas D, Markovitsi D, Marguet S, et al. Fluorescence properties of DNA nucleosides and nucleotides: a refined steady-state and femtosecond investigation. J. Phys. Chem. B 2002;106:11367–11374.

28. Brautigam CA. Calculations and publication-quality illustrations for analytical ultracentrifugation data. Methods Enzymol 2015;562:109-133.

29. Ghisaidoobe ABT, Chung SJ. Intrinsic tryptophan fluorescence in the detection and analysis of proteins : a focus on förster resonance energy transfer techniques. Int J Mol. Sci. 2014;15:22518-22538.

30. Lakowicz, J. R. Protein fluorescence. Principles of fluorescence spectroscopy. New York: Springer Science+Business Media, 2006. 529-575.

31. Guidance for Industry Q2B Validation of Analytical Procedures : Methodology. U.S. Department of health and human services food and drug administration center for drug evaluation and research (CDER). Center for biologics evaluation and research (CBER) November 1996 ICH.

32. Bioanalytical Method Validation Guidance for Industry. U.S. Department of health and human services food and drug administration. Center for drug evaluation and research (CDER). Center for veterinary medicine (CVM). 2018.

33. Flotte, T. R. Empty Adeno-Associated Virus Capsids : Contaminant or natural Decoy ? Hum. Gene. Ther 2017; 28:147–148.

Chapter 7 General discussion

In the last two decades, the AAV manufacturing sector has seen sustained developments with the emergence of new mammalian and insect cell-based AAV production systems. However, because of exponential growth in the demand for clinical-grade AAV material as a result of the rapidly expanding AAV-gene therapy clinical pipeline, the high-yield production of recombinant AAV vectors remains one of the limiting factors for current manufacturing processes. Traditional adherent mammalian cells-based production protocols were effective at a smaller scale and could generate AAV material in sufficient quantities for *in vitro* transduction studies or pre-clinical testing in animal models. However, implementing these non-scalable methods to generate AAV material for human clinical studies presented significant technical and operational challenges. For example, to generate approximately 10^{15} VGs necessary to conduct a large-scale animal study or phase-I human clinical trial, around 500 to 1000 traditional 175 cm^2 T-flask are required, with the demand further growing up to 100 times more flasks for phase-II/III studies. This prompted the eventual development of various modular adherent cell culture systems or novel bioreactor configurations for propagation and expansion of adherent cells growing on a suspended or static solid support.

In contrast to the adherent cell culture's operational complexity and relatively limited scalability, the suspension cell-culture based AAV production systems offer a straightforward mean of linear production scalability expanding from 20 mL to 20,000 L scale. Suspension adapted HEK293 or BHK cells and insect-cell baculovirus expression vector systems (IC-BEVS) have been the workhorse in the last two-decades for AAV production in suspension cell cultures. Of these systems, insect-cell systems exhibit better ease of scalability and ability of insect-cells to grow and produce the protein of interest in high-cell density cultures, which in turn, offer higher volumetric

yields. In this thesis, employing a recent modification of the one baculovirus system: One-Bac 3.0, an improved AAV manufacturing process was developed using AAV5 as a model serotype. In contrast to the other insect cell production system based on three or two baculoviruses (Three-Bac or Two-Bac, respectively), the herein used One-Bac system, requiring only a single baculovirus infection, offers operational simplicity over other systems. The AAV *rep* and *cap* gene sequences, integrated into the insect cell line, exhibited robust induction and amplification at an optimal MOI of 3 with stable expression levels up to 35 cell passage numbers (maximum passages tested). This was a critical outcome as the traditional Three-Bac, or Two-Bac system showed stable expression and sustained AAV yield up to seven baculovirus passages only, both of which gradually dropping over additional baculovirus passages. Despite being isolated from an entire baculovirus genome context, which is necessary for inducible expression of AAV proteins, 28-fold amplification of *rep* and *cap* gene expression at an optimal MOI of 3 was achieved. This resulted in cell-specific titer in the range of 20,000 VG/cell and volumetric titer of approximately $4x10^{10}$ VG/mL of cell culture in low-cell density cultures (~ $2x10^{6}$ cells/mL), which were comparable to that of other insect cell and mammalian cell production platforms.

Next, to increase the volumetric titer of AAV production, a high-cell density fed-batch production process was developed. The challenging aspect was to attain a linear increase in volumetric yield (VG/mL) with a corresponding increase in cell-densities, which was only possible if the cell-specific yield (VG/cell) was maintained at high cell densities. The cells were fed with a nutrient cocktail in a timely fashion to help reach high cell-densities while maintaining them in the mid-exponential growth phase before baculovirus infection. Post-infection, the cell culture shifted to the AAV-production phase from the growth phase, and the cells were supplemented with nutrients to support elevated demand. Among various cell-densities tested as high as 30 million cells/mL,

the suitable cell-density for AAV production was 10-12 million cells/mL. At higher cell-densities, the cell culture was unsustainable in a productive infection phase resulting in a sudden drop of cell-viability and AAV yield potentially because of nutrient exhaustion or accumulation of toxic-metabolites, a phenomenon commonly reported as a metabolic limitation of the cell-culture. Implementing higher-cell density cultures without a corresponding increase in AAV yield was impractical. Moreover, the co-extraction of a substantial amount of cellular components along with AAV and their removal exert a significant burden on the downstream processing.

At an optimal cell density of 10 million cells/mL for infection, the insect cell culture transitioned to a productive infection phase within 48 hours, allowing sufficient time for AAV protein expression and AAV vector production before they were harvested at 96 hpi. An approximately 50-fold increase in AAV *rep/cap* gene expression resulted in sustained cellular productivity even at 6x higher cell densities (~12 million cells/mL) compared to the control low-cell density culture (~ 2 million cells/mL). Corresponding 6-fold increase in AAV viral genome yield (VG/mL) and 18-fold increase in functional vector yield (ETU/mL) suggested that the optimal nutrient feeding employed effectively sustained cells in the productive and processive phase. The AAV fed-batch production process was validated at a 3L bioreactor scale. The overall volumetric titer as high as $3x10^{14}$ VG/L was one of the highest yields reported for AAV production, in general, and for AAV5 in particular. Notably, this volumetric titer was up to 6-fold higher than the current routine manufacturing process ($5x10^{13}$ VG/L), signifying that with our proposed process, an equal amount of AAV material can be generated employing 6-time smaller manufacturing scale or at the same production scale, 6-times higher AAV yield can be achieved.

Comparable with widely used triple plasmids transient transfection mammalian production process, the AAV5 produced using the One-Bac3.0 system with the reported fed-batch process

also showed substantial excess of empty capsids over genome-containing functional viral capsids. The *sv*-AUC analyses data indicated that in the affinity-purified material, the genome-containing vector capsids (GC) were only 10%, while 90% of capsids were genome-less empty capsids. Due to their reported immunogenic properties, the removal of this excess of empty capsids was essential to generate high-quality GC-enriched AAV5 preparations suitable for clinical studies. Because of the relatively limited availability and implementability of ultracentrifugation technology for preparing GC-enriched AAV material at a large scale, an alternative, more feasible ion-exchange chromatographic approach was developed exploring the minute differences in ionic charge characters of AAV EC and GC capsids.

During the salt-screenings study, AAV5 elution in a continuous NaCl gradient, a commonly used salt gradient for AAV, displayed poor resolution and separation with substantial overlapping between EC and GC peaks. Differently from this, in the previous reports of AAV5, the separation was achieved by using either weak anion exchanger (POROS PI) and salt of monovalent chloride anions (KCl)[86] or strong anion exchanger (POROS HQ) and salt of acetate (Tris-acetate)[72] or chloride (NaCl)[87,88]. To address the peak overlapping issue, divalent anionic displacer salts, sodium monohydrogen phosphate (HPO_4^{2-}), and sodium sulfate (SO_4^{2-}), with higher ionic strength, were selected for further screening. It was hypothesized that due to strong ionic interaction of divalent ions with ammonium ligand, these salts might strongly elute less negatively charged AAV EC preferentially before the beginning of GC elution, resulting in less EC peak tailing and reduced overlap as opposed to a low ionic strength NaCl salt. As expected, these salts eluted AAV5 EC and GC with better resolution and less overlap between EC and GC. The sharp and narrow peaks with reduced co-elution of EC and GC indicated better GC enrichment compared to chloride, as shown by $A_{260/280}$ ratio.

The intrinsic difference between elution points of AAV5 EC and GC was amplified employing a shallow elution gradient, which resulted in improved resolution and separation. A discontinuous (step) gradient elution approach was employed to further simplify the process and to address partial co-elution of EC and VC, which necessitates discarding overlapping peak fractions and selectively collecting later fractions containing enriched vector capsids to achieve higher purity, although at the expense of the total recovery (**Table S2**). The partial co-elution with empty capsid fraction suggests that the net negative charge of the intermediate population encapsidating small size DNA is close to that of the empty capsids. In contrast, vector capsids encapsidating full-length large size genome may have a higher net negative charge.

The step-gradient process enabled empty and genome-containing vector capsids, each collected in single, highly concentrated fractions in a reproducible manner. Moreover, this step-gradient protocol can also be adapted with better ease than the continuous gradient elution approach to an up-scale operation[89,90]. Identical elution profiles of AAV8-*gfp* capsid under the shallow continuous gradient run in both monolith and packed bed resin columns suggest an easy to adapt AAV-AEX process to a widely used chromatography medium without significant changes. Finally, the sulfate based AEX process showed reproducible and comparable results with other serotypes such as AAV6 and AAV8. This signifies the generic character of the proposed AEX method and its potential to be applicable to other AAV serotypes produced in mammalian on insect-cell cultures without requiring significant modifications.

Chapter 8 Conclusion and summary

The field of AAV manufacturing is interdisciplinary and has undergone substantial improvements in the first generational AAV production systems, including the insect cell baculovirus platform. Improvements in molecular design aspects of the AAV production system and their consequent adaptation to the upstream and downstream processing have resulted in a more simplified and streamlined production process. A recent modification of a more simplified IC-BEVS, One-Bac 3.0, was employed in this doctoral research work to improve the overall manufacturing process using AAV5 as a model. This work was the first report of the high-yield production of functional AAV5 vectors in high-cell density fed-batch cultures of One-Bac Sf9 cells. These results were of prime importance as the previous attempts of AAV5 production using other insect-cell systems were limited to low-cell density production cultures, and the AAV5 produced were biologically inactive. The fed-batch approach integrating an optimal feeding regime resulted in 18-fold higher volumetric yields of functional AAV5 vectors. The reported yield of around 2-3x10^{14} VG/L, both at a small shaker flask scale and 3L bioreactor scale, were one of the highest yield ever reported for AAV5 in any AAV production system. These findings reinforced the stance of One-Bac as a suitable system for AAV vector production.

Next, the downstream processing work focused on understanding the effect of important components of anion-exchange chromatography on AAV5 EC and GC separation efficiency and GC enrichment. The systemic screening of various ionic salts indicated the better suitability of stronger divalent salts for better enrichment of AAV5 GC capsids. This finding was different from previous reports where conventional monovalent salts have been used for this purpose. The selection and implementation of divalent salts in the chromatography process provided 8-fold enrichment of AAV5 GC capsids with an overall recovery of 75% while operating under a step-

gradient elution process. These values of degree of enrichment and % recovery were the highest among the reported values as compared to previous reports where the recovery has been consistently below 60%. The optimal chromatographic process showed universal characteristics as it demonstrated the separation of EC and subsequent enrichment of GC for other clinically relevant serotypes such as AAV6 and AAV8. More importantly, the GC enrichment and process recovery were consistently higher than any of the previous reports signifying the importance of fundamental salt-screening studies. Demonstrating the robustness, the proposed IEX-chromatography process provided similar separation characteristics for both the packed-bed and monolith column. These results also provided evidence for the suitability of ease of scale-up of the proposed IEX-process using two-widely used chromatography media.

The reported IEX-HPLC method for AAV5 EC and GC analysis demonstrated the suitability of very strong phosphate salts for the separation and resolution of AAV capsids in the analytical column. Notably, the proposed IEX-HPLC method was effective for the sample where the EC content, the main AAV-related impurity, was 10x higher than the product of interest, the GC. Differently from previous reports utilizing a continuous-elution gradient, the step-gradient approach provided the required degree of separation to enable accurate and precise quantification of EC and GC capsids in the samples with a significantly higher proportion of the impurity. Moreover, the reported method for AAV5 may be easily adapted to other serotypes applying serotype-specific adjustments in the chromatographic conditions.

Incorporating all three phases of AAV manufacturing: upstream processing, downstream processing, and analytics, this thesis provides implementable and straightforward solutions for high-yield, high-quality AAV production.

8.1 Future perspective

The research work performed in this thesis highlights several areas that would be an appropriate starting point for future work towards further improving the AAV manufacturing process. Following are the critical points that call for a further in-depth investigation to better understand the AAV production systems and process.

- The discovery of essential baculovirus helper function elements and understanding their effect on AAV yield and quality is an important sector that lacks detailed studies. The outcome of such studies would help design improved IC-BEVS systems for AAV production.
- The generation of insect cell-based producer cell lines for AAV production offers an exciting opportunity to simplify the overall AAV manufacturing at the commercial scale. Dedicated efforts in generating Sf9 or Hi-5 insect-cell based producer cell line remains an open area for further investigation.
- The development of insect-cell metabolomics-based newer growth media and nutrient feed formulations to support sustained AAV yield at higher cell-densities is critical for next-generation process-intensification.
- Strategies to sustain higher cell viability during the AAV production phase and compartmentalize AAV capsids in the extracellular environment (cell-culture supernatant) remain an important area of investigation to simplify the primary recovery and overall downstream purification steps. This also provides an opportunity to overcome any existing limitation of the AAV-extraction process.

- The development of novel non-affinity chromatography methods for the primary capture step is also desirable to enable purification of serotypes that are not complemented via affinity-ligands used in currently available affinity-resins.
- The development of chromatography ligands with specificity towards either AAV empty capsids or genome-containing vector capsids also offers an exciting opportunity to simplify GC enrichment and the overall downstream purification process.
- Chromatographic strategies capable of distinguishing the vector capsids (encapsidating full-length vector expression cassette) from genomic capsids encapsidating non-vector sequences (fragmented genome, host cell genome, or baculovirus backbone sequences) remains open to an in-depth investigation.
- Finally, the development of novel analytical chromatography media or methods suitable for analysis of AAV EC and GC capsids in crude-cell lysate are crucial to integrate the HPLC method as a suitable process analytical technology for upstream production process manufacturing and control.

Chapter 9 Appendices: Supplemental Information

9.1 Supplemental information 1 Achieving High-Yield Production of Functional AAV5 Gene delivery Vectors via Fedbatch in an Insect Cell-One Baculovirus system (Chapter 4)

Supplemental data

Figure S1

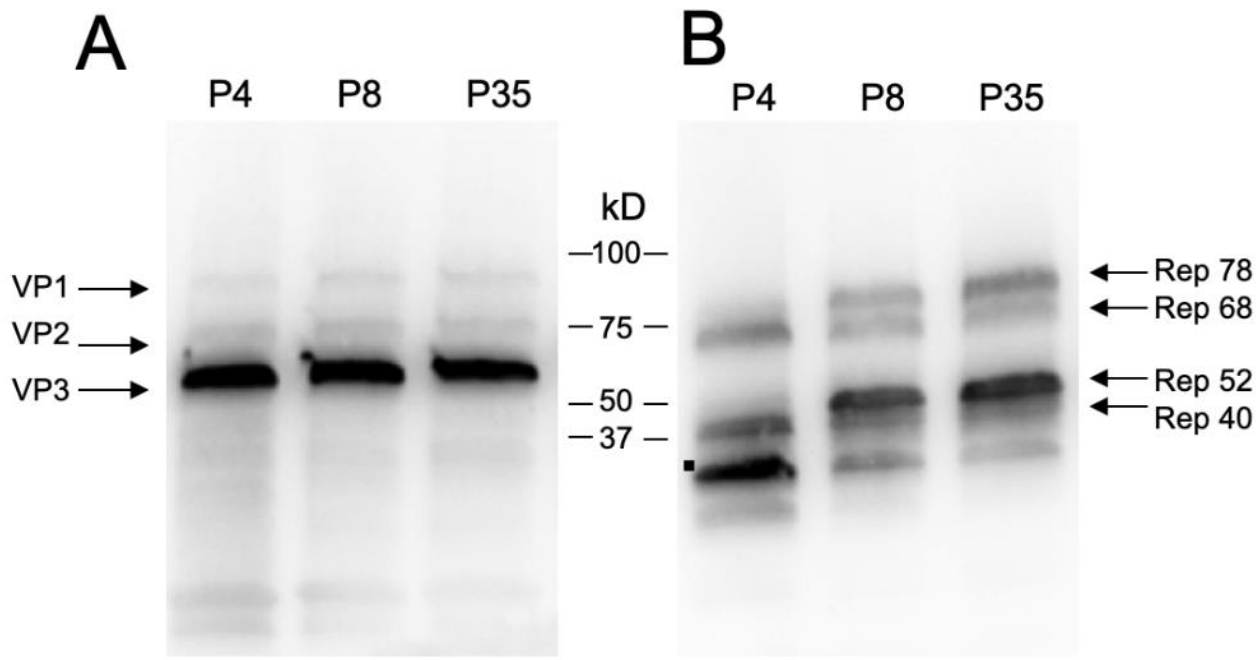

Genetic stability of rep2cap5 packaging Sf9 cell line

(A) Anti AAV5 capsid Western blot of cell lysate samples from different passage number production runs. Three capsid subunits were detected and identified from their respective molecular weights. **(B**) Anti AAV replicase 2 Western blot of cell lysate samples from different passage number production runs. Four different replicase subunits were detected and were identified based on their respective molecular weights. Two essential rep proteins responsible for genome replication and encapsidation: Rep 78 and Rep 52 profile shows a progressive increase in expression over the passage numbers. Note the additional smaller spliced variants of Rep 52 pointed with a dot.

Figure S2

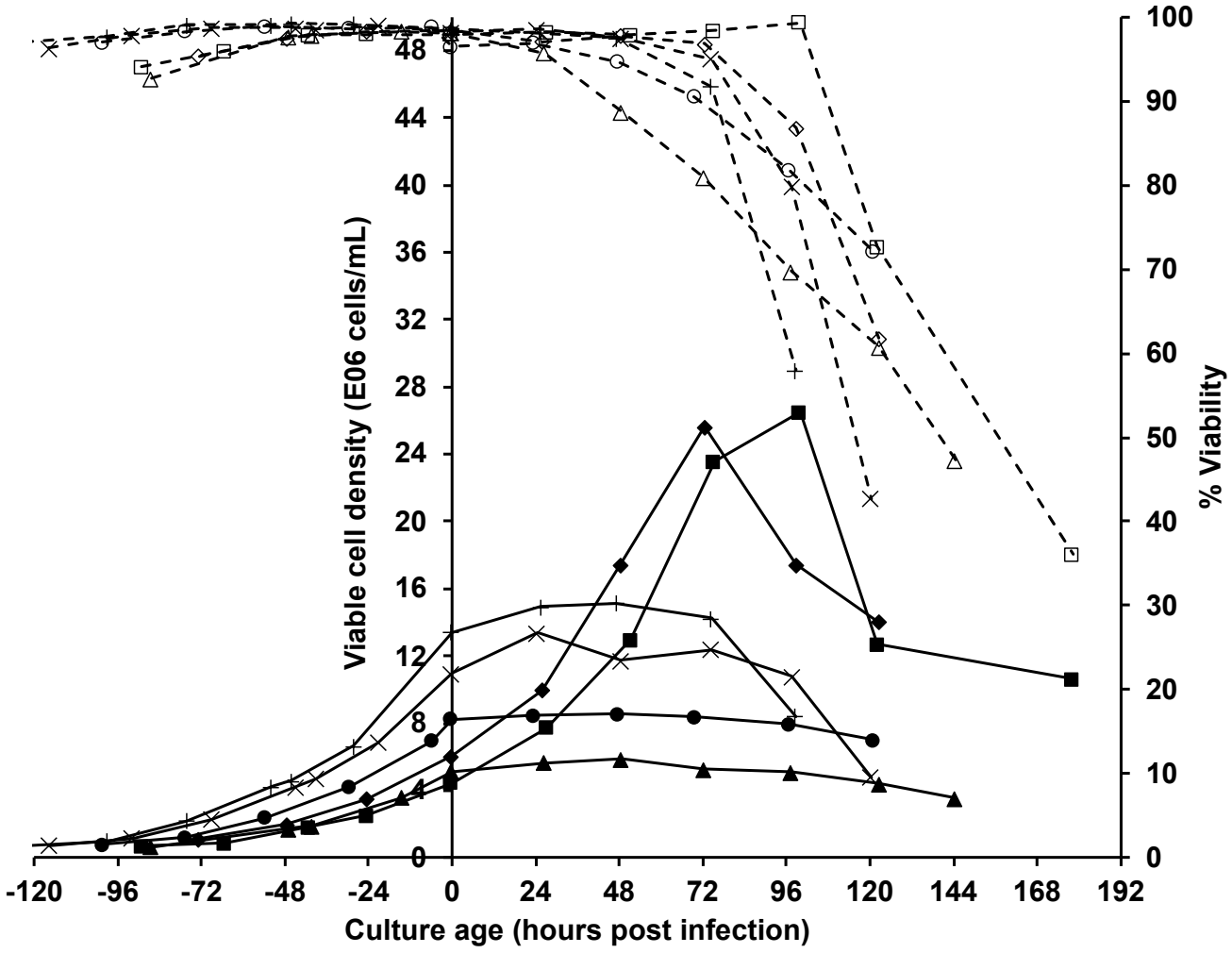

Cell culture data for preliminary work on feeding regime and cell density at the time of infection in fedbatch mode of operation using B8 cell line

B8 packaging cell line showed different growth characteristics compared to what has been published by our group previously. This can be attributed to the possible metabolic changes upon transformation. A feeding regime tailored for B8 cell line was developed as reported in the paper and different cell density at the time of infection were screened. The graph shows data from representative runs. A fedbatch production run with overall cell density above 10-12 million cells resulted in a reduced yield of genomic and functional virus particles and hence 10 million cells/mL at the time of infection was selected for further work. The cell density data are shown via solid line and filled symbols (__) whereas the data of % cell viability is shown via dotted lines and empty symbols (----).

[Legends: ◊: No infection and feeding in three shots as per the published report by our group, **• :** No infection and extended and multiple shots feeding, Δ**:** infection at 5million cells/mL**, 0:** infection at 8 million cells/mL**. X:** Infection at about11 million cells/mL**,** and **+:** infection at about 14 million cells/mL**]**.

Figure S3

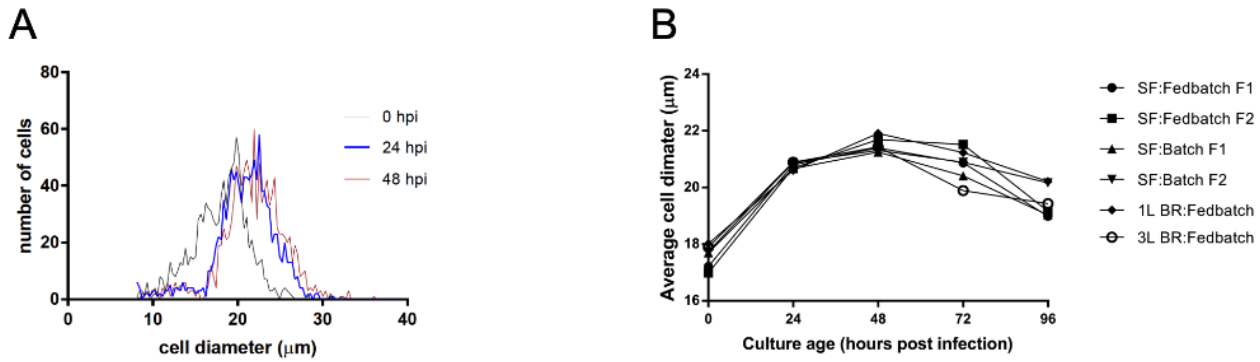

Synchronous infection characteristics at MOI of 3

(A) A histogram showing Sf9 cell size distribution before and after baculovirus infection at MOI 3 during a fedbatch production in a bioreactor run. Note the right-hand side shift at 24 hpi, a direct indication of infection that resulted in an increase in cell dimeter. **(B)** Average cell diameter profile in pre- and post-infection phases. An immediate increase of around 3µm in average cell diameter at 24 hpi and subsequent plateau at 48 hpi is an indication of synchronous infection at MOI of 3. BR: bioreactor, hpi: hours post infection, SF: shake flask,

Figure S4

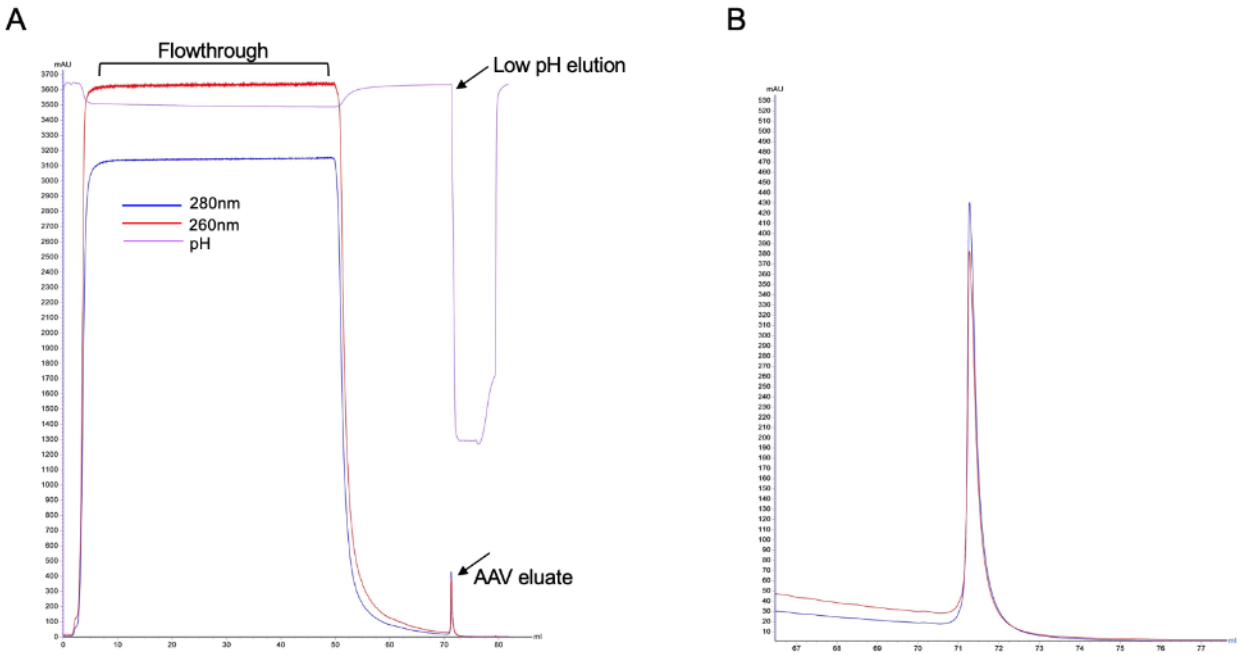

(A) AAV5 affinity purification chromatogram. **(B)** The magnified image of an AAV eluate peak. (To fig. 3)

Figure S5

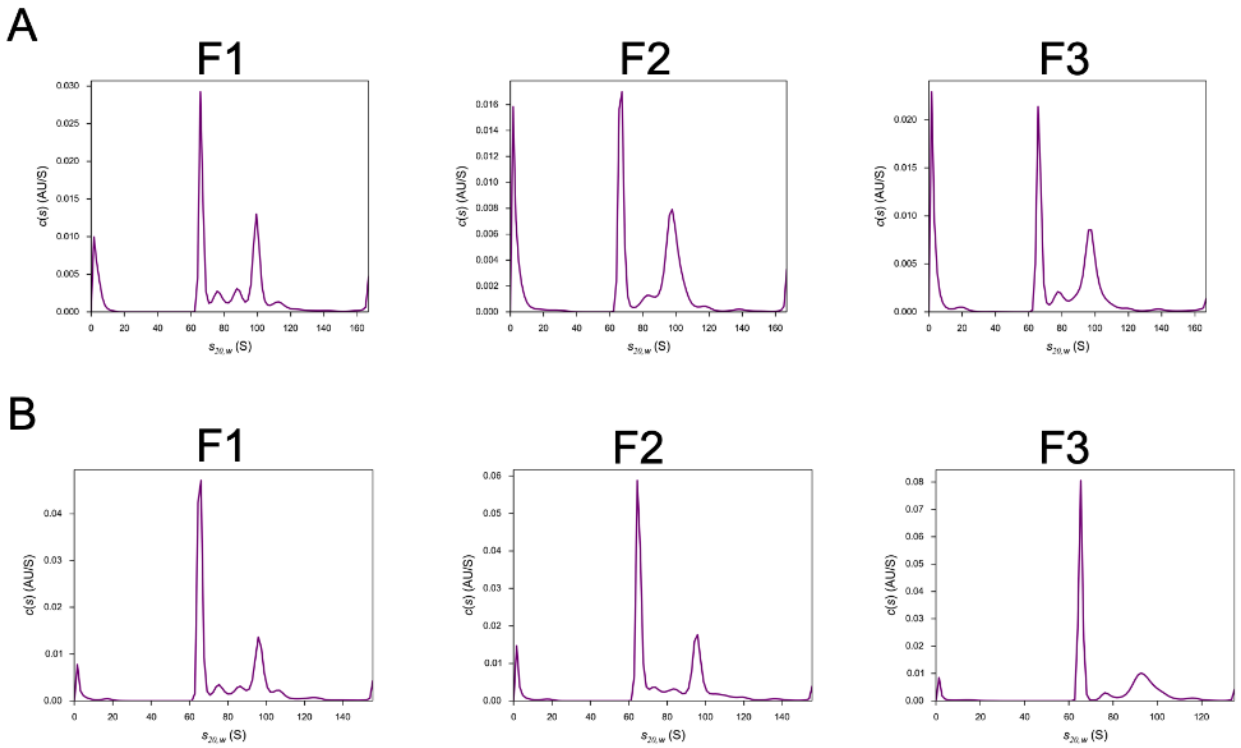

AUC histograms of AAV5 production in shake flasks in batch and fedbatch mode of operation

(A) AAV5 production in triplicate shake flask production runs in batch mode. **(B)** AAV5 production in triplicate shake flask production runs in fedbatch mode. A very sharp peak around 62-67s represents the presence of an empty capsid and a major peak around 93-98s and intermediate population between these two major peaks represent genomic capsids. The peaks corresponding to the intermediate population may represent the form of a particle with encapsidation of partial AAV genome or collaterally packaged contaminating DNA. (To Fig. 3)
F: flask

Figure S6

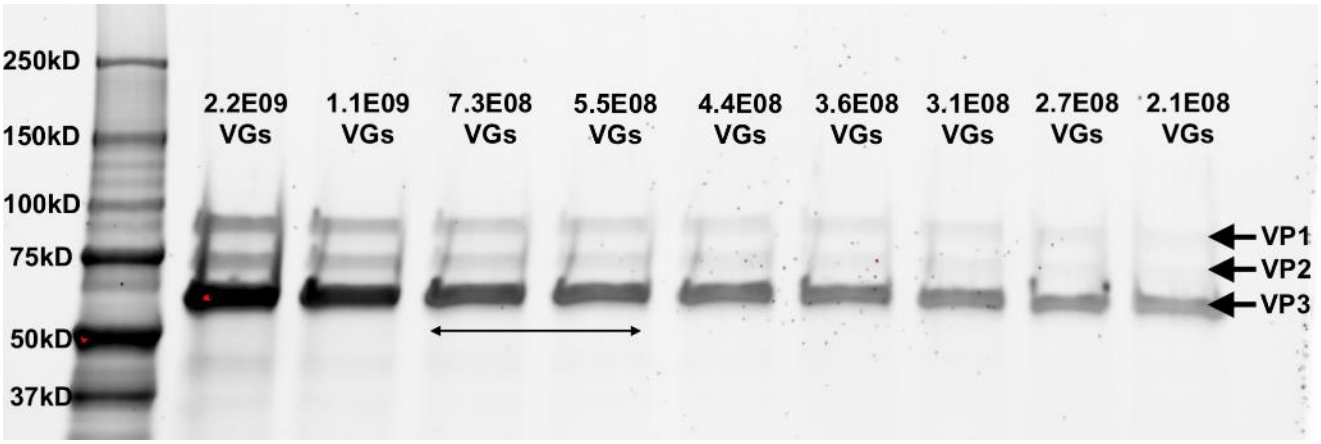

AAV capsid VP composition analysis

VP stoichiometry analysis via Flamingo™ stained SDS-PAGE gel of affinity purified sample. Each lane is labelled with its corresponding amount of total VG loading and the linear range of quantification ($5.5x10^8$-$7.3x10^8$ VG) is marked with a double headed arrow. The average of VP band intensities in a given range is 1.7:1.6:10 = VP1:VP2: VP3. (To Fig. 3)
VGs: viral genome.

Table S1. Relative proportion of empty and genomic capsid in AAV5 samples from multiple AAV production runs in batch and fedbatch modes of operation

Sample	Sedimentation coefficient (S Value)		Relative proportion (%)	
	Empty capsid	Major genomic capsid	Empty capsids	Genomic population
SF Batch F1	66	98	74.17	25.83
SF Batch F2	67	98	73.45	26.54
SF Batch F3	66	97	74.70	25.30
SF Fedbatch F1	65	94	80.81	19.05
SF Fedbatch F2	65	95	81.61	18.39
SF Fedbatch F3	65	96	79.48	20.52

(To Fig.3)
SF: shake flask

Table S2. VP composition analysis of affinity purified samples from multiple AAV production runs

	SF Batch F1	SF Batch F2	SF Batch F3	SF Fedbatch F1	SF Fedbatch F2	SF Fedbatch F3	Fedbatch 1L Bioreactor	Fedbatch 3L Bioreactor
VP1	1.5	1.5	1.6	1.4	1.6	1.3	1.7	1.4
VP2	2.2	2.1	2.4	1.4	1.7	1.5	1.6	1.4
VP3	10	10	10	10	10	10	10	10

(To Fig.3)
SF: shake flask

Table S3. Primer sequence for *rep/cap* copy number analysis

Cap5 F	5’-tcagcagcatcaagatcaagcc-3’
Cap5 R	5’-cctgttgacaggctctcctc-3’
Rep2 F	5’-gcaagaccggatgttcaaat-3’
Rep2 R	5’-cctcaaccacgtgatccttt-3’

(To Fig. 4)

Supplemental methods

Calculation of relative proportion of empty and genomic particles from AUC data

The following calculation is performed from the AUC data of a representative AAV production run as described in the manuscript.

Molar absorption coefficient and Molecular weight values for AAV2 empty capsid has been previously reported[1] and are as following:

$\varepsilon_{260\ (empty\ capsid)} = 3.72x10^{6}\ \mathbf{M^{-1}cm^{-1}}$

Molecular Weight $_{(empty\ capsid)} = 3.74x10^{6}$ **g/mol**

Above values can be theoretically adopted for AAV5 empty capsid due to capsid amino acid sequence homogeneity of AAV serotypes with AAV2

The molecular weight of vector DNA was calculated, and Molar absorption coefficient was determined from spectroscopic analysis of vector DNA extracted from purified AAV5 preparation. The values are as following:

$\varepsilon_{260\ (vector\ DNA)} = 9.26x10^{6}\ \mathbf{M^{-1}cm^{-1}}$

Molecular weight $_{(vector\ DNA)} = 4.63x10^{5}$ **g/mol**

The molar absorption coefficient of AAV5 vector particle can be derived by combination of those values of empty capsid and vector DNA

$\varepsilon_{260\ (vector\ DNA)} + \varepsilon_{260\ (empty\ capsid)} = (9.26x10^{6} + 3.72x10^{6}) = 1.3x10^{7}\ \mathbf{M^{-1}cm^{-1}}$

Molecular weight $_{(vector\ DNA\ +\ empty\ capsid)} = 4.20x10^{6}$ **g/mol**

The molar concentration **C** of the empty capsid can be determined from the area of the empty capsid peak using Beer`s equation:

$$\mathbf{C}_{(empty\ capsid)} = \mathbf{A}_{260} / (b * \varepsilon_{260\ (empty\ capsid)})$$
$$= 0.074 / (1.2 * 3.72x10^{6})$$
$$= 1.66x10^{-8}\ \mathbf{M}$$

Where b is the pathlength of AUC sample cell, and $\mathbf{A_{260}}$ is the area under the peak when measured at 260 nm

Consequently, the concentration **W**(g/L) of the empty capsid can be calculated from basic equation of molarity

$\mathbf{W}_{(\text{empty capsid})}$ = (**C** * Molecular weight) = ($1.66\text{x}10^{-8}$ * $3.74\text{x}10^{6}$) = $6.20\text{x}10^{-2}$ **g/L**

Similarly, the molar concentration of genomic particle (vector particle or full particle) can be derived too

$\mathbf{C}_{(\text{vector})} = \mathbf{A}_{260\ (\text{DNA + capsid})} / (b * [\ \varepsilon_{260\ (\text{vector DNA})} + \varepsilon_{260\ (\text{empty capsid})}])$

$= 0.093 / (1.2 * 1.3\text{x}10^{7}) = 5.96\text{x}10^{-9}$ **M**

$\mathbf{W}_{(\text{vector})} = (\mathbf{C}_{(\text{DNA + capsid})} * \text{Molecular weight}_{\ (\text{DNA+ capsid})})$

$= (5.96\text{x}10^{-9} * 4.20\text{x}10^{6}) = 2.50\text{x}10^{-2}$ **g/L**

For equimolar composition, the relative amount of individual component is in proportion to their relative molecular weights. Hence, the concentration **W**(g/L) of capsid in the genomic particle (genomic capsid) can be given by the following equation:

W(genomic capsid) = ($\mathbf{W}_{(\text{vector})}$ * [Molecular weight $_{(\text{capsid})}$ / Molecular weight $_{(\text{vector DNA + empty capsid})}$])

$= (2.50\text{x}10^{-2}) * (3.74\text{x}10^{6} / 4.20\text{x}10^{6})$

$= 2.23\text{x}10^{-2}$ **g/L**

From the total amount of empty capsid and genomic capsid, their relative proportion can be given as following:

$\%_{(\text{genomic capsid})} = 100 * \mathbf{W}_{(\text{genomic capsid})} / (\mathbf{W}_{(\text{genomic capsid})} + \mathbf{W}_{(\text{empty capsid})})$

$= 100 * (2.23\text{x}10^{-2}) / (2.23\text{x}10^{-2} + 6.20\text{x}10^{-2})$

$= 26.45\%$

$\%_{(\text{empty capsid})} = 100 - \%_{\ (\text{genomic capsid})}$

$= 73.55\%$

Hence, the relative proportion of empty and genomic particles is ~74% and ~26% respectively.

Supplemental References:

1. Sommer, JM., Smith, PH., Parthasarathy, S., Issacs, J., S, Vijay., Kieren, J. et al. (2003). Quantification of adeno associated virus particles and empty capsids by optical density measurement. Mol Ther. 7(1):122-128.

9.2 Supplemental Information 2 Development of a Scalable and Robust Anion-Exchange Chromatographic Method for Enriched Recombinant Adeno-Associated Virus Preparations in Genome Containing Vector Capsids of Serotypes- 5, 6, and 8 (Chapter 5)

Supplemental Data

Figure S1

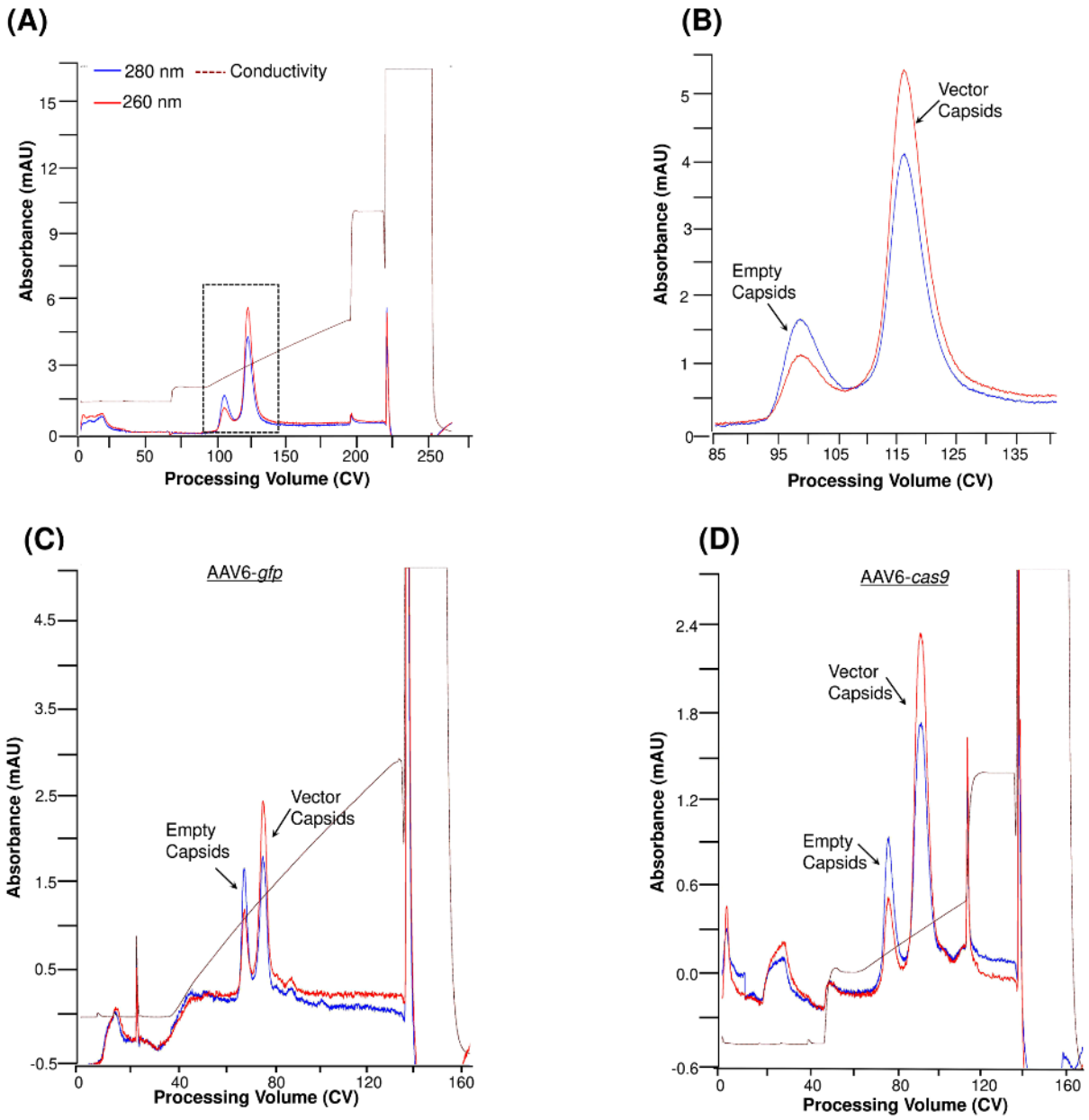

AAV6 and AAV8 Serotypes elution profiles under optimal conditions of continuous gradient AEX process

(A) AAV8-*gfp* elution profile under optimal conditions of AEX processing (10 mM BTP, pH 9.0, and $MgSO_4$) operated under a shallow continuous gradient of salt (0.4 mM salt/CV). **(B)** Enlarged image of two distinctly separate peaks corresponding to AAV8 EC and VC. **(C)** AAV6-*gfp* and **(D)** AAV6-*cas9* elution profiles under

optimal conditions of the AEX process (10 mM BTP, pH 9.0, and $MgSO_4$) operated under a shallow gradient of the salt (0.4 mM salt/CV).
AEX, anion-exchange chromatography; CV, column volume; EC, empty capsids; VC, vector capsids.

Figure S2

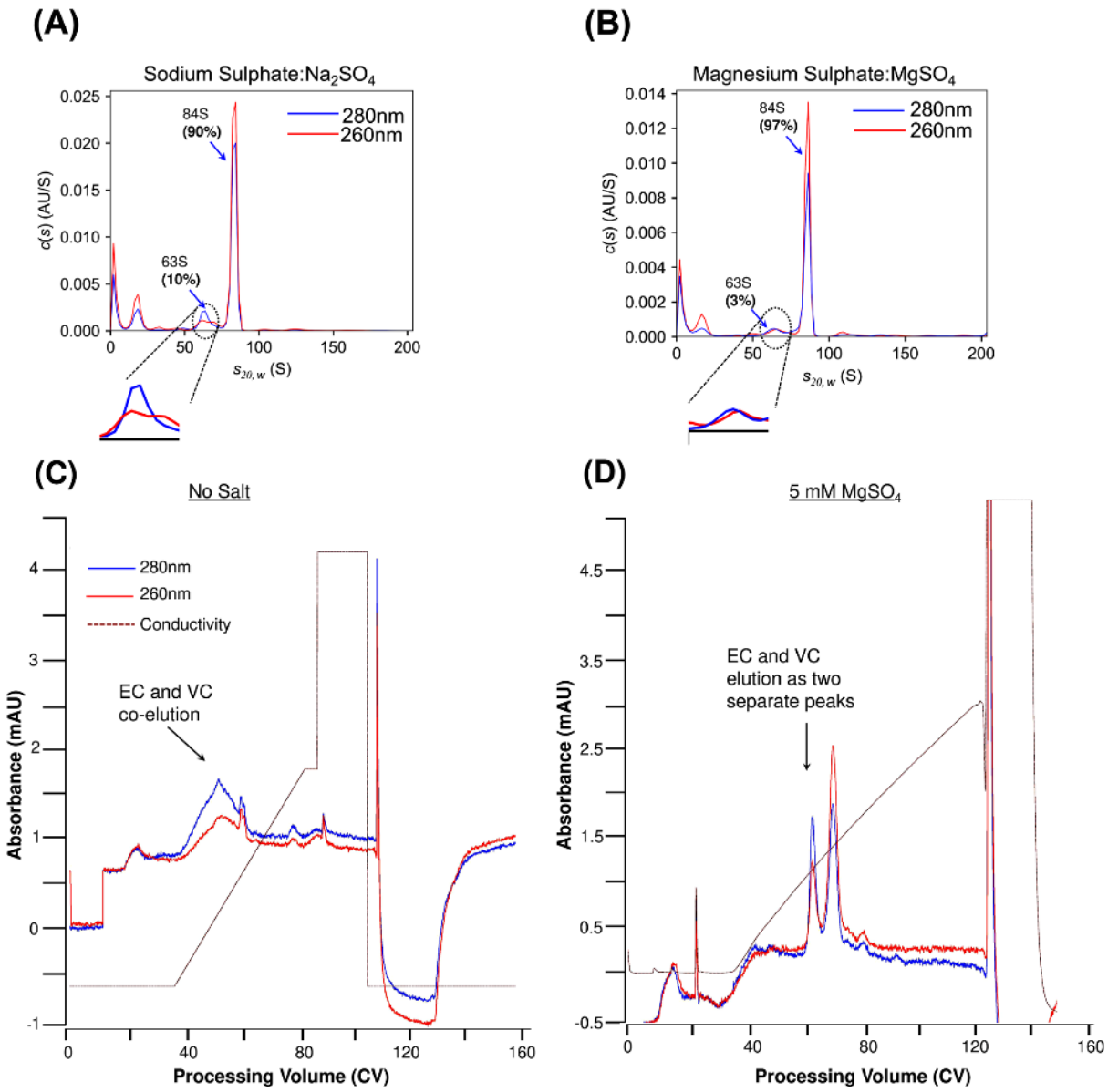

Effect of buffer composition on AAV VC enrichment and separation

sv-AUC profile of AAV8-*gfp* VC peak fraction collected under Na_2SO_4 **(A)** and $MgSO_4$ **(B)** salt gradient. In Na_2SO_4 elution fraction, the relative proportion of EC (63S) and VC (84S) are 10% and 90%, respectively. The peak at 63S (enlarged) also shows a higher 280 nm signal profile and $A_{260/280}$ =0.69. In the $MgSO_4$ elution fraction, the peak at 63S, though present, does not represent the $A_{260/280}$ profile representative of EC, indicating a possibility of UV signal noise in *sv*-AUC. Nevertheless, upon calculation, the relative proportions of 63S and 84S peaks were 3% and 97%, respectively. AAV6-*gfp* vector elution profile without **(C)** and with **(D)** additional

salt in the exchange buffer and column equilibration buffer. $A_{260/280}$, the ratio of peak area measured at 260 nm and 280 nm absorbance: *sv*-AUC, sedimentation velocity analytical ultracentrifugation.

Table S1. Chromatographic parameters of AAV5 elution under different salts

Condition	Peak resolution (R_s)	$A_{260/280}$		% Peak area[d]			
		Empty Capsid	Vector Capsid	Empty Capsid (280 nm)	Vector Capsid (280 nm)	Empty Capsid (260 nm)	Vector Capsid (260 nm)
AAV5/*sv*-AUC	NA	0.53	0.97[c]	61[e]	39[e]	48[e]	52[e]
AAV5/NaCl	0.31[a]/0.5[b]	0.63	0.89	72	28	24	76
AAV5/Na_2HPO_4	0.55 [a]/1.06[b]	0.71	1.21	38	62	28	72
AAV5/Na_2SO_4	0.49 [a]/0.90 [b]	0.62	1.19	53	47	35	65

NA, not applicable; $A_{260/280}$, the ratio of peak area measured at 260 and 280 nm absorbance

[a] Calculation of resolution of based on the equation for peak width and peak distance: [$R_s=2(V_2- V_1)/(W_1+W_2)$]. V_1 and V_2 are the elution points of peak 1 and 2, respectively. W_1 and W_2 are peak width of peak 1(empty capsid) and 2 (vector capsid), respectively; see figure below. The retention time was converted to retention volume by multiplying with the flow rate: 0.5 mL/min.

[b] Calculation of resolution based on an alternative equation.
Rs = $(\sqrt{N}/4)*((\alpha-1)/\alpha)*(k'/(k'+1))$
Where α = selectivity factor, k' = retention factor of peak 2, N = theoretical plates.
$N= 16\ (tr/tw)^2$, where tr is retention time (or volume) and tw is peak width (in time or volume).
The retention time was converted to retention volume by multiplying with the flow rate: 0.5 mL/min.

[c] calculation based on the combined peak area of 79S and 95S peaks.

[d] calculation based on peak area from valley-to-valley integration of the peaks shown in the HPLC chromate gram (see figure below).

[e] calculation based on peak area determined using Gussi software applying baseline peak integration of peaks shown in AUC histogram.

(To Fig. 1)

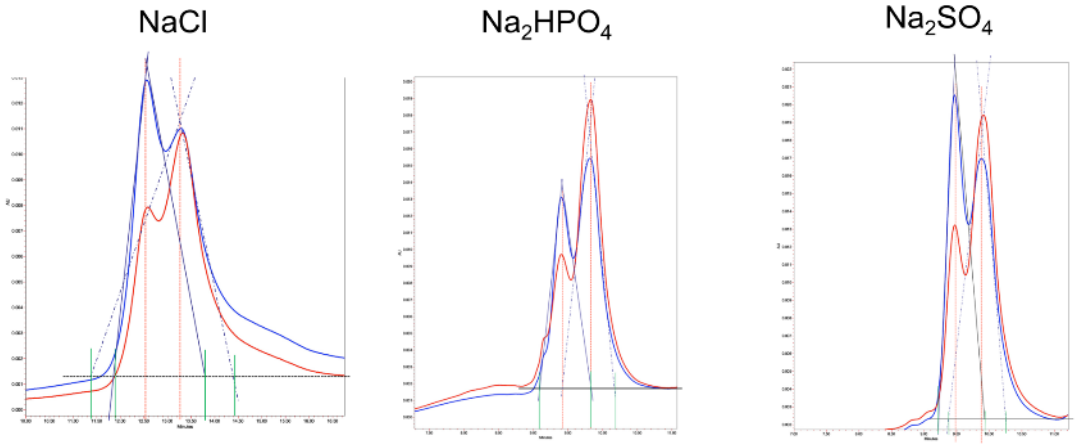

Table S2. AAV5 vector capsid recovery under sodium sulfate continuous gradient elution

Fraction	Fraction number	% VG eluted	% VG Recovery
Empty capsid fractions	1	0.87	4.79%
	2	1.3	
	3	1.11	
	4	1.51	
Overlapped fractions	5	8.11	19.51%
	6	11.4	
Vector capsid fraction	7	22.8	57.09%
	8	18.05	
	9	10.2	
	10	6.04	

(To Fig 1)

Table S3 Summary of AEX step gradient process characteristics

Sample	VG/mL	Volume (mL)	Total VGs	% VG Recovery[a]
AAV5-*gfp*[b]				
Feed	8.50×10^{11}	10	8.50×10^{12}	-
Flowthrough and column wash	1.98×10^{09}	30	5.94×10^{10}	0.7
EC peak fraction	2.42×10^{10}	45	1.09×10^{12}	12.8
VC peak fraction	4.12×10^{11}	15	6.18×10^{12}	72.7
High salt washes:100%B and 2 M NaCl[c]	1.58×10^{10}	30	4.74×10^{11}	5.6
AAV8-*gfp*[b]				
Feed	2.0×10^{11}	10	2.0×10^{12}	-
Flowthrough and column wash	2.0×10^{08}	30	6.0×10^{09}	0.3
EC peak fraction	1.50×10^{09}	50	7.5×10^{10}	3.7
VC peak fraction	1.09×10^{11}	15	1.6×10^{12}	81.7
High salt washes:100%B and 2 M NaCl[c]	2.13×10^{09}	30	6.4×10^{10}	3.2
AAV6-*gfp*				
Feed	1.5×10^{11}	10	1.5×10^{12}	-
Flowthrough and column wash	2.5×10^{08}	30	7.5×10^{09}	0.5
EC peak fraction	1.6×10^{09}	25	4.0×10^{10}	2.7
VC peak fraction	8.0×10^{10}	15	1.2×10^{12}	79.9
High salt washes:100%B and 2 M NaCl[c]	9.0×10^{08}	30	2.7×10^{10}	1.8
AAV6-*cas9*				
Feed	3.0×10^{11}	10	3.0×10^{12}	-
Flowthrough and column wash	7.0×10^{08}	30	2.1×10^{10}	0.7
EC peak fraction	1.97×10^{09}	35	6.9×10^{10}	2.3
VC peak fraction	1.66×10^{11}	15	2.5×10^{12}	83.0
High salt washes:100%B and 2 M NaCl[c]	1.7×10^{09}	30	5.1×10^{10}	1.7

EC, empty capsids; VC, vector capsids; VG, vector genome copies

[a] VGs recovery reported with respect to the total VGs loading in feed being 100%. The difference in the overall VG mass balance may represent the error associated with ddPCR analyses.

[b] Values reported as an average of triplicate runs

[c] VGs reported combinedly for both wash fractions

Table S4. Chromatographic characteristics of AAV capsids elution under continuous salt gradient elution

rAAV Vector	Peak Resolution[a] (R_S)
AAV5-*gfp*	0.78
AAV8-*gfp*	1.27
AAV6-*gfp*	1.16
AAV6-*cas9*	1.10
AAV8-*gfp*, Monolith[b] Vs. Packed-bed[b]	
AAV8-*gfp*/ POROS™ HQ	0.91
AAV8-*gfp*/ CIMmultus™ QA	1.59

[a, b] calculations based on data from continuous gradient run with a gradient slope value of 0.16 mM salt/CV and 0.25 mM salt/CV, respectively. CV, column volume:1 mL.

[a] Calculation of resolution of based on the equation for peak width and peak distance: [$R_s=2(V_2-V_1)/(W_1+W_2)$]. V_1 and V_2 are the elution points of peak 1 (empty capsid) and 2 (vector capsid), respectively. W_1 and W_2 are peak width of peak 1and 2, respectively,

9.3 Supplemental information 3 Development and Validation of an Anion-Exchange High-Performance Liquid Chromatography Method for Analysis of Empty and Genome-Encapsidating Capsids in a Purified Preparation of Recombinant Adeno-Associated Virus Serotype 5 (Chapter 6)

Supplementary data

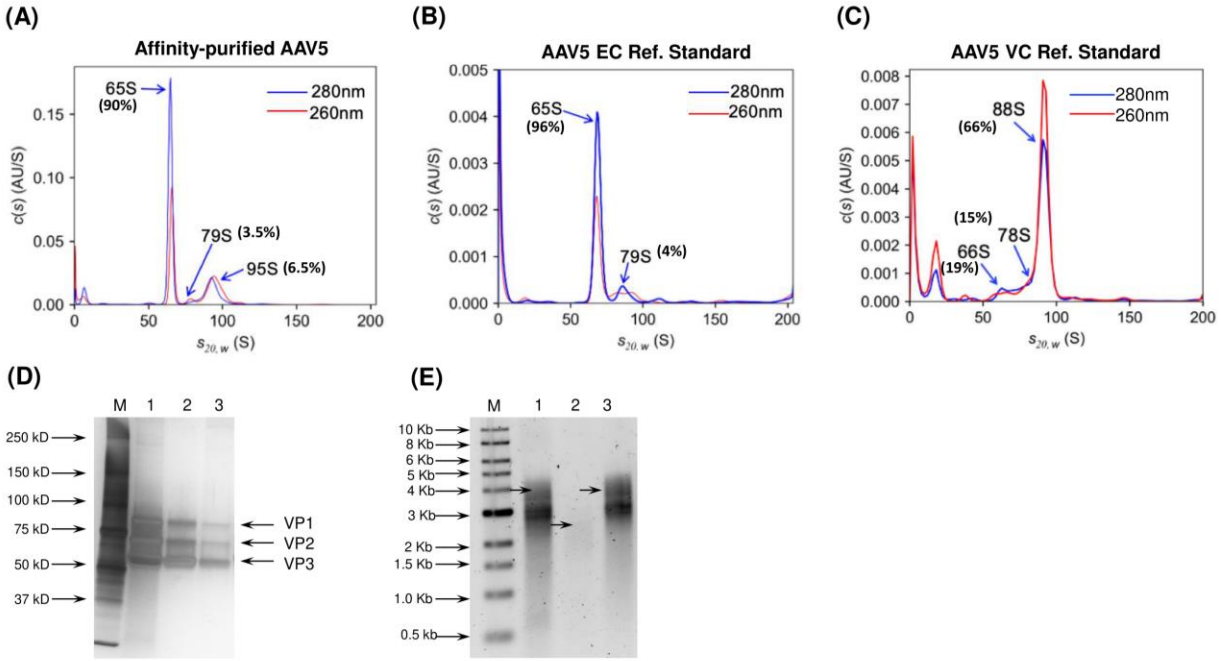

Supplementary Figure S1. AAV5 affinity-purified sample and reference standards characterization. *sv*-AUC analyses of AAV5 affinity-purified sample **(A)**, empty capsid (EC) reference standard **(B),** and vector capsid (VC) reference standard **(C)**. Peaks representing empty capsid, vector capsid, and intermediate population correspond to 65S, 95S, and 79S, respectively. **(D)** SDS-PAGE and **(E)** alkaline agarose gel electrophoresis profile. Lane 1, 2, and 3 represent the AAV5 affinity-purified sample, EC reference standard, and VC reference standard, respectively. Note the visible bands of encapsidated genome up to ~4.5 kb in the affinity-purified sample **(1)** and vector capsid standard **(3)**. The empty capsid standard shows low molecular weight DNA bands (2.5 kb and below), indicating the intermediate population, which is also visible in the *sv*-AUC profile (79S, B). EC: empty capsids, M: molecular weight marker, *sv*-AUC: sedimentation velocity analytical ultracentrifugation, VC: vector capsids.

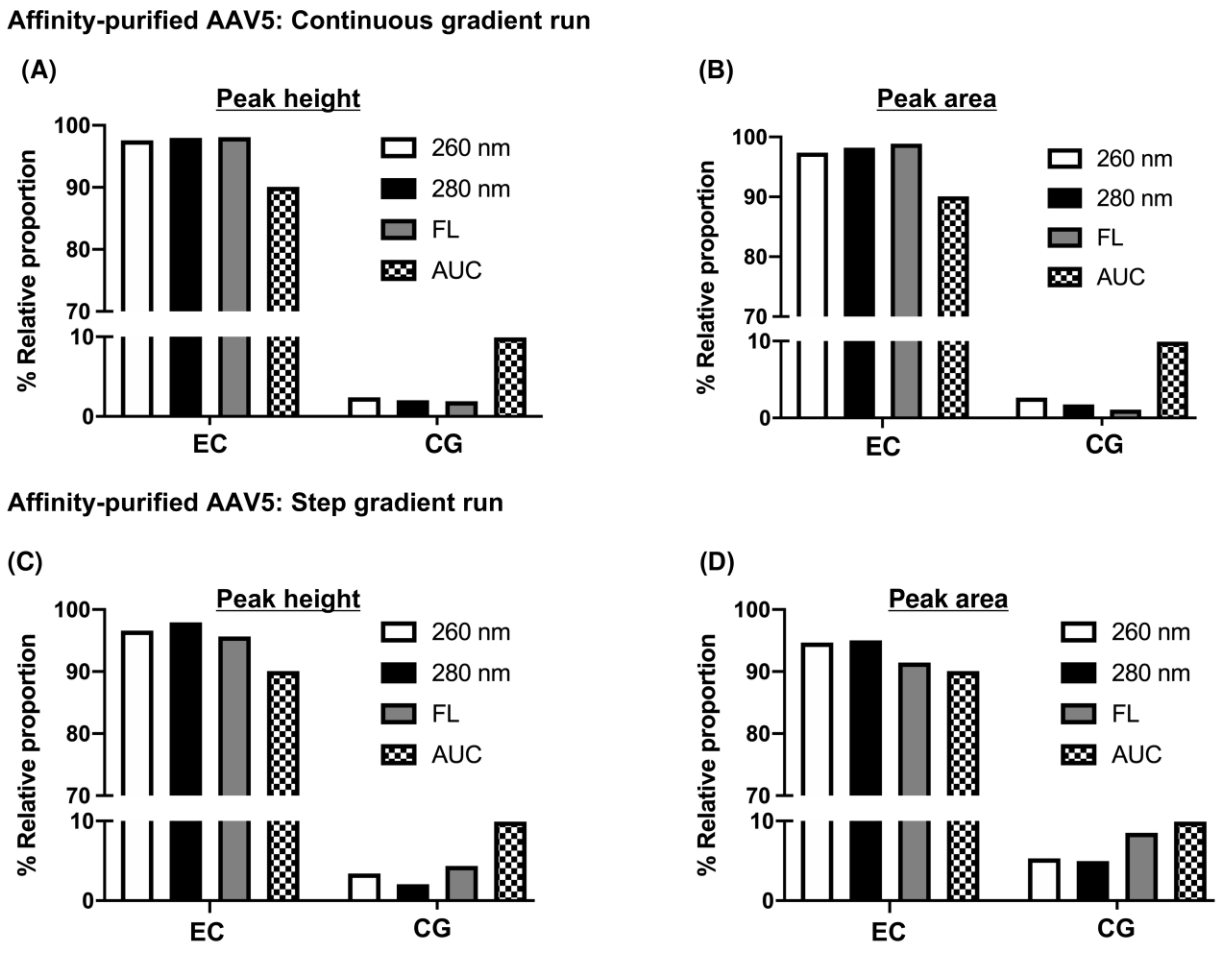

Supplementary Figure S2. Determination of the % relative proportion of EC and CG in affinity-purified AAV5 sample as analyzed from the data of three different signals (260 nm, 280 nm, and FL) and two different modes (peak height and peak area)**.** In a continuous gradient run, for both peak height **(A)**- and peak area **(B)**- based analyses, the % of EC (>95%) and CG (<5%) values differ significantly from the values of the *sv*-AUC (EC:90% and CG:10%). For the step-gradient run, as compared to peak height-based analyses (EC: 90-95% and CG:5-10%) **(C)**, the values from peak area-based analyses (EC: 95-98% and CG:2-5%) **(D)** for all three signals have a better agreement with the values from *sv*-AUC analysis (EC:90% and CG:10%) with FL signal being the most accurate. CG: capsids encapsidating genetic material, FL: fluorescence.

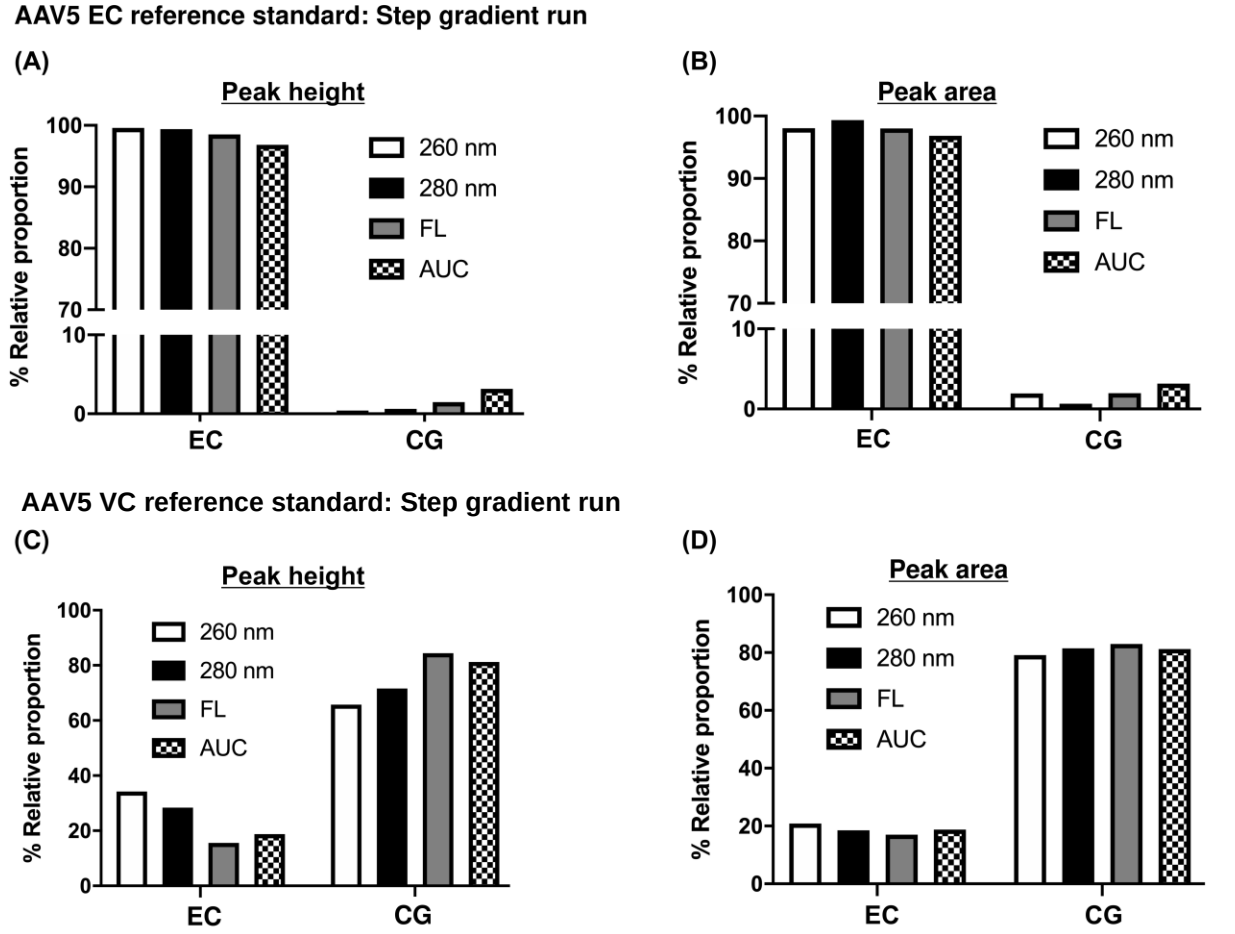

Supplementary Figure S3. Determination of the relative proportion of % of EC and CG in EC and VC reference standards of AAV5 as analyzed from the data of three different signals (260 nm, 280 nm, and FL) and two different modes (peak height and peak area)**.** In the EC reference standard, for both **(A)** peak height (EC: 98-99.5% and CG:0.5-2%) - and **(B)** peak area (EC:97-99.5% and CG: 0.5-3%) -based analyses, the % of EC values were comparable with values from the *sv*-AUC analysis (EC: 96% and CG 4%). For the step-gradient run, as compared to peak height-based analyses (EC: 16-34% and CG 66-84%) **(C)**, the values from peak area-based analyses (EC: 17-20% and CG: 80-83%) **(D)** have a better agreement with the values from the *sv*-AUC analysis (EC: 19% and CG: 81%) for all three signals. FL: fluorescence.

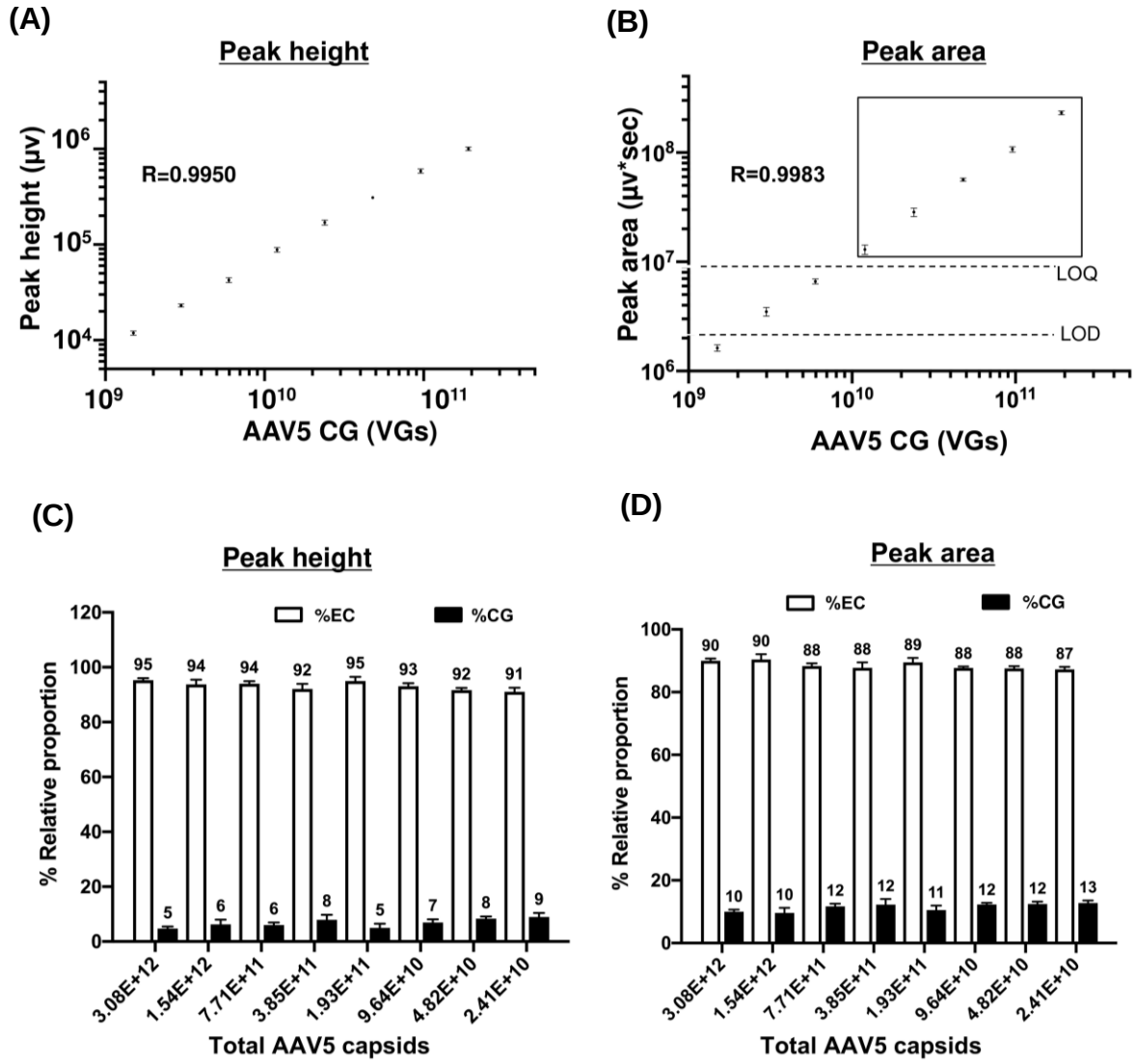

Supplementary Figure S4. Linearity curve of VC reference standard and relative percentages of EC and CG in affinity-purified AAV5 sample. Linearity curve for VC reference standard where CG peak signals: peak height (A) and peak area (B) were plotted as a function of total VGs. The LOD ($2.6x10^6$) and LOQ ($1x10^7$) values reported for peak area (B) correspond to those based on the standard deviation of y-intercept of the regression line. The error bar represents the % relative standard deviation for the triplicate injections. The actual range of reliable quantification is shown in the rectangle. The values reported on the X-axis correspond to the amount of VGs recovered in CG peak from 40 µL injection of the serially diluted VC reference standard of the $0.5x10^{13}$ VG/mL concentration (Table S1). The relative proportion of EC and CG determined from the fluorescence peak height (C) and peak area (D) data of the serially diluted affinity-purified AAV5 sample over the two-log range. The values reported on the X-axis correspond to the total capsids in 40 µL injection of two-fold serial dilution of the affinity-purified sample with $8.5x10^{12}$ VG/mL ($7.7x10^{13}$ Capsids/mL) concentration (Table S1). The error bar represents the % relative standard deviation for the triplicate injections.

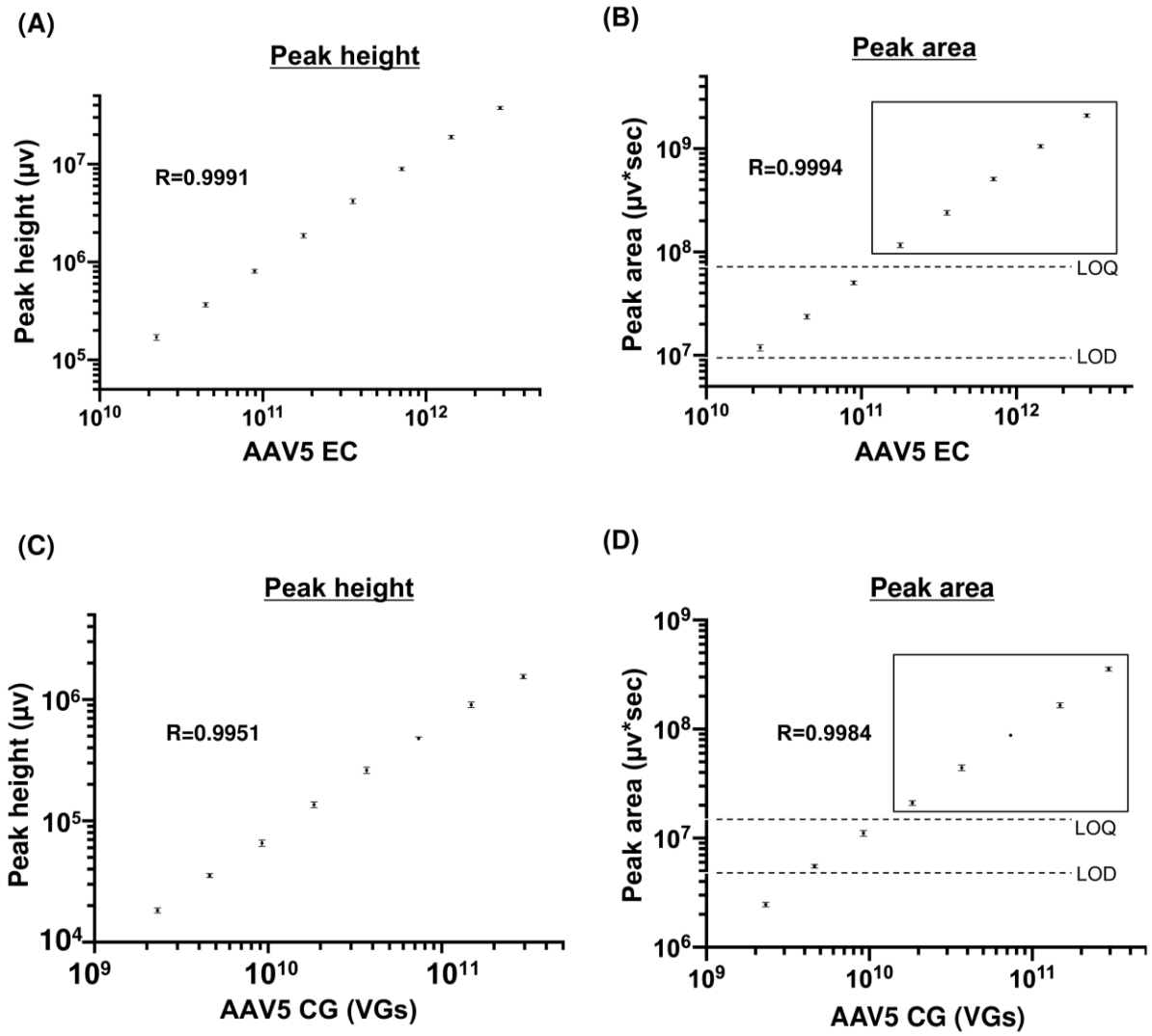

Supplementary Figure S5. Linearity curve for EC and CG peak signals in an affinity-purified sample. Linearity curve for EC peak signals: peak height **(A)** and peak area **(B)** plotted as a function of total EC. The LOD ($9.6x10^6$) and LOQ ($5.7x10^7$) values reported for peak area **(B)** correspond to those based on the standard deviation of y-intercept of the regression line. Linearity curve for CG peak signals: peak height **(C)** and peak area **(D)** plotted as a function of total VGs. The LOD ($4.5x10^6$) and LOQ ($1.6x10^7$) values reported for peak area **(D)** correspond to those based on the standard deviation of y-intercept of the regression line. The rectangle represents the actual range for reliable quantification. The values reported on the X-axis correspond to the amount of corresponding capsid population in 40 µL injection of two-fold serial dilution of affinity-purified sample with $8.5x10^{12}$ VG/mL ($7.7x10^{13}$ Capsids/mL) concentration. The error bar for each point represents the % relative standard deviation for the triplicate injections.

Supplementary Table S1. *Orthogonal quantitative analysis of the affinity-purified AAV5 sample and VC reference standard used in the AEX-HPLC method validation studies*

Analytical Method	Affinity purified AAV5 (mixture of EC and CG)	VC reference Standard
ddPCR	$8.5x10^{12}$ VG[a]/mL	$0.5x10^{13}$ VG[a]/mL
	$7.7x10^{13}$ Cp[b]/mL	$6.8x10^{12}$ Cp[b]/mL
Optical Density measurement	$6.8x10^{12}$ VG/mL	$7.1x10^{12}$ VG/mL
Total Protein assay and Avogadro`s equation-based calculation	$8.9x10^{12}$ VG/mL[c]	$9.2x10^{12}$ VG/mL[b]
	$9x10^{13}$ Cp/mL	$1.1x10^{13}$ Cp/mL

[a] VG values from ddPCR assay.

[b] Total capsid calculated from VGs and % relative proportion determined from *sv*-AUC data (**Table 1**).

[c] VGs calculated from the total capsid value (Cp), and % relative proportion of EC and CG determined from *sv*-AUC data (Table 1).

Cp, total capsid particles; VG, viral genome copies.

Supplementary Table S2. *Linearity curve characteristics determined for EC and CG peaks from an AEX-HPLC run of an affinity-purified sample of AAV5*

Linearity curve characteristics	EC peak fraction	CG peak fraction
Detection mode/Signal	Fluorescence/ Peak area	
Parameter	Value	Value
Linearity curve equation	$Y=0.000742X-1.38x10^{7}$	$Y=0.001197X-1.18x10^{6}$
R^2	0.9990	0.9969
Linearity range tested	$2.3x10^{10}$-$2.8x10^{12}$ capsids	$2.3x10^{9}$-$2.9x10^{11}$ capsids
Linearity range tested (combined)	$2.3x10^{9}$-$2.8x10^{12}$ capsids	
Based on the residual standard deviation of the regression line		
LOD (Peak area)	$7.4x10^{7}$	$2.1x10^{7}$
LOQ (Peak area)	$2.6x10^{8}$	$6.6x10^{7}$
The actual combined range for reliable quantification based on LOQ values when expressed as total capsids	$5.6x10^{10}$- $2.8x10^{12}$	
Based on the standard deviation of y-intercept of the regression line		
LOD (Peak area)	$9.7x10^{6}$	$4.5x10^{6}$
LOQ (Peak area)	$5.7x10^{7}$	$1.6x10^{7}$
The actual combined range for reliable quantification based on LOQ when expressed as total capsids	$1.4x10^{10}$- $2.8x10^{12}$	

Supplementary Table S3. *Accuracy and recovery analyses of AAV5 VC reference standard spiking (4.80x10^{10} VGs) in three different concentrations of affinity-purified AAV5 samples*

VGs in Affinity-purified AAV5 CG peak[a]	Non-spiked CG peak area (µV*sec)	CG peak area after spiking[b] (µV*sec)	VGs in CG peak after spiking	Recovered AAV5 VC	% Recovery of spiked AAV5 VC
2.9x10^{11} (1x)	3.5x10^{8}	4.1x10^{8}	3.4x10^{11}	4.5x10^{10}	93.80
2.9x10^{10} (1:10)	3.4x10^{7}	9.1x10^{7}	7.7x10^{10}	4.7x10^{10}	98.80
1.5x10^{10} (1:20)	1.7x10^{7}	7.4x10^{7}	6.2x10^{10}	4.8x10^{10}	99.20

[a] Values correspond to the capsid amount in 40 µL injection of the highest concentration 8.5x10^{12} VG/mL sample (**Table S1**). The values in the parenthesis correspond to the dilution factor of the concentrated sample.

[b] The spiking of 4.8x10^{10} VGs corresponds to the capsid amount in 40 µL injection in 1:4 dilution of the concentrated stock (0.5x10^{13} VG/mL) VC reference standard (**Table S1**).

All values reported above are means of triplicate injections. The % RSD value for all injections was below 4%.

Supplementary Table S4. *Carryover analysis*

Sample	EC peak area	CG peak area
$2.9x10^{11}$ VGs[a]	$2.3x10^{9}$	$3.9x10^{8}$
Buffer blank	$1.0x10^{7}$	$1.8x10^{6}$
Carryover (% of LOQ) LOQ based on the residual standard deviation of the regression line[b]	4.183%	2.770%
Carryover (% of LOQ) LOQ based on the y-intercept of the regression line[c]	19.164%	11.375%

[a] Values represent the capsid amount in 40 µL injection of the highest concentration sample ($8.5x10^{12}$ VG/mL). The average VG recovery of 87% in the VC peak is used in the calculation.
[b, and c] Values of LOQ correspond to different criteria as presented in **Table S2**.

Supplementary calculation

Parameters	Affinity-purified AAV5 (mixture of EC and CG)	Empty capsid reference standard	Vector capsid reference standard
A_{260}	0.64	0.143	0.228
A_{280}	0.80	0.186	0.166
$A_{260/280}$	0.80	0.77	1.37
VG/mL	$6.72x10^{12}$	$1.3x10^{12}$	$5.06x10^{12}$
Cp/VG	9.27	11.67	1.10
% Filled capsids	10.78	8.57	90.76
% Empty capsids	89.22	91.43	9.24

Calculation method

1. Calculation of the titer

$$(\mathrm{VG/mL}) = \frac{4.47 \times 10^{19}(A_{260} - 0.59A_{280})}{MW_{DNA}}$$

Size of the expression cassette (ITR-to-ITR): 3.79 kb

Molecular weight of the expression cassette (MW_{DNA})= $1.15x10^{6}$

2. Calculation of the total capsids (Cp) to viral genome (VG) ratio

$$\text{Capsid ratio (Cp/VG)} = MW_{DNA} \times \frac{1.76 \times 10^{-6}(1.80 - A_{260}/A_{280})}{A_{260}/A_{280} - 0.59}$$

References

[1] Wirth, T., and Ylä-Herttuala, S. (2006). Gene technology based therapies in the brain. Advances and technical standards in neurosurgery (pp. 3-32). Springer, Vienna.

[2] Waehler, R., Russell, S. J., and Curiel, D. T. (2007). Engineering targeted viral vectors for gene therapy. Nature reviews genetics, 8(8), 573-587.

[3] Wang, D., Tai, P. W., and Gao, G. (2019). Adeno-associated virus vector as a platform for gene therapy delivery. Nature reviews Drug discovery, 18(5), 358-378.

[4] Li, C., and Samulski, R. J. (2020). Engineering adeno-associated virus vectors for gene therapy. Nature Reviews Genetics, 1-18.

[5] Masri, F., Cheeseman, E., and Ansorge, S. (2019). Viral vector manufacturing: how to address current and future demands. Cell and Gene Ther Insights, 5, 949-970.

[6] Wright, J. F. (2014). Product-related impurities in clinical-grade recombinant AAV vectors: characterization and risk assessment. Biomedicines, 2(1), 80-97.

[7] Mingozzi, F., and High, K. A. (2007). Immune responses to AAV in clinical trials. Current gene therapy, 7(5), 316-324.

[8] Mingozzi, F., and High, K. A. (2011). Therapeutic in vivo gene transfer for genetic disease using AAV: progress and challenges. Nature reviews genetics, 12(5), 341-355.

[9] Mingozzi, F., and High, K. A. (2013). Immune responses to AAV vectors: overcoming barriers to successful gene therapy. Blood, The Journal of the American Society of Hematology, 122(1), 23-36.

[10] Ayuso, E., Mingozzi, F., Montane, J., Leon, X., Anguela, X. M., Haurigot, V., ... and Bosch, F. (2010). High AAV vector purity results in serotype-and tissue-independent enhancement of transduction efficiency. Gene therapy, 17(4), 503-510.

[11] Mueller, C., Ratner, D., Zhong, L., Esteves-Sena, M., and Gao, G. (2012). Production and Discovery of Novel Recombinant Adeno-Associated Viral Vectors. Current protocols in microbiology, 26(1), 14D-1.

[12] Zolotukhin, S., Byrne, B. J., Mason, E., Zolotukhin, I., Potter, M., Chesnut, K., ... and Muzyczka, N. (1999). Recombinant adeno-associated virus purification using novel methods improves infectious titer and yield. Gene therapy, 6(6), 973-985.

[13] Qu, W., Wang, M., Wu, Y., and Xu, R. (2015). Scalable downstream strategies for purification of recombinant adeno-associated virus vectors in light of the properties. Current pharmaceutical biotechnology, 16(8), 684-695.

[14] Kronenberg, S., Kleinschmidt, J. A., and Böttcher, B. (2001). Electron cryo-microscopy and image reconstruction of adeno-associated virus type 2 empty capsids. EMBO reports, 2(11), 997-1002.

[15] Subramanian, S., Maurer, A. C., Bator, C. M., Makhov, A. M., Conway, J. F., Turner, K. B., ... and Hafenstein, S. L. (2019). Filling Adeno-Associated Virus Capsids: Estimating Success by Cryo-Electron Microscopy. Human Gene Therapy, 30(12), 1449-1460.

[16] Burnham, B., Nass, S., Kong, E., Mattingly, M., Woodcock, D., Song, T., ... and O'Riordan, C. (2015). 556. Analytical Ultracentrifugation as an Approach to Characterize Recombinant AAV Vectors. Molecular Therapy, 23, S223.

[17] Pierson, E. E., Keifer, D. Z., Asokan, A., and Jarrold, M. F. (2016). Resolving adeno-associated viral particle diversity with charge detection mass spectrometry. Analytical chemistry, 88(13), 6718-6725.

[18] Omenn, G. S., Lane, L., Lundberg, E. K., Beavis, R. C., Overall, C. M., and Deutsch, E. W. (2016). Metrics for the Human Proteome Project 2016: progress on identifying and characterizing the human proteome, including post-translational modifications. Journal of proteome research, 15(11), 3951-3960.

[19] Thul, P. J., and Lindskog, C. (2018). The human protein atlas: A spatial map of the human proteome. Protein Science, 27(1), 233-244.

[20] Loewe, L., and Hill, W. G. (2010). The population genetics of mutations: good, bad and indifferent.

[21] Carlin, J. L. (2011). Mutations are the raw materials of evolution. Nature Education Knowledge, 3(10), 10.

[22] Lagassé, H. D., Alexaki, A., Simhadri, V. L., Katagiri, N. H., Jankowski, W., Sauna, Z. E., and Kimchi-Sarfaty, C. (2017). Recent advances in (therapeutic protein) drug development. F1000Research, 6.

[23] Ginn, S. L., Amaya, A. K., Alexander, I. E., Edelstein, M., and Abedi, M. R. (2018). Gene therapy clinical trials worldwide to 2017: An update. The journal of gene medicine, 20(5), e3015.

[24] Griffith, F. (1928). The significance of pneumococcal types. Epidemiology and Infection, 27(2), 113-159.

[25] Dawson, M. H., and Sia, R. H. (1931). In vitro transformation of pneumococcal types: I. A technique for inducing transformation of pneumococcal types in vitro. The Journal of experimental medicine, 54(5), 681.

[26] Alloway, J. L. (1933). Further observations on the use of pneumococcus extracts in effecting transformation of type in vitro. The Journal of experimental medicine, 57(2), 265-278.

[27] Avery, O. T., MacLeod, C. M., and McCarty, M. (1944). Studies on the chemical nature of the substance inducing transformation of pneumococcal types: induction of transformation by a desoxyribonucleic acid fraction isolated from pneumococcus type III. The Journal of experimental medicine, 79(2), 137-158.

[28] Zinder, N. D., and Lederberg, J. (1952). Genetic exchange in Salmonella. Journal of bacteriology, 64(5), 679.

[29] Szybalska, E. H., and Szybalski, W. (1962). Genetics of human cell lines, IV. DNA-mediated heritable transformation of a biochemical trait. Proceedings of the National Academy of Sciences of the United States of America, 48(12), 2026.

[30] Temin, H. M. (1961). Mixed infection with two types of Rous sarcoma virus. Virology, 13(2), 158-163.

[31] Rogers, S., and Pfuderer, P. (1968). Use of viruses as carriers of added genetic information. Nature, 219(5155), 749-751.

[32] Rosenberg, S. A., Aebersold, P., Cornetta, K., Kasid, A., Morgan, R. A., Moen, R., ... and Merino, M. J. (1990). Gene transfer into humans—immunotherapy of patients with advanced melanoma, using tumor-infiltrating lymphocytes modified by retroviral gene transduction. New England Journal of Medicine, 323(9), 570-578.

[33] Rosenberg, S. A., Anderson, W. F., Blaese, M., Hwu, P., Yannelli, J. R., Yang, J. C., ... and Ettinghausen, S. E. (1993). The development of gene therapy for the treatment of cancer. Annals of surgery, 218(4), 455.

[34] Blaese, R. M., Culver, K. W., Miller, A. D., Carter, C. S., Fleisher, T., Clerici, M., ... and Greenblatt, J. J. (1995). T lymphocyte-directed gene therapy for ADA− SCID: initial trial results after 4 years. Science, 270(5235), 475-480.

[35] Goswami, R., Subramanian, G., Silayeva, L., Newkirk, I., Doctor, D., Chawla, K., ... and Betapudi, V. (2019). Gene therapy leaves a vicious cycle. Frontiers in oncology, 9, 297.

[36] Lundstrom, K. (2018). Viral vectors in gene therapy. Diseases, 6(2), 42.

[37] Ibraheem, D., Elaissari, A., and Fessi, H. (2014). Gene therapy and DNA delivery systems. International journal of pharmaceutics, 459(1-2), 70-83.

[38] Huang, S., and Kamihira, M. (2013). Development of hybrid viral vectors for gene therapy. Biotechnology advances, 31(2), 208-223.

[39] Atchison, R. W., Casto, B. C., and Hammon, W. M. (1966). Electron microscopy of adenovirus-associated virus (AAV) in cell cultures. Virology, 29(2), 353-357.

[40] Cheung, A. K., Hoggan, M. D., Hauswirth, W. W., and Berns, K. I. (1980). Integration of the adeno-associated virus genome into cellular DNA in latently infected human Detroit 6 cells. Journal of Virology, 33(2), 739-748.

[41] Srivastava, A. R. U. N., Lusby, E. W., and Berns, K. I. (1983). Nucleotide sequence and organization of the adeno-associated virus 2 genome. Journal of virology, 45(2), 555-564.

[42] King, J. A., Dubielzig, R., Grimm, D., and Kleinschmidt, J. A. (2001). DNA helicase-mediated packaging of adeno-associated virus type 2 genomes into preformed capsids. The EMBO journal, 20(12), 3282-3291.

[43] Collaco, R. F., Kalman-Maltese, V., Smith, A. D., Dignam, J. D., and Trempe, J. P. (2003). A biochemical characterization of the adeno-associated virus Rep40 helicase. Journal of Biological Chemistry, 278(36), 34011-34017.

[44] Kotterman, M. A., and Schaffer, D. V. (2014). Engineering adeno-associated viruses for clinical gene therapy. Nature Reviews Genetics, 15(7), 445-451.

[45] Nonnenmacher, M., and Weber, T. (2012). Intracellular transport of recombinant adeno-associated virus vectors. Gene therapy, 19(6), 649-658.

[46] Huang, L. Y., Halder, S., and Agbandje-McKenna, M. (2014). Parvovirus glycan interactions. Current opinion in virology, 7, 108-118.

[47] Xiao, P. J., and Samulski, R. J. (2012). Cytoplasmic trafficking, endosomal escape, and perinuclear accumulation of adeno-associated virus type 2 particles are facilitated by microtubule network. Journal of virology, 86(19), 10462-10473.

[48] Nicolson, S. C., and Samulski, R. J. (2014). Recombinant adeno-associated virus utilizes host cell nuclear import machinery to enter the nucleus. Journal of virology, 88(8), 4132-4144.

[49] Kelich, J. M., Ma, J., Dong, B., Wang, Q., Chin, M., Magura, C. M., ... and Yang, W. (2015). Super-resolution imaging of nuclear import of adeno-associated virus in live cells. Molecular Therapy-Methods and Clinical Development, 2, 15047.

[50] Fisher, K. J., Gao, G. P., Weitzman, M. D., DeMatteo, R., Burda, J. F., and Wilson, J. M. (1996). Transduction with recombinant adeno-associated virus for gene therapy is limited by leading-strand synthesis. Journal of virology, 70(1), 520-532.

[51] Ferrari, F. K., Samulski, T., Shenk, T., and Samulski, R. J. (1996). Second-strand synthesis is a rate-limiting step for efficient transduction by recombinant adeno-associated virus vectors. Journal of virology, 70(5), 3227-3234.

[52] Berns, K. I., Pinkerton, T. C., Thomas, G. F., and Hoggan, M. D. (1975). Detection of adeno-associated virus (AAV)-specific nucleotide sequences in DNA isolated from latently infected Detroit 6 cells. Virology, 68(2), 556-560.

[53] Penaud-Budloo, M., Le Guiner, C., Nowrouzi, A., Toromanoff, A., Chérel, Y., Chenuaud, P., ... and Snyder, R. O. (2008). Adeno-associated virus vector genomes persist as episomal chromatin in primate muscle. Journal of virology, 82(16), 7875-7885.

[54] Bryant, L. M., Christopher, D. M., Giles, A. R., Hinderer, C., Rodriguez, J. L., Smith, J. B., ... and Wilson, J. M. (2013). Lessons learned from the clinical development and market authorization of Glybera. Human gene therapy Clinical development, 24(2), 55-64.

[55] Russell, S., Bennett, J., Wellman, J. A., Chung, D. C., Yu, Z. F., Tillman, A., ... and Cross, D. (2017). Efficacy and safety of voretigene neparvovec (AAV2-hRPE65v2) in patients with RPE65-mediated inherited retinal dystrophy: a randomised, controlled, open-label, phase 3 trial. The Lancet, 390(10097), 849-860.

[56] Mahajan, R. (2019). Onasemnogene abeparvovec for spinal muscular atrophy: The costlier drug ever. International Journal of Applied and Basic Medical Research, 9(3), 127.

[57] Chahal, P. S., Schulze, E., Tran, R., Montes, J., and Kamen, A. A. (2014). Production of adeno-associated virus (AAV) serotypes by transient transfection of HEK293 cell suspension cultures for gene delivery. Journal of virological methods, 196, 163-173.

[58] Grieger, J. C., Soltys, S. M., and Samulski, R. J. (2016). Production of recombinant adeno-associated virus vectors using suspension HEK293 cells and continuous harvest of vector from the culture media for GMP FIX and FLT1 clinical vector. Molecular Therapy, 24(2), 287-297.

[59] Thorne, B. A., Takeya, R. K., and Peluso, R. W. (2009). Manufacturing recombinant adeno-associated viral vectors from producer cell clones. Human gene therapy, 20(7), 707-714.

[60] Martin, J., Frederick, A., Luo, Y., Jackson, R., Joubert, M., Sol, B., ... and Vincent, K. (2013). Generation and characterization of adeno-associated virus producer cell lines for research and preclinical vector production. Human Gene Therapy Methods, 24(4), 253-269.

[61] Clément, N., Knop, D. R., and Byrne, B. J. (2009). Large-scale adeno-associated viral vector production using a herpesvirus-based system enables manufacturing for clinical studies. Human gene therapy, 20(8), 796-806.

[62] Thomas, D. L., Wang, L., Niamke, J., Liu, J., Kang, W., Scotti, M. M., ... and Knop, D. R. (2009). Scalable recombinant adeno-associated virus production using recombinant herpes simplex virus type 1 coinfection of suspension-adapted mammalian cells. Human gene therapy, 20(8), 861-870.

[63] Urabe, M., Ding, C., and Kotin, R. M. (2002). Insect cells as a factory to produce adeno-associated virus type 2 vectors. Human gene therapy, 13(16), 1935-1943.

[64] Smith, R. H., Levy, J. R., and Kotin, R. M. (2009). A simplified baculovirus-AAV expression vector system coupled with one-step affinity purification yields high-titer rAAV stocks from insect cells. Molecular Therapy, 17(11), 1888-1896.

[65] Aslanidi, G., Lamb, K., and Zolotukhin, S. (2009). An inducible system for highly efficient production of recombinant adeno-associated virus (rAAV) vectors in insect Sf9 cells. Proceedings of the National Academy of Sciences, 106(13), 5059-5064.

[66] Xiao, X., Li, J., and Samulski, R. J. (1998). Production of high-titer recombinant adeno-associated virus vectors in the absence of helper adenovirus. Journal of virology, 72(3), 2224-2232.

[67] Kang, W., Wang, L., Harrell, H., Liu, J., Thomas, D. L., Mayfield, T. L., ... and Knop, D. R. (2009). An efficient rHSV-based complementation system for the production of multiple rAAV vector serotypes. Gene therapy, 16(2), 229-239.

[68] Mena, J. A., Aucoin, M. G., Montes, J., Chahal, P. S., and Kamen, A. A. (2010). Improving adeno-associated vector yield in high density insect cell cultures. The Journal of Gene Medicine: A cross-disciplinary journal for research on the science of gene transfer and its clinical applications, 12(2), 157-167.

[69] Joshi, P. R., Cervera, L., Ahmed, I., Kondratov, O., Zolotukhin, S., Schrag, J., ... and Kamen, A. A. (2019). Achieving high-yield production of functional AAV5 gene delivery vectors via fedbatch in an insect cell-one baculovirus system. Molecular Therapy-Methods and Clinical Development, 13, 279-289.

[70] Grieger, J. C., Soltys, S. M., and Samulski, R. J. (2016). Production of recombinant adeno-associated virus vectors using suspension HEK293 cells and continuous harvest of vector from the culture media for GMP FIX and FLT1 clinical vector. Molecular Therapy, 24(2), 287-297.

[71] Mietzsch, M., Casteleyn, V., Weger, S., Zolotukhin, S., and Heilbronn, R. (2015). OneBac 2.0: Sf 9 cell lines for production of AAV5 vectors with enhanced infectivity and minimal encapsidation of foreign DNA. Human gene therapy, 26(10), 688-697.

[72] Nass, S. A., Mattingly, M. A., Woodcock, D. A., Burnham, B. L., Ardinger, J. A., Osmond, S. E., ... and O'Riordan, C. R. (2018). Universal method for the purification of recombinant AAV vectors of differing serotypes. Molecular Therapy-Methods and Clinical Development, 9, 33-46.

[73] Savy, A., Dickx, Y., Nauwynck, L., Bonnin, D., Merten, O. W., and Galibert, L. (2017). Impact of inverted terminal repeat integrity on rAAV8 production using the baculovirus/Sf9 cells system. Human Gene Therapy Methods, 28(5), 277-289.

[74] Chahal, P. S., Aucoin, M. G., and Kamen, A. (2007). Primary recovery and chromatographic purification of adeno-associated virus type 2 produced by baculovirus/insect cell system. Journal of virological methods, 139(1), 61-70.

[75] Segura, M. M., Kamen, A. A., and Garnier, A. (2011). Overview of current scalable methods for purification of viral vectors. In Viral Vectors for Gene Therapy (pp. 89-116). Humana Press.

[76] Zolotukhin, S., Potter, M., Zolotukhin, I., Sakai, Y., Loiler, S., Fraites Jr, T. J., ... and Flotte, T. R. (2002). Production and purification of serotype 1, 2, and 5 recombinant adeno-associated viral vectors. Methods, 28(2), 158-167.

[77] Clark, K. R. (1999). Liu X, McGrath JP, Johnson PR. Highly purified recombinant adeno-associated virus vectors are biologically active and free of detectable helper and wild-type viruses. Hum Gene Ther, 10, 1031-1039.

[78] Anderson, R., Macdonald, I., Corbett, T., Whiteway, A., and Prentice, H. G. (2000). A method for the preparation of highly purified adeno-associated virus using affinity column

chromatography, protease digestion and solvent extraction. Journal of virological methods, 85(1-2), 23-34.

[79] Harris, J. D., Beattie, S. G., and Dickson, J. G. (2003). Novel tools for production and purification of recombinant adeno-associated viral vectors. In Viral Vectors for Gene Therapy(pp. 255-267). Humana Press.

[80] O'Riordan, C. R., Lachapelle, A. L., Vincent, K. A., and Wadsworth, S. C. (2000). Scaleable chromatographic purification process for recombinant adeno-associated virus (rAAV). The Journal of Gene Medicine: A cross-disciplinary journal for research on the science of gene transfer and its clinical applications, 2(6), 444-454.

[81] Auricchio, A., O'connor, E., Hildinger, M., and Wilson, J. M. (2001). A single-step affinity column for purification of serotype-5 based adeno-associated viral vectors. Molecular Therapy, 4(4), 372-374.

[82] Koerber, J. T., Jang, J. H., Yu, J. H., Kane, R. S., and Schaffer, D. V. (2007). Engineering adeno-associated virus for one-step purification via immobilized metal affinity chromatography. Human gene therapy, 18(4), 367-378.

[83] Stachler, M. D., and Bartlett, J. S. (2006). Mosaic vectors comprised of modified AAV1 capsid proteins for efficient vector purification and targeting to vascular endothelial cells. Gene therapy, 13(11), 926-931.

[84] Qu, G., Bahr-Davidson, J., Prado, J., Tai, A., Cataniag, F., McDonnell, J., ... and Smith, P. (2007). Separation of adeno-associated virus type 2 empty particles from genome containing vectors by anion-exchange column chromatography. Journal of virological methods, 140(1-2), 183-192.

[85] Urabe, M., Xin, K. Q., Obara, Y., Nakakura, T., Mizukami, H., Kume, A., ... and Ozawa, K. (2006). Removal of empty capsids from type 1 adeno-associated virus vector stocks by anion-exchange chromatography potentiates transgene expression. Molecular Therapy, 13(4), 823-828.

[86] Kaludov, N., Handelman, B., and Chiorini, J. A. (2002). Scalable purification of adeno-associated virus type 2, 4, or 5 using ion-exchange chromatography. Human gene therapy, 13(10), 1235-1243.

[87] Brument, N., Morenweiser, R., Blouin, V., Toublanc, E., Raimbaud, I., Chérel, Y., ... and Moullier, P. (2002). A versatile and scalable two-step ion-exchange chromatography process for the purification of recombinant adeno-associated virus serotypes-2 and-5. Molecular Therapy, 6(5), 678-686.

[88] Davidoff, A. M., Ng, C. Y., Sleep, S., Gray, J., Azam, S., Zhao, Y., ... and Nathwani, A. C. (2004). Purification of recombinant adeno-associated virus type 8 vectors by ion exchange chromatography generates clinical grade vector stock. Journal of virological methods, 121(2), 209-215.

[89] Gallant, S. R., Kundu, A., and Cramer, S. M. (1995). Optimization of step gradient separations: consideration of nonlinear adsorption. Biotechnology and bioengineering, 47(3), 355-372.

[90] Antos, D., and Seidel-Morgenstern, A. (2002). Continuous step gradient elution for preparative separations. Separation science and technology, 37(7), 1469-1487.